ODF2L is a negative regulator of ciliogenesis

Paulu SRP De Saram

Royal Holloway University of London

This thesis is resubmitted for the degree of Doctor of Philosophy

April 2018

Declaration of Authorship

I, Paulu SRP De Saram, hereby declare that this thesis and work presented in it is entirely my own. Where I have consulted the work of others, this is clearly stated.

Signed: _____

Date:_____

Acknowledgment

It is a pleasure to thank the many people who made this thesis possible.

I would like to express gratitude to my supervisor, Christopher Wilkinson for his support and for his guidance and reassurance. I would also like to thank my secondary supervision Jenny Murdoch for her support and advice. I wish to express my gratitude to all the academic staff for their support and allowing me use of their laboratories and research equipment.

A very special thanks is also due to my advisor Philip Chen, and his laboratory members for the support.

I would like to thank all the research technicians for their help and instruction. I am particularly grateful for the assistance given by Chris Gerrish, and Kayvan Hakim-Red for taking time from their own busy schedule to introduce me to mass spectrometry and support me throughout. I also very grateful to Julia Smith for her continued help and for inviting me to Bruker for training.

A very special thanks is also due to my lab partners Kayvan Hakim-Rad and Anila Iqbal for their support, encouraging words and advices.

I wish to thank my family and friends for their solid support and understanding. Lastly, and most importantly, I wish to thank my mother. She, raised me, supported me, taught me, and loved me. To her I dedicate this thesis.

Abstract

The centrosome is a subcellular organelle whose main role is acting as a microtubule organising centre (MTOC). It consists of two barrel-shaped centrioles surrounded by the pericentriolar matrix. Further out are electron-dense protein particles called centriolar satellites. In quiescent cells, centrioles migrate to the apical surface of the cell and act as the template (basal body) for hair-like projections called cilia and flagella. Control of ciliogenesis is still not fully understood. Here, I have studied three proteins to determine their contribution to ciliogenesis: zebrafish Cep72 and Odf2b, and human ODF2L. Human CEP72 has been previously identified as a PCM-1 interacting centriolar satellite protein which contributes to ciliogenesis in cultured cells. I tested whether Cep72 depletion in zebrafish embryos would disrupt ciliogenesis and cause a developmental phenotype. A 'ciliary' phenotype was observed, consisting of the typical morphology following ciliary disruption, yet with no obvious change in cilium numbers or length.

ODF2 is a component of the distal appendages of the mother centriole, shown previously to regulate ciliogenesis. Related proteins include human ODF2L and zebrafish Odf2a and Odf2b. Here, I show that depletion of *odf2b* led to reduced cilium length in the zebrafish embryo pronephros. I also observed localisation of ODF2L to the centriolar satellites in proliferating cells in culture, using immunofluorescence-labelling. Intriguingly, at the onset of ciliogenesis ODF2L disappeared from centriolar satellites but then reappeared after ciliation was complete. Overexpression of ODF2L in cultured cells suppressed ciliogenesis, even after initiation of ciliation by serum deprivation. Furthermore, ODF2L knockdown resulted in cilia being formed in cells cultured in serum-supplemented media, when they would not normally produce cilia. Pull-down of ODF2L-interacting partners and identification with mass spectrometry, coupled with in silico structural analysis, suggest that ODF2L may be involved in Golgi trafficking to the cilium which is necessary for ciliogenesis to begin.

Table of Contents

Table of Figures

Index of tables

Abbreviations

Ab	Antibody
ADIP	Afadin and alpha-actin binding
APG	Autophagy protein
ATCC	American Type Culture Collection
ATP	Adenosine 5’-Triphosphate
BBS	Bardet-Biedl syndrome
BCAP	Basal body Centriole-Associated Protein
C2CD3	C2 calcium dependent domain containing 3
CaM	Calmodulin
cAMP	Cyclic AMP
CANX	Calnexin
CCDC	Coiled-coil domain-containing protein
CDK	Cyclin-dependent kinase
cDNA	Complementary DNA
CEP	Centrosome protein
CFP	Cyan fluorescent proteins
CID	Collision-induced dissociation
CMA	Chaperones-mediated autophagy
CNAP	Chromosome Condensation-related SMC-associated Protein
COG	Clusters of Orthologous Groups of proteins
CO-IP	Co-immunoprecipitation
COP	Coatomer Protein
CPAP	Centrosomal P4.1-associated protein
CPC	Ciliary pore complexes
DAPI	4’,6-Diamidino-2-phenylindol
DMEM	Dulbeccos's Modified Eagle's Medium
DNA	Deoxyribonucleic Acid
dNTP	Deoxynucleotide triphosphates
Dr	*Danio rerio*/Zebrafish
E coli	*Escherichia coli*
EDTA	EDTA
EEF	Elongation factor
eGFP	Enhanced Green Fluorescent Protein
ER	Endoplasmic Reticulum
ERK	Extracellular-signal-regulated kinases
EST	Expressed sequence tag
FACS	Fluorescence-activated cell sorting
FGF	Fibroblast growth factor
FOP	FGFR1 Oncogene Partner
FOR20	FOP-related protein
FRET	Förster resonance energy transfer
GDP	Guanosine 5’-Diphosphate
GFP	Green Fluorescent Protein

GM130	Golgi Matrix 130 kDa (GOLGA2)
GMAP-210	Golgi Microtubule Associated Protein of 210 kDa
GPS	Group-based Prediction System
GSK	Glycogen synthase kinase
GTP	Guanosine 5'-Triphosphate
HDAC	Histone deacetylase
HEF	Human enhancer filamentation
HEK293T	Human embryonic kidney 293 cells, large T antigen
HPLC	High-performance liquid chromatography
HSP	Heat shock protein
hTERT	Human telomere reverse transcriptase
IFT	Intraflagellar Transport
IP	Immunoprecipitation
kb	kilobase
kDa	kilo Dalton
KIF	Kinesin-like protein
LAG	Lymphocyte-Activation Gene
LAMP	Lysosome-associated Membrane Protein
LB	Luria Bertani
LC-MS	Liquid chromatography–mass spectrometry
MAPK	Mitogen-activated protein kinases
MCD	Mucociliary differentiation
MKS	Meckel-Gruber syndrome
MS	Mass spectrometer
MT	Microtubule
MTOC	Microtubule organising centre
NLS	Nuclear localisation sequence
NPC	Nuclear pore complex
NPHP	Nephronophthisis
NPM	Nucleophosmin
Nubp	Nucleotide-binding protein
NUP	Nucleoporins
ODF2	Outer dense fiber protein 2
ODF2L	Outer dense fiber protein 2 like
OFD1	Oral-facial-digital syndrome 1 protein
PAGE	Polyacrylamide Gel Electrophoresis
PBS	Phosphate Buffered Saline
PCM	Pericentriolar material
PCNT	Pericentrin
PCP	Planer cell polarity
PCR	Polymerase Chain Reaction
Pifo	Pitchfork
PKA	Protein kinase A
PKC	Protein kinase C
PLK	Polo-like kinase
PMT	Post-transitional modifications

POC	Protein of Centriole
PTM	Post translation modifications
RA	Retinoic acid
RFP	Red fluorescent proteins
RNA	Ribonucleic acid
RPE1	Retina Pigment Epithelium 1
RPGR	Retinitis pigmentosis GTPase regulator
RPGRIP	RPGR-interacting protein
S.cerevisiae	*Saccharomyces cerevisiae*
SCLT1	Sodium channel and clathrin linker 1
SDS	Sodium Dodecyl Sulphate
Shh	Sonic hedgehog
SIM	SUMO-interacting motifs
siRNA	Small interfering RNA
SNARE	Soluble NSF attachment protein receptor
SSX2IP	Synovial Sarcoma, X Breakpoint 2 Interacting Protein
SUMO	Small ubiquitin-like modifiers
TE	Tris-EDTA
TGN	*trans*-Golgi network
TRAM	Translocation associated membrane protein
Tris	Trishydroxymethylaminomethane
TZ	Transition zone
VCP	Valosin-containing protein
VPS	Vacuolar protein sorting
WASP	Wiskott–Aldrich Syndrome protein
WB	Western blotting
YFP	Yellow fluorescent protein
Zf	Zebrafish
γ-TuRC	γ-tubulin ring complex

Chapter 1:

Centrosome, Cilia and Golgi Coalition

1.1 Introduction

Since its discovery 140 years ago (Flemming, 1875; van Beneden, 1876), the centrosome has been a puzzle in cell biology. Two main theories emerged regarding its function. Theodor Boveri, who introduced the name centrosome (Boveri, 1887; Boveri, 1900) hypothesised that the centrosome is a cellular organelle found closer to the nucleus with a functionally important role in cell division. In 1887 he stated in his short communication that the centrosome represents the dynamic centre of the cell and that its division creates the centres of the forming daughter cells around which all the other cellular components arrange themselves symmetrically (translated by Scheer, 2014). A second theory by Henneguy-Lenhossek (1898) argued that the centrosome and basal body were the same organelle located in two distinct sites, with the centrosome located at the cell centre near the nucleus, and the basal body existing at the base of the cilia at the plasma membrane. This was the earliest remark to highlight the important and functional relationship between the centrosome and cilia. Flemming even mentioned that the discovery of the centrosome was as important as the discovery of the nucleus (Flemming, 1891) yet research on the centrosome proved to be restrictive until the advancement of modern cell and molecular biology techniques. This slow progress of centrosome research was mainly because electron microscopy studies could not reveal the function of the centrosome (Schatten, 2008), although a greater number of early electron microscopy studies were able to describe the ultrastructural organisation of the centrosome. The structure of the centrosome from electron microscopy studies was described as loosely as amorphous osmiopholic material surrounding a well-structured centriole (Sathananthan *et al.*, 1991). These observations focussed the attention of the research community towards the centrioles but understanding the function of the centrosome was largely neglected and became less appreciated. However, the development of new antibodies and tagged proteins, coupled with the advances in immunofluorescent and other microscopy techniques, have greatly advanced research providing a deeper understanding of centrosome structure and function.

The centrosome is a subcellular non-membrane bound semi-conserved organelle, approximately 1 µm in size consisting of a pair of cylindrical centrioles orientated perpendicular to each other and surrounded by a proteinaceous scaffold containing a large number of centrosome proteins (Schatten, 2008) (Figure 1.1A,B). The centrioles are 0.1-0.5 µm long and 0.1-0.2 µm in diameter cylindrical structures composed of nine triplets of microtubules arranged to resemble a cartwheel (Preble *et al.*, 2000; Marshall, 2001; Dong, 2015). The protein scaffolding surrounding the centrioles is referred to as the pericentriolar material (PCM) (Bobinnec *et al.*, 1998; Woodruff *et al.*, 2014). The PCM lacks a defined boundary as the centrosome is not a membrane-bound organelle. The PCM consists of a large number of proteins including γ-tubulin and the γ-tubulin ring complexes (γ-TuRC) (Gunawardane *et al.*, 2000; Moritz *et al.*, 2000; Schiebel, 2000; Kollman *et al.*, 2011). The centrosome is the major microtubule anchoring site and provides a dynamic platform to anchor the microtubules at their minus ends (Bornens, 2002) allowing them to extend by the addition of tubulin to the plus end (McIntosh and Euteneuer, 1984). The centrosome is considered the cell's main microtubule organising centre (MTOC) and plays a pivotal role in numerous cell processes including intracellular trafficking, cell polarity, signal transduction and cell division (Nigg and Raff, 2009). The centrosome's three-dimensional architecture is maintained through special protein-protein interactions (Azimzadeh and Marshall, 2010) and the PCM is the main area of these transient interactions. The PCM also plays a pivotal role in duplication of the centrioles (Loncarek *et al.*, 2008) and formation of the cilia, hair-like projections from the cells (Moser *et al.*, 2010). At the onset of building the cilium, the centrosome migrates to the apical surface of the cell and docks to the membrane via the mother centriole, to start nucleating the microtubule-based cilium (Alieva and Vorobjev, 2004; Dawe *et al.*, 2007a; Satir and Christensen, 2007). In this context, centrioles are called basal bodies (Figure 1.1A) and become a major recruitment site for large numbers of proteins involved with the cilium and cell signalling (Michaud and Yoder, 2006; Singla and Reiter, 2006; Goetz and Anderson, 2010). In addition to these structures, early electron

microscopy studies identified electron-dense spherical granules of 70-100 nm in diameter, localised around the centrosome (Figure 1.1C,D) (Bernhard and de Harven, 1960; Theg, 1964; Berns *et al.*, 1977). These granules have been called massules (Bessis and Breton-Gorius, 1958) or satellites (Bernhard and de Harven, 1960). They were occasionally shown to be associated with microtubules radiating from centrosomes (Theg, 1964) and their number decreased and increased during mitosis and interphase, respectively (Rattner, 1992).

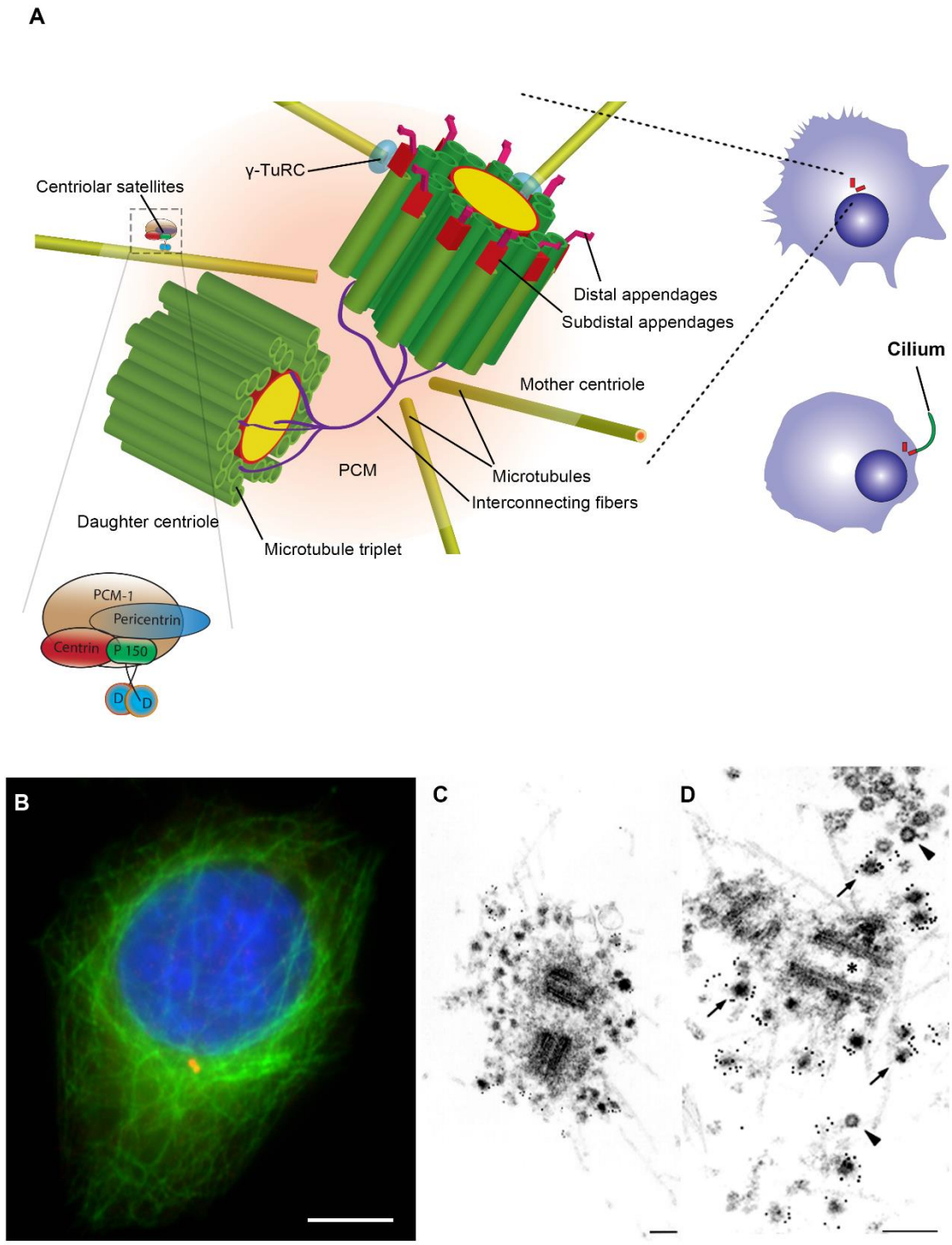

Figure 1-1 Illustration of the structural organisation of the vertebrate centrosome

The centrosome is the microtubule-organizing centre (MTOC) of most animal cells. **(A)** The centrosome is formed by two cylinder-shaped microtubule-based structures, the centrioles, which are surrounded by a protein matrix cloud, the pericentriolar material (PCM). Each centrosome is composed of a mature (mother) and an immature (daughter) centriole. While both centrioles are initially built around a 9-fold symmetric scaffold of microtubules, the cartwheel, only the mother centriole matures to form the distal and subdistal appendages. Distal appendages are required for centrioles to anchor at the plasma membrane when forming the cilium; in this context, the centrosome is known as the basal body, with the cilium extending from this. The PCM facilitates the anchoring of the microtubules to the centrosome via γ-Tubulin ring complexes (γ-TuRC). Microtubules provide the transport pathways for

the large protein complexes called satellites to deliver cargos to the centrioles. **(B)** Immunofluorescent image of a cell showing the location of the centrioles (red dots), with the microtubule cytoskeleton shown in green and the nucleus in blue. Scale bar 5 μm. **(C)** Electron micrograph of the centrosome. Scale bar 200 nm. **(D)** Higher power electron micrograph of the centrosome, showing centriolar satellites (arrows) organised around centrioles (asterisks). Microtubules are also visible (arrowheads). Black dots show gold immunostaining for PCM1. Scale bar 200 nm. Image credit: Christopher J Wilkinson, B; (Kubo *et al.*, 1999), C and D.

1.2 The Centrosome - structure and function

1.2.1 Centrioles

The centrioles are found in all eukaryotic species that form cilia or flagella but are absent from higher plants and from yeast. Therefore, it has been suggested that the evolution of centrioles coincides with the evolution of cilia (Marshall, 2009). In the G1 phase, cells contain two centrioles; the older centriole is termed as the mother centriole and the younger centriole is termed as the daughter centriole. In a proliferating cell, centrioles duplicate exactly once per cell cycle and each centriole's proximal area becomes the site of the assembly of the new procentriole.

Structurally, centrioles are made of nine triplets of microtubules where each triplet consists of a complete microtubule (the A-tube) onto which two additional partial microtubules are assembled (the B and C tubules respectively) to create a highly stable microtubule triplet structure (Figure 1.2A,B) (Azimzadeh and Marshall, 2010). This triplet microtubule structure is further stabilised by post-translational modification of α- and β- tubulin and by additional associated proteins (Bornens and Gonczy, 2014). Microtubules in the centrioles are also modified through detyrosination, acetylation and polyglutamylation to further stabilise the whole structure (Janke and Bulinski, 2011; Magiera and Janke, 2014; Song and Brady, 2015). As microtubule-based structures, centrioles are highly polarised with the microtubule minus ends positioned at the proximal end of the centriole (Figure 1.2A). The proximal microtubule region of the centrioles is also the site where new procentrioles are built using the cartwheel structure (Figure 1.2B).

1.2.1.1 Building the centriole

Procentrioles start forming perpendicularly to the existing centrioles around the G1/S transition. The biogenesis of centrioles requires at least five gene products in *Caenorhabditis elegans* and these components are evolutionarily conserved among species, although some species may need additional proteins for the biogenesis of centrioles (Strnad and Gonczy, 2008). The key players involved in centriolar biogenesis are PLK4 (also known as SAK in *Drosophila*), ZYG-1 in *C. elegans* (which is distinct from PLK4 but functionally homologous) and SAS-6 (Azimzadeh and Marshall, 2010).

The cartwheel structure of the centriole consists of a hub at the centre, with nine spokes radiating from the hub and pinheads at the end of the spokes that connect with the A-tubule of the microtubule triplets (Jana *et al.*, 2014) (Figure 1.2 B). The assembly of the cartwheel is regulated by Polo-like kinase 4 (PLK4), recruited to the proximal end of the mother centriole (Bettencourt-Dias *et al.*, 2005; Habedanck *et al.*, 2005). SAS-6 is essential for the formation of both the central hub and the radiating spokes of the cartwheel (Strnad and Gonczy, 2008; van Breugel *et al.*, 2011). Interestingly, SAS-6 is also shown to localise to the proximal region of the ciliary axoneme and to the basal body in mature medullary thymic epithelial (mTEC) cells, revealing the possible involvement with ciliary assembly or function (Vladar and Stearns, 2007). In *C. elegans*, recruitment of SAS-6 to the cartwheel is controlled by SAS-5 (Ana-2 is the possible *Drosophila* homologue), another key protein in centriolar duplication (Delattre *et al.*, 2004; Leidel *et al.*, 2005). In addition to those proteins, the assembly of the cartwheel is also dependent on conserved Cep135 (homologue of *Chlamydomanas* Bld10p), a recognised component of the cartwheel spoke (Matsuura *et al.*, 2004).

The assembly of the centriole microtubule triplet occurs sequentially. First, the A-tube is attached to the pinhead of the spoke in the cartwheel then the B- and C-tubules are added to create the triplets (Dippell, 1968; Guichard *et al.*, 2010). This attachment and elongation is

mediated by several other proteins including SAS-4 (also known as CPAP in humans), POC5, OFD1 and CP110 (Azimzadeh and Marshall, 2010). SAS-4 is thought to stabilise the microtubules by associating with γ-tubulin and therefore creating a nucleation site to extend the microtubules (Dammermann *et al.*, 2008; Schmidt *et al.*, 2009). Furthermore, SAS-4 depleted *C. elegans* embryos fail to attach microtubules, although the cartwheel structure was elongated and fully present, confirming its vital role in microtubule attachment (Pelletier *et al.*, 2006). Once the SAS-4 mediated centriolar elongation is initiated, CP110 localises to the distal end of the extending centriole and possibly functions as a cap to limit the microtubule extension (Schmidt *et al.*, 2009). Furthermore, recruitment of CP110 to centrioles is mediated by CEP97 and depletion of either of these proteins initiates ciliation in cycling RPE-1 cells (Spektor *et al.*, 2007). Conversely, overexpression of Cep97 or CP110 prevented centrioles from assembling cilia even after the induction of ciliation (Spektor *et al.*, 2007). Interestingly, in non-ciliating cell lines like U2OS or HeLa, depletion of CP110 and CEP97 induced the assembly of elongated structures resembling primary cilia (Spektor *et al.*, 2007) though later reported to be abnormally elongated centrioles (Schmidt *et al.*, 2009; Tang *et al.*, 2009). Therefore, these findings suggest that CEP97 and CP110 are required for controlling the length of the centrioles. SAS-4 (and human homologue CPAP) would promote elongation by favouring the tubulin incorporation at the plus end of the centriolar microtubules while CP110 capping would limit the growth of the microtubules.

Another human protein, OFD1 (mutated in Orofaciodigital syndrome 1) is also known to regulate centriolar length (Singla *et al.*, 2010). OFD1 has been localised to both the basal body and the stalk of the cilium (Romio *et al.*, 2004). In recent years, OFD1 has also been shown to be localised to the distal end of the centrioles (Singla *et al.*, 2010) and to centriolar satellites (Lopes *et al.*, 2011; Tang *et al.*, 2013). In OFD1-deficient cells, centrioles show excessive elongation and a defect in ciliogenesis (Ferrante *et al.*, 2006; Singla *et al.*, 2010). Finally, POC1, another protein conserved across species, may also regulate the elongation of centrioles (Keller *et al.*, 2009).

Although the cartwheel structure is required to assemble the 9-fold symmetry, it is not required to stabilise the centrioles once assembly is completed. Therefore, the cartwheel structure is dissembled once the centriolar maturation completes (Strnad *et al.*, 2007).

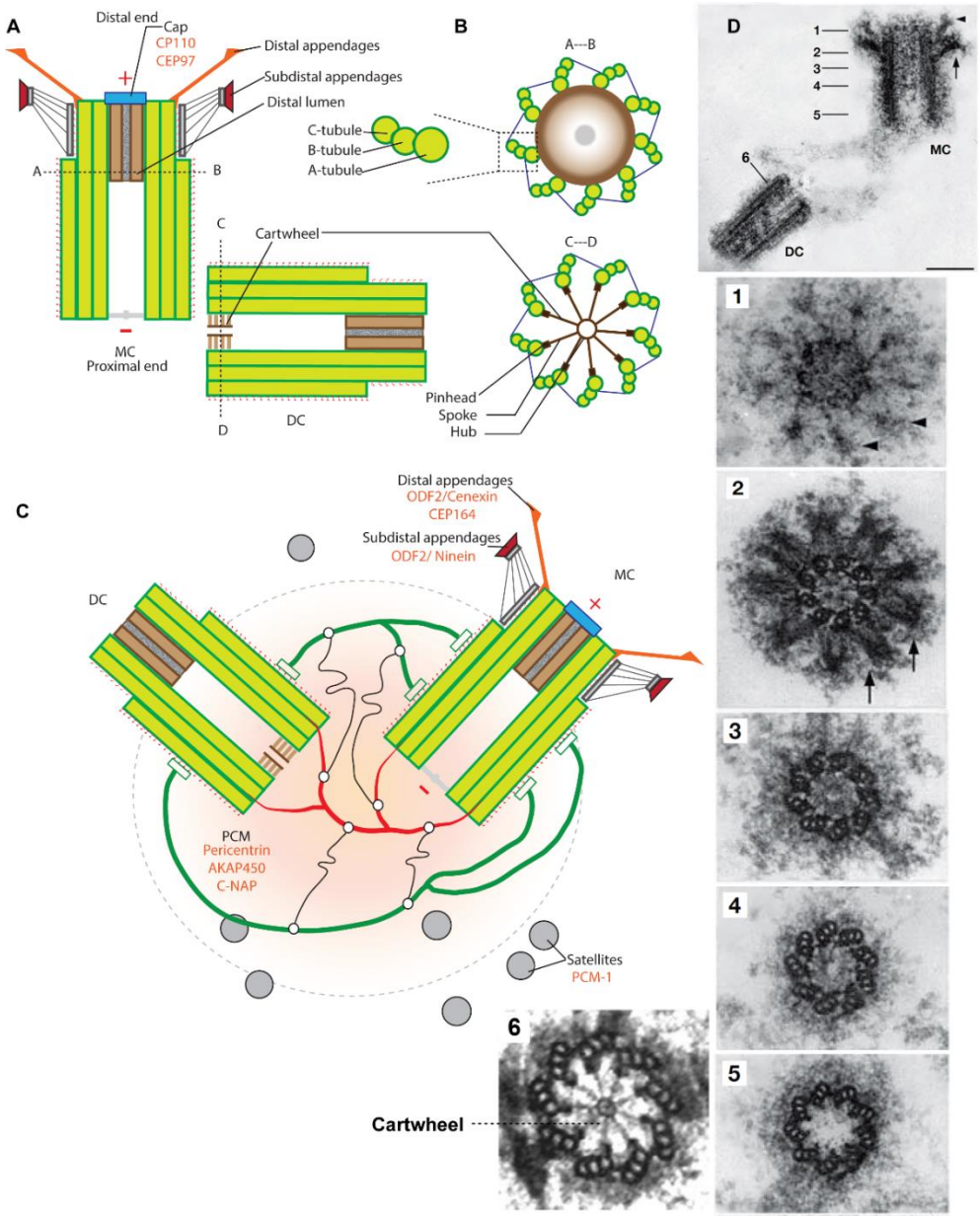

Figure 1-2 Schematic drawings and electron micrographs of the centriole organisation and structure

(A) Centrioles are microtubule arrays composed of nine triplets of microtubules organized around a cartwheel structure. The mother centriole looses its cartwheel structure after maturation. The mother centriole contains additional structures such as distal and subdistal appendages which consist of ODF2, CEP164 and Ninein. The distal end of the centrosome is capped by the CP110/CEP97 complex. **(B)** Cross section through **A-B** and **C-D** regions illustrating the microtubule triplet organisation. The triplets are connected to the cartwheel through the A-tubule, the first to assemble during centriole assembly and the only complete microtubule in a triplet. The B- and C-tubules are incomplete microtubules. **(C)** The centrosome from G1 cells is composed of a mother centriole (MC) and a daughter centriole (DC) linked by a matrix. Matrix assembly is thought to be triggered by centrioles through two subsets of microtubule-binding proteins. One (shown in red) is able to bind to the proximal end of the centrioles (the minus microtubule ends), while the other (shown in green) is able to bind to the centriole walls in a polyglutamylation-dependent manner (red dots). Other proteins (black) could interact and cross-link centriole-binding proteins and participate in the fully assembled matrix (dotted line). The satellite proteins (grey circles) shuttle other proteins in and out of the centrosome**. (D)** Electron micrographs of

the centrioles, with transverse sections at levels 1-6 shown below; images were adapted from (Paintrand *et al.*, 1992). Scale bar: 0.2 µm. A-C modified from (Bornens, 2002).

1.2.1.2 Building the distal end of the centriole and centriole maturation

Centriolar elongation also involves the assembly of the intra-luminal structures at the distal end of the centrioles. There is a great degree of variation among the species in composition of the ultrastructure of intra-luminal structures in mammals and other ciliating eukaryotes. The intra-luminal space is known to consist of centrin (Paoletti *et al.*, 1996; Geimer and Melkonian, 2005). Centrin is a calcium-binding protein related to calmodulin (CaM). However, the exact role of centrin within the centriole remain elusive. Centrin interacts with POC5 and co-immunoprecipitates with CP110 (Chen *et al.*, 2002; Azimzadeh *et al.*, 2009).

In vertebrates, the centrosome contains only one mature centriole that shows additional distal and sub-distal appendages named as the mother centriole (Figure 1.2 A). These distal and sub-distal appendages, whose distribution mirrors the ninefold symmetry of the centriole, are only added at the end of the cell cycle following the one in which the procentrioles emerged. The formation of the distal and sub-distal appendages marks the centriole maturation and takes 1.5 cell cycles to complete (Kobayashi and Dynlacht, 2011). Only the mother centriole can attach with the plasma membrane using the distal appendages, and initiate ciliogenesis (Ishikawa *et al.*, 2005). Once the mother centriole is docked to the plasma membrane it is referred to as the basal body (Bornens and Gonczy, 2014).

ODF2, initially isolated as a major component of the sperm tail fibre (Petersen *et al.*, 1999), is known to localise to distal appendages and is essential for the construction of the distal appendages (Ishikawa *et al.*, 2005). In mouse cells, removal of ODF2 resulted in centrioles without distal appendages which failed to anchor onto the plasma membrane and ciliogenesis

was inhibited (Ishikawa *et al.*, 2005). The sub-distal appendages are also thought to play a role in microtubule anchoring, and consist of ODF2 and Ninein (Ibi *et al.*, 2011).

More recently, a study conducted by Chang *et al*., (2013), elegantly demonstrated that only ODF2 isoform 9 (also known as cenexin-1 (Huber and Hoyer-Fender, 2007)) is localised to distal/sub-distal appendages and this isoform is also localised to the axonemes of primary cilia. Chang *et al*., (2013) also demonstrated that cenexin-1 is essential for ciliogenesis but not ODF2 and cenexin-1 functions independently of other ODF2 isoforms. They also proposed that multiple isoforms of ODF2 may have distinct and diverse roles in the cell and may function independently to each other. Furthermore, cenexin-1 can interact with GTP-bound RAB8A and mediate the correct localisation of Chibby (CBY1) to the basal body; both are essential for proper ciliogenesis (Chen and Megraw, 2013). CEP164 is also known to localise to distal appendages and depletion of this protein inhibits ciliogenesis in RPE-1 cells (Graser *et al.*, 2007). CEP83 (ccdc41), CEP89 (ccdc123), SCLT1 and FBF1 have also been identified as exclusive components of distal appendages, not present in sub-distal appendages (Tanos *et al.*, 2013). Interestingly, the finding that SCLT1 (sodium channel and clathrin linker 1) associates with distal appendages raises the possibility that centrioles may directly associate with clathrin-coated vesicles via SCLT1. CEP83 is also shown to be required for ciliogenesis and to partially localise with the Golgi complex (Joo *et al.*, 2013). Furthermore, CEP83 interacts with IFT20 (Failler *et al.*, 2014) which also localises to Golgi and cilia, therefore may mediate ciliary vesicle docking (Follit *et al.*, 2006). Recently, CEP164 has been shown to mediate ciliogenesis via regulating vesicular docking to the mother centriole (Schmidt *et al.*, 2012). C2CD3 (C2 calcium dependent domain containing 3) also localises to both the distal end of the centrioles and to the centriolar satellites and is required for recruitment of appendage proteins SCLT1, CEP83, CEP89, FDF1 and CEP164 (Ye *et al.*, 2014). Clearly, many proteins are involved in the function of the centriolar appendages.

1.2.2 Pericentriolar material (PCM)

The microtubule network in the cell is a dynamic network comprising of α/β tubulin polymers that facilitate transport of protein complexes, organelles and segregation of genetic material via the mitotic spindles (Nicklas *et al.*, 1982; Gadde and Heald, 2004). This microtubule network is assembled by the cell's MTOC. The centrosome consists of two structural elements: the centrioles and the pericentriolar material (PCM) (Figure 1.2C). The centrioles act as a primary scaffold to promote the organisation of the PCM. The PCM's primary function is to provide a structural scaffold for the microtubule network to anchor via γ-tubulin ring complexes (γ-TuRCs) (Kollman *et al.*, 2011). The PCM consists of a dynamic structure; during centriole maturation the PCM increases its size dramatically to increase the microtubule nucleating capacity via recruiting large number of γ-TuRCs from the cytosol. This is particularly important as a large number of astral and spindle microtubules are involved with spindle orientation and cytokinesis. The maturation process is orchestrated by PLK1 and Aurora A kinase activity and is essential for robust mitotic spindle assembly (Glover *et al.*, 1995; Barr *et al.*, 2004). The PCM also plays an essential part in centriolar duplication and ciliogenesis providing a protein matrix for signalling, docking, regulating and transporting proteins to and from the centrioles and cilia, using motor proteins and the microtubule network (Zimmerman and Doxsey, 2000).

The techniques to define the PCM structure were not available until recently. The limitation of the techniques and methodologies utilised previously did not provide enough resolution to understand the structural composition of the PCM (Woodruff *et al.*, 2014). The earliest electron micrographs depicting the centrosome described the PCM as a densely staining amorphous mass surrounding the centrioles (Robbins *et al.*, 1968). The later studies of the centrosome isolated from mammalian cells did little justice to resolve this "amorphous mass" but confirmed the origination of microtubules from the PCM (Gould and Borisy, 1977). The development of electron tomography and immunolabelling techniques in later years enabled enough resolution to get a glimpse into the structural organisation of the PCM (Moritz *et al.*, 2000). Also,

development of deconvolution microscopy, Förster resonance energy transfer (FRET), and subdiffraction-resolution techniques such as 3D structured-illumination microscopy (3DSIM), stochastic optical reconstruction microscopy (STORM), and stimulated emission depletion (STED) have been successfully employed to study protein interactions and structural organisation, taking advantage of the improved resolution (Woodruff *et al.*, 2014).

In recent years, there has been an increase in research into the PCM to identify the constituent molecules. One of the first PCM components to be identified was pericentrin (PCNT) as an essential protein involved in spindle organisation (Doxsey *et al.*, 1994). Now, there has been a number of additional PCM components identified, such as CEP120, CEP192/SPD-2, CDK5RAP2/Cnn, CEP152/Asterless, CG-NAP (AKAP450) and SPD-5 (Andersen *et al.*, 2003; Lawo *et al.*, 2012; Woodruff *et al.*, 2014). All these proteins share a coiled-coil domain in their structure and coiled-coil domains are known to mediate protein-protein interactions (Lupas *et al.*, 1991). Therefore, it has been proposed that these coiled-coil structures might be mediating a robust inter-molecular interaction to form the scaffolding structure in the PCM (Andersen *et al.*, 2003; Salisbury, 2003).

Although originally described as an amorphous mass, the PCM has recently been shown to be structurally organised. The PCM proteins are distributed in “concentric toroids” each of a discrete diameter around the centriole (Woodruff *et al.*, 2014). Human CDK5RAP2, CEP120, CEP192, and CEP152, and *Drosophila* Asterless and PCNT-like protein (D-PLP) form a highly ordered toroidal organisation around the proximal end of the centrioles in interphase (Lawo *et al.*, 2012). Lawo *et al*. (2012) have also shown that PCNT is anchored near the centriole through its C-terminus region and the N-terminus extends away from the centrioles and is required for the toroid organisation of other proteins. On the contrary, when the localisation of these proteins was studied during metaphase, no ordered structure and a minimal co-localisation between the proteins was observed (Lawo *et al.*, 2012). Therefore, these findings raise the

question of whether this ordered PCM structure is first assembled in interphase and then serves as the foundation to expand the PCM towards metaphase. In recent years, the historic view of PCM as the binding platform for γ-tubulin-containing complexes has been challenged. This is due to γ-tubulin complexes being poor microtubule nucleators *in vitro* (Kollman et al., 2015) and microtubule asters can also be formed in the absence of γ-tubulin complexes *in vitro* (Srayko *et al.*, 2005; Wiese and Zheng, 2006) by using other complexes such as tumor overexpressed genes (TOGs) (Gard and Kirschner, 1987), transforming acidic coiled coil proteins (TACC) (O'Brien *et al.*, 2005) and targeting protein for the *Xenopus* kinesin-like protein (TPX2) (Wittmann *et al.*, 2000) through yet unknown mechanisms (Wiese and Zheng, 2006). Historically, the PCM was studied in cells that do not possess a cilium and therefore these studies mostly focused on the centrosome-centriole-PCM relationship. The development of new techniques and expansion of understanding the organisation of the PCM have now been able to expand the understanding of the function PCM and its relationship with the basal body and the cilium. Due to the transient nature of the proteins associated with the PCM, such as pericentriolar satellite proteins, and the dynamic restructuring that happens during cell cycle progression, the PCM is an interesting area to study, particularly with regard to how the protein dynamics influence and regulate ciliogenesis.

1.2.3 Centriolar satellites

Centriolar satellite is a term used to describe the small, spherical granules that are clustered close to the centrosome (Kubo *et al.*, 1999). They are about 70-100 nm in diameter and can be seen as electron dense particles scattered around the centrosome in an electron micrograph and as small punctate structures by epifluorescence microscopy (Balczon *et al.*, 1994; Kubo *et al.*, 1999; Kubo and Tsukita, 2003) (Figure 1.1 and 1.2C). Interest in centriolar satellites has increased recently, as it's been reported that they are involved with several centrosome-related

functions including ciliogenesis, cell polarity, cell migration, microtubule organisation, and cell cycle progression.

When centriolar satellites were studied by live cell imaging, it became apparent that the satellites move along cytoskeletal microtubules in the minus end direction, towards the centrosome (Balczon *et al.*, 1999). Centriolar satellites are present in almost all mammalian cells; however, the molecular composition, size, and the localisation varies considerably. Furthermore, satellites only can be observed in the interphase of the cells and in mitosis, they rapidly disperse after cytokinesis and reform in interphase (Kubo and Tsukita, 2003).

PCM-1 was the first satellite protein to be discovered (Balczon *et al.*, 1994; Kubo *et al.*, 1999) and is considered to be a fundamental component of the satellites. Therefore, PCM-1 has become a standard marker for studying satellite organisation and function (Balczon and West, 1991; Balczon *et al.*, 1994; Kubo *et al.*, 1999; Kubo and Tsukita, 2003). Kubo et al. (1999) have also shown that the movement of PCM-1 is dependent on dynein, but not kinesin, and moves towards the centrosome along microtubules. Furthermore, loss of PCM-1 results in reduction and disorganisation of centrin, pericentrin, and ninein, suggesting that PCM-1 is involved with delivering proteins from the cytoplasm to the centrosome (Dammermann and Merdes, 2002). Therefore, at a functional level, PCM-1 is suggested to provide a scaffold for other proteins to interact with and to allow them to be transported. This notion of "transporter scaffold" especially becomes plausible when the domain organisation is considered; PCM-1 consists of 8 coiled-coil motifs, most of which are located close to the N-terminus. The coiled-coil motif is known to mediate protein-protein interactions and is commonly present in proteins that interact with a number of other proteins such as centrosome, Golgi, and transporter proteins (Lopes *et al.*, 2011; Wang *et al.*, 2013). To date, over 30 satellite proteins have been identified. A list of the identified satellite proteins and the references can be found in Table 1.1.

For the centrosome to conduct its different functions, proteins need to be present at the centrosome in a timely manner. The satellite proteins ensure the delivery of the required proteins to the centrosome, at the times they are needed, enabling the normal function of the centrosome (Barenz *et al.*, 2011). Another proposed satellite function is that it may provide a favourable environment for the proper folding of centrosome and ciliary proteins, regulating their biological activity before being transported to their final destinations (Hames *et al.*, 2005).

Dynein/dynactin-dependent satellite transport relies on the microtubule network to localise the cargos to the correct location. The association of dynein motors with satellites can be mediated by several satellite proteins such as BBS4, Par6α and CEP290 (Kim *et al.*, 2004; Kim *et al.*, 2008; Kodani *et al.*, 2010). BBS4 and CEP290 both interact with PCM-1 to act together in centriolar satellites for protein recruitment and microtubule organisation (Kim *et al.*, 2004). CEP290 was reported to be required for efficient recruitment of Rab8 to the primary cilium via a PCM-1 dependent pathway (Kim *et al.*, 2008). However, knocking down CEP290 also disrupted the organisation of the microtubule network and caused concentric aggregation of PCM-1 granules at the centrosome in RPE-1 cells (Kim *et al.*, 2008). Therefore, it is plausible that CEP290 is not required for centrosomal recruitment of PCM-1 but to regulate the plus end transport of PCM-1. This is supported by the evidence that CEP290 can interact with both dynein and kinesin motor machineries (Chang *et al.*, 2006; McEwen *et al.*, 2007); kinesin-based movement will carry PCM-1 back to the cytoplasm, as microtubule plus end transport is facilitated by kinesin motors. Indeed, overexpression of CEP290 resulted in dispersing PCM-1 back into the cytoplasm (Kim *et al.*, 2008). On the other hand, knockdown of BBS4 caused PCM-1 to disperse into the cytoplasm (Kim *et al.*, 2004) therefore, PCM-1's ability to interact with both CEP290 and BBS4 may mediate the coordination of PCM-1 movement (Kim *et al.*, 2008). OFD1, another satellite protein, has also been shown to associate with BBS4, CEP290 and PCM-1 (Lopes *et al.*, 2011). Depletion of OFD1 leads to complete disappearance of BBS4 and PCM-1 from the satellites and causes CEP290 to move from the satellites to the centrosome. Furthermore, disruption of PCM-1

increased the centrosomal localisation of several other satellite proteins such as CEP72 and CEP90 (Oshimori *et al.*, 2009; Kim *et al.*, 2012; Stowe *et al.*, 2012).

Hence, these data suggest that localisation of these proteins to centriolar satellites are mutually dependent on other satellite proteins. However, in some cases, it has been shown that localisation of some proteins to the satellites is independent of satellite proteins and may depend on other recruitment mechanisms such as LIS1 homology (LisH) or coiled-coil domain interactions found in non-satellite proteins to recruit them to the centrosome (Tollenaere *et al.*, 2015).

Satellite proteins	References
AZI1 (CEP131)	Chamling *et al.* (2014)
BBS4	Kim *et al.* (2004); Lopes *et al.* (2011)
C11orf49	Gupta *et al.* (2015)
C2CD3	Ye *et al.* (2014)
CCDC11	Silva *et al.* (2016)
CCDC112	Gupta *et al.* (2015)
CCDC13	Staples *et al.* (2014)
CCDC138	Gupta *et al.* (2015)
CCDC14	Firat-Karalar *et al.* (2014)
CCDC18	Gupta *et al.* (2015)
CCDC66	Gupta *et al.* (2015)
CDK1	Spalluto *et al.* (2013)
CEP126	Bonavita *et al.* (2014)
CEP290	Valente *et al.* (2006); Kim *et al.* (2008)
CEP350	Gupta *et al.* (2015)
CEP63	Firat-Karalar *et al.* (2014)
CEP72	Oshimori *et al.* (2009); Stowe *et al.* (2012)
CEP90	Kim and Rhee (2011)
FOP	Lee and Stearns (2013)
FOR20	Sedjai *et al.* (2010)
HAP1	Engelender *et al.* (1997)
HOOK3	Ge *et al.* (2010)
HTT	Keryer *et al.* (2011)
KIAA0753	Firat-Karalar *et al.* (2014)
LRRC49	Gupta *et al.* (2015)
MED4	Gupta *et al.* (2015)
MIB1	Akimov *et al.* (2011); Villumsen *et al.* (2013)
OFD1	Romio *et al.* (2003)
Para6α	Kodani *et al.* (2010)
PCM1	Kubo *et al.* (1999)
PIBF1	Gupta *et al.* (2015)
SDCCAG8	Insolera *et al.* (2014)
SSX2IP/MSD1	Barenz *et al.* (2013)
TBC1D31	Gupta *et al.* (2015)
TEX9	Gupta *et al.* (2015)
WDR8	Kurtulmus *et al.* (2016)

Table 1-1 Satellite proteins reported in the literature.

1.2.3.1 Centriolar satellites function in centriolar maturation, maintenance and mitosis.

Several satellite proteins such as CEP72, CEP90, CEP131 (also known as AZI1), SSX2IP and CCDC13 have been shown to associate with the spindle pole to maintain accurate chromosome segregation during mitosis (Staples *et al.*, 2012; Barenz *et al.*, 2013; Hori *et al.*, 2014; Staples *et al.*, 2014). CEP72 and CEP90 are required for maintaining spindle stability and chromosome alignment during metaphase through the recruitment of Kizuna and γ-tubulin (Oshimori *et al.*, 2009; Kim and Rhee, 2011). CEP11 and CCDC13 are required for the correct chromosome segregation and both proteins interact with PCM-1 to localise to satellites and to the centrosome (Staples *et al.*, 2012; Staples *et al.*, 2014).

At the onset of mitotic entry, these proteins are moved from satellites to the centrosome and this localisation change may ensure that an adequate protein concentration of components is present during the chromosome segregation process (Blagden and Glover, 2003). Perhaps, in this context, the localisation of centriolar satellites to the centrosome might serve as a temporary storage area during mitosis or may protect them from degradation or unwanted protein-protein interactions, perhaps through interaction with chaperones (Chamling *et al.*, 2014).

Centriolar satellites also play a role in centriole duplication and maturation. As previously mentioned, OFD1 can localise to the centrosome, basal body and cilium and is reported to control centriolar length and maturation (Singla *et al.*, 2010). Also, NEK2A, a cell cycle-regulated kinase is reported to interact with PCM-1 and this mediates the recruitment of NEK2A to the centrosome (Hames *et al.*, 2005). C2CD3, a centrosome maturation factor and essential protein for recruiting centriolar distal appendage proteins, also localises to centriolar satellites in a PCM-1 dependent manner (Ye *et al.*, 2014). In a recent study, a factor required for centriolar duplication, CEP63, was also shown to localise to centriolar satellites (Brown *et al.*, 2013). The targeting of CEP63 to the centrosome is dependent on its interacting partner, CEP152, and

influenced by CCDC14 and KIAA0753. CCDC14 and KIAA0753 both localise to centriolar satellites. Interaction of these proteins with CEP63 can limit the availability of CEP63 to interact with CEP152 therefore regulating centriole duplication (Firat-Karalar *et al.*, 2014).

1.2.3.2 Centriolar satellite involvement with ciliogenesis

Primary cilia are hair-like projections from the cell (as will be discussed in detail in section 1.3) and are responsible for a plethora of functions including sensing, signalling and defining left right symmetry in embryogenesis. The cilium is assembled from the mother centriole which in this context is known as the basal body. In recent years, centriolar satellites have been identified as one of the key regulators of ciliogenesis. As described previously, OFD1 and C2CD3 play important roles in recruiting proteins such as CEP164, TTBK2 to the distal appendages. Distal appendages are essential for centriolar docking to the plasma membrane at the onset of ciliogenesis. TTBK2 is crucial for the removal of CP110, which is an important prerequisite for ciliogenesis (Goetz *et al.*, 2012). One of the best ways to understand the satellites involvement with ciliogenesis is by studying the BBSome. The BBSome is a multi-protein complex localised to the ciliary transition zone. It consists of highly conserved seven core proteins (BBS1, BBS2, BBS4, BBS5, BBS7, BBS8 and BBS9) and a novel protein BBIP10 (Jin and Nachury, 2009). In humans, loss of any of these proteins results in the ciliopathic disease, Bardet-Biedl syndrome, in which loss of the cilia causes a range of characteristic phenotypes including polydactyly, polycystic kidneys and retinitis pigmentosa (Forsythe and Beales, 2013). The current assigned function for the BBSome is to extend microtubules from the base of the growing cilium to the cell periphery to recruit proteins to the growing cilium (Jin *et al.*, 2010). Assembly of the BBSome occurs in a highly hierarchical manner, with BBS4 being the last added component (Zhang *et al.*, 2012). The recruitment of BBSome to the ciliary base is mediated by BBS4. CEP290 interacts with CEP72 and both proteins can interact with BBS4 and disruption of these proteins disrupts the localisation

of BBS4 and therefore disrupts the recruitment of the BBSome to the ciliary base (Kim *et al.*, 2004; Kamiya *et al.*, 2008; Stowe *et al.*, 2012). Furthermore, PCM-1 and DISC1 also interact with BBS4 and are known to regulate the recruitment of BBSome to the ciliary base (Kamiya *et al.*, 2008; Soares *et al.*, 2011). In a recent study, CEP131 (AZI1) has also been recognised to interact with BBS4 (Chamling *et al.*, 2014). CEP131 not only binds with PCM-1 and BBS4, it can also inhibit the recruitment of BBS4 to the basal body. Knockdown of CEP131 causes BBS4 to accumulate and the BBSome to form at the ciliary transition zone (Chamling *et al.*, 2014). However, the mode of regulation of BBSome by CEP131 remains unclear.

Tang *el al*. (2013) discovered that OFD1 negatively regulates ciliogenesis. OFD1 not only localises to centriolar satellites but also to centrioles and it has been suggested to play a role in centriolar maintenance and cilia assembly (Romio *et al.*, 2004; Singla *et al.*, 2010; Lopes *et al.*, 2011). OFD1 is associated with ciliopathic diseases such as oral-facial-digital syndrome, Joubert syndrome and nephronophthisis-related disease (Lopes *et al.*, 2011). It is known to facilitate the membrane docking of the centrosome at the onset of ciliogenesis and recruitment of IFT88 to the distal appendages of the centriole. In OFD1-deficient cells, the centrioles show excessive elongation and failure to properly assemble the distal appendages, which leads to defects in attachment of the mother centrioles to the membrane when ciliation is initiated and defects in primary cilia formation (Ferrante *et al.*, 2006). OFD1 is localised to the centrioles and to centriolar satellites in cycling RPE-1 cells however, in quiescent RPE-1 cells, OFD1 localisation to the satellites is dramatically reduced upon ciliation (Tang *et al.*, 2013). Indeed, Tang *el al*. (2013) demonstrated that removal of OFD1 from satellites through an autophagy pathway encourages ciliogenesis in contrast to the inhibition of ciliogenesis when OFD1 is removed from the centrosome. Therefore, Tang and colleagues concluded that the two populations of OFD1 regulate ciliogenesis independently; the centrosomal pool is positively regulating ciliation by assisting the docking of the centrosome to the membrane whereas the satellite pool acts to negatively regulate ciliation by affecting BBS4 localisation to the centrioles. The knowledge on centriolar

satellite involvement in ciliogenesis is rapidly expanding. The other centriolar satellite protein such as SSX2IP, CCDC13, FOP, FOR20 have also been implicated in ciliogenesis however, their exact molecular mechanism involved in ciliogenesis is yet to be discovered (Sedjai *et al.*, 2010; Lee and Stearns, 2013; Staples *et al.*, 2014).

1.3 Structure and function of cilia

Cilia are membrane bound, centriole-derived, microtubule-containing hair-like projections from the surface of most eukaryotic cells (Figure 1.3). The occurrence of cilia within all major eukaryotes and evolutionary conservation of the core ciliary proteins indicate that the last common eukaryotic ancestor already had sophisticated motile and sensory cilia (Hodges *et al.*, 2010). Although initially studied for their role in motility, it is now known that they serve as a complex signalling centre that performs a diverse sensory function in both unicellular and multicellular organisms (Duldulao *et al.*, 2010; Oh and Katsanis, 2012). Much of the structural understanding of the ciliary components comes from the studies and observations made from flagella isolated from a green alga *Chlamydomonas* (Dutcher, 1995). The major part of the cilium is the axoneme which nucleates out from the mother centriole, which becomes termed as the basal body in this context; the mother centriole and basal body are structurally similar apart from having additional proteins recruited to assemble the structures required for docking to the plasma membrane, such as transition fibres, basal feet, and the ciliary rootlet during the onset of cilium formation (Marshall, 2008; Kobayashi and Dynlacht, 2011). Transition fibers and basal feet are ultrastructurally similar to distal and subdistal appendages, respectively. Transition fibers are believed to aid the anchoring of the basal body to the membrane in the transition zone (Anderson, 1972). The rootlet extends from the proximal end of the basal body into the cytoplasm, providing the structural support for the cilium extending from the distal end of the basal body (Tachi *et al.*, 1974). The cilium axoneme is comprised of nine peripheral fused pairs

of microtubules surrounding a central pair of microtubules; this is termed the "9+2" axoneme organisation. The doublets consist of α/β tubulin heterodimers with the fast polymerising plus end at the distal ciliary tip. Some cilia lack the central pair of microtubules and are deemed to have the "9+0" organisation. Eukaryotic cilia and flagella come in various forms, and are often classified by whether they have a 9+2 or 9+0 axoneme organisation, but another way is to classify by the presence or absence of motility (Figure 1.3; (Leigh *et al.*, 2009). The 9+2 cilia also contain radial spokes, and outer and inner dynein arms attached to microtubules; the presence of the dynein arms confers the ability to move to these cilia.

The general consensus is that 9+2 structures are motile and 9+0 structures are non-motile but there are some cilia found in eukaryotes which do not follow this rule. For instance, non-motile 9+2 cilia can be found in some sensory receptors, such as in the mammalian olfactory epithelium and hair cells of the vestibular apparatus in some vertebrates. Conversely, while most of the 9+0 vertebrate cilia are non-motile, the 9+0 cilia found in the embryonic node are motile; this is due to the additional dynein arms present in the axoneme in these cilia (Leigh *et al.*, 2009). In the early days of cilia studies, much of the attention was given to the motile cilia but in recent years the attention has been shifted towards what was once thought of as a vestigial organ, the primary cilium. The primary cilium is non-motile with the 9+0 axoneme organisation. The primary cilium has now been established as an important cell signalling centre which acts by regulating intracellular Ca^{+2} levels and has a key role in Hedgehog (Hh), planer cell polarity (PCP), Wnt and PDGFR-α signalling pathways (Singla and Reiter, 2006; Goetz and Anderson, 2010; Pan *et al.*, 2013).

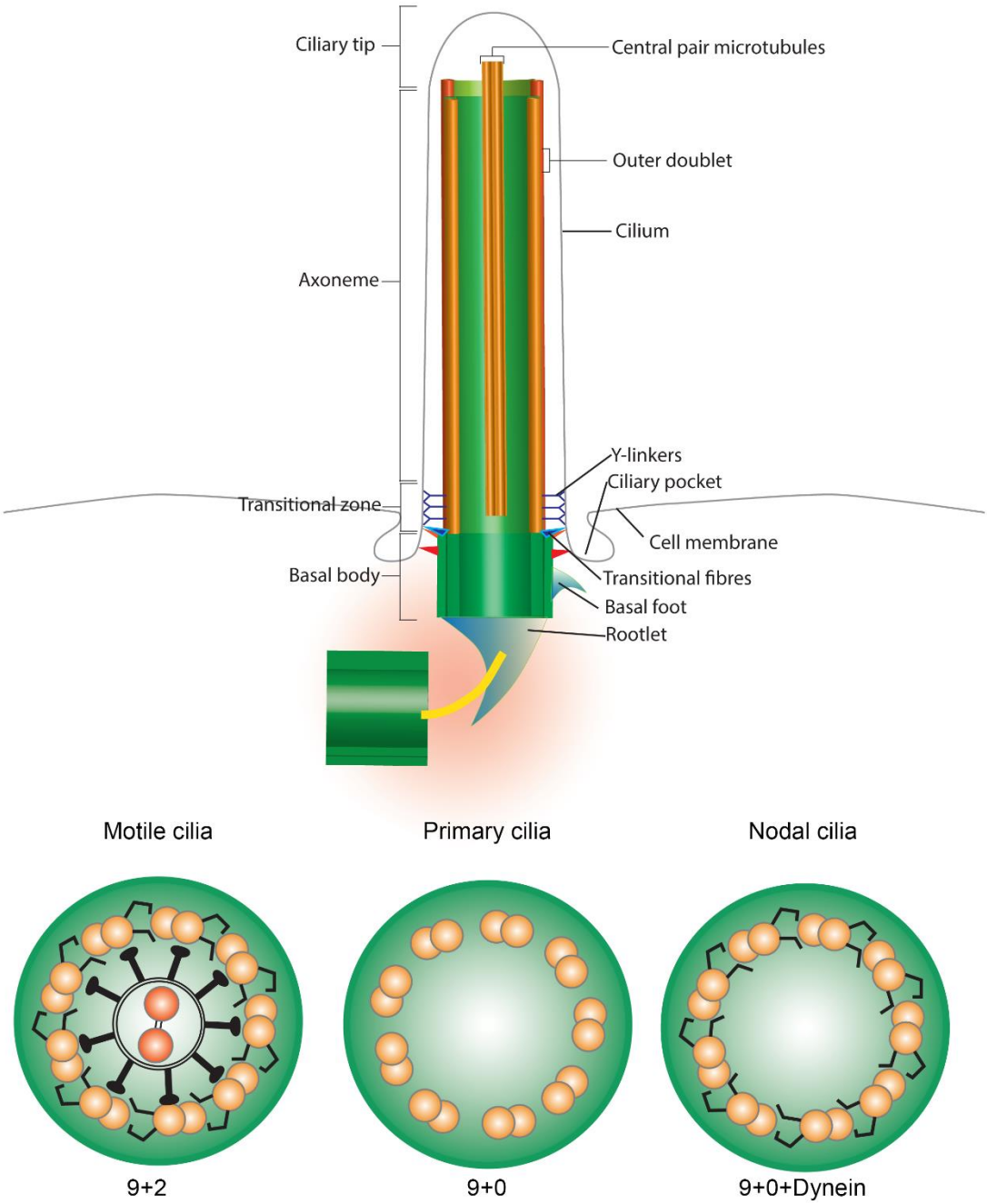

Figure 1-3 Schematic diagram of the structural organisation of the vertebrate cilium.

Cilia are tethered to the apical surface of the cell at the basal body, surrounded by pericentriolar material. Nine radially organized microtubule triplets protrude from the basal body to the transition zone, and then extend as microtubule doublets in the ciliary axoneme. Bottom illustrations show the structural differences in the different type of cilia present in vertebrates; motile cilia consist of 9+2 axoneme organisation whereas primary cilia completely lack the central pair and the dynein arms rendering them immotile. Nodal cilia found in the embryonic node lack the central pair of microtubules however, contains the dynein arms making them motile.

The assembly and maintenance of the cilium is tightly regulated by a number of proteins and is synchronised with cell cycle regulation. Therefore, genetic disorders that alter the proteins associated with the centrosome, basal body, or cilia result in functionally or structurally compromised cilia that can profoundly affect cellular homeostasis (Waters and Beales, 2011). In recent years, a growing number of cilia-associated diseases have been identified, and are collectively named as ciliopathies (Adams *et al.*, 2008). These diseases are characterised by phenotypes that range from organ-specific defects, such as in polycystic kidney disease, to pleiotropic effects as is the case in Bardet-Biedl syndrome (BBS), Meckel-Gruber syndrome (MKS) and Joubert syndrome (Waters and Beales, 2011). Ciliopathies include cystic diseases of the kidney, liver and pancreas, as well as some neural tube defects, postaxial polydactyly, nephronophthisis (NPHP), Oral-facial-digital syndrome 1 (OFD1), situs inversus, and retinal degeneration (Adams *et al.*, 2007; Bujakowska *et al.*, 2017). In recent years, ciliary defects have also been implicated in cancer and obesity (Mukhopadhyay and Jackson, 2013; Vaisse *et al.*, 2017). A list of ciliopathies is given in Table 1.2.

Condition/Defects	**Gene(s)**	**Systems/ organs**
Pleiotropic conditions associated with ciliary dysfunction		
Alstrom syndrome	*ALMS1*	Eye, Ear, Heart, Brain
Bardet-Biedl syndrome	*BBS1, BBS2, ARL6, BBS4, BBS5, MKKS, BBS7, TTC8, BBS9, BBS10, TRIM32, BBS12, CEP290, BBS15*	Eye, Brain, Bone, Kidney
Joubert syndrome	*INPP5E, TMEM216, AHI1, NPHP1, CEP290, TMEM 67, RPGRIP1L, ARL13B, CC2D2A, BRCC3*	Liver, Heart, Bone
Meckel-Gruber syndrome	*MKS1, TMEM67, TMEM216, CEP290, RPGRIP1L, C C2D2A*	Eye, Kidney
Senior-Loken syndrome	*NPHP1, NPHP4, IQCB1, CEP290, SDCCAG8*	Bone, Kidney
Orofaciodigital syndrome	*OFD1*	Brain, Bone, Kidney
Leber's congenital amaurosis	*LCA5,GUGY2D, RPE65, SPATA7, AIPL1, RPGRIPL1, CRX, CRB1, IMPD1, RD3, CEP290, NPHP5, RDH12*	Eye
Jeune asphyxiating thoracic dystrophy	*IFT80*	Bone, Lungs, Eye, Kidney
Ellis van Creveld syndrome	*EVC1, EVC2*	Heart, Bone
Sensenbrenner syndrome	*IFT122, WDR35*	Bone, Kidney
Primary ciliary dyskinesia (Kartagener syndrome)	*DNAI1, DNAH5, TXNDC3, DNAH11, DNAI2, KTU, R SPH4A, RSPH9, LRRC50*	Lungs, Ear
Organ-specific conditions associated with ciliary dysfunction		
Polycystic kidney disease (ADPKD and ARPKD)	*PKD1, PKD2, PKHD1*	Kidney
Nephronophthisis (NPHP)	*NPHP1–NPHP11, NPHP1L, SDCCAG8*	Kidney
Retinal dystrophy	*ALMS1, AHI1, CEP290,ARL6, MAK, RP1, RP2, TOPORS, RP1L1, BBS4, LCA5, MYO7A, TMEM67, TTC8*	Eye
Situs inversus/Isomerism	*DNAI1, DNAH5, TXNDC3, DNAH11, DNAI2, KTU, R SPH4A, RSPH9, LRRC50*	Heart

Table 1-2 Ciliopathies in human patients with the associated genes and showing the organs affected.

The cilium consists of the axoneme extending from the basal body. The basal body is anchored to the cell surface by the basal foot (Figure 1.3). Between the basal body and the cilium lies the "ciliary gate", an evolutionary conserved ciliary sub-domain structurally characterised by

transitional fibres and the transition zone (Figure 1.3, 1.4) (Omran, 2010). The ciliary gate can be identified at the very early onset of ciliogenesis with electron microscopy but the actual function has remained elusive until recent years (Omran, 2010; Williams *et al.*, 2011). In motile cilia, the boundary between the axoneme and the transition zone is known as the basal plate and this has been identified as the zone that takes part in the nucleation of the central pair of microtubules (Gilula and Satir, 1972). The microtubule arrangement in the basal body and transition zone is different to that of the axoneme, in that each microtubule doublet in fact contains a third microtubule member (Figure 1.4A). The outermost microtubule component of each triplet in the basal body extends only to the transition zone of the ciliary gate.

Transitional fibres emerge from the distal appendages on B tubes of the basal body microtubule triplets and form a "pinwheel-like" structure on TEM cross-sections (Figure 1.4 B, G). In mammals, the pinwheel structure consists of CEP164, OFD1 and other distal centriolar components such as POC5 (Azimzadeh and Marshall, 2010). In recent years, some additional components such as CCDC123 (CEP89), SCLT1, and FBF1 (Fas binding factor 1) have also been identified to co-localise to the distal appendages which are essential for recruiting CEP164 to distal appendages to form the transitional fibres (Jana *et al.*, 2014). Failure to recruit any of these proteins impairs the recruitment of TTBK2 and impairs the removal of the capping protein CP110 from the basal body (Oda *et al.*, 2014). In fact, removal of CP110 is essential for initiating microtubule extension and, therefore, leads the way for building the axonemal structure. Indeed, CP110 and its stabilising protein CEP97 are removed from maternal centrioles before the ciliogenesis commences (Schmidt *et al.*, 2009).

Additionally, CP110 has been demonstrated to interact with human ciliopathic protein CEP290 (also known as BBS14, NPHP6, MKS4, LCA10) and Rab8a (Tsang *et al.*, 2008). CEP290 localises to the distal region of the basal body, ciliary transition zone and to centriolar satellites and is attributed to the migration and anchoring of the basal body to the plasma membrane during the

early stages of ciliogenesis (Craige *et al.*, 2010). The depletion of CEP290 prevents ciliation in cells without compromising centrosome function (Tsang *et al.*, 2008). The protein expression level of CEP290 remains relatively constant during the cell cycle (Tsang *et al.*, 2008) but it is thought that CP110 restrains the activity of CEP290 through direct protein-protein interaction; once the cell enters to quiescent state to undergo ciliogenesis, CP110 is thought to release CEP290 from inhibition (Tsang *et al.*, 2008). However, the exact mechanism of these proteins' interplay in ciliation is not clear. CEP104, a microtubule plus-end tracking protein also interacts with both CEP97 and CP110 as shown by co-immunoprecipitation (Jiang *et al.*, 2012) and also localises to the distal end of centrioles (Jiang *et al.*, 2012; Satish Tammana *et al.*, 2013). CEP104 is an essential protein for ciliogenesis, suggesting it may be involved with axonemal growth in the beginning of ciliogenesis by counteracting the activities of CEP97 and CP110. KIF24, a kinesin family member, also interacts with CEP97 and CP110 and appears to reinforce the role of CP110 as a negative regulator of ciliogenesis; depletion of KIF24 promotes ciliation whereas overexpression inhibits ciliogenesis (Kobayashi *et al.*, 2011). KIF24 normally localises with CP110 therefore, KIF24 is capable of depolymerising the centriolar microtubules and inhibiting the axoneme growth (Kobayashi *et al.*, 2011). At the onset of ciliogenesis, the abundance of KIF24 around the centrioles dramatically reduces to facilitate the axoneme growth by polymerising tubulin (Schmidt *et al.*, 2009; Kobayashi *et al.*, 2011).

The distal appendages have been proposed to facilitate the anchoring of the centriole onto the cell membrane through the formation of the pinwheel like transition fibre structure (Figure 1.4B) observed in electron microscopy analysis (Anderson, 1972). It has also been suggested that distal appendages form a part of the ciliary gate or "ciliary pore complex" working with the septin ring barrier (Hu *et al.*, 2010), nucleoporins (Kee *et al.*, 2012) and ciliary transition zone (Chih *et al.*, 2012) to target ciliary cargo into and out of the cilium.

In the ciliary gate lies the transition zone, an evolutionary conserved subdomain immediately distal to the transition fibres (Figure 1.4A). The transition zone is characterised by distinctive Y-shaped fibres that connect the doublet microtubules of the axoneme to the ciliary membrane and the ciliary necklace (Figure 1.4C). The ciliary necklace is a specialised structure (effectively a modified membrane) that consists of several parallel strands of intra membrane particles which are species- and cell-specific (Figure 1.4C, H). However, the exact composition of the necklace and the structural organisation are still unknown. Few proteins have been identified to localise to the transition zone during ciliogenesis. CEP290/NPHP6 in *Chlamydomonas* (Craige *et al.*, 2010), RPGRIP1L in *C. elegans* (Fisch and Dupuis-Williams, 2011), and mammalian TMEM237 (Huang *et al.*, 2011) have been shown to localise to the ciliary transition zone and may be components of the Y-shaped fibres.

The distal end of the cilium is known as the ciliary tip and is the site of axonemal growth and reabsorption. It is thought to be the main point of regulating and remodelling by intra-flagellar transport (IFT) proteins. IFTs are microtubule dependent bidirectional transport proteins responsible for moving large protein cargo complexes along the axoneme and play an essential role in building and maintaining the cilium (Fisch and Dupuis-Williams, 2011). In primary cilia, the ciliary tip consists of an electron-dense plug; however, the composition and the actual function remains a mystery.

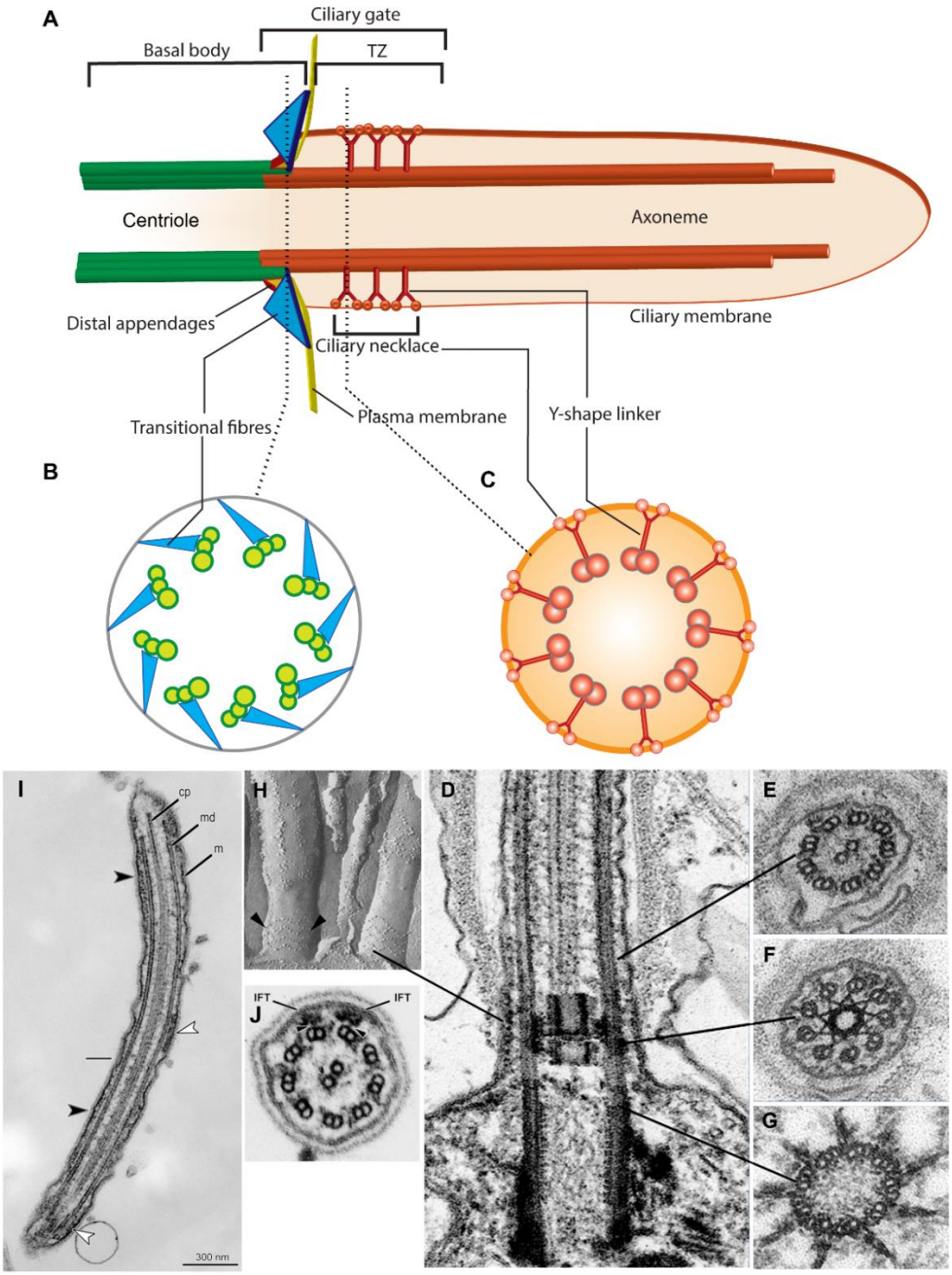

Figure 1-4 Ultrastructure of the cilium and transition zone.

(**A**) Illustration of the longitudinal structure of the cilium, showing the relationship between the basal body, ciliary gate and axoneme. The transitional fibres, transition zone (TZ) and ciliary necklace organisation form the ciliary gate. (**B**) Transverse section through the ciliary gate at the level of the transitional fibres. Microtubules exist in a triplet arrangement, and transitional fibres form a pinwheel arrangement extending from the B tubules of each triplet. (**C**) Transverse section through the ciliary gate at the level of the ciliary necklace. The ciliary necklace is a modified plasma membrane (shown as beads) and Y-shaped fibres link the ciliary necklace to the microtubules. (D) Longitudinal transmission electron micrograph (TEM) through the basal body and the cilium of *Paramecium* showing the continuity between the basal body and the ciliary microtubule. (**E-G**) Tranverse section TEMs through the basal body and cilium at the levels shown in **(D**). Sections demonstrate the 9+2 arrangement of microtubules in the axoneme **(E),** the more complex arrangement of structures in the transition zone

(F) and the ciliary gate complex with the pinwheel arrangement of transitional fibres (G). (**H**) Freeze-fracture of the *Elliptio* cilia showing the ciliary necklace with rows of membrane beads (arrowheads). (I & J) Longitudinally and transverse sections of *C. reinhardtii* flagellum showing the IFT particles (white and black arrows). CP: central pair of microtubules; md: microtubule doublet; m: flagellar membrane. Image credits: D-G adapted from (Beisson and Wright, 2003), H adapted from (Gilula and Satir, 1972), I and J from (Pigino *et al.*, 2009).

1.3.1 Early ciliogenesis

Building a primary cilium is tightly linked to the cell cycle and occurs from the distal end of the mother centriole as cells enter growth arrest/G1 phase (Pan and Snell, 2007). Early electron microscopy studies described three distinct early stages of primary cilium assembly (Sorokin, 1962). First, a Golgi-derived vesicle attaches to the distal end of the mother centriole, from which the axoneme begins to extend. Then, the vesicle invaginates as the axoneme extends and accumulation of accessory structures around the mother centriole occurs for it to become the basal body (Figure 1.5). Secondly, nearby secondary vesicles fuse with the new membrane forming at the ciliary base to create a sheath surrounding the elongating axonemal shaft. Finally, the membrane bound axoneme migrates to the plasma membrane (Figure 1.5) and the ciliary membrane fuses with the plasma membrane to form a cup-like structure called the ciliary pocket surrounded by the ciliary necklace (Gilula and Satir, 1972). The initiation of ciliogenesis occurs close to the Golgi apparatus and to the nucleus and is regulated by vesicular trafficking from the Golgi apparatus.

Although some of the recruitment and structural components of the early ciliary vesicle-basal body structure have been identified, the exact mechanisms of the ciliary vesicle targeting the mother centriole is unknown. In recent years, studies identified small GTPases, Rab8a and Rabin8, to localise to the membrane of the ciliary vesicle and potentially mediate its transport from the Golgi apparatus to the mother centriole (Nachury *et al.*, 2007; Westlake *et al.*, 2011). Rabin8 is a downstream effector of the GTP-bound Rab11, which regulates vesicle transport

from the trans-Golgi network (TGN), post-Golgi vesicle and recycling endosomes (Welz et al., 2014), implicating a Rab11-Rabin8-Rab8 based pathway in ciliary vesicle formation during cilium assembly (Knodler *et al.*, 2010; Westlake *et al.*, 2011). Moreover, Rabin8 interacts with the trafficking protein particle complex TRAPPII, which regulates intra-Golgi transport through vesicle tethering and together, this complex targets Rab11-Rabin8 to the basal body (Hutagalung and Novick, 2011). The localisation of Rab8a to the basal body is also regulated by Sorting Nexin 10 (SNX10) (Dixon-Salazar *et al.*, 2004), V-ATPase (Chen *et al.*, 2012) and Ahi1 (Jouberin) which is disrupted in Joubert Syndrome (Dixon-Salazar *et al.*, 2004). The activated Rab8 and Rab11 recruit Sec15, a component of actin-based motor protein Myosin. Sec15 is also a component of an exocytosis complex which contains eight subunits (Sec3, Sec5, Sec6, Sce8, Sec10, Exo70, and Exo84) in *S. cerevisiae* and in mammalian cells. This complex is required for constitutive secretion and for polarised exocytosis (TerBush *et al.*, 1996; Kee *et al.*, 1997). Therefore, recruitment of Sec15 may participate in tethering and transporting of the exocytic vesicle (Das and Guo, 2011). Another GTPase-GEF pair implicated for ciliogenesis is CDC42-TUBA which, interacts with the exocytic complex and is required for its localisation to primary cilia (Zuo *et al.*, 2011). It has also been proposed that specific SNARE (Soluble N-ethylmaleimide-sensitive factor activating protein receptor) proteins, such as syntaxin 3 and SNAP-25, might be involved with ciliary membrane expansion by vesicular fusion on a Rab8-dependent manner especially in photoreceptor cells (Mazelova *et al.*, 2009). All the above data suggest that the process of ciliary vesicle formation, fusion and tethering may be governed by the exocytic pathway. However, further studies are needed to ascertain how the subsequent stages are controlled in ciliogenesis.

Following the fusion of the ciliary vesicle with the distal appendages of the mother centriole, although in most cases this leads to cilia formation by causing association of the centriole and membrane-bound axoneme with the plasma membrane, this does not always happen. The migration to the plasma membrane seems to be governed by re-arrangement of the actin

cytoskeleton and membrane-associated components of the transition zone such as MKS1 and MKS3 (Lemullois *et al.*, 1988; Dawe *et al.*, 2007b; Dawe *et al.*, 2009). Filamentous actin (F-actin) forms branched F-actin and stress fibres (Chhabra and Higgs, 2007). Branched F-actin is nucleated by the ARP2/3 complex and becomes distributed mainly in the cell cortex (also known as the actin cortex or actomyosin cortex) located on the inner face of the plasma membrane. The actin-severing factor Gelsolin and nucleator ARP2/3 complex were implicated recently as positive and negative regulators of ciliogenesis respectively (Kim *et al.*, 2010). The actin cortex is also involved in the formation of lamellipodia at the leading edge of migrating cells, as well as being involved with vesicle sorting and trafficking (Goley and Welch, 2006). Yan and Zhu (2013) have shown that formation of branched F-actin negatively regulates ciliogenesis and that when cells are treated with cytochalasin D, an F-actin destabiliser, this provoked ciliogenesis in cells within 1-2 h (Bershteyn *et al.*, 2010; Kim *et al.*, 2010; Sharma *et al.*, 2011; Cao *et al.*, 2012). Breakup of the branched F-actin cortex seems to be required to allow the fusion of the membrane-bound axoneme with the plasma membrane.

Furthermore, inhibition of branched F-actin also resulted in longer cilia implying that cilia formation is promoted through the inhibition of certain types of F-actin. Actin-binding proteins also may regulate cilium length. For example, monomeric globular actin (G-actin) binding protein, MIM, promotes ciliogenesis by antagonising cortactin phosphorylation by a Src-dependent pathway (Bershteyn *et al.*, 2010). Cortactin is a class II nucleation-promoting factor (NPF) of the ARP2/3 complex and promotes formation of branched F-actin by associating with class I NPFs such as WASP family proteins (Goley and Welch, 2006). Therefore, active cortactin can promote actin polymerisation and branching which inhibits ciliogenesis. Several other actin dynamic modifiers such as ARP3 have also been implicated in ciliogenesis and cilium length control. In RPE-1 cells, when ARP3, a component of ARP2/3 was downregulated, ciliogenesis was promoted and caused cilium length to increase (Kim *et al.*, 2010). Furthermore, depletion of actin-severing proteins such as GSN and AVIL also resulted in decreased cilium numbers.

Branched F-actins appear to regulate ciliogenesis by modulating membrane trafficking. These observations suggest that branched actins inhibit ciliogenesis and restrict the cilium elongation however the exact mechanism of this is obscure.

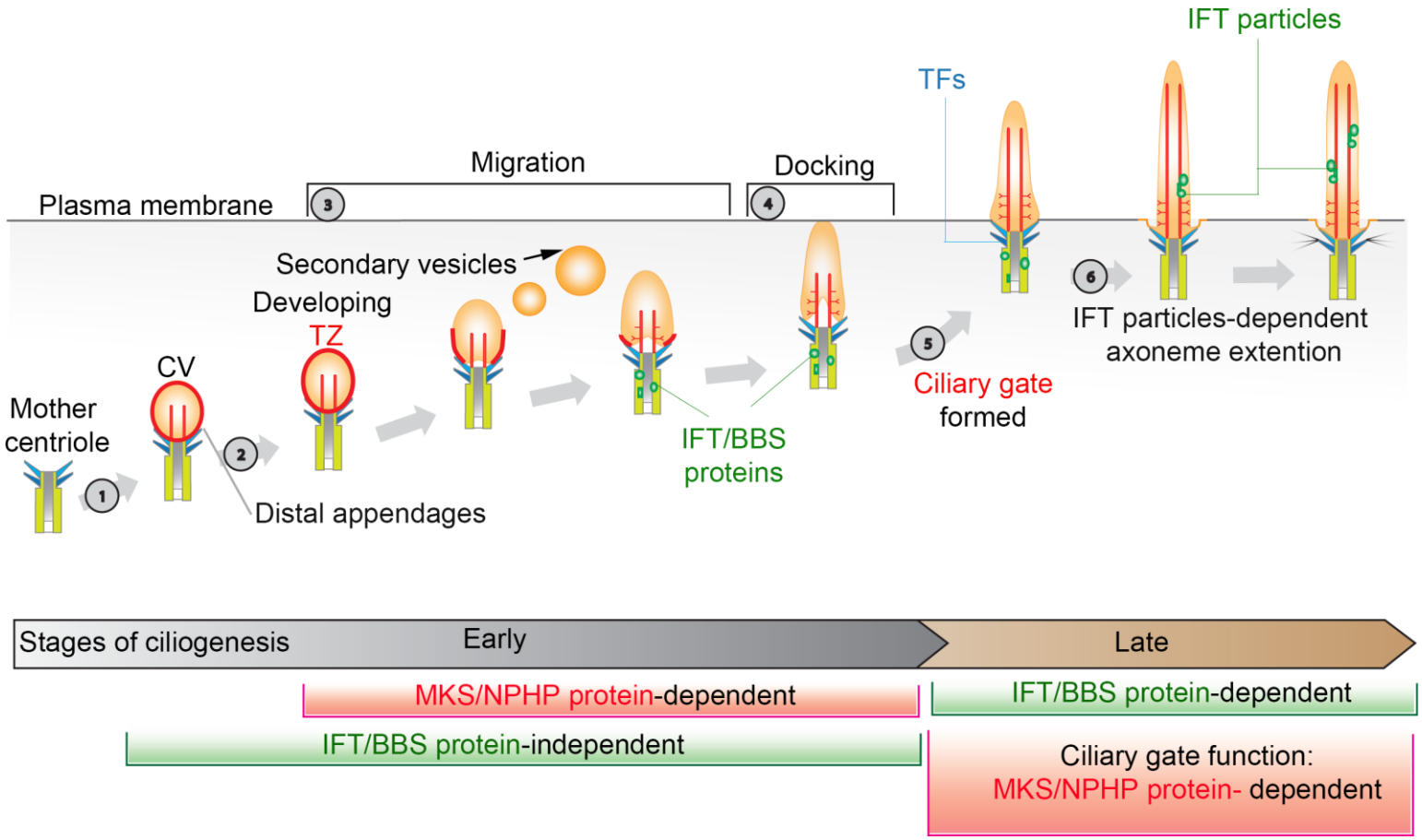

Figure 1-5 Illustration of primary cilium formation.

In many mammalian cell types, the first ciliogenic event involves the binding of a ciliary vesicle (CV) to the distal end of the mother centriole, probably through distal appendages (1). The initial CV fusion creates the transition zone (TZ; 2) and initiates microtubule extension to form the axoneme. The mother centriole is now known as the basal body. Secondary vesicles fuse to the ciliary vesicle, extending the membrane surface (3), as the basal body-vesicle complex migrates to the plasma membrane. IFT and BBS proteins are recruited to the basal body although the early stages of ciliogenesis occur independently of IFT/BBS proteins; they may simply be trafficked there for eventual assembly as functional IFT particles. (3-4). The distal tip of the ciliary membrane fuses with the plasma membrane (4), at which point the maturing TZ forms the ciliary gate (5). Complete formation of the axoneme and a functional cilium is an IFT/BBS protein-dependent process (6) and in the functional cilium IFT/BBS proteins shuttle cargoes into and out of the cilium. MKS/NPHP proteins are required in both early and late stages of ciliogenesis. IFT, intraflagellar transport; BBS, Bardet–Biedl syndrome. Image was adopted from Reiter *et al.* (2012).

1.3.2 Ciliary cargo delivery and length control

Once the basal body is formed, the microtubules extend from the distal end, to form the ciliary axoneme. Since the basal body lacks the protein synthesis machinery, the growing axoneme recruits proteins from the cell body using IFT machinery (Pedersen and Rosenbaum, 2008). IFT was first described by Kozminski *et al.* (1993) as a bidirectional movement of granule-like particles along the axoneme of the *Chlamydomonas* flagella (Kozminski *et al.*, 1993). IFT involves two complexes, IFT-A and IFT-B, which direct the retrograde and anterograde movement of ciliary proteins respectively (Lechtreck, 2015). Increasing the expression of IFT-B complex proteins leads to elongated cilia while reducing the abundance, activity or mobility of IFT-B proteins generates shorter cilia or absence of cilia (Brazelton *et al.*, 2001; Marshall and Rosenbaum, 2001; Marshall *et al.*, 2005; Hou *et al.*, 2007). Conversely, restricting IFT-A complex protein activity or expression, or ablating Tctex-1, a putative component of IFT-associated dynein, leads to elongated cilia or misshapen cilia (Iomini *et al.*, 2009; Palmer *et al.*, 2011). It is thought that all ciliating cells utilise IFT proteins to deliver cargo into the cilium and regulate ciliary growth, whereas basal body docking, anchoring, or transition zone formation occur independently of IFT. For example, transition zone formation appears normal in *Chlamydomonas IFT52* mutant, which cannot otherwise build the rest of the axoneme, as well as in IFT gene mutants in *C. elegans* (Perkins *et al.*, 1986; Brazelton *et al.*, 2001). However, the exact coordination of events are not understood.

At least two IFT proteins, IFT20 and Elipsa/DYF-11, BBS proteins, and vesicular transport components such as Rab8, Rab11, Rabin8 might be also involved in facilitating the cargo delivery from the Golgi-apparatus to the ciliary base when building the axoneme (Follit *et al.*, 2006; Yen *et al.*, 2006; Follit *et al.*, 2008; Omori *et al.*, 2008). Once the cargo proteins reach the base of the cilium, ciliary entry is thought to be coordinated by the transition zone (Czarnecki and Shah, 2012; Garcia-Gonzalo and Reiter, 2012). The transitional fibres in the ciliary gate represent the functional region of the basal body which serve as the coordinating unit for ciliary entry of the

proteins and provide the main attachment point for transport vesicles. Moreover, the ciliary gate represents a physical barrier to vesicle movement as the electron micrographs indicate that the inter-fibre spaces are too small to allow the passage of vesicles (Doolin and Birge, 1966; Geimer and Melkonian, 2004). Therefore, the points where the transitional fibres attach to the plasma membrane function as the physical limit for the ciliary-targeted vesicles to fuse and off load their contents. The transitional zone also contains a large number of proteins associated with ciliopathies and is thought to control the entry of cargos into the cilium (Lim and Tang, 2013). It has been observed that various proteins such as RP2 and SEPT2 are targeted to the transitional fibre region and localise to the area in a doughnut-like fashion at the ciliary base (Stephan *et al.*, 2007; Hu *et al.*, 2010).

Immunofluorescent studies have indicated that a pool of IFT proteins accumulate at the base of the cilium, immediately proximal to the transition zone, including IFT52 (Deane *et al.*, 2001; Sedmak and Wolfrum, 2010). The BBSome also localises to the transition zone and is known to be involved with the coordination of recruitment of the ciliary proteins to the cilium. Furthermore, several IFT proteins, IFT57, IFT88, IFT140 are also observed at the groove between the ciliary and periciliary membrane (Sedmak and Wolfrum, 2010). Depletion of some of the transition zone proteins including Mks6/CC2d2a, inhibits cilium formation in some tissues in vertebrates (Garcia-Gonzalo *et al.*, 2011) or causes abnormal ciliary entry of TRAM proteins and membrane associated RP2 homologue in *C. elegans* (Williams *et al.*, 2011). Another prominent feature of the known transition zone proteins is that they all consist of a basal body-targeting transmembrane and lipid-interacting C2/B9 domain (Zhang and Aravind, 2010). The presence of this domain is consistent with them being transition zone proteins and implicates them in having a role in regulating the diffusion of membrane-associated proteins. However, the precise mechanism of regulating the diffusion barrier and the transport of ciliary proteins by the transition zone proteins remain to be fully explored (Reiter *et al.*, 2012).

Recent investigation of the gated entry to the cilium has proposed a mechanism that may be analogous to that of regulated entry of nuclear proteins into the nucleus. Nuclear transport is mediated by nucleporins (NUPs) in large complexes known as nuclear pore complexes (NPCs). When a protein is targeted to the nucleus, the active transport of the protein into the nucleus is dependent on having a nuclear localisation sequence (NLS) to be recognised by the transport receptors, such as importins, to shuttle the protein across the NPC. The idea of regulation of ciliary entry by nuclear transport proteins came about by the discovery that numerous nuclear transport proteins are present in the ciliary proteome (Gherman *et al.*, 2006). In the cilium, these complexes have been called ciliary pore complexes (CPC). Recently, a ciliary localisation sequence (CLS) analogous to the NLS has been identified for the IFT component kinesin-2 motor KIF17 (Dishinger *et al.*, 2010) and a peripheral membrane protein transported by IFT, retinitis pigmentosa 2 (RP2) (Hurd *et al.*, 2011). Both of these CLS motifs are recognised by importin β2 for transport across the ciliary barrier in a RanGTP/GDP-dependent manner (Dishinger *et al.*, 2010; Hurd *et al.*, 2011). The retinitis pigmentosis GTPase regulator (RPGR) has also been shown to interact with another nuclear transporter protein, nucleophosmin (NPM), for its localisation to the basal body (Shu *et al.*, 2005). NPM is a multifunctional protein chaperone that shuttles between the nucleoli and cytoplasm and has also been associated with 'licensing' the centrosome division (Okuda *et al.*, 2000; Grisendi *et al.*, 2005). Thus cilium entry may be controlled in a similar manner to nuclear entry and may utilise the same protein subsets for cargo delivery.

1.3.3 Cilia disassembly

When the cilium axoneme is assembled, ciliary tubulins undergo a set of post-translational modifications, including acetylation, detyrosination, polyglutamylation, and glycylation that stabilise the axoneme. These post-translational modifications, especially the ones central for the

axoneme stability, are disrupted during the disassembly of the cilium. It has been demonstrated that growth factor stimulation of ciliated cells triggers the stabilisation of human enhancer filamentation -1, HEF1 (also known as NEDD9 or Cas-L) which then activates the Aurora A kinase (Pugacheva *et al.*, 2007). Aurora A then phosphorylates and stimulates histone deacetylase-6 (HDAC6) found in the basal body and ciliary stalk, ultimately resulting in deacetylation of the axonemal microtubules rending them unstable (Pugacheva *et al.*, 2007). It has also been shown that Pitchfork (Pifo) which is localised in the basal body of the embryonic nodal cilia, interacts with Aurora A and encourages cilium disassembly (Kinzel *et al.*, 2010). In addition, PLK1 is recruited by PCM-1 and is also found to activate HDAC6 by phosphorylation and therefore is involved with cilium disassembly (Wang *et al.*, 2013). Therefore, cilium deacetylation can be a plausible model to regulate the cilium length.

1.4 Golgi and centrosome, the functional relationship

The Golgi apparatus plays a pivotal role in the secretory pathway and is known to coordinate a functional relationship with the centrosome and ciliogenesis. The regulation of this relationship is especially apparent during the interphase of the cell cycle. The Golgi always localises close to the centrosome and the positioning requires the microtubule and actin cytoskeleton (Brownhill *et al.*, 2009). It has been shown that the Golgi apparatus can nucleate microtubules (Chabin-Brion *et al.*, 2001; Miller *et al.*, 2009) and together with the microtubules that originate from the centrosome they play a part in keeping the close association between the Golgi and centrosome. First a subset of microtubules nucleated from the Golgi is necessary for the assembly of the Golgi fragments into a connected ribbon from the cell periphery. Second, the centrosome microtubules provide tracks to transport Golgi membranes to the cell centre (Cole *et al.*, 1996). Both of these process are dependent on the minus end-directed motor protein complex dynein (Miller *et al.*, 2009) and re-arrangement of the actin cytoskeleton. Actin fibres have been shown

to localise to the Golgi apparatus and provide tracks for myosin, and actin based motor proteins to shuttle proteins out of the Golgi complex (Sahlender *et al.*, 2005; Vicente-Manzanares *et al.*, 2007). The functional relationship between the Golgi apparatus and centrosome is important for specialised functions such as cell polarization and for cell migration (Li *et al.*, 2005). Cell polarisation is dependent on the directional transport of proteins from the Golgi apparatus. During this process, the centrosome is orientated towards the leading edge of the cell. In recent years, GMAP210 and Golgin160 have been recognised to coordinate directional transport from the Golgi ribbon during cell migration and polarisation (Yadav *et al.*, 2009). Depletion of these proteins results in disruption of the orientation of the Golgi apparatus, so that it's no longer oriented towards the leading edge, and thus disrupts the directional transport of proteins to the cell surface. Furthermore, the depleted cells were unable to migrate in the wound healing assay (Yadav *et al.*, 2009). This indicates that directional protein transport is crucial for cell migration. GMAP210 also functions as a receptor for IFT20 at the Golgi apparatus which is also recruited to the basal body and primary cilium (Follit *et al.*, 2008). IFT20 is a critical component of the IFT machinery which is required for ciliogenesis and extension of the cilium (Follit *et al.*, 2006). Absence of GMAP210 in mouse embryonic kidney cells resulted in shorter cilia that contained a reduced amount of membrane protein polycystin-2 suggesting that GMAP210 and IFT20 function together at the Golgi apparatus, possibly sorting the proteins destined for ciliary membrane travel (Follit *et al.*, 2008).

Another protein that has been found to regulate cell polarisation is GM130 (Kodani and Sutterlin, 2008; Rivero *et al.*, 2009). Depletion of GM130 is shown to alter the localisation of the centrosome so that the centrosome failed to nucleate microtubules or to re-orientate in response to a polarisation stimulus. Furthermore, GM130 is involved in regulating the small GTPase, Cdc42 at the centrosome which is a known regulator of cell polarisation (Kodani *et al.*, 2009). GM130 is known to be required for recruitment of Golgi microtubule nucleating factor and a centrosome protein AKAP450 to the Golgi (Rivero *et al.*, 2009). Moreover, GM130 is known

to activate the protein kinase YSK1 which is a regulator of cell migration (Preisinger *et al.*, 2004). Therefore, all these findings suggest that GM130 may affect cell migration and polarisation through its effect on centrosome and Golgi organisation, Cdc42 activation and through YSK1 activation.

It is becoming evident in recent years that the relationship between the centrosome and the Golgi extends beyond the physical proximity and represents a functional relationship. For an example, Golgi proteins are known to control centrosome organisation and positioning whereas centrosome nucleating microtubules are necessary for directional protein transport and pericentriolar Golgi positioning (Sutterlin and Colanzi, 2010; Rios, 2014). This emphasises the functional relationship between two organelles. Further studies are necessary to understand how these relationships are orchestrated.

1.5 Zebrafish as a model to study ciliary defects

Zebrafish has been used for many years as a model organism to investigate proteins implicated in ciliogenesis and ciliary function. Zebrafish are the model organism of choice for many laboratories given their short gestation and relatively easy maintenance under laboratory conditions. Perhaps more importantly, the transparency of the embryo enables easier observation of developmental processes, high nucleotide and amino acid identity with humans and versatility in genetic analyses compared to many other model organisms, Zebrafish became a promising model organism for studying human development and diseases (Howe *et al.*, 2013). Gene function can be tested by disruption, using approaches such as siRNA and morpholinos with microinjection as a delivery method, or by creating genetic mutations using gene targeting technologies such as TALEN and CRISPR (Bedell *et al.*, 2012; Chang *et al.*, 2013b). Alternatively, transgenic animals can be created, to over-express genes of interest (Sun *et al.*, 2004).

A number of previous reports have investigated the phenotypes that arise following disruption of proteins required for the structure or function of cilia or centrosomes. A common "ciliary phenotype" is observed in zebrafish when known centrosome/ciliary proteins such as PCM-1 (Stowe *et al.*, 2012), IFT proteins (Sun *et al.*, 2004; Tsujikawa and Malicki, 2004), CEP proteins (Wilkinson *et al.*, 2009; Baye *et al.*, 2011), PKD proteins (Sullivan-Brown *et al.*, 2008) or FoxJI-induced genes (FIGs; (Choksi *et al.*, 2014) were disrupted. This ciliary phenotype is characterised by a curved body axis, ectopic otoliths, polycystic kidneys, hydrocephalus or microcephalus, situs inversus, and retinal degeneration (Figure 1.6) (Song *et al.*, 2016; Shi *et al.*, 2017). Otoliths are commonly known as "earstones" and are visible structures within the otic vesicle of bony fishes, formed from a proteinaceous core that is biomineralised by calcium carbonate; normally an otic vesicle would contain only two otoliths (Waterman and Bell, 1984; Kimmel *et al.*, 1995; Stooke-Vaughan *et al.*, 2015).

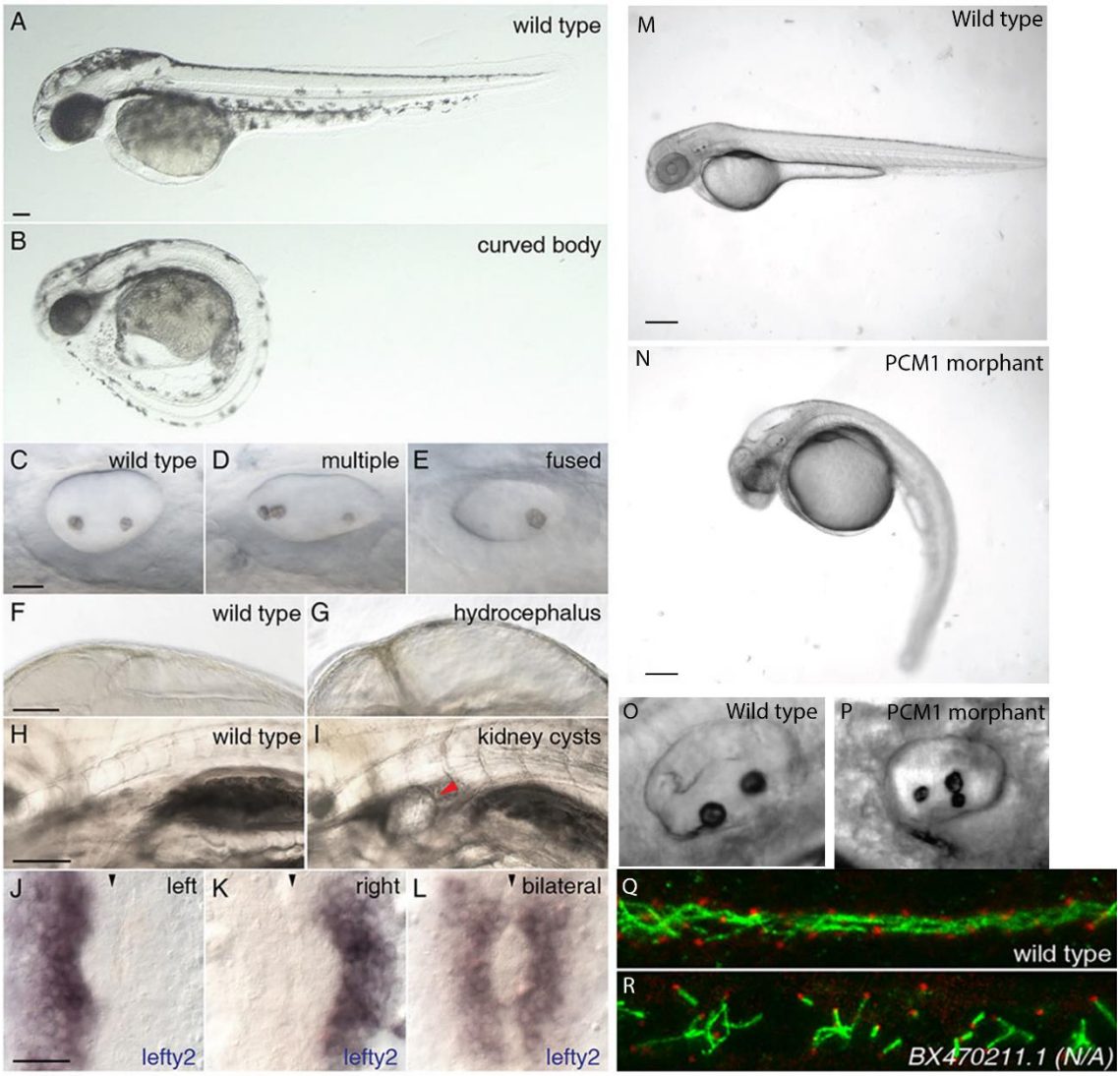

Figure 1-6 Typical phenotypes of zebrafish embryos with ciliary defects.

Comparison of wild-type zebrafish embryos **(A,C,F,G,J,M,O,Q)** with embryos injected with morpholinos targeting the 50 FoxJI-induced genes (FIGs) which disrupt ciliogenesis **(B,D,E,I,K,L,R)** or with morpholinos targeting PCM1 **(N,P)**. Typical morphant morphology following disruption to ciliogenesis includes curved body axis **(B,N),** otolith defects in the inner ear with either multiple otoliths **(D,P)** or fused otoliths **(E),** swelling of the brain ventricles (hydrocephalus, **G**), kidney cysts (I), and disruption of *lefty2* expression to give right-sided expression **(K)** or bilateral expression **(L).** Cilia of the pronephric duct stained with anti-Arl13b antibody (green) and basal bodies stained with anti-γ-tubulin (red) in 24 hpf embryos show long cilia of uniform length in wild-type embryo (Q), whereas FIGs morphants exhibit shortened cilia **(R).** Figure adapted from Choksi *et al*., 2014 (A-L,Q,R) and Stowe *et al*., 2012 (M-P).

1.6 Aim of the project

A large number of proteins have been identified to associate with ciliogenesis and the centrosome in the last decade. However, many of these still remain to be fully characterised to understand their functional role in ciliogenesis and centrosome function.

CEP72 and ODF2L (BCAP) are two partially characterized proteins that are implicated in centrosome function and ciliogenesis. The aim of this study is to investigate more fully the functions of these proteins.

The mammalian CEP72 protein is required for microtubule nucleation activity on the gamma-tubulin ring complexes (γ-TuRCs) and has critical roles in forming a focused bipolar spindle, which is needed for proper tension generation between sister chromatids (Oshimori *et al.*, 2009). It is also involved with localization of KIZ/PLK1S1, AKAP9, CG-NAP and γ-TuRCs to the centrosome (Oshimori *et al.*, 2009) Furthermore, it has been shown that mammalian CEP72 functions as a component in the centriolar satellites and cooperates with PCM-1 in the recruitment of CEP290; depletion of either CEP72 or CEP290 interferes with BBS4 localization (Stowe *et al.*, 2012). In addition, disruption of satellite protein PCM-1 in zebrafish results in developmental defects that may indicate the primary cilium function is compromised (Stowe *et al.*, 2012). Therefore, this invites the question whether zebrafish Cep72 also functions in a similar manner to PCM-1. Moreover, previous studies on mammalian CEP72 have shown it to be involved in mitotic spindle formation. Therefore, in this study, I am testing the hypothesis that zebrafish Cep72 may play an important role in ciliogenesis.

Human protein Outer Dense Fiber 2 (ODF2; also known as cenexin) was initially identified as the main component of the sperm tail cytoskeletal protein. ODF2 is a centriolar structural scaffolding protein specifically localized at the distal/subdistal appendages of mother centrioles (Nakagawa *et al.*, 2001; Ishikawa *et al.*, 2005). A protein deemed to be ODF2-like (ODF2L), also named as Basal body Centriole-Associated Protein (BCAP), is present in the protein databases,

although this shares only 20% amino acid similarity with ODF2 (Ponsard *et al.*, 2007). ODF2L is conserved in evolution and homologues have been found in a number of species that possess cilia and flagella including some mammals and vertebrates (Ponsard *et al.*, 2007). Ponsard *et al*., (2007), have shown that ODF2L is expressed in cilia- and flagella- containing tissues and is localized to the basal bodies and centrioles in ciliated cells. However, the exact role of ODF2L in ciliated cells is yet unknown.

Preliminary work carried out in this laboratory suggested that zebrafish morphant phenotypes of Odf2 and Odf2l were to some extent dissimilar, and that the Odf2l morphant phenotype was more closely related to the Pcm-1 morphant phenotype. Therefore, this thesis aims also to further investigate the hypothesis that Odf2l is involved in ciliogenesis.

The specific objectives of this thesis are:

a. To knockdown Cep72 function in zebrafish using morpholinos in order to investigate the consequence on embryo development and ciliogenesis (Chapter 3);
b. To knockdown Odf2l function in zebrafish using morpholinos in order to investigate the consequence on embryo development and ciliogenesis (Chapter 4);
c. To investigate the localisation of ODF2L in human cell lines and the changes in ciliogenesis (Chapter 5);
d. To knockdown and over-express ODF2L in human cell lines and observe the consequences on ciliogenesis and cell behaviour (Chapter 5);
e. To identify ODF2L-interacting partners in human cell lines following over-expression of GFP-tagged ODF2L, affinity purification and mass spectrometry (Chapter 6).

Chapter 2:

Materials and Methods

2.1 Materials and reagents and plasmids

Reagents were purchased from Sigma, FisherScientific, Merck or Melford, unless otherwise stated. Frequently used buffers are summarised in Table 2.1.

Solutions	Composition
LB (Luria Bertani)	10 g/L Bacto-tryptone, 5 g/L Bacto-yeast extract, 10 g/L NaCl
LB-Agar	LB plus 15 g/L Bacto-agar
Phosphate buffer saline (PBS)	8 g/L NaCl, 0.2 g/L KCl, 1.44 g/L Na_2HPO_4, 0.24 g/L KH_2PO_4, pH 7.4
TAE 50X	242.4 g/L Tris, 57.2 mL/L glacial acetic acid, 100 mL/L 0.5 M EDTA pH 8.0
Tris-EDTA (TE) buffer	10mM Tris-HCl, pH 7.4, 1mM EDTA
Cell lysis buffer	50 mM Tris-HCL (pH 7.5), 150 mM NaCl, 1 mM EDTA, 10% Glycerol, 1% Triton X-100
SDS-PAGE Tris-Glycine running buffer 10X	30.2 g/L Tris, 188 g/L Glycine, 10 g/L Sodium dodecylsulphate, pH 8.3
SDS-PAGE transfer buffer	25 mM Tris base, 0.2 M glycine, 10% (v/v) Methanol
2X SDS sample buffer	120 mM Tris-HCl pH6.8, 20% Glycerol, 4% SDS, 0.04% Bromophenol blue, 10% β-mercaptoethanol
TBS 10X	23.23 g/L Tris-HCl, 80.06 g/L NaCl, pH 7.6
TBST	1x TBS + 0.5% Tween 20
PBST	PBS + 0.5% Tween 20
Coomassie Blue (Candiano Recipe)	0.12% (w/v) CBB G-250, 10% (w/v) Aluminium sulphate, 20% (v/v) methanol, 10% (v/v) Orthophosphoric acid

Table 2-1 Often used buffers.

Vectors and Plasmids: The plasmids used in this study are based on commercially available vectors which were modified as appropriate. The plasmids used in this study were created by the methods described in section 2.4.1.6. The parental vectors and plasmids created are given in Table 2.2.

Vector Name	Organism	Description	Selective marker
pCS2P+EGFPN	*E. coli*	N-terminal, enhanced GFP-Tag, Mammalian expression (parental)	Ampicillin
pBluescriptSK(-) (pBS)	*E. coli*	Standard cloning vector (parental)	Ampicillin
*pCS2P-EGFPN-ODF2L	*E. coli*	N-terminal, enhanced GFP-Tag, ODF2L Mammalian expression	Ampicillin

*pBS-ODF2L	*E. coli*		Ampicillin

Table 2-2 Vectors and plasmids.

2.2 Cell culture methods

2.2.1 Cell lines

Human HeLa (human cervix adenocarcinoma cells), mouse fibroblast NIH 3T3 cells (ATCC cat# CRL-1658) and human embryonic kidney cells (HEK293T) were provided by Professor George Dickson's laboratory at Royal Holloway University of London (RHUL). The hTERT-immortalised human retinal pigment epithelial cell line (hTERT-RPE-1, ATCC cat#: CRL-4000) was kindly provided by Professor Eric Nigg's laboratory, Basel, Switzerland. Human hepatocyte derived cellular carcinoma cells (HuH-7) were kindly provided by Professor Robin William's laboratory at RHUL.

Sterilised plastic (Corning Inc, UK) and media were used, and all the equipment was either washed with 70% ethanol or 1X Distel (Tristel, Cambridge, UK) and solutions were pre-warmed to 37°C prior to use. All the cell culture was performed inside a Class II microbiological safety cabinet after irradiating the cabinet with Ultraviolet (UV, 254nm wave length) light for 30 min prior to use.

The HeLa, NIH 3T3 and HEK293T cells were grown in Dulbecco's Modified Eagle's Medium (Sigma D6546) supplemented with 2 mM L-Glutamine (Sigma, G7513), 10% Foetal Bovine Serum (Gibco, 10500-064) and 1X antibiotic-antimycotic mixture (Gibco, 15140-122). The hTERT-RPE-1 cells were grown in Dulbecco's Modified Eagle's Medium with nutrient mixture F-12 Ham (Sigma, D6421) supplemented with 10% Foetal Bovine Serum, 0.348% sodium bicarbonate (Gibco, 25080-094) and 1X antibiotic-antimycotic mixture. The HuH-7 cells were cultured in Dulbecco's

Modified Eagle's Medium (Sigma, D6546) supplemented with 10% Foetal Bovine Serum and 1X antibiotic-antimycotic mixture.

2.2.2 Cell plating, passaging and freezing

Frozen cell aliquots were rapid-thawed in a 37°C water bath with gentle shaking and transferred into a 15 mL Falcon conical tube (Corning, CLS430829) containing 4 mL of pre-warmed growth medium, then the cells were centrifuged at 1000 x *g* for 10 min. The medium was discarded and cells were re-suspended in fresh medium and transferred to a T75 cell culture flask (Corning, CLS3290). Cells were incubated at 37°C with 5% CO_2 in a humidified incubator and confluence was assessed by microscopy. Once cells had reached 85-90% confluence, cells were passaged to new cell culture flasks to maintain the cultures.

To passage cells, the culture medium was aspirated from the flask and cells washed with pre-warmed Hank's balanced salt solution (HBSS; Gibco, 14185045) or PBS without calcium and magnesium (Gibco, 14190144) twice. Then cells were trypsinised off the flask by incubating in TryPLE Select (Gibco, 12563-029) for 2-3 min at 37°C (1 mL for a T75 flask and 0.5 mL for T25 flask) to detach cells from the flask. The flask was gently shaken to lift the cells and 5 mL of pre-warmed medium was added to the flask to inhibit TryPLE. Then, cells were transferred into a 15 mL Falcon tube and centrifuged for 10 min at 1500 x *g*. The medium was then discarded and the pellet re-suspended in 10 mL of fresh pre-warmed medium. Approximately 20 µL of the cell suspension was taken out and applied to a haemocytometer. Cells were counted in 5 individual squares of the grid (each 0.2 x 0.2 x 0.1 mm) and multiplied by 5 to calculate the number of cells in 0.1 mm^3 and then multiplied by 10^4 to get an estimation of the number of cells in 1 mL. Approximately $1X10^6$ cells were transferred to T75 flask and the final volume adjusted to 10 mL, then incubated as described above.

To make the frozen stocks, cells were trypsinised and centrifuged as described above and the pellet was re-suspended in Recovery™ cell culture freezing medium (Gibco, 12648-010) at 1 million cells per mL concentration. Cells were then aliquoted into 1.5 mL cryotubes (Nunc, V7634) and stored at -80°C overnight in a CoolCell SV2 (BioCision, BCS-172) to ensure the correct temperature drop before transferring to a liquid nitrogen dewer for long term storage.

2.2.3 Transient transfection of mammalian cells with DNA

HeLa, hTERT-RPE1, HEK293 and HuH-7 cells were transiently transfected with DNA constructs for expression in mammalian cells by using lipid-based delivery methods. Cells were plated 24 h in advance in a 6-well plate (Corning, CLS3516 or Nunc, 140675) and grown up to 80-90% confluence and transfected with Lipofectamine 2000 (Invitrogen, 11668019) according to manufacturers' protocols. For a 6-well plate, 7 µL of Lipofectamine 2000 was diluted in 243 µL of Opti-MEM (Gibco, 11058021). For all the transfections in 6-well format, 2.5 – 3 µg of plasmid DNA was used and diluted in 250 µL Opti-MEM. Both Lipofactamine 2000 and DNA mixtures were incubated for 5-10 min at room temperature before combining together. The Lipofectamine 2000-DNA combination was mixed well and incubated for 10-15 min at room temperature. Cell medium was aspirated from the flask and replaced with serum and antibiotic free medium and then the Lipofectamine-DNA mixture was added drop-wise to the cells. Cells were then incubated for 5-6 h (37°C with 5% CO_2) and replaced with serum positive, antibiotic free medium and incubated for 24-48 h. For large culture dishes (T25 and T75), the protocol was scaled up in relation to the increased amount of cell culture medium used.

2.2.4 RNA interference

Specific knockdown of ODF2L mRNA level was achieved by transfecting small interfering RNA oligonucleotide duplexes (siRNA) into HeLa and hTERT-RPE1 cells as described (Elbashir *et al.*,

2001). The siRNAs were designed with custom RNA synthesis tools (siDESIGNE Center) provided by GE Dharmacon to ODF2L transcripts: XM_005271056, NM_001184766, NM_020729, XM_005271057, NM_001184765, NM_001007022, XM_005271055, XM_005271054. The siRNA oligo sequences were designed to have an overlap of 19 nucleotides and 2 nucleotide overhangs on the 3'-end of both the sense and anti-sense strands (Table 2.3). Oligos were supplied as 20 nmol stocks (pre-annealed; Dharmacon), oligos were resuspended in 200 µL of RNase-free water to make a stock solution of 100 µM and stored at -80°C. The working concentration of 10 µM aliquots were also made by diluting 100 µM stock with RNase free water and stored in -80°C. For delivering siRNAs to mammalian cells, Lipofectamine RNAiMAX (Invitrogen, 13778150) was used according to the manufacturer's protocol. For transfection of mammalian cell lines, a reverse transfection procedure was used. Transfection complexes were prepared in sterile 6-well plates and for each well, 2.5 -3 µL of siRNA (from 10 µM working stock) and 7.5 µL of Lipofectamine RNAiMAX were diluted in 500 µL of Opti-MEM and the mixture incubated at room temperature for 10-15 min to allow the complexes to form. Cells were pelleted and resuspended in Lipofectamine RNAiMAX at about $1x10^6$ cells/mL; about $1x10^6$ cells were added to each well containing siRNA-RNAiMAX complexes and diluted with culture medium without

antibiotics to make a final volume of 2.5 mL per well. After 24-96 h of incubation (37°C, 5% CO_2) the transfected cells were processed further for immunofluorescence microscopy (Section 2.3.1).

Custom siRNA		
Name	**Catalogue number**	**sequence**
ODF2L siRNA1	TMOSLR-005597	Sense: GCAAGAAGCAGCUGAAAUAUU Antisense : UAUUUCAGCUGCUUCUUGCUU
ODF2L siRNA2	TMSOLR-005599	Sense: GGAGAAGGCUGUAAAUGAUUU Anisense: AUCAUUUACAGCCUUCUCCUU
ON-TARGETplus™ Non-targeting pool		
Non-Targeting pool	D-001810-10-05	Unknown

Table 2-3 siRNA sequences.

2.3 Cell biology methods

2.3.1 Indirect immunofluorescence microscopy

For immunofluorescence microscopy, cells were grown on glass coverslips sterilised with 80% ethanol in 6-well plates. Cell numbers plated depended on cell line and the time until fixation. Cells were fixed in either 4% paraformaldehyde (PFA) (v/v) or ice cold methanol.

Paraformaldehyde fixation: stock of 16% PFA (w/v) was purchased from Agar Scientific (AGR1026) and 1% or 4% PFA (v/v) working solution was freshly prepared by diluting the stock with PBS with 0.2% Triton X-100 (v/v) (Sigma, X100-100ML). The cells on the coverslips were washed three times in PBS and fixed immediately for 5 min at room temperature. The coverslips were then washed three times with PBS and proceeded for immunostaining.

Methanol fixation: The coverslips were washed three times with PBS and fixed immediately with ice cold methanol for 5-10 min on ice. The coverslips were then washed three times with PBS.

Antibody labelling of fixed cells: The coverslips were blocked in 1% or 3% BSA in PBS for 30 min at room temperature with gentle shaking. After blocking, coverslips were removed from wells and placed on top of parafilm on a flat surface. Then 100-200 µL of primary antibody solution was added to the top of the coverslips. The coverslips were incubated with the primary antibody

for 60-120 min at room temperature or overnight at 4°C in a humidified chamber. After the incubation, coverslips were transferred back to the 6-well plate and washed three times with PBS at room temperature. Then the coverslips were incubated with the secondary antibodies identically to the procedure described above and incubated for 60 min at room temperature. After the incubation, coverslips were transferred back to a 6-well plate and washed again with PBS three times and then mounted with 10 -15 µL of Vectashield™ mounting media with DAPI (Vectorlabs, H-1200) onto glass slides for microscopy. The mounted coverslips were sealed with nail varnish and left to dry for a couple of hours in a dark chamber before microscopy.

Immunofluorescence microscopy: Images were collected with either a Nikon Eclipse TE300 inverted microscope (Nikon, UK) with 40X Plan Fluor objective (Nikon) or 60X Plan Apochromat oil immersion objective with NA 1.4 standard filter sets (Nikon) attached to a 1.3 megapixel ORCA-100 cooled CCD camera (model C4742-95, Hamamatsu, Japan) and Hamamatsu HCImageLive (Hamamatsu Corporation, Japan) software or Nikon Eclipse Ni-E microscope (CF160 optical system, Nikon) with 60X Plan Apochromat oil immersion objective attached to 1.5 megapixel monochrome DS-Qi1MC cooled CCD camera and NIE Br (Nikon, UK) software.

Confocal microscopy: Confocal microscopy stacks were obtained with the Olympus IX81/FV-1000 laser confocal system with 63X Plan Apochromat oil immersion objective (Olympus) using Argon gas laser and Helium-Neon diode laser. Image Z-stacks were analysed using Olympus FV-1000 Fluoview 2.0 C software.

Name	Description	Organism	Dilution		Supplier, Cat#
Primary antibodies			**IF**	**WB**	
Acetylated α-Tubulin	Monoclonal, reacts with: human, bovine, invertebrates, rat, hamster, plant. Clone 6-11B-1	Mouse	1:500		Sigma-Aldrich, T7451
Anti-γ-Tubulin	Monoclonal, reacts with: human, rat, bovine, mouse. Clone GTU-88	Mouse	1:2500		Sigma-Aldrich, T6557
Anti-γ-Tubulin	Polyclonal, reacts with: chicken, human	Rabbit	1:1000		Sigma-Aldrich, T5192
Anti-Golgin-97	Monoclonal, reacts with: Human Clone: CDF4	Mouse	1:1000		ThermoFisher, Q92805
Anti-β-Actin	Monoclonal, reacts with: cat, human, mouse, pig. Clone AC-74	Mouse		1:5000	Sigma-Aldrich, A2228
Anti- ODF2L	Polyclonal, Human	Rabbit	1:100	1:1000	Biorbyt, orb31049
Anti- ODF2L	Polyclonal, Human	Rabbit	1:50 1:100	1:500 1:1000	Novus Biologicals, NBP1-82922
Anti- ODF2L	Polyclonal, Human	Rabbit	1:50 1:100	1:500 1:1000	Novus Biologicals, NBP1-56559
Anti- ODF2L	Polyclonal, Human	Rabbit	1:50 1:100	1:500 1:1000	Novus Biologicals, NBP1-82921
Anti- ODF2L	Polyclonal, Human	Rabbit	1:100	1:1000	Proteintech, 23887-1-AP
Anti-GFP	Polyclonal	Rabbit		1:2000	ThermoFisher, G10362
Secondary antibodies					
IRDye 680RD anti-mouse	React with : mouse	Goat		1:15000	Li-Cor, 925-68070
IRDye 800CW anti-rabbit	React with : rabbit	Goat		1:15000	Li-Cor, 925-32211
Alexa Fluor 594	React with : mouse	Goat	1:1000		Invitrogen, Z25007
Alexa Fluor 488	React with : rabbit	Goat	1:1000		Invitrogen, Z25302

Table 2-4 Antibodies and dilutions.

2.3.2 Cell migration assay (Scratch-Wound Assay)

To assess the cell migration pattern and polarity, a scratch-wound assay was performed on siRNA knockdown hTERT-RPE1 cells. The cells were seeded on to a glass coverslip placed in a 6-well plate and grown in an incubator as described in section 2.2.1 to reach about 90% confluency. Then a linear scratch wound was made using a blunt sterile P200 tip between parallel edges of the coverslip as described in (Wells and Parsons, 2011). The coverslips were washed twice with PBS and incubated with fresh medium for 24 h until the wound was closed. The coverslips were fixed in cold methanol at different time points as described in section 2.3.1 and proceeded to immunostaining.

2.3.3 Cell cycle synchronization

For cell cycle synchronization at G2/M transition phase, hTERT-RPE1 cells were seeded and cultured until 70-80% confluency followed by treatment with 1.5 µM nocodazole (Sigma, M1404) for 24 h as described (Uetake and Sluder, 2007). To release from G2/M arrest, cells were washed twice with PBS and incubated in serum free growth medium and then allowed to grow until analysed. For the analysis, cells were fixed in 1% PFA and immunostained with anti-γ-tubulin, anti-ODF2L and anti-acetylated α-tubulin.

2.3.4 Cell cycle analysis using fluorescence activated cell sorting (FACS)

For the FACS-based cell cycle analysis, hTERT-RPE-1 cells were grown under normal culture conditions in a 6-well plate. Once the cells reached 80-90% confluency, cells were trypsinised and harvested as described in section 2.2.1 and washed twice with PBS. The cells were then fixed in ice cold 70% ethanol for at least 30 min on ice and washed twice with PBS. For the FACS analysis, cells were treated with 100 µg/ml RNaseA solution (Thermo Scientific, EN0531) in PBS followed by 50 µg/ml propidium iodide (PI) (Sigma, P4864) for staining (400 µL per million cells).

Cells were stained overnight in a dark chamber at room temperature and data were collected using a BD FACSCANTO I flow cytometer (BD Bioscience, Oxford, UK) set to collect in the linear scale. Cell cycle analysis was performed using BD FACSDiva (BD Bioscience) and FlowJo version X.

2.3.5 Förster resonance energy transfer (FRET) analysis

For the sensitised emission assay, pCSP2-GFP-CDK5RAP2-CNN2 and pCSP2-mCherry-PCNT-PACT (supplied by Dr Rivka Isaacson and Ewelina Krysztofinska at King's College, London) were transfected into HeLa cells and images were acquired using an Olympus Fluoview FV1000 confocal microscopy system. The eGFP donor channel was acquired using donor excitation (λ = 488 nm) and donor filter set. The acceptor channel (mCherry) was acquired using acceptor (λ =587 nm) and the acceptor filter set. FRET was acquired using excitation (λ=610 nm) and the FRET filter set. Images were taken from donor, acceptor and FRET samples using the same acquisition parameters. Donor and acceptor images were used to evaluate signal cross-talk caused by image setting and fluorophore properties. The acquired data was analysed using Olympus Fluoview FV1000 Toolbox software.

2.4 Molecular biology methods

2.4.1 Nucleic acid methods

2.4.1.1 RNA extraction

Total RNA was extracted from hTERT-RPE-1 cells using the Trizol-chloroform method as described (Chomczynski and Sacchi, 1987) and reviewed in (Chomczynski and Sacchi, 2006). TRI reagent was purchased from Sigma-Aldrich (T9424).

2.4.1.1.1 Cells

Cells were harvested and homogenised with 0.5 mm glass beads (Thistle Scientific, Glasgow, Scotland) in 500 µL of TRI solution with vortexing. For the phase separation, 100 µL (1/5 of the volume of TRI solution) of Chloroform was added followed by a short vortex and incubated for 5 min at room temperature. Then the mixture was centrifuged at 1200 x *g* for 15 min at 4°C for the three phase separation. The colourless upper aqueous phase was then transferred to a fresh tube followed by RNA precipitation with isopropanol (1/2 of the volume of TRI). The solution was centrifuged at 12000 x *g* for 10 min at 4°C and the pellet was washed with 50 µL of 70% ethanol. Then the RNA pellet was resuspended in 20 µL RNase free water and stored at -80°C for long term storage.

2.4.1.1.2 Zebrafish

Zebrafish total RNA was extracted from 20 embryos at 48 hours post-fertilization (h.p.f) with TRIzol method as described above. Prior to extraction, embryos were transferred into a 2 mL Eppendorf tube and cooled on ice for 3 min, excess embryo medium was carefully removed from the tube and 500 µL of TRizol (Sigma-Aldrich, T9424) reagent was added to each tube. Tubes were then homogenised for 30 s in a Mini-beadbeater-16 homogeniser (BioSpec Products Inc, Oklahoma, USA) with 0.5 mm glass beads (Thistle Scientific, Glasgow, Scotland) and continued to RNA extraction.

2.4.1.2 cDNA synthesis (reverse transcription)

Approximately 2-5 µg of RNA was used to synthesise first strand complimentary DNA (cDNA) in 20 µl reactions using AccuScript Hi-Fi (Agilent Technologies, 200820) or GoScript (Promega, A5003) reverse transcription kits according to manufacturers' instructions. For all the cDNA synthesis reactions Oligo$(dT)_{20}$ primers (Invitrogen, 18418020) were used.

2.4.1.3 Polymerase chain reaction (PCR)

The DNA was amplified by PCR using 1.5 mM $MgCl_2$, 1x GoTaq Buffer, 1.25 Units GoTaq (Promega, M3005) DNA polymerase and 1 mM dNTPs. For each reaction, approximately 0.5 µg of cDNA was used in a total reaction volume of 50 µL. For high fidelity PCR, *Pfu* DNA polymerase was used, with 1x *Pfu* buffer, 0.5 Unit *Pfu* DNA polymerase (Promega, M7741) in 50 µL reaction volumes without $MgCl_2$.

The reactions were amplified with a Chromo4 thermocycler (MJ research) with appropriate primer combinations. The thermocycler program comprised of initial denaturing step for 5 min at 95°C followed by 30 cycles of denaturing for 30s at 95°C, annealing for 30 s (with the temperature depending on primer melting point) and extension at 72°C (extension time depended on the amplicon length) followed by final extension of 5 min at 72°C.

PCR amplicon	**Forward sequence**	**Reverse sequence**
Zebrafish β actin	5'-GATGCCCCTCGTGCTGTTTTC-3'	5'-ACCTCCCTTTCCAGTTTCCGC-3'
Human β actin	5'-ATTCCTATGTGGGCGACGAG-3'	5'-GGAGTTGAAGGTAGTTTCGTGG-3'
zOdf2l MO1	5'-GGCAGCTATTGTTGTCCGTGCGAGA-3'	5'-GGCAGCTATTGTTGTCCGTGCGAGA-3'
zOdf2l MO2	5'-TCTGATTGGCAGCTATTGTTGTCCG-3'	5'-CGACATTAGGCTTTCGAGTTTTCTCTCA-3'
zCep72 MO1	5'-GTAGACGGTTTGCCCATAACAG-3'	5'-CATTCATTCTCGCAGCGGAC-3'
zCep72 MO2	5'-GTAGACGGTTTGCCCATAACAG-3'	5'-TCTTATAATCCGAGCTCTTGGAGG-3'
hODF2L siRNA	5'-ATGGAGAAGGCTGTAAATGA-3'	5'-CTTTCAACTTATCGTTCTCG-3'

Table 2-5 PCR primer sequences.
Primers to check the morpholinos are marked as MO

2.4.1.4 Agarose gel electrophoresis

The PCR products and plasmid DNA were size-fractioned and visualised on 1-2% agarose gels containing 1 µL of Web Green (Web Scientific, Crewe, UK) (per 100 mL of gel) for DNA staining in 1 x TAE buffer. Samples were prepared with 1 x DNA loading buffer (Bioline, BIO-37045) containing 1 µg plasmid or 5 µL PCR product per well. The Bioline HyperLadder 1 kb (BIO-33053)

or Hyperladder 25 bp (BIO-33057) was used as a molecular maker on agarose gels. The gels were run in an electrophoresis tank at constant voltage of 75-80 V and visualised using a GeneFlash gel documentation system (Syngene Bio Imaging, Cambridge).

2.4.1.5 Sequencing

The PCR fragments and plasmids were sent for sequencing with the relevant primers to the Department of Biochemistry, Cambridge University, UK. The results were analysed by using sequence analysis tools in CLC workbench (CLC Bio) version 5.

2.4.1.6 Cloning and sub-cloning

2.4.1.6.1 Bacterial transformation

Escherichia coli (E. coli) DH5α electro competent (prepared in our lab) or α-select silver efficiency chemically competent (Bioline, 85026) cells were used for all the transformations. The chemically competent cells were thawed on ice and to a 50 µL aliquot 1-50 pg of plasmid DNA was added and gently mixed, then cells were incubated on ice for 30 minutes. These cells were then transformed by heat shocking for 45 s at 42°C following the manufacturer's instructions. For electroporation, 50 µL competent cells were gently transferred to cold 0.2 cm cuvette and gently mixed with 1-50 pg of DNA. These cells were then pulsed at 2.5 kV in a BioRad Gene Pulser II set at 25 mF and 200 Ω. After the transformation, 1 mL of pre warmed LB broth was immediately added to the cells and they were allowed to recover for 1 h in a 37°C shaking incubator. After the initial incubation, cells were streaked on to LB-agar plates made with the selective antibiotic (ampicillin 50 µg/mL (Sigma, A9393) or kanamycin 25 µg/mL (Sigma, 10106801001)). Plates were incubated overnight at 37°C and individual colonies were picked the following day and inoculated into LB broth with the appropriate antibiotic.

2.4.1.6.2 Plasmid preparation and purification

Plasmids used for cloning and sequencing were purified using the Qiagen QIAfilter Plasmid Midi kit (12245) or Promega PureYield Plasmid midiprep kit (A2492) as described by the manufacturers. The purified plasmids were re-suspended in Tris-EDTA (TE) buffer and quantified using a NanoDrop ND-100 (Thermoscientific) spectrophotometer by reading the absorbance at 260 nm.

2.4.1.6.3 Cloning strategy

The strategy used for this work was to use a PCR product which could be subcloned into a wide variety of vectors. For this strategy, full length mouse Odf2l I.M.A.G.E clone (cDNA clone MGC: 28123, IMAGE:3979963, Gene bank accession BC020075.1, Gene ID 52184) was purchased from Source BioScience, (Nottingham, UK) and *Bam*HI restriction sites on the 5'-end and *Xho*I restriction sites on the 3'-end were generated during amplification of the gene by PCR. The ATC sequence of the *Bam*HI restriction site was designed to be in-frame with the start codon of the insert as shown below:

ttttggatcctc**ATG**GA *Bam*HI

The restriction site is underlined and the start codon is marked with capitalised bold; as *Bam*HI cuts after the –ATC-, the cut site is in-frame with the start codon.

The pCS2P+eGFPN plasmid was cut with restriction enzymes *Bgl*II (NEB, R0144S) and *Sal*I (NEB, R0138T) and pBluescript plasmid was cut with *Bam*HI (NEB, R0 136S) and *Xho*I (NEB, R0146S). Both linearised plasmids were gel purified using Bioline Isolate II PCR and Gel clean up kit (BIO-52059) according to the manufacturer's instructions. Full length ODF2L amplicons were generated with primers that contain restriction sites to allow the amplicons to be restriction digested and cloned into pCS2P+eGPN and pBluescript vectors using Bioline T4 ligase (BIO-

27026) according to the manufacturer's instructions. The inserts were then sequenced as described in section 2.4.1.5. The plasmids used and created are listed in Table 2.2.

2.4.2 Protein methods

2.4.2.1 Protein extraction

Cells were harvested and lysed in 500 µL of cell lysis buffer containing 5 µL of 100X protease inhibitor cocktail (Sigma, P8340) for 30 min at 4°C with gentle shaking. Then the cell debris were removed by centrifuging at 12000 x *g* at 4°C for 20 min. The supernatant was removed and aliquoted into 100 µL aliquots and stored at -80°C.

2.4.2.2 Determination of protein concentration

To determine the protein concentration, BioRad Detergent Compatible (DC) assay (BioRad, 5000112) was used. The assay uses a modified Lowry assay which is based on protein reacting with copper, causing reduction of Folin reagent and development of the blue colour such that intensity reflects protein concentration. DC reagent A (an alkaline tartrate solution) was mixed with DC reagent S (50:1 ratio) and combined with sample or protein standard (5 µl) in a flat bottom 96 well plate. DC reagent B, Folin reagent (200 µl) was added and the mixture incubated (30 min, RT). The absorbance at 750 nm was measured in µ Quant (Bio-tek Instruments). Quantification of each sample and standards was performed in duplicate and absorbance values of the standards were used to generate a standard curve and to compare the absorbance values of the samples.

2.4.2.3 Sodium dodecyl sulfate-Polyacrylamide gel electrophoresis (SDS-PAGE)

Small 10% SDS polyacrylamide gels (8 x 6.5 cm) with 0.75 mm thickness were hand cast using a Biorad Mini-Protein II casting chamber. Approximately 5-15 µg of protein samples were

prepared in 20 µl volumes with 1x Orange sample loading buffer and 1x NuPAGE™ reducing agent (Invitrogen, NP0009), heated for 10 min at 70°C to denature the proteins, and kept on ice until loaded. PageRuler Plus prestained protein ladder (ThermoFisher Scientific, 26619) was used as a molecular weight marker. Gels were run with SDS-PAGE running buffer (Table 2.1) in a BioRad Mini Protein II gel chamber at 100 V for around 90 minutes.

2.4.2.4 Coomassie staining of SDS-PAGE gels

SDS-PAGE gels were stained using Colloidal Coomassie G-250 staining (Invitrogen, LC6025) method as described (Candiano *et al.*, 2004). The gel was fixed in fixing solution (12% w/v tricarboxylic acid, TCA) for 1 h at room temperature followed by Coomassie staining for 2 h to overnight at room temperature on a shaker. After the incubation, gels were destained for 30 min in 25% (v/v) methanol. Stained gels were then digitised using an HP flatbed scanner at 300 dpi resolution.

2.4.2.5 Western blotting

The proteins separated on an SDS-PAGE gel were subsequently transferred onto activated PVDF-FL (Millipore, IPFL00005) membrane with the aid of a BioRad mini protein II wet blotting system filled with transfer buffer (Table 2.1). The transfer was performed at 100 V for 1h and the transfer tank kept cold until the transfer was complete by placing an ice pack and a magnetic stirrer inside the tank.

2.4.2.6 Immunodetection

Once the transfer was complete, the membrane was blocked in either Odyssey blocking solution (Licor) or 1x casein buffer (Sigma, B6429) in PBS for 1 h at room temperature. After blocking, the

membrane was incubated in diluted primary antibody solution for 1-2 h at room temperature or overnight at 4°C. Primary antibodies and dilutions are given in Table 2.4. The membrane was subsequently washed 5 times in TBST or PBST at room temperature for 15 min each to remove excess primary antibody and then incubated in secondary antibody solution for 1 h at room temperature. Secondary antibodies and dilutions are given in Table 2.4. The membrane was then washed 5 times with PBST or TBST for 15 min each and processed for detection. The Odyssey SA near infrared fluorescent detector (Licor) was used to detect the fluorescent bands at 700 nm and 800 nm. The images were captured using Image studio software (Licor) version 3.

2.4.3 Mass spectrometric protein preparation and analysis

2.4.3.1 ODF2L over expression and anti-GFP magnetic beads pull-down

HEK 293T cells were cultured according to section 2.2 to reach 60-70% confluency. Then the cells were transfected with plasmid pCS2P+EGFPN+mOdf2l as described in section 2.2.3. After 48 h, cells were harvested and proteins were extracted as described in 2.4.2.1.

The GFP-Trap magnetic agarose (MA), anti-GFP antibody-conjugated magnetic beads (gtma-20), and binding control magnetic particles (bmp-20) were purchased form Chromotek GmbH (Planegg, Germany). To pre-clear the protein lysate, 25 µL of the binding control particles were prepared by resuspending in 500 µL dilution buffer (10 mM Tris-HCl pH7.5, 150 mM NaCl, 0.5mM EDTA) then separating using a magnetic separation rack (Ambion, AM10055) and removing the supernatant. This process was repeated twice and then the particles were resuspended in 200 µL of the protein lysate diluted in 300 µL of dilution buffer. The binding control particles were incubated with the protein lysate on a gentle shaker for 30 min at 4°C and then magnetically separated. The pre-cleared lysate was then used with the GFP-Trap magnetic beads for the pull-down. For the GFP pull-down, 25 µL GFP-Trap MA magnetic beads were re-suspended in 500 µL of the dilution buffer and magnetically separated as described above. After two washes, GFP-

Trap magnetic beads were incubated in the pre-cleared lysate at 4°C for 1 h on a tube rotator. After the incubation, beads were magnetically separated and the supernatant was discarded. Then the separated magnetic beads were resupended in 500 µL of dilution buffer and magnetically separated as described above. The process was repeated twice and then re-suspended finally in 25 µL SDS-sample buffer (for SDS-PAGE) or in 20 µL of 50 mM ammonium bicarbonate buffer (ABC buffer, for the trypsin digest).

The beads re-suspended in SDS-sample buffer were heated for 10 min at 95°C and subjected to SDS-PAGE as described in section 2.4.2.3. After the SDS-PAGE, gels were stained in Coomassie blue as described in section 2.4.2.4 or silver stained using Sigma ProteoSilver™ silver staining kit (PROTSIL1) as per manufacturer's instructions.

2.4.3.2 On-bead trypsin digest

The beads re-suspended in ABC buffer were subjected to trypsin digest for LC-MS/MS study. After re-suspending beads in ABC buffer, 20 µL of 45 mM DTT (in ABC buffer) was added to the sample and incubated at 50°C for 30 min. Samples were then incubated for 15 min at room temperature in the dark after adding 20 µL of 100 mM iodoacetamide (IAA) (in ABC buffer). To remove IAA activity, further 20 µL of 45 mM DTT was added. Then the sample was subjected to trypsin digest; 20 µL of 12 ng/µL trypsin in ABC buffer was added to the sample and incubated overnight at 37°C. After the incubation 10 µL of formic acid was finally added. Digested protein fragments were then concentrated using a C^{18} column packed Zip tip (Merck Milipore, ZTC18S096) following manufacturer's instructions.

2.4.3.3 Mass spectrometric analysis – AmaZon electron transfer dissociation (ETD)

The LC-MS/MS analysis was performed on an Ultimate™ 3000 RSLCnano HPLC system (Thermo Scientific Dionex) coupled to an Amazon ion trap mass spectrometer (Bruker) with a CaptiveSpray nano Booster ion source (Bruker). Tryptic peptide mixtures were automatically injected (3 µL) and loaded at a flow rate of 4 µL/min in loading solvent (2% acetonitrile and 0.1% formic acid in HPLC-grade water) onto a nano trap column (75 µm i.d. × 2 cm, packed with Acclaim PepMap100 C18, 3 µm, 100 Å; Dionex). Peptides were eluted and separated on the analytical column (75 µm i.d. × 25 cm, Acclaim PepMap RSLC C18, 2µm, 100 Å; Dionex) by a multi-step gradient. Starting conditions consisted of 96% solvent A (0.1% formic acid in HPLC grade water), 4% solvent B (0.1% formic acid in acetonitrile) at a flow rate of 250 nL/min. Peptides were eluted from the column by graduated introduction of solvent B to 25% at 70 minutes, the rate was increased up to 60% at 90 min and to 90% at 90.5 minutes. The column was washed with solvent B (90%) for 10 min before equilibration in the starting conditions for a further 20 min. The complete run time was 120 min.

The eluted peptides were analysed using an AmaZon ion trap ETD mass spectrometer. From the mass spectrometry (MS) survey scan with a mass range of 300–1,500 Da, the five most intense multiply charged ions were selected for fragment analysis in the ion trap if they exceeded an intensity of at least 2500 counts. Every ion selected for fragmentation was excluded for 20 seconds by dynamic exclusion. Fragmentation was actioned consecutively by both collision-induced dissociation (CID) and electron transfer dissociation (ETD). The normalised collision energy for CID was optimised automatically by Smartfrag (Bruker).

For the qualitative peptide search, the raw data was analysed using Mascot (Matrix Science version 2.4.0) and Bio Tools (Bruker). All the MS/MS spectra were searched against the SwissProt database using Mascot. The search was restricted to the mammalian database, assuming the digestion enzyme trypsin, a fragment ion mass tolerance of 0.5 Da and a parent ion

tolerance of 0.5 Da. Carbamidomethylation of cysteine was specified as a fixed modification and oxidation of methionine as a variable modification.

2.5 Zebrafish Methods

2.5.1 Maintenance

Both AB and TL wild-type zebrafish strains (https://zfin.org/action/genotype/view/ZDB-GENO-960809-7, and https://zfin.org/action/genotype/view/ZDB-GENO-990623-2) were maintained and bred at 26.5°C and the embryos were raised at 28.5°C as previously described (Westerfield, 1993).

2.5.2 Embryo production, collection and mounting

The night prior to the microinjection, eight fish pairs were set up in breeding tanks with the separators in place and on the following morning (after the day-light cycle turned on) separators were removed from all the tanks for the fish to begin mating. Tanks were monitored at 30 minute intervals and embryos were collected immediately after laying by using a strainer. The collected embryos were then rinsed with embryo medium (EM3: NaCl, 13.7 mM; KCl, 0.54 mM; $MgSO_4$, 1.0 mM; $CaCl_2$, 1.3 mM; Na_2HPO_4, 0.025 mM; KH_2PO_4, 0.044 mM; $NaHCO_3$, 4.2 mM) and transferred to a Petri dish. Unfertilized eggs were removed with a plastic transfer pipette. To prepare embryos for microinjection, the embryos were carefully lined up against the edge of a glass slide mounted on a polycarbonate plastic embryo holding tray as described (Rosen *et al.*, 2009) with the aid of a transfer pipette.

2.5.3 Needle pulling and loading morpholinos

For the microinjection, 1.0 mm x 0.5 mm glass capillaries (Borosil, India) were used. To create the capillary needles, the glass capillaries were pulled in a Flaming Brown micropipette puller (Sutter instruments, CA, USA) and stored in a Petri dish prior to use. The morpholinos were loaded onto a capillary needle using a syringe attached to a micromanipulator-mounted micropipette attached to a microinjector (World Precision Instruments, Sarasota, FL, USA). After loading the morpholinos into the needle, the injection volume was calculated and adjusted accordingly and the injection pressure adjusted as needed.

2.5.4 Microinjection

All the microinjections were performed when the embryos were at the one- or two-cell stage. Each embryo was carefully injected with 1-5 nL (0.5-2.5 pmol) of morpholinos, into the embryo yolk; the yolk circulation carries the morpholinos into the cells of the embryo. After completing the injection of a row of embryos (about 50 embryos) the embryos were collected using a gentle stream of embryo medium into a clean Petri dish. Approximately 40-60 embryos were injected per concentration and all the embryos were raised in an incubator at 28.5°C. At the end of day one, all the dead embryos were removed and the embryo medium replaced to minimise the chance of infection. All the embryos were observed for 2-3 days and the number of dead embryos recorded, as well as carefully assessing any for phenotypic differences. Control embryos were injected with a matching volume and similar concentration of control morpholinos, directed against eGFP. The embryo pictures were captured using a Nikon SMZ1500 microscope attached to a 1.2 megapixel DXM1200 temperature cooled CCD camera (Nikon, UK).

2.5.5 Morpholino design

The morpholinos were designed either to include an intron or to skip an exon by hindering the spliceosome activity; this splicing change will induce a frame-shift to create an early stop codon downstream to result in a truncated form of the protein or complete knockdown of the protein. All the exon-intron boundaries were subjected to exonic splicing enhancer/ suppressor sequence prediction by using ESEfinder (Cartegni *et al.*, 2003) to obtain a graphical representation of the putative splicing enhancer sequences and exonic splicing suppressor

sequences within the exons of interest. From these sequences, morpholinos (PMO) were designed to bind with the sequences predicted to be involved in recognition by ESE elements. Also in the design process, the predicted secondary structure of the pre-mRNA was considered by using RNA folding software mfold, and PMOs were only designed to the areas of open

Gene	**PMO sequence**	**Target**
Zebrafish *odf2-likest*	CGGAGAAGACGACCGTGTTTTCATC	Start codon
Zebrafish *odf2likeE1i1*	GGAGGATATGGTCAAACCTGGCTCC	Exon1 intron 1 boundary
Zebrafish *cep72st1*	TTATGGGCAAACCGTCTACCGCCAT	Start codon
Zebrafish *cep72E2i2*	GAATAAATAATATTCACCTGAACTG	Exon 2 intron 2 boundary
Zebrafish *cep72i2E3*	ATCCCCTACAAACATCCACATGACC	Intron 2 exon 3 boundary
eGFPst	ACAGCTCCTCGCCCTTGCTCACCAT	GFP start codon

Table 2-6 Site directed PMO sequences.

confirmation or have their ends in open loop structures, as described (Duan, 2011). All the PMOs were purchased from Gene Tools (Philomath, OR, USA) and stored in aliquots at -20°C. PMO sequences are given in Table 2.6; further information about their design is included in the Results chapters 3 and 4.

2.5.6 Whole-mount immunostaining

For whole-mount preparation, 1-day old embryos were fixed in cold methanol overnight and then washed twice for 30 min each in PBS with 0.2% Triton X-100 and then in PBS for 30 min. Embryos were then blocked for 4 h in 10% heat-inactivated goat serum, 1% bovine serum albumin, and 0.2% Triton X-100 in PBS.

To observe embryos beyond the 1-day stage, embryos were incubated in embryo medium containing PTU (0.2 mM phenylthiocarbamide; Sigma-Aldrich, P7629) to prevent pigment formation. Once the embryos had developed to the required stage, embryos were washed with embryo medium then fixed in 2% TCA for 3 h at room temperature. After fixation, embryos were washed three times in PBS for 5 min each. Fixed embryos were then washed twice in PBS with 0.8% Triton X-100 (PBT) at room temperature and then chilled on ice prior to permeabilization. Embryos were permeabilized by incubation in 0.25% trypsin-EDTA in Hank's balanced salt solution (Gibco, 14170112) for 5 min on ice and then washed five times for 5 min in PBT at room temperature. Embryos were blocked by incubation for 1 h in 10% heat-inactivated goat serum at room temperature.

Embryos were incubated with primary antibody diluted in blocking solution for 48 h at 4°C. Embryos were washed in PBS for at least 5 washes over the course of a day and overnight. Embryos were then incubated with secondary antibody in blocking solution for 24 h at 4°C. The primary antibodies used were rabbit anti-γ-tubulin (Sigma-Aldrich, T5192), 0.6 µg/mL, and mouse anti–acetylated tubulin (Life Technologies, 32-2700,) 1 µg/mL. Secondary antibodies used were Alexa 594-conjugated goat anti-mouse IgG (Invitrogen) (1:1000), and Alexa 488-conjugated goat anti-rabbit IgG (Invitrogen) (1:1000). Cell nuclei were co-stained with TO-PRO-3 Iodide (Molecular Probes, T3605) (1:1000) with the secondary antibodies. Confocal stacks were obtained with the Olympus FX81/FV-1000 laser confocal system using Argon gas laser and

Helium-Neon diode laser. Image Z-stacks were analysed using Olympus FV-1000 Fluoview software.

2.6 Statistical methods

Student's t-test was used to test for statistically significant differences in the means of the control and treated samples. The software package SPSS version 20 was used to perform these statistical tests. Where there were three (or more) treatment groups, one-way Analysis of Variance (ANOVA) was used to test for statistically significant differences in the means, to avoid Type I statistical errors. For ANOVA, Statistica (StatSoft) version 10 software package was used. For nonparametric, categorical variables, Fisher's exact test was used to test the statistical significance of the effects between the experimental groups. For Fisher's exact test, SPSS version 20 software package was used. Differences were considered statistically significant if $p<0.05$ (*).

Chapter 3:

The Investigation of the Role of Cep72 in Zebrafish

3.1 Introduction

The human CEP72 protein (KIAA1519) is encoded by the *CEP72* gene (Gene ID: 55722) located on Chromosome 5p15.33. The gene was first recognised and the cDNA isolated from a library by Nagase *et al.* (2000) and was further characterised structurally and functionally by Oshimori *et al.* (2009); and Stowe *et al.* (2012). Mouse Cep72 was first described as a centrosome protein (Andersen *et al.*, 2003) and as a Kizuna (Kiz) targeting protein that might be playing a role in microtubule organisation via further associating with γ–tubulin ring complexes (γ-TuRC) and CG-NAP (Oshimori *et al.*, 2009). It was also demonstrated to associate with centrosome satellite protein PCM-1 in high-throughput yeast two-hybrid screening (Rual *et al.*, 2005; Xin *et al.*, 2009) and in co-immunoprecipitation methods (Stowe *et al.*, 2012). However, a study conducted by Stowe *et al.*, (2012) formally identified CEP72 as a centriolar satellite protein which is required for recruitment of CEP290 to centriolar satellites and might be negatively regulating ciliary recruitment of another satellite-associating protein, BBS4.

CEP72 is related to Leucine Rich Repeat Complex 36 (LRRC36) protein and it has been suggested that CEP72 and LRRC36 are part of a duplicated genome region in mammals (Stowe *et al.*, 2012). However, CEP72 is only localised to centriolar satellites whereas LRRC36 is localised to centrosomes and with γ-tubulin; this suggests that despite the stuctural relationship, the two proteins are functionally divergent (Stowe *et al.*, 2012). Furthermore, orthlogues of CEP72 can be found in chordates, deuterostomes, schistosomes and in ciliated placozoan but not in *Chlamydomonas* or *Caenorhabditis* and the similar protein domain structure to that of PCM-1 suggests the functional co-evolution relationship between these two satellite proteins (Hodges *et al.*, 2010; Stowe *et al.*, 2012).

NCBI predicted 4 splice variant transcripts for the human *CEP72* gene (Ensembl ID: ENSG00000112877) and only one transcript has been identified to encode protein (Ensemble Trenscript ID: CEP72-001 ENST00000264935) (Figure 3.1 A). The CEP72 protein coding variant

(CEP72-001) consists of 12 exons and encodes a protein of 647 amino acids with two leucine-rich repeats (LLR) flanked by LLRCap domain in its N-terminus and a putative coiled-coil domain in its C-terminus region (Figure 3.3).

Previous work published by Stowe *et al.* (2012) identified human CEP72 as a centriolar satellite protein that associates with CEP290 and PCM-1. They also demonstrated that CEP72 is essential for relocating BBS4 from satellites to the cilium. Depletion of PCM-1 in mammalian cells results in CEP72 and CEP290 being localised to the centrosome from satellites. Furthermore, depletion of PCM-1 does not affect the localisation of BBS-4 to the cilium. Therefore, BBS4 might be relying on CEP72 to localise to the cilium during ciliogenesis. Although reduction of ciliogenesis is observed in CEP72 or CEP290 depleted cells, this reduction might have been due to the ineffective recruitment of BBS4 and the BBsome to the cilium rather than through a direct role in ciliogenesis of these proteins. Therefore, the role of CEP72 in ciliogenesis is subtle and unclear. The primary cilium plays a pivotal role in development from defining the left-right symmetry to cell migration and in signalling pathways such as Wnt and Shh. Therefore, it raises the question of whether CEP72 plays any role in development. CEP72 has also been implicated to target Kiz to the spindle pole and is essential for forming the focused bipolar spindle, needed for proper tension generation between sister chromatids (Oshimori *et al.*, 2009). Furthermore, CEP72 is also involved in γ-TuRC recruitment to the centrosome and CG-NAP, therefore facilitating the microtubule organising activity and structural integrity of the centrosome. At the onset of mitosis, centrosome maturation occurs through the expansion of PCM by recruiting many components essential for mitosis and this seems to be needed to nucleate an adequate number of microtubules for spindle organisation (Blagden and Glover, 2003). During this expansion process, PCM is stabilised by Kiz and is essential for the correct spindle formation (Oshimori *et al.*, 2006). Therefore, Kiz-CEP72 interaction also suggests a probable involvement of CEP72 with the cell cycle progression.

All of the previous studies were conducted using immortal cell lines to explore the function of CEP72 in centrosome and ciliogenesis. Although, *in vitro* models are important in understanding the basic function of a protein, *in vivo* studies are essential for understanding the complete manifestation of a protein in a biological system. Furthermore, parallels can be drawn between primary cilia and developmentally important nodal cilia; however, functional differences exist between the two cilium types making it impossible to study the effect on development by just using *in vitro* models alone.

Zebrafish is an attractive model for studying early developmental defects and has been used as a model to study vertebrate ciliogenesis. Mutagenesis and gene knockdown experiments have been able to identify numerous proteins involved in maintaining ciliary structure, function, ciliogenesis and signalling (Sun *et al.*, 2004; Kramer-Zucker *et al.*, 2005; Wilkinson *et al.*, 2009).

Morpholino oligonucleotides (MOs or PMOs) have been used as an effective tool for gene-specific knockdown in model systems such as zebrafish (Ekker, 2000; Choksi *et al.*, 2014) and in cells (Morcos, 2001) (excellent reviews of morpholinos can be found in (Summerton and Weller, 1997; Summerton, 1999; Heasman, 2002; Summerton, 2007)). Morpholino oligos can be used to block the initiation of translation, by binding over and preventing recognition of the start codon. Alternatively, morpholinos can be used to experimentally manipulate splicing machinery. This is a powerful technique to study the function of an individual transcript by altering splicing to generate “loss of function” (knockdown) by means of exon deletion or by inclusion of an intron. The mechanism of altering the transcript structure is due to the interference with the pre-mRNA processing steps by preventing splice-directing small nuclear ribonucleoprotein (snRNP) complexes from binding to their targets at the junctions of exon-introns on the strand of pre-mRNA, or by blocking the nucleophilic adenine base and preventing it from forming the splice lariat structure, or by interfering with the binding of splice regulatory

proteins such as splice silencers and splice enhancers (Draper *et al.*, 2001; Bruno *et al.*, 2004; Morcos, 2007).

Therefore, in this chapter, I sought to investigate whether *Cep72* plays a role in zebrafish development and in ciliogenesis.

3.2 Cep72 in zebrafish

Human *CEP72* has four splice variants (Figure 3.1 A). In contrast, the zebrafish (*Danio rerio*) *Cep72* gene (Ensembl ID: ENSDART00000163151), located on chromosome 16, is predicted to have only a single transcript (Figure 3.1B). The human CEP72 protein consists of 647 amino acids, while zebrafish Cep72 is 532 amino acids (Figure 3.2). Pairwise comparison shows that zebrafish Cep72 protein is 25% identical to the human homologue, overall (Figure 3.2). The most conserved region of the sequence is over the first 200 amino acids, with 48% identity (Figure 3.2); this region contains the leucine rich repeat (LRR) domains (from 60-160 amino acids) in the human CEP72 protein (Figure 3.3). Both the human and zebrafish amino acid sequences were analysed using SMART (Simple Modular Architecture Research Tool: http://smart.embl-heidelberg.de) domain search database (Schultz *et al.*, 1998; Letunic *et al.*, 2015). However, while the SMART search identified the LRR domains in the human protein, no LRR domains were identified in zebrafish. Instead, SMART predicted an LRRcap domain (a motif which normally occurs after leucine rich repeats and is typical in LRR-containing proteins) in the N-terminus of the zebrafish Cep72 and a putative coiled-coil domain in the C-terminus (Figure 3.3).

Since zebrafish Cep72 is the closest zebrafish homologue to the human CEP72, I expected to have a high degree of domain conservation between homologues. However, the above results suggest that the protein is not highly conserved.

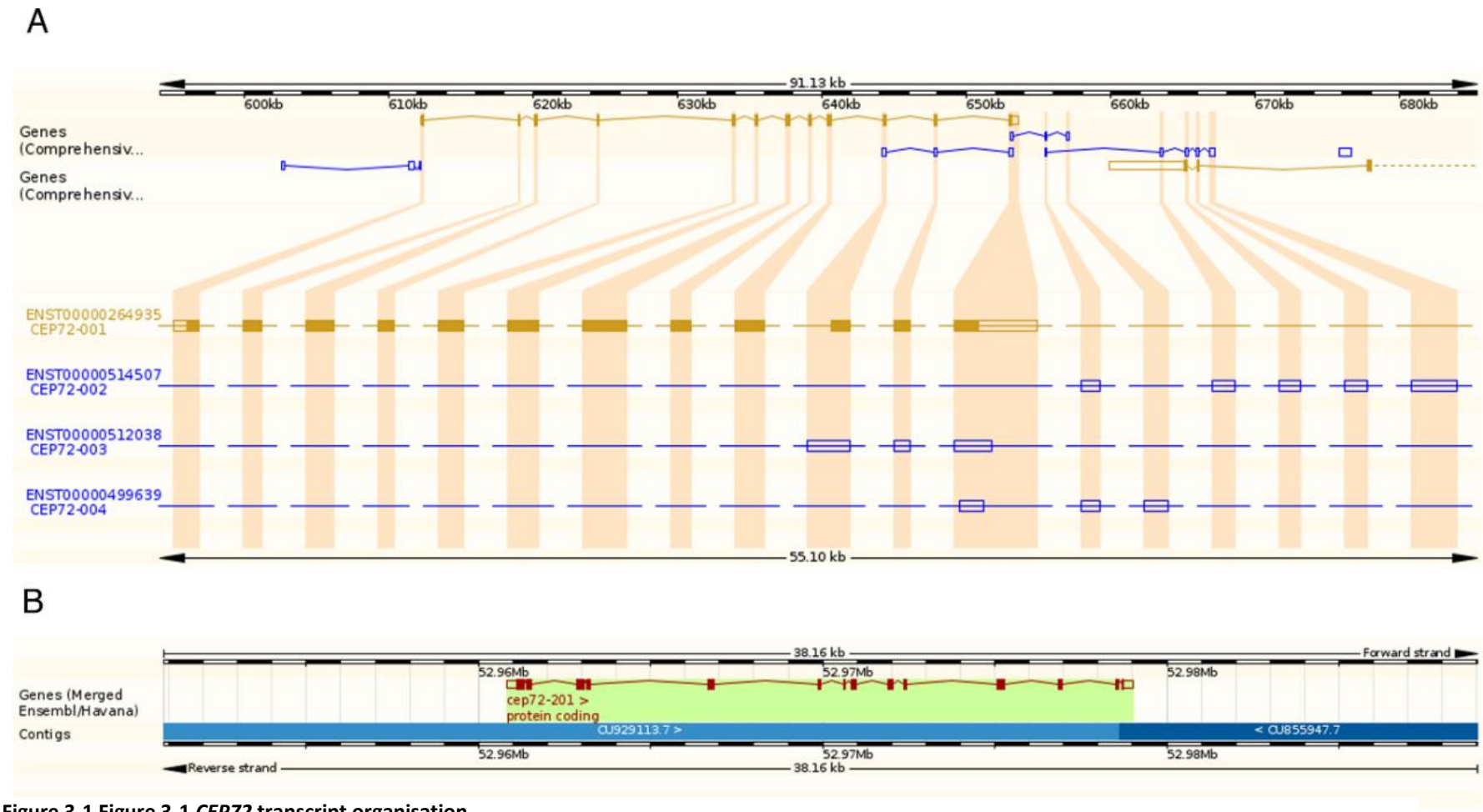

Figure 3-1 Figure 3-1 *CEP72* transcript organisation.

(A) Human *CEP72* gene organisation and 4 predicted transcripts, taken from Ensembl. **(B)** Zebrafish *cep72* gene organisation and single predicted transcript.

Figure 3-2 Amino acid comparison between human CEP72 and zebrafish Cep72.

Pairwise comparison of human (HsCEP72) and zebrafish (ZfCep72) Cep72 using EMBOSS Needle. The alignment show 25% amino acid identity (44% similarity) with the most conserved region being the first 200 amino acids, where the proteins show 48% identity. Vertical lines indicate amino acid identity; colons show similarity. Dashed lines represent gaps.

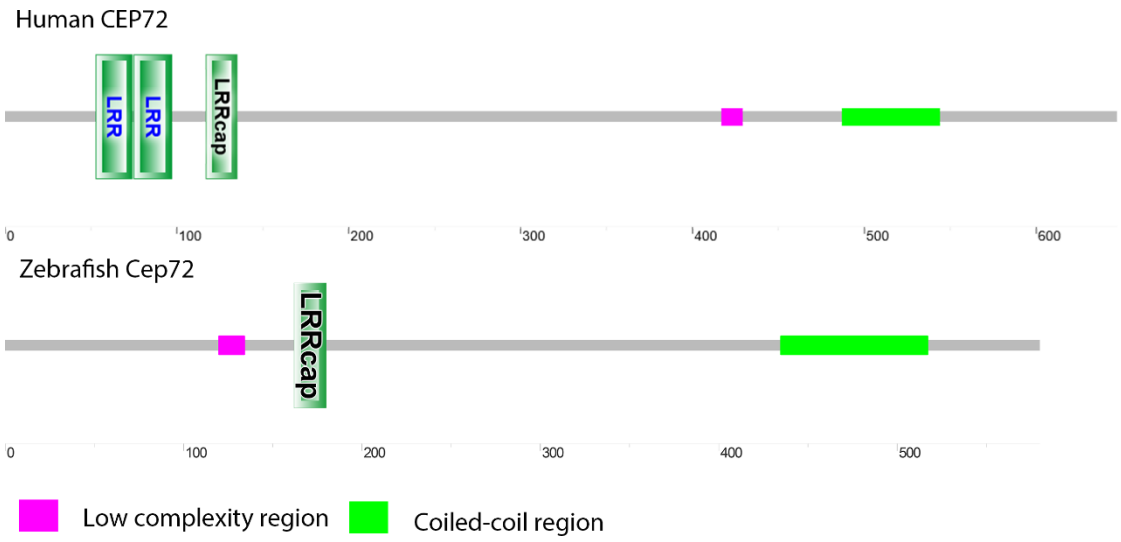

Figure 3-3 Schematic diagram of the domain organisation of human and zebrafish Cep72 obtained from SMART domain search.
Low complexity regions are highlighted in pink; coiled-coil domains are highlighted in green. The SMART search recognised the coiled-coil domain in both of the homologues, however Leucine-rich repeats (LRR) were only recognised in human Cep72.

These findings were contradicting since Cep72 is a member of leucine-rich-repeat super family of proteins and earlier studies were reported that LRR domains are conserved in vertebrates and sea urchins (Oshimori *et al.*, 2009). Therefore, to validate the above finding further, I also analysed both human and zebrafish Cep72 sequences using NCBI conserved domain search database (CDD) (http://www.ncbi.nlm.nih.gov/Structure/cdd/cdd.shtml) (Marchler-Bauer *et al.*, 2009; Marchler-Bauer *et al.*, 2015). The full search using CDD v3.14 recognised the N-terminus LRR domains (LLR4 and LLR8) in both human and zebrafish Cep72 homologues, while domains for APG6 (Autophagy protein 6), LAG3 (Lymphocyte-Activation Gene 3) and COG (Clusters of Orthologous Groups of proteins) were found only in the C-terminus region in zebrafish Cep72 (Figure 3.4). The unique APG6, LAG3 and COG domains may indicate that zebrafish Cep72 might also be involved with other cellular functions, additional to human Cep72. However, further studies are needed to ascertain the existence and the roles of these domains.

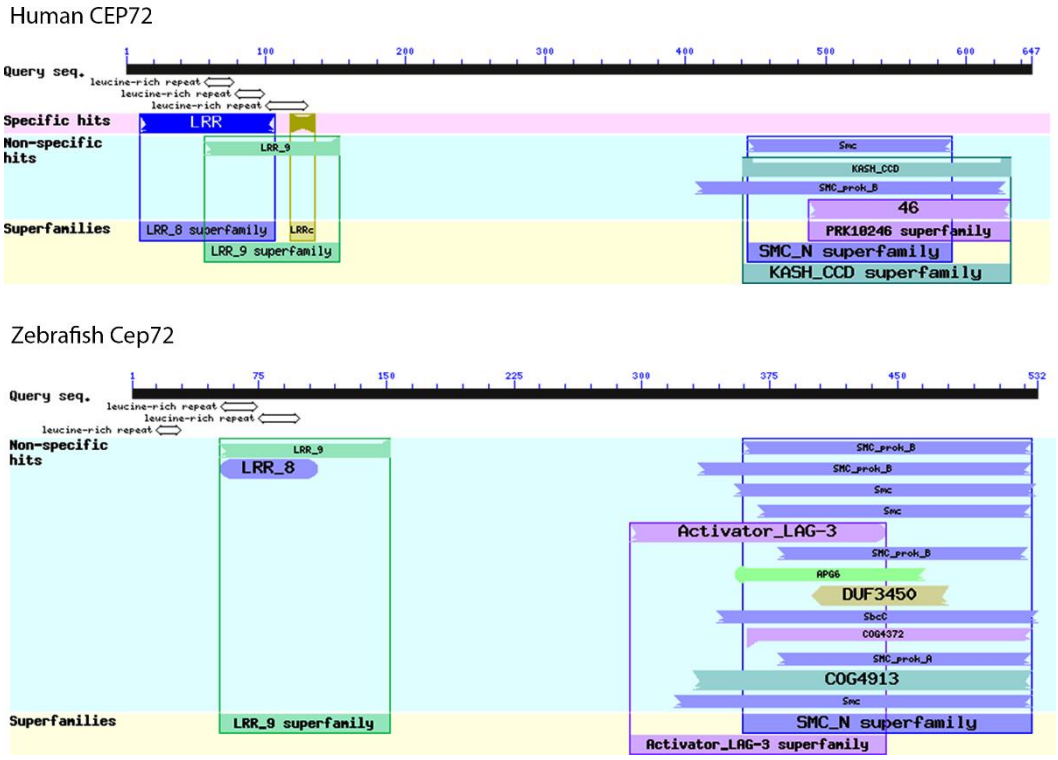

Figure 3-4 Schematic diagram of the human and zebrafish Cep72 domain organisation outputted from NCBI CDD search.
Both homologues of the Cep72 contain 3 Leucine-rich repeats (LRR) in the N-terminus. The C-terminus of the zebrafish Cep72 contains additional APG6, COG and LAG3 domains.

To evaluate the early developmental and embryological function of Cep72 in zebrafish, morpholino oligos (MO) were used to knock down the *cep72* gene expression in zebrafish.

3.3 Designing the morpholinos for cep72 knockdown

The design of morpholinos was based around previously published work from Draper *et al.* (2001), Howard *et al.* (2004) and Morcos (2007). One morpholino was designed to block the initiation of translation, and another to create a frame-shift by introducing an intron or by skipping an exon in the mRNA transcript.

To knock down the Cep72 transcripts in zebrafish, three morpholinos were designed. The first morpholino was designed to target the start codon (*cep72st*) to block translation. The next two

were designed to modify the splice machinery by targeting the exon 2-intron 2 boundary (*cep72E2i2*) to retain an intron within the transcript and by targeting intron 2-exon 3 boundary (*cep72E2i3*) to skip an exon from the mRNA strand. The two splice modifying morpholinos were optimally designed to block the spliceosome binding regions by designing anti-sense MOs to hybridise with the mRNA sequence motif to block the five small nuclear RNAs (snRNA: SRSF1, 2 ,4, 5 ,6) of the spliceosome (Figure 3.5 A,C). To design morpholinos, first the exon-intron boundaries (50 bases upstream and downstream from the exon-intron boundary) were analysed using ESEfinder version 3 to identify the snRNA binding regions and 25-mer oligonucleotide sequences were selected as the MO target sequences to provide optimal coverage and block the maximum number of snRNA binding sites (Figure 3.5 A,C). Secondly, I analysed the predicted secondary structure of the pre-mRNA to find an open confirmation or having their ends in open loop structure by using *in silico* RNA folding program mfold (Zuker, 2003) by inputting the exon sequence of interest together with 50 nt of intronic sequence both upstream and downstream of the exon. Only the sequences qualified with both the above requirements were used for morpholino design (Figure 3.5 B, D).

When designing the MOs, the position of the LRR region was also taken into consideration. Both splice modifying MOs were designed to target the LRR domain regions to disrupt the LRR domain by adding intron 2 after the exon 2 or by completely removing exon 3 from the transcript (Figure 3.5, E). These inclusions of intron and exclusion of exon should result in a frameshift, creating a premature stop codon and therefore disrupting the protein synthesis; the truncated protein that is made is likely to be misfolded and degraded. Once the morpholinos were designed, the sequences were submitted for the Gene Tools LLC (Philmath, OR, USA) for further validation. In addition, the sequences were assessed for specificity by searching for nearly exact matches in other genes, using BLASTn (optimized for short input sequences). The only hits identified in zebrafish were for *cep72*. While this does not fully rule out the possibility of non-specific effects,

we subsequently analysed *cep72* mRNA expression as a direct test of the effect of the morpholinos (described later, Section 3.4.1).

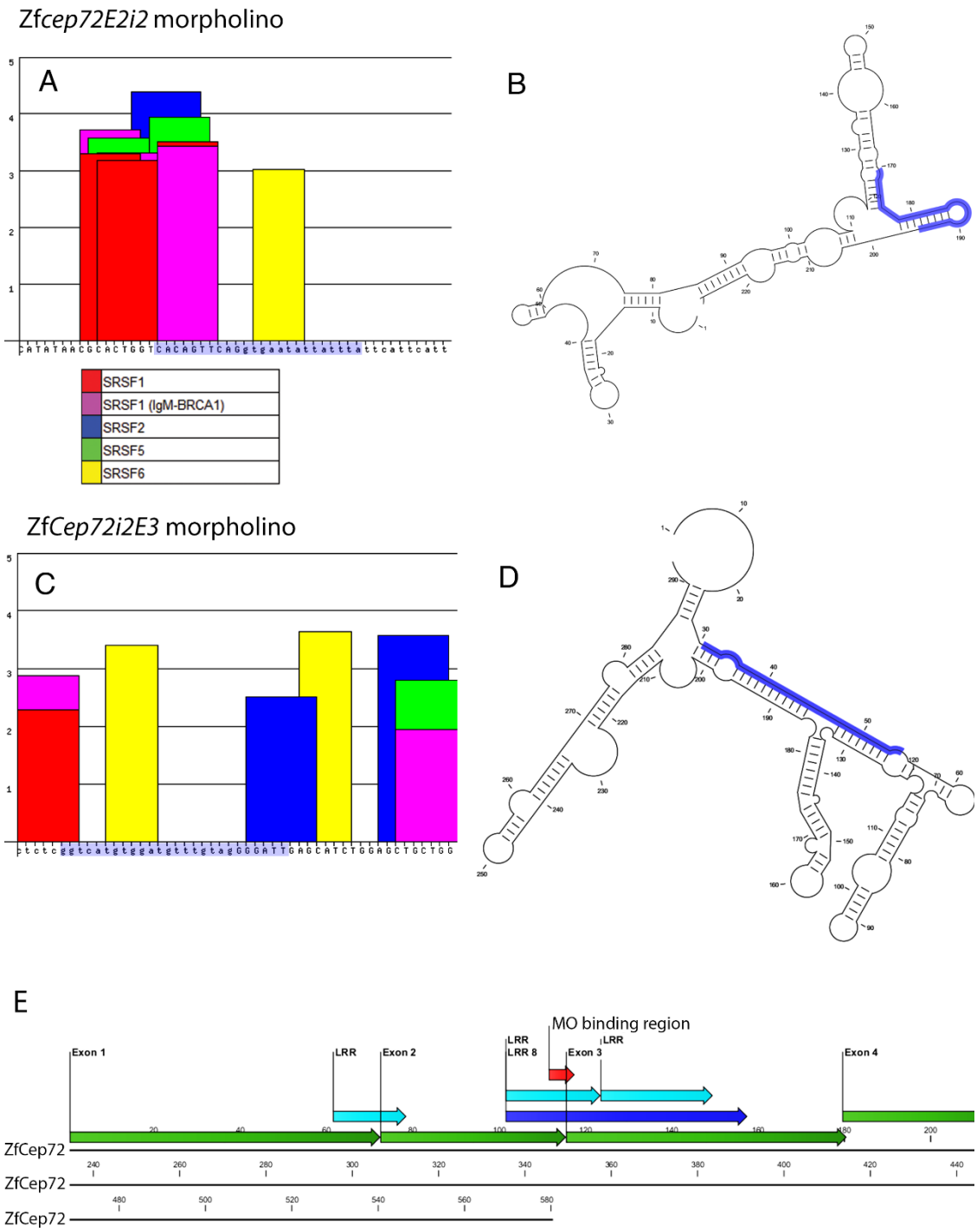

Figure 3-5 Schematic summary of the tools used for designing phosporodiamide morpholino oligomers (MO) to exon 2/exon 3 region.
(A) and **(C)** shows the results of ESEfinder analysis showing locations of SRp55, SRp40, SF2/ASF, SF2/ASF, and SC35 binding motifs above the established threshold value for each motif. Designed MO sequences are shown in blue. **(B)** and **(D)** Mfold secondary structure prediction for exon 2 and exon 3 of the zebrafish *cep72* gene. All the mfold analysis was performed using exon2 or exon3 plus 50 nucleotides of the upstream and downstream intron sequence and with maximum base-pairing distance of 100 nucleotides. The highlighted blue areas indicate the position of the MO target sites. **(E)** Schematic diagram to showing the sequence location of the leucine-rich repeat (LRR) domains in the nucleotide sequence and the MO targeting region. Targeting exon2-exon3 region will alter the LRR

domain in the protein and cause a frame shift. Figure 3-5 Schematic summary of the tools used for designing phosporodiamide morpholino oligomers (MO) to exon 2/exon 3 region.

3.4 Cep72 morphants in Zebrafish

To establish the effective concentration of morpholinos to use, embryos were injected with varying concentrations. The injected embryos were monitored for 48h and the number that died or showed morphological phenotypes were recorded (Figure 3.6).

The first morpholino tested was *cep72st*, which blocks the start codon and prevents translation. I found that increasing doses of the *cep72st* MO caused increasing mortality, as expected from the commonly reported toxicity of MOs (Figure 3.6A). I also observed an increasing proportion of embryos with ectopic otoliths, as *cep72st* MO dose increased, as well as a reasonable proportion of embryos showing morphological deformation in embryogenesis (Figure 3.6B-C). These highly deformed embryos were often characterised with a curved body axis, severe developmental delay, truncated tail and somewhat smaller brain (Figure 3.7D,H).

Similar experiments were conducted using two further morpholinos, to help confirm the phenotypes are caused by a specific effect on *cep72*. The *cep72i2E3* morpholino targets the splice junction between intron2-exon3, and should cause exclusion of exon 3 and therefore a frameshift; the remaining (truncated) protein is likely to be misfolded and degraded. A similar pattern of increasing mortality, increasing proportion of embryos with morphological abnormalities, and increasing proportion with ectopic otoliths was seen, with increasing dose of *cep72i2E3* MO (Figure 3-6 D-F). The *cep72E2i2* morpholino targets the splice junction between exon2-intron2, and should cause inclusion of intron 2 and therefore a frameshift. This morpholino appeared from initial tests to be highly toxic (Figure 3.6G) and was therefore not used further in this study.

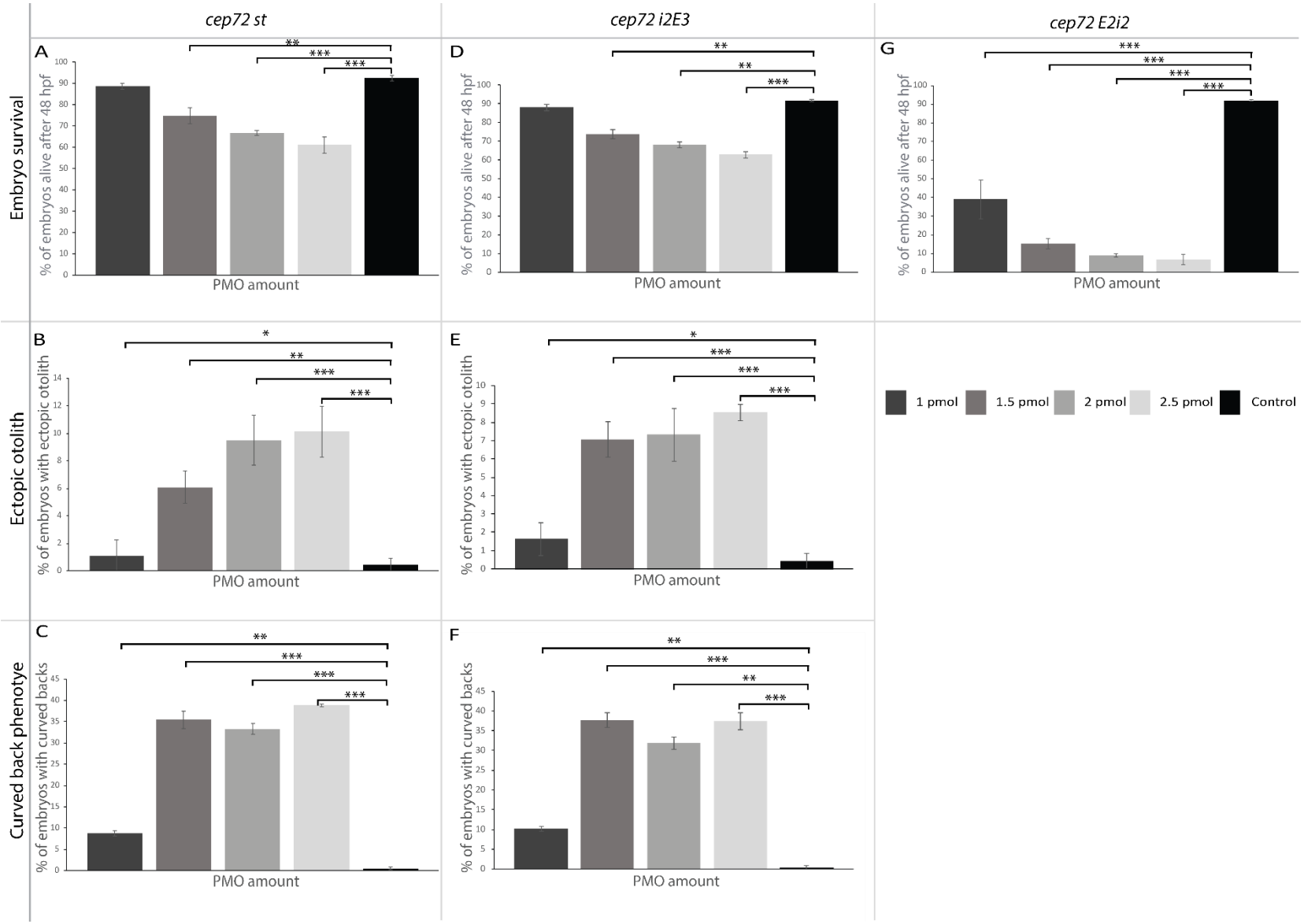
cep72 st
cep72 i2E3
cep72 E2i2
Embryo survival
Ectopic otolith
Curved back phenotye
A
B
C
D
E
F
G
% of embryos alive after 48 hpf
% of embryos with ectopic otolith
% of embryos with curved backs
PMO amount
1 pmol
1.5 pmol
2 pmol
2.5 pmol
Control

Figure 3-6 Efficiency of Cep72 morpholino injections.

Embryos were injected with 1 to 2.5 pmol of *cep72st* morpholino **(A-C)**, *cep72 i2E3* morpholino **(D-F)**, or *cep72E2i2* morpholino **(G)** or the GFP morpholino as a control, and cultured for 48 hours. **(A,D,G)** Percentage of embryos surviving after 48 h. **(B,E)** Percentage of embryos showing ectopic otoliths. **(C,F)** Percentage of MO injected embryos showing a curved body morphology, a phenotype typical of ciliary defects. Error bars: standard error of the mean percentage of 3 independent experiments. Fisher's exact test was used to statistically analyse significance; P value < 0.05 (*), 0.01 (**) and 0.001 (***).

Both the *cep72st* and *cep72i2E3* morpholinos generated a similar set of phenotypic defects in the morphants. The most apparent external phenotypic trait of the morphants was the curved body axis (Figure 3.7). Higher doses of morpholino caused exacerbation of this phenotype, and at the higher doses tested (2 and 2.5 pmol), embryos exhibited a truncated body axis and smaller brain (Figure 3.7 D,H). In addition, ectopic otoliths were observed in a higher proportion of the Cep72 morphants compared to the control (Figure 3.6, 3.7 I,J). Expanded brain ventricles were also seen in some of the morpholino treated embryos, compared to control embryos, indicative of hydrocephalus (Figure 3.7 K,L). During the third day of life, wild type and control MO injected embryos hatched and body curvature straightened over time in contrast to morphants which remained curved even after hatching.

The phenotypes observed match with the "ciliary phenotype" in zebrafish when known centrosome/ciliary proteins such as PCM-1 (Stowe *et al.*, 2012), IFT proteins (Sun *et al.*, 2004; Tsujikawa and Malicki, 2004), CEP proteins (Wilkinson *et al.*, 2009; Baye *et al.*, 2011) and PKD proteins (Sullivan-Brown *et al.*, 2008) were affected.

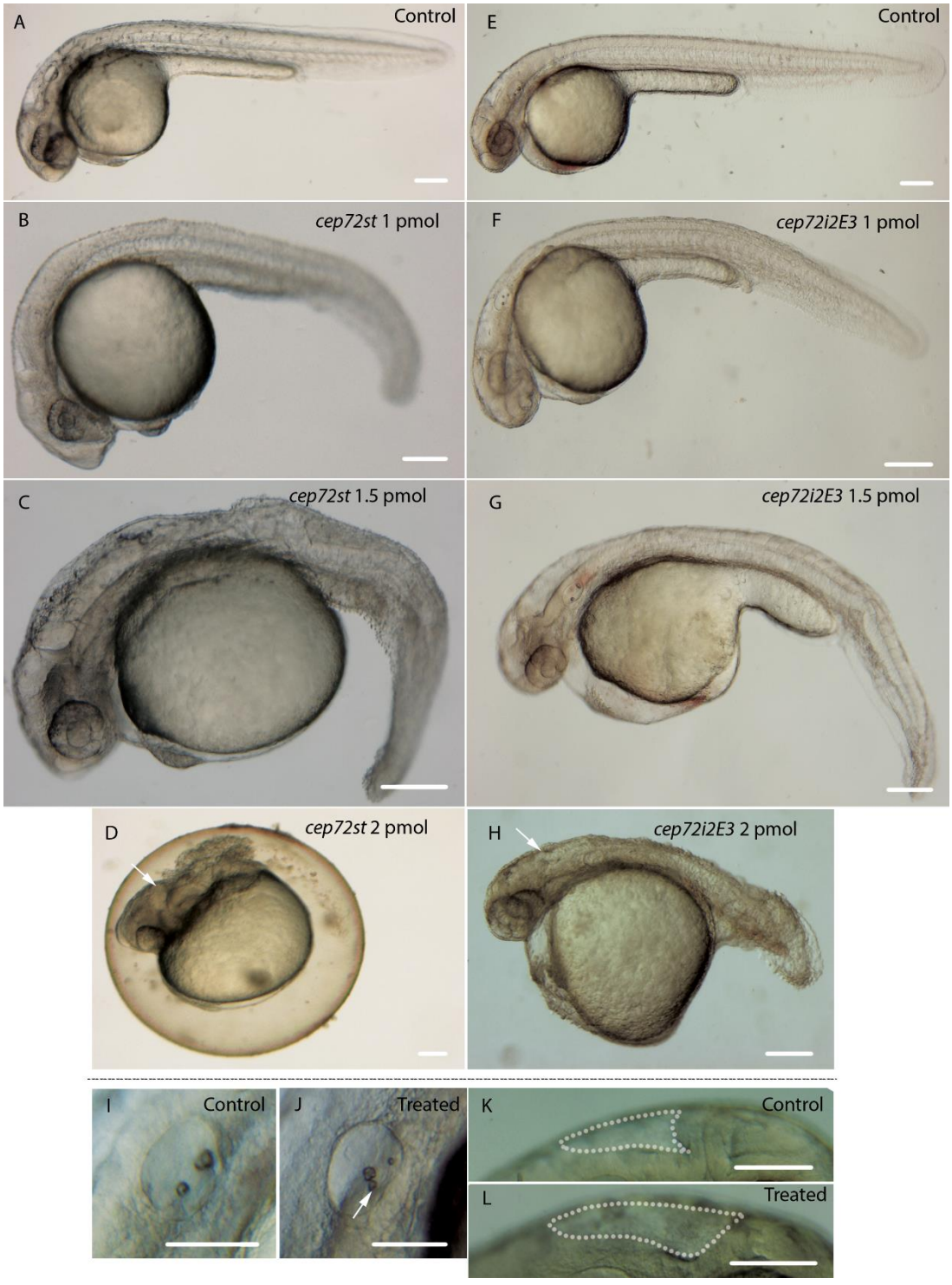

Figure 3-7 Morpholino knockdown of Cep72 with Cep72st causes multiple phenotypes associated with ciliary dysfunction in zebrafish embryos.
(A,E) Control MO injected zebrafish embryos. **(B-D)** *cep72st* morpholino injected zebrafish embryos showing a curved body phenotype **(B, C)**; higher concentrations of MOs cause a more severe form of the morphology, with truncated axis and smaller brain **(D)**. **(F-H)** *cep72i2E3* morpholino injected zebrafish embryos again showing a curved body phenotype (F-H) and higher MO concentrations cause more severe defects, with truncated axis and smaller brain (H). (**I,J**) Otolith organisation in control MO injected embryo **(I)** and abnormal multiple otolith phenotype in *cep72st* morpholino embryo **(J)**. **(K,L)** Brain ventricles in control MO treated embryo **(K)** and hydrocephalic phenotype in *cep72st* MO embryo **(L)**. Scale bar: 100 µm.

3.4.1 Validation of Cep72 knockdown

The Cep72 morpholinos were designed to either block initiation of translation or cause a splicing alteration. The splicing morpholinos are expected to cause exclusion of exon 3 (*cep72i2E3*) or inclusion of intron 2 (*cep72E2i2*), by interfering with the splicing process. The efficiency of these altered splicing events can be effectively analysed by using RT-PCR with appropriate primer pairs to amplify the region of interest. In the RT-PCR, altered splicing can be observed as a band shift in gel electrophoresis (Figure 3.8B). However, in some cases of intron inclusion, only partial inclusion of the intron occurs due to activation of cryptic splicing sites within the intron and this also can be confirmed through the RT-PCR system by having a much smaller product than the expected product. Translation blocking morpholinos generally do not cause degradation of their RNA targets, so RT-PCR is not a suitable method for assessing the effectiveness of this approach.

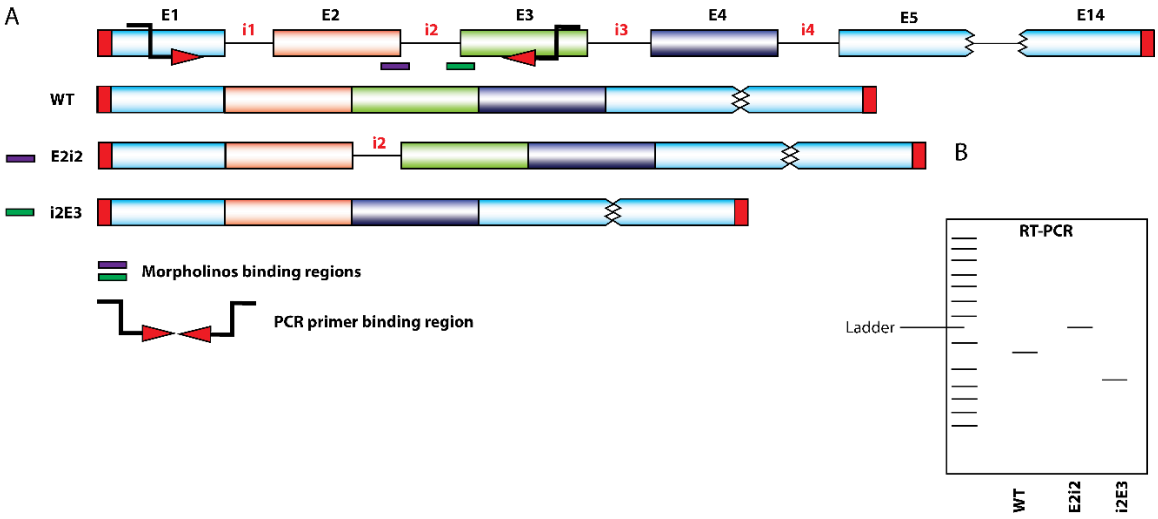

Figure 3-8 Schematic diagram showing the effect of the splice modifying morpholinos and the RT-PCR approach used for verifying the results.
(**A**) Exon-intron structure of the *cep72* gene, showing the splicing morpholino binding sites and the expected mRNA strands that result. The typical splice-blocking scenario involves deletion of an internal exon by masking spliceosome binding site in the intron-exon boundary (i2E3), or insertion of an intron by targeting junctions of the exon- intron boundary (E2i2) of a transcript. These splicing modifications can be assayed through a RT-PCR system, using primers that flank the modified region. (**B**) Theoretical gel image showing the expected outcomes from RT-PCR with the primer sites shown in **(A).** Removal of an exon (i2E3) should result in a shorter band than the wild type (WT) and addition of an intron (E2i2) should result in a much larger PCR product when amplified with the correct primer pair. The lane on the left depicts a marker ladder.

I used three different MOs to induce the knockdown of zebrafish *cep72*. The first was the translation blocking morpholino (*cep72st*) which binds with part of the 5'-untranslated region and the start codon of the mRNA; the effect of this morpholino cannot be tested by RT-PCR. The second morpholino is the *cep72E2i2* splice modifying morpholino which binds where the exon 2-intron 2 boundary occurs and results in the inclusion of the intron 2 sequence in the final mRNA. To confirm the effectiveness of this morpholino, RT-PCR was used to amplify the region between exon 1 and exon 3. This is predicted to give an amplicon of 1728 bp with this primer 1-2 combination (Figure 3.9A). The *cep72i2E3* splice modifying morpholino (the third morpholino) binds where the intron 2 and exon 3 boundary occurs and should result in the exclusion of exon 3 from the final mRNA sequence. RT-PCR amplifying between exons 1 and 5 (primers 1 and 3) is expected to produce an amplicon of 463 bp (Figure 3.9A).

For the RT-PCR, only the embryos showing the ciliary phenotype were used, to ensure that the embryos selected had been successful in the MO injection (as is standard practice with this type of experiment). cDNA quality was checked using β-actin primers as a control; all cDNA samples demonstrated β-actin amplification (Figure 3.9B,D).

For the *cep72i2E2* morpholino injected embryos, RT-PCR shows a band of ~400 bp, corresponding to the predicted wild-type fragment of 394 bp, and a second band of ~600 bp (Figure 3.9 C). The absence of this 600 bp band from both control samples indicates that the 600 bp band is unique to MO injected embryos and therefore seems to be a consequence of the MO action. However, it was expected to see a much larger amplicon product. If the full intron sequence was included in the transcript, the RT-PCR should have produced a band of 1728 bp. It is possible that the MO resulted in only partial inclusion of the intronic sequence into the transcript. This may due to activation of a cryptic splicing site within the intron, causing a different size insertion. Furthermore, the 400 bp band intensity from morphant samples was lower than in the controls indicating that there is a partial knockdown of the wild-type Cep72

transcript in zebrafish with this morpholino. I tried to sequence the 600 bp band by separating and amplifying the fragment using Band-stab PCR (Bjourson and Cooper, 1992) however this was unsuccessful in the time available.

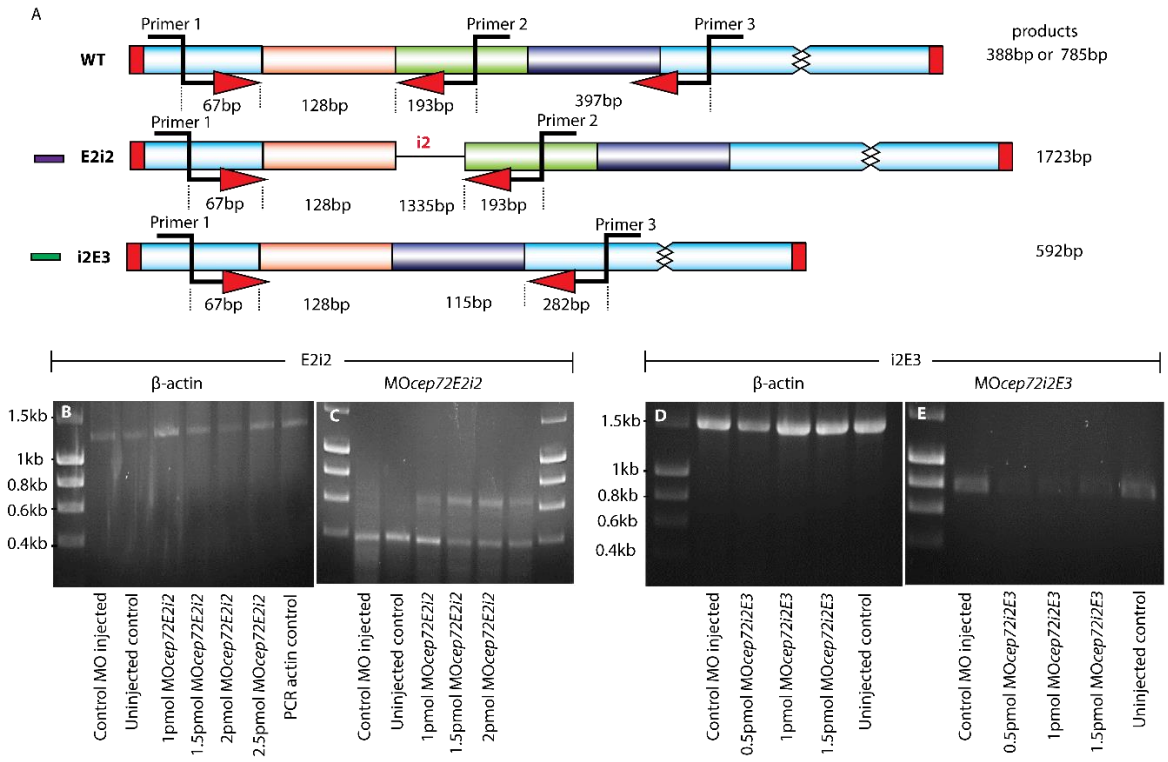

Figure 3-9 RT-PCR analysis of the splice-altering morpholino oligos on the zebrafish Cep72 transcript.

(A) Schematic diagram showing the expected amplicon sizes with the selected primers, and how these have been calculated. **(B)** and **(D)** Amplification of *β-actin* fragments (A: ~1.2kb, B:~1.5kb) using cDNA from controls and morpholino-injected embryos. **(C)** Amplification of *Cep72* using primers 1 and 2 from cDNA from MO*cep72E2i2* injected morphants, as well as control MO and uninjected embryos. A ~400 bp band can be observed in all samples, corresponding to the fragment expected from wild-type mRNA. Note that a band of approximately 600 bp is evident from all the MO*cep72E2i2* injected morphants samples, but is absent from the control MO injected and uninjected control. The extra ~200 bp might be due to intronic insertion but with activation of cryptic splicing. The reduced intensity of the 400 bp band from all the *cep72E2i2* MO injected samples indicates a corresponding partial knockdown of wild-type *cep72*. **(E)** PCR amplification of *cep72* using primers 1 and 3 from cDNA from MO*cep72i2E3* injected morphants, as well as control MO and uninjected embryos. The control MO and uninjected embryos produce a band of the expected size, while this band disappears from MO*cep72i2E3* injected morphants, confirming the knockdown of the *cep72* mRNA.

Similarly, the RT-PCR was performed to check the effect on the mRNA in the *cep72i2E3* morpholino injected morphants. If exon skipping had occurred, the product size expected from the RT-PCR would be expected to decrease from 661 bp to 463 bp. The full length (661 bp) product was observed from the control MO and uninjected embryos. The RT-PCR results also show a near-complete disappearance of the 661 bp band in the MO*cep72i2E3* injected embryos, although the 463 bp band was not observed (Figure 3.9 E). This is perhaps as expected since effective exon skipping has been reported to induce complete degradation of the mRNA transcript (Eisen and Smith, 2008; Sud *et al.*, 2014). Also the MO*cep72i2E3* was more effective in generating the curved phenotype even with lower concentrations of the morpholinos than the *cep72E2i2* morpholino. Hence it can be concluded that *cep72i2E*3 morpholino was more effective in knocking down zebrafish *cep72*. The specific effects evident on the *cep72* mRNA suggest that off-target effects from these morpholinos is unlikely and the results represent a genuine knockdown of the *cep72* mRNA. We selected embryos with a phenotype for this analysis; it would be interesting in future experiments to compare the extent of knockdown in MO injected embryos that did not show an abnormal phenotype.

3.5 Zebrafish Cep72 does not mediate ciliogenesis

The phenotypes observed in embryos injected with the Cep72 MOs are typical of those seen when cilia or the centrosome are affected: curved body axis, ectopic otoliths, hydrocephalus and situs defects. To test whether Cep72 regulates ciliogenesis in zebrafish, 1-cell stage embryos were injected with MO*cep72i2E3* and morphants were collected at 27-30 hpf. Embryos were fixed with 4% formaldehyde and stained with anti-γ-tubulin and anti-acetylated α-tubulin to stain the centrioles and cilia respectively. Cilium length was measured using confocal microscopy. The proximal and distal ends of each individual cilium were determined by careful

examination through the range of optical sections (Figure 3.10A). Once these ends were marked, the horizontal length of each cilium was measured (Figure 3.10 B,C).

The morphants did not show a difference in cilium length in the pronephric duct (Figure 3.11) compared to the wild type and control morpholino injected embryos. The average cilium length for control and *cep72i2E3* morphants was 8.22 ± 0.41 µm and 8.12 ± 0.47 µm respectively. Therefore, knockdown of *cep72* does not appear to affect ciliogenesis in zebrafish. The function of Cep72 may be in ciliary function, or centrosome function, rather than in growth or maintenance of the cilium.

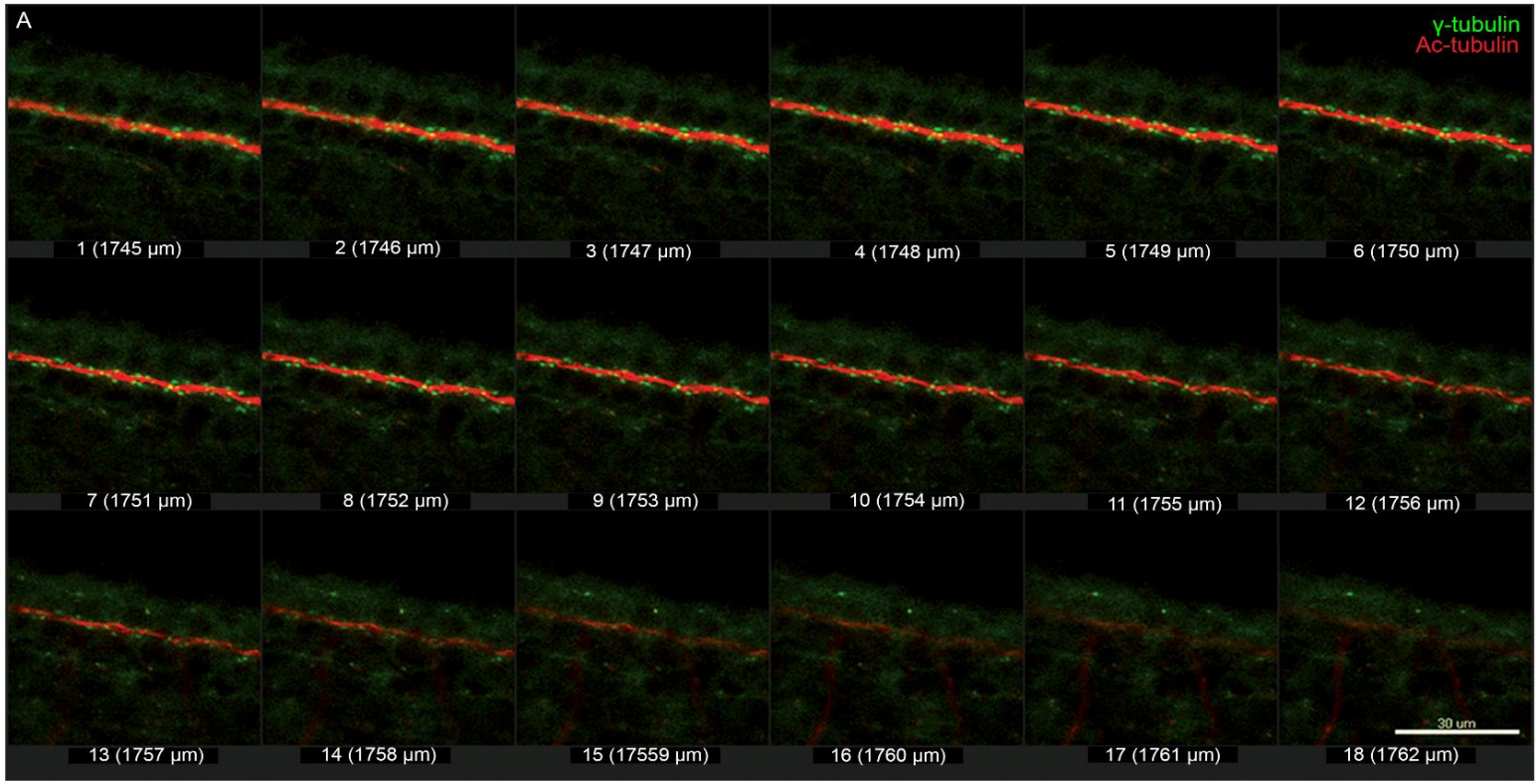
A
γ-tubulin
Ac-tubulin
1 (1745 µm)
2 (1746 µm)
3 (1747 µm)
4 (1748 µm)
5 (1749 µm)
6 (1750 µm)
7 (1751 µm)
8 (1752 µm)
9 (1753 µm)
10 (1754 µm)
11 (1755 µm)
12 (1756 µm)
13 (1757 µm)
14 (1758 µm)
15 (17559 µm)
16 (1760 µm)
17 (1761 µm)
18 (1762 µm)
30 µm
B
C
Cilium 2
Cilium 3
Cilium 1

Figure 3-10 Measuring pronephric cilia.

(A) Consecutive optical sections through the pronephros, showing the cilia stained with anti-acetylated tubulin (red) and the centrosomes stained with anti-γ-tubulin (green). Numbers refer to z-plane positioning; sections were taken at 1 µm intervals. Scale bar: 30 µm.

(B) Schematic representation of a cilium, protruding through multiple optical sections.

(C) Sections were examined carefully through the entire z-stack and the proximal and distal ends of individual cilia were marked. The horizontal measurement of the cilium was then determined. The vertical displacement of the cilium was not taken into account, however this would have altered the length by only around 6-7 µm, with the same discrepancy between both control and Cep72 MO-treated embryos.

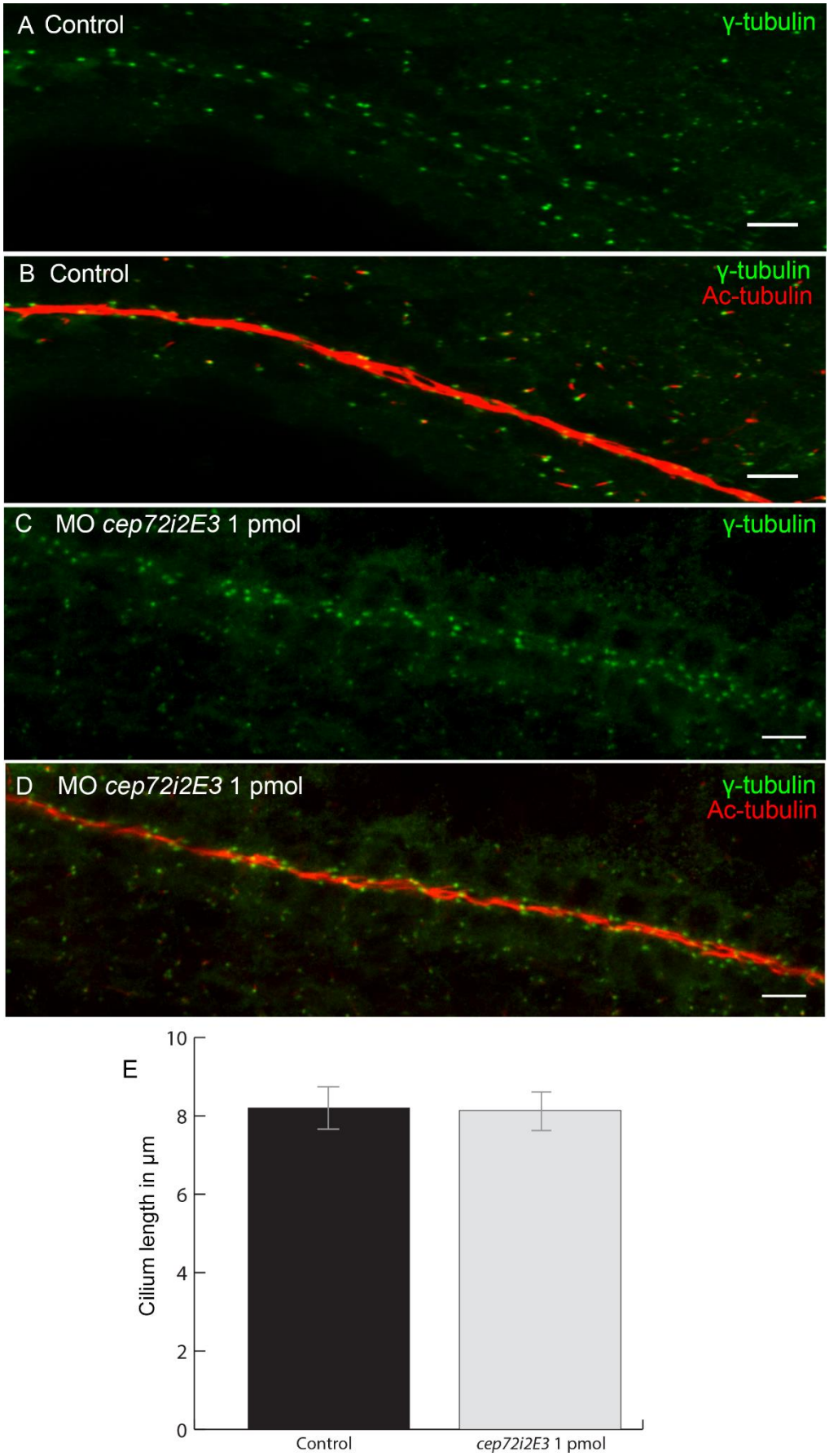
A Control
γ-tubulin
B Control
γ-tubulin
Ac-tubulin
C MO cep72i2E3 1 pmol
γ-tubulin
D MO cep72i2E3 1 pmol
γ-tubulin
Ac-tubulin
E
Cilium length in µm
0
2
4
6
8
10
Control
cep72i2E3 1 pmol

Figure 3-11 Knockdown of Cep72 in zebrafish does not affect ciliogenesis.

(A-D) *cep72i2E3* morpholino-injected **(C,D)** or control MO-injected **(A,B)** embryos were stained with acetylated α-tubulin and γ-tubulin to stain cilia (red) and centrosomes (green). Control and Cep72-morpholino injected embryos show similar pronephric cilia. Smaller cilia in the surrounding tissue appear different in these images, however this is due only to the level of the optical sections and no real differences exist. Scale bar 10 µm. **(E)** Cilium length comparison for the pronephric cilia, between the control and morphants. The average cilium lengths measured in control and morphants were 8.2 ± 0.41 µm and 8.12 ± 0.47 respectively. n =60. Error bars: SD.

3.6 Summary

In this chapter, I investigated whether Cep72 in zebrafish plays a role in ciliogenesis or cilium function. I have demonstrated that morpholino injections caused phenotypes to develop. The use of translation blocking and splice altering morpholinos gave comparable morphant phenotypes, making it likely that the effects are specific to Cep72 knockdown, rather than any off target effect.

Cep72 morphant phenotypes were comparable to the phenotypes observed with disruption of other ciliary proteins (Wilkinson *et al.*, 2009; Baye *et al.*, 2011; Stowe *et al.*, 2012; Choksi *et al.*, 2014). This is consistent with Cep72 playing a role in ciliary function. Although the pronephric cilia in Cep72 morphants appeared to be of normal length, it is possible that Cep72 disruption may affect development by compromising ciliary function or cilia mediated cell signalling, rather than through an effect on ciliary structure. This notion is especially true since Stowe *et al*. (2012) have shown that depletion of CEP72 significantly increased the amount of pericentriolar distribution of PCM-1 and corresponding centriolar satellites. However only a modest reduction in ciliogenesis was observed in CEP72 depleted cells. Furthermore, over expression of CEP72 severely affected ciliogenesis and sequestered PCM-1 reducing the pericentrosomal distribution of the centriolar satellites (Stowe *et al.*, 2012). Therefore, depletion of Cep72 may not directly affect ciliogenesis but may act through an indirect satellite protein recruitment mechanism, essential for ciliary function. Moreover, CEP72 plays a pivotal role in recruiting other proteins to

the cilium, including BBS4, CDK5RAP2, CEP152, WDR62 and CEP63 to the centrioles (Kodani *et al.*, 2015). Most of these proteins are implicated in centriolar duplication through the CDK2 dependant pathway and associate with primary microcephaly (MCPH) (Kodani *et al.*, 2015). The observation of smaller brain in higher morpholino doses in Cep72 morphants therefore may be due to the effect on the above proteins. Hence, the phenotypes observed in the Cep72 morphants may be due to some compromise of the interplay in these complex molecular systems. Therefore, further studies are required to explain exactly what mechanisms are involved in creating such phenotypes.

3.7 Future work

The ciliary phenotype observed may be caused by the compromised ciliary function, therefore studying functional aspects of the cilium may validate the phenotypical relationship with the depletion. Motile cilium functional assay can be performed using fluorescent micro-beads introduced into the Kupffer's vesicle (KV) and measuring the beads movement within the KV with live video microscopy as described (Okabe *et al.*, 2008). Perhaps sectioning of the brain and the eye and staining for the appropriate markers to MCPH also can confirm whether depletion Cep72 cause MCPH. However, I did not pursue this project further as it deviated from studying centriolar satellites and regulation of ciliogenesis.

Chapter 4:

Investigation of the Role of *odf2b* in Zebrafish

4.1 Characterisation of zebrafish odf2b protein

A previous study conducted in this laboratory has shown that knocking down the ODF2 homologue in zebrafish, *odf2a*, resulted in a failure to generate cilia in pronephric duct (Anila Iqbal, unpublished data). This is expected since Odf2 is a component of the distal appendages and essential for ciliogenesis (Ishikawa *et al.*, 2005). Zebrafish Odf2a protein (831 amino acids) shows 48% identity to human ODF2 (822 amino acids; Table 3.1), and is considered to be the homologue of ODF2. In fact, the zebrafish genome contains a second gene which encodes a protein with similarity to human ODF2: *odf2b*. Zebrafish Odf2a and Odf2b proteins share 48% identity (68% similarity), and Odf2b protein (810 amino acids) shows 38% identity with human ODF2 (Table 3-1). The zebrafish frequently has two homologues for every mammalian gene due to a duplication event during zebrafish evolution (Taylor *et al.*, 2003). Another protein in the sequence database is named ODF2-like (ODF2L); sequence comparisons show this has only 21% identity to ODF2, despite the name. The pairwise comparisons to zebrafish Odf2a and Odf2b show 19-21% identity, between the 4 different ODF2L isoforms (a-d) and either Odf2a or Odf2b (Table 4-1). ODF2L will be considered further in Chapter 4. Sequence information is given in Appendix 1.

Pairwise amino acid identity (similarity)						
	ZfOdf2a	HsODF2	HsODF2L-a	HsODF2L-b	HsODF2L-c	HsODF2L-d
ZfOdf2a		48% (67%)	20% (39%)	19% (38%)	20% (38%)	21% (39%)
ZfOdf2b	48% (68%)	38% (61%)	19% (38%)	19% (37%)	20% (37%)	20% (38%)
HsODF2	48% (67%)		21% (39%)	21% (37%)	21% (40%)	21% (39%)

Table 4-1 Comparison of zebrafish Odf2a and Odf2b with human ODF2 and ODF2L.

Numbers show amino acid identity (and similarity) determined from pairwise alignments generated with EMBOSS Needle.

While *odf2a* knockdown in zebrafish resulted in the loss of cilia in embryos, the function of odf2b has never previously been investigated. Therefore, I tested the role of Odf2b by knockdown in zebrafish embryos.

4.2 Knockdown of *odf2b* in zebrafish causes a ciliary phenotype

We therefore sought to deplete Odf2b from zebrafish embryos to examine the phenotype and the effect on ciliogenesis, in order to assess the functional effect of Odf2b.

To confirm the presence of the predicted sequence of zebrafish *odf2b*, the full length cDNA was amplified by RT-PCR. Due to the sequence similarities of the N-terminus of *odf2b* with *odf2a*, specific primers were designed to bind to unique sequences in the 5' UTR and just upstream from the stop codon, for both *odf2b* and *odf2a*. Both primer sets amplified an amplicon of the predicted size, around 2.5 kb, from 24 hpf embryos. The intensity of the bands for each PCR product, amplified from the same cDNA mixture, suggests that *odf2a* was more abundantly expressed in embryos than *odf2b* (Figure 4.3B).

For the knockdown of zebrafish *odf2b,* two morpholinos were designed: a translation blocking morpholino which targets the start codon (ATG) and a splice altering morpholino to target the intron1-exon2 boundary to skip exon 2 from the final mRNA. In both cases, morpholinos were designed to be specific to *odf2b* and not bind to *odf2a*. Both morpholinos target the untranslated regions – the 5'UTR or introns – where the sequence homology between *odf2a* and *odf2b* is very low. The morpholinos are therefore predicted to bind only to *odf2b* and not affect *odf2a*. The exclusion of exon 2 would result in a frame-shift in the sequence to induce a premature stop codon. This premature stop codon would create a truncated version of *odf2b*. The morpholinos were injected into single cell embryos as described in the Materials and Method section.

To establish the effective concentration of morpholinos, embryos were injected with a series of doses ranging from 1 pmol-4 pmol. For each concentration, viability and the morphant phenotype frequencies were recorded (Figure 4.1). From these experiments, 1-3 pmol doses were established as the most effective range for the embryos (Figure 4.1). Although, 4 pmol doses produced the highest number embryos with a phenotype, at this dose the embryo viability was severely affected (Figure 4.1).

The phenotypes observed in *odf2b* knockdown morphants resembled the ciliary phenotypes in zebrafish following knock down of other centrosomal proteins (Sullivan-Brown *et al.*, 2008; Wilkinson *et al.*, 2009; Stowe *et al.*, 2012; Huang *et al.*, 2014). The phenotype observed with *odf2b* morphants included extended body curvature (Figure 4.2B-H) with otolith defects (Figure 4.2J), swelling of the brain ventricles (hydrocephaly) (Figure 4.2N) and pericardial oedema (Figure 4.2L). A curved tail phenotype is first observed after 22 hpf-24 hpf, which was the first time point where the morphants were visually distinguishable. Both translation blocking (*odf2b*st) and splice altering (*odf2bE1i1*) morpholinos produced similar phenotypes (Figures 4.1 & 4.2).

Knockdown of *odf2a* also produces a phenotype similar to the “ciliary phenotype” observed in zebrafish. However, the *odf2a* morphant phenotype also has additional features such as reduced retinal size, reduced overall body size and marked reduction in size of the brain (microcephaly) making them more closely resemble an autosomal recessive primary microcephaly (MCPH) phenotype in zebrafish (Novorol *et al.*, 2013).

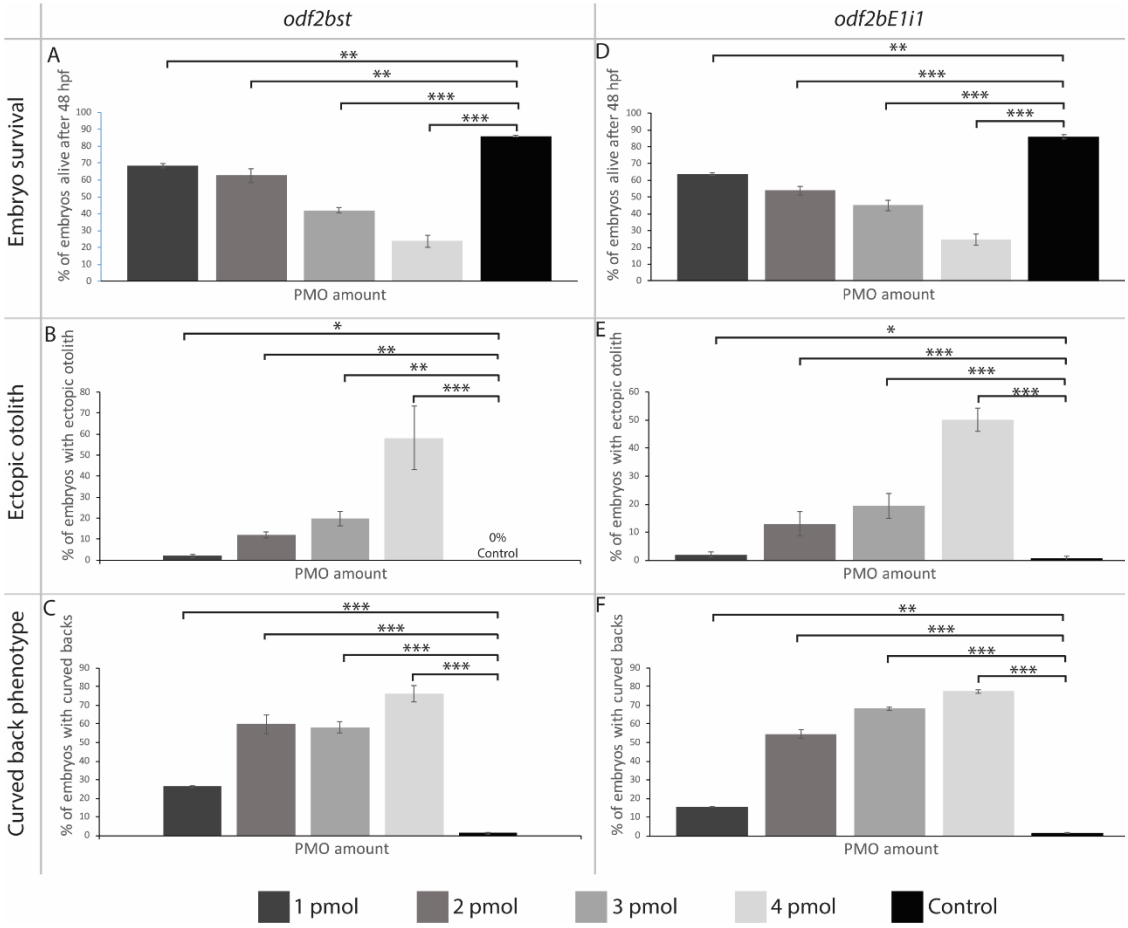

Figure 4-1 Efficiency of Odf2b morpholino injections.

Embryos were injected with 1 to 4 pmol of *odf2bst* morpholino **(A-C),** *odf2bE1i1* morpholino **(D-F)**, or the GFP morpholino as a control, and cultured for 48 hours. **(A,D)** Percentage of embryos surviving after 48 h. **(B,E)** Percentage of embryos showing ectopic otoliths. **(C,F)** Percentage of MO injected embryos showing a curved body morphology, a phenotype typical of ciliary defects. Error bars: standard error of the mean percentage of 3 independent experiments. Embryos were injected with 1 to 4 pmol of o*df2bst* morpholino (A-C), *odf2bE1i1* morpholino (D-F), or the GFP morpholino as a control, and cultured for 48 hours**. (A,D)** Percentage of embryos surviving after 48 h. **(B,E)** Percentage of embryos showing ectopic otoliths. **(C,F)** Percentage of MO injected embryos showing a curved body morphology, a phenotype typical of ciliary defects. Error bars: standard error of the mean percentage of 3 independent experiments. Fisher's exact test was used to statistically analyse significance; P value < 0.05 (*), 0.01 (**) and 0.001 (***).

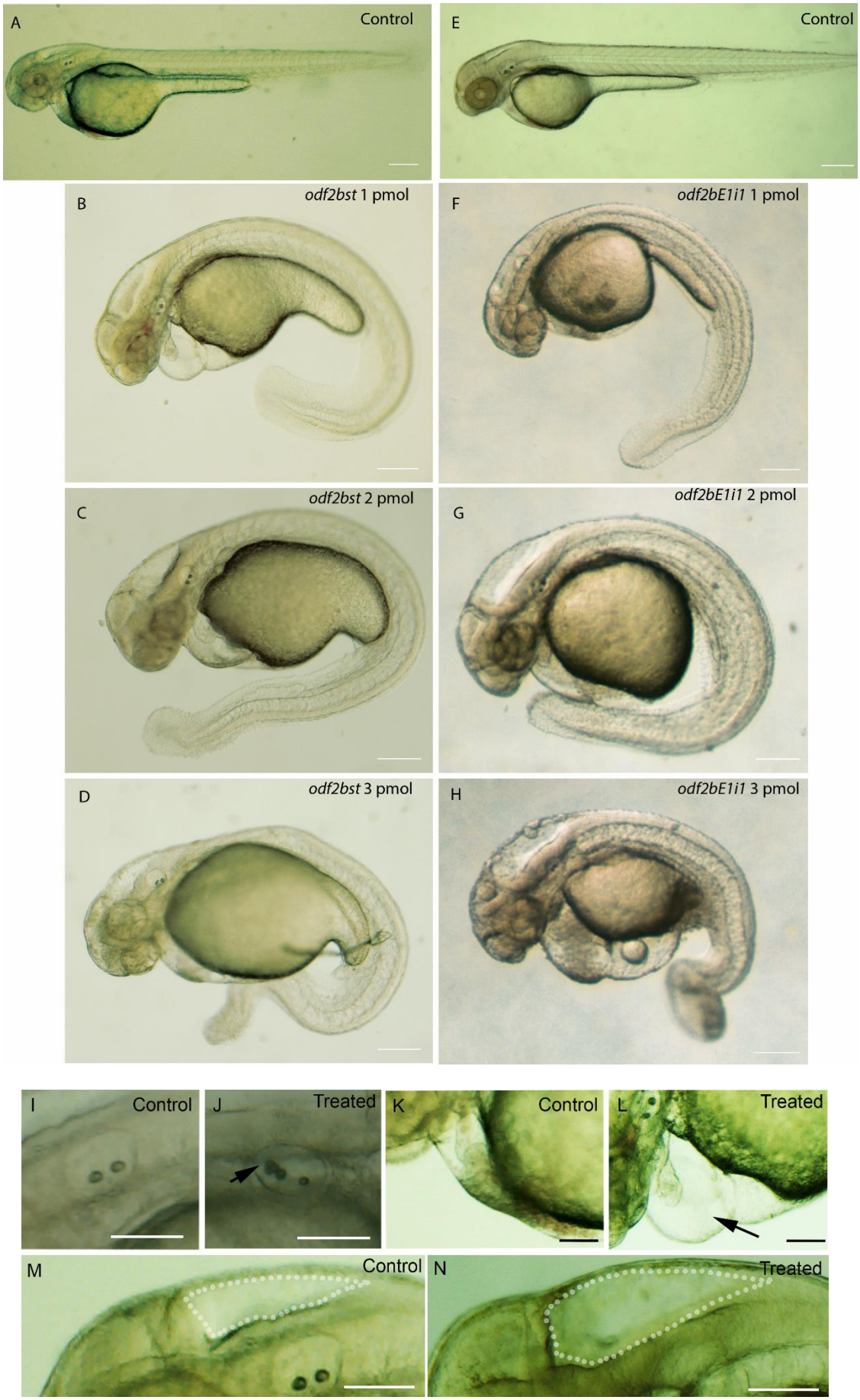
A
Control
E
Control
B
odf2bst 1 pmol
F
odf2bE1i1 1 pmol
C
odf2bst 2 pmol
G
odf2bE1i1 2 pmol
D
odf2bst 3 pmol
H
odf2bE1i1 3 pmol
I
Control
J
Treated
K
Control
L
Treated
M
Control
N
Treated

Figure 4-2 Morpholino knockdown of odf2b causes multiple phenotypes associated with ciliary dysfunction in zebrafish embryos.
(A,E) Control GFP-MO injected zebrafish embryos. (**B-D**) Odf2b-st morpholino injected zebrafish embryos showing a curved body phenotype **(B-D**); higher concentrations of MOs cause a more severe form of the morphology **(D)**. (**F-H**) *odf2bE1i1* morpholino injected zebrafish embryos again showing a curved body phenotype **(F-H)**; higher MO concentrations cause more severe defects **(H)**. (**I,J**) Otolith organisation in control MO injected embryo (I) and abnormal multiple otolith phenotype in *odf2bst* morpholino embryo **(J)**. **(K,L)** Enlarged magnification view of the heart in control **(K)** and splice altering morphants **(L)** with pericardial oedema. (**M,N**) Enlarged magnification view of the hindbrain region in control MO treated embryo (M) and splice altering morphants with swelling of the brain ventricles (hydrocephaly) **(N)**. Scale bar: 100 µm.

4.2.1 Confirmation of the knockdown

To confirm the effect of the splice altering morpholino, RT-PCR was used to assess the alteration in the mRNA transcript. The primers were designed to amplify a region between the 5' UTR and exon 3 in the *odf2b* mRNA that would produce an amplicon of 694 bp from the wild-type control. Conversely, following exposure to the *odf2b* splice altering morpholino, a 280 bp product was expected as the binding of the morpholino should cause skipping of exon 2 from the transcript (Figure 4.3A).

The RT-PCR experiments gave products of the expected sizes, with bands apparent at approximately 280 bp from the splice altering MO injected embryos (Figure 4.3C in yellow dotted lines) and approximately 700 bp from the wild-type control. Therefore, it can be concluded that the splice morpholino was effective in causing exon skipping in *odf2b*. The morpholinos are designed so that they should be specific to *odf2b*, and not affect *odf2a* transcripts; nevertheless, formal evidence for lack of an effect on *odf2a* requires amplification of the *odf2a* transcript in the control and treated samples, which was not done. This would need to be done to eliminate the possibility of any contribution of *odf2a* depletion to this phenotype.

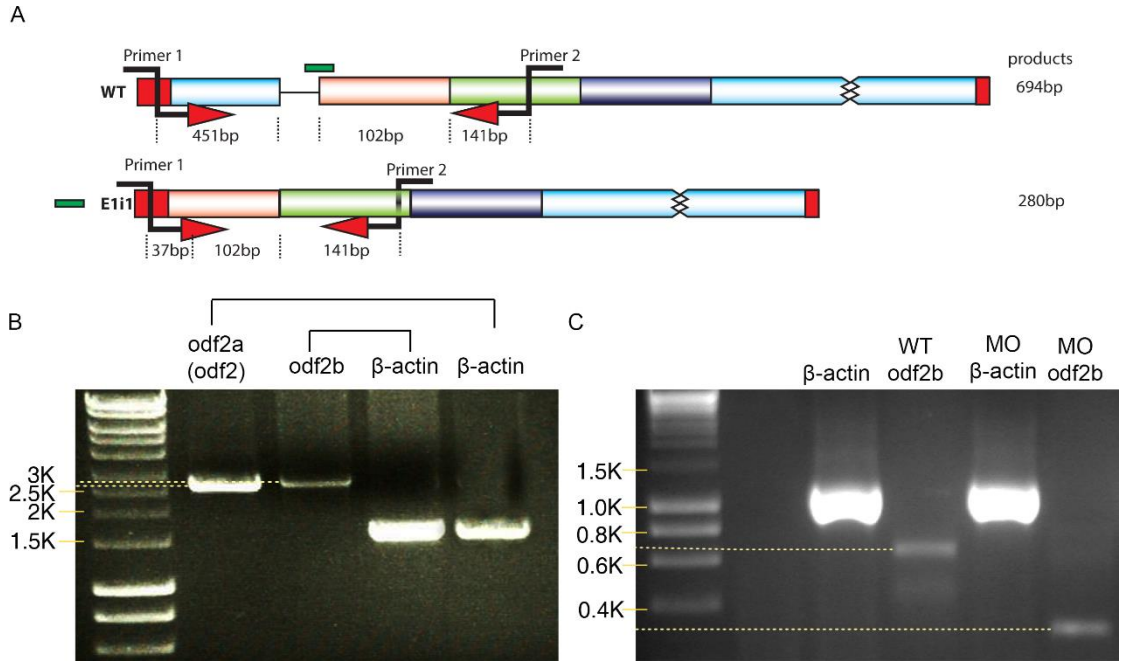

Figure 4-3 Semi quantitative analysis of RT-PCR results from *odf2b* splice altering morpholinos in zebrafish.
(A) Schematic diagaram of expected amplicon sizes with the selected primers. The wild type mRNA should produce a product of 694 bp with the primers used and 280 bp product from knockdown embryos. **(B)** verification of *odf2a* and *odf2b* expression in zebrafish shows both genes were expressed in embryos at 24 hpf. **(C)** RT-PCR amplification of products from wild type (WT) and *odf2b* splice altering morphant embryos show products of about the expected size. β-actin was used as a control to check cDNA quality.

4.3 The knockdown of *odf2b* in zebrafish resulted in shorter cilia

Given the connection between cilia and polycystic kidney disease (PKD) and the similarity of the observed morphants' phenotypes to other zebrafish ciliary phenotypes, it is possible that ciliogenesis was affected in the morphants. To investigate if the developmental and physiological phenotypes were linked to ciliary dysfunction, pronephric cilia of the morphants were studied with whole-mount immunostaining using confocal microscopy. Antibodies raised against acetylated α tubulin and γ-tubulin were used to immunostain the zebrafish cilia and centrosome respectively. The cilium length, number of cilia, and basal body numbers were recorded using the in-built measurement toolbox function found in the Olympus FV10 software. The confocal microscopy analysis verified the presence of cilia protruding from the apical surface of tubular and ductal cells into the lumen of the pronephros, in both morphants and control

embryos (Figure 4.4). The basal bodies appeared closer to the lumen in the morphants compared to the wild-types (Figure 4.4B-F). The number of basal bodies and the number of cilia protruding into the lumen per 100 µm length of the pronephros were counted. No difference was found between the number of basal bodies in the morphants (40 ± 1.4) and the control (41 ± 1.3. However, the cilia length was significantly reduced in morphants (7.08 ± 1.3 µm) compared to the wild-type embryos (9.5 ± 1.1 µm); (P<0.001, students t-test) (Figure 4.4G). This shortening of the cilium in morphants was observed with morpholino doses as low as 0.5 pmol. The previous work conducted in this laboratory observed that knockdown of *odf2a* also resulted in shorter cilia (Anila Iqbal, unpublished data). However, *odf2a* knockdown had a greater effect than observed here for *odf2b,* with complete disappearance of the cilium in some cases. Therefore, zebrafish *odf2a* morphants show a closer parallel than *odf2b* morphants to the effect of depletion of human *ODF2* in cultured cells and mouse *Odf2* null which result in severe ciliogenesis defects and disappearance of the cilia (Ishikawa *et al.*, 2005). Therefore, *odf2b* may have a different biological role to *odf2a* in zebrafish. Furthermore, the *odf2b* morphants were very similar to the *pcm-1* morphants (Stowe *et al.*, 2012), therefore it is plausible that *odf2b* functions similarly to satellite protein PCM-1.

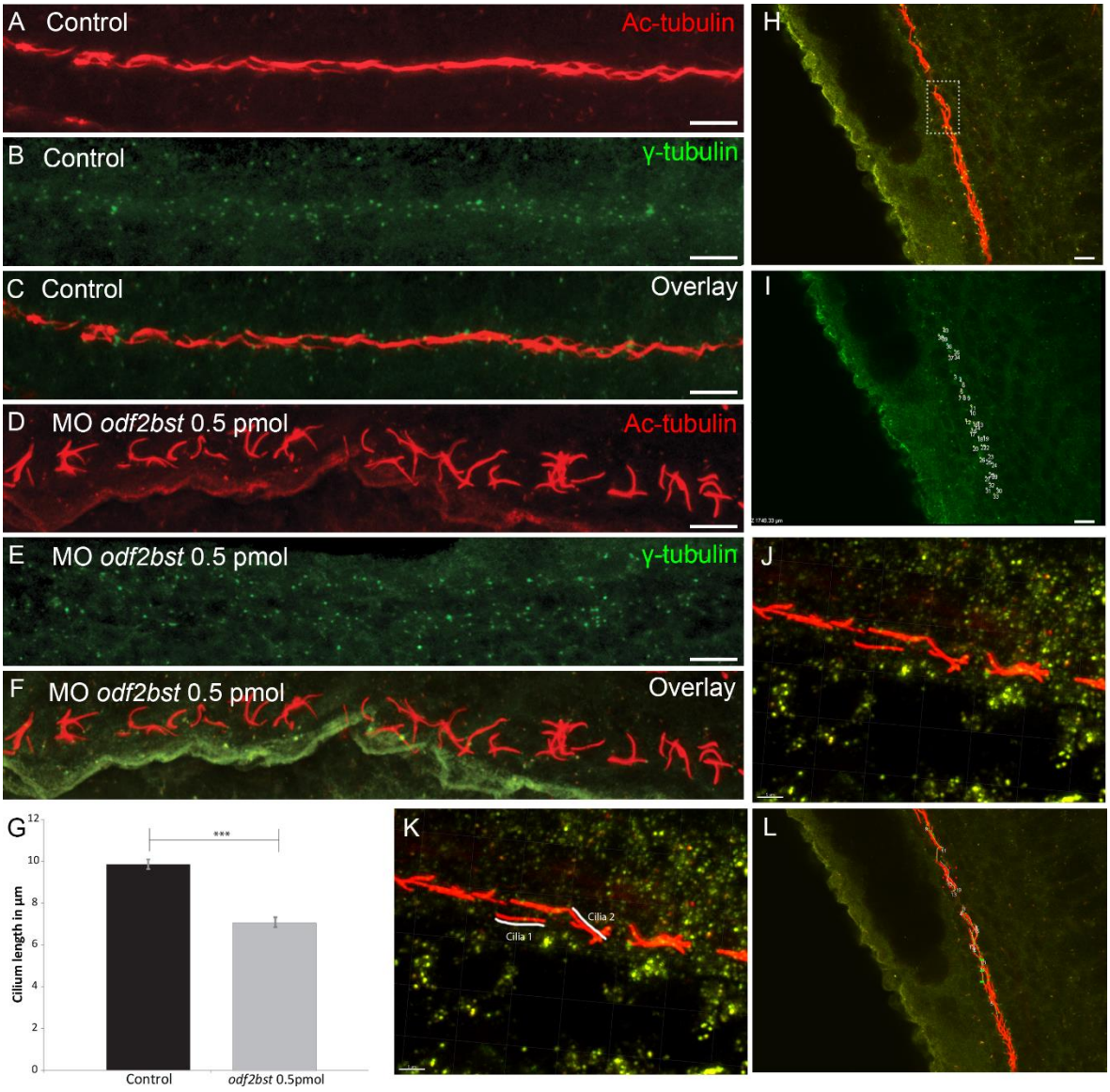

Figure 4-4 Knockdown *odf2b* in zebrafish causes shortened cilia in the pronephros.

(A-F) The embryos were stained for acetylated α-tubulin and γ-tubulin to identify cilia (red) and centrosomes (green). **(A-C)** Control MO-injected embryos showing the cilia in the pronephros. **(D-F)** Translation blocking *odf2b-st* morpholino injected embryos showing the cilia in the pronephros. **(G)** Comparison of cilium length in control and Odf2b-st morpholino injected embryos; Odf2b knockdown causes a significant shortening of the pronephric cilia. Student's t-test was used to statistically analyse significance; P<0.001. n=3 embryos for each condition; over 200 cilia measured for each embryo. Error bar shows the SEM. **(H-L)** Methodology used to measure cilium length. For each region of the pronephros **(H)** the basal body is identified and marked **(I)** and the distal tip of each cilium is found by scanning through the magnified optical sections **(J),** allowing the horizontal length of each individual cilium to be measured **(K,L).** Scale bar: 10 µm **(A-F,H,I,L)** or 5 µm **(J,K).**

4.4 Summary

In this chapter, the function of *odf2b* in development and ciliogenesis in zebrafish was studied by using morpholinos to knockdown the mRNA. A preliminary experiment conducted in this laboratory showed that depletion of *odf2a* causes zebrafish embryos to lose their pronephric cilia (Anila Iqbal, unpublished). This is expected as Odf2a is thought to be homologous to ODF2, which is a structural component of the distal appendages and crucial for docking the centriole to the plasma membrane at the onset of ciliogenesis (Novorol *et al.*, 2013). Therefore, it could be predicted that losing Odf2a should cause ineffective membrane docking of the centriole and render cells unable to form cilia.

Although depletion of *odf2b* produced a ciliary phenotype somewhat comparable to the *odf2a* phenotype, *odf2b* morphants were still able to form cilia. Furthermore, *odf2a* morphants have shown some phenotypes that were not observed with *odf2b* morphants, such as microcephaly and reduced retina size (Novorol *et al.*, 2013). Therefore, these observations suggest that *odf2a* and *odf2b* are functionally divergent. Morpholinos were designed to be specific to *odf2b* and not affect *odf2a*, however, the experimental analysis to test this has not been completed. Indeed, it remains possible that knockdown of *odf2b* itself has an effect on *odf2a*, or vice versa; further investigation would be needed to assess this, at both the mRNA and protein level.

The cilia observed in *odf2b* morphants were shorter than in wild-type embryos. A shortened cilia phenotype was observed in a number of satellite protein morphants, including *pcm-1* (Stowe *et al*, 2012). From the phenotypic parallels observed between *odf2b* morphants and centriolar satellite morphants, I wondered if *odf2b* was a centriolar satellite protein. However further investigation of zebrafish *odf2b* was not feasible at this time, owing to a lack of suitable reagents. This led us to consider using an alternative model system.

Chapter 5:

Investigation of the Role of ODF2L in Ciliogenesis

5.1 Introduction

The previous chapter investigated the possible role of zebrafish Odf2b in ciliogenesis. In order to investigate this further, we wanted to use an alternative model system, as the lack of available antibodies limited the experiments that could be performed using zebrafish. BLAST searches of the human protein database identified ODF2 as the closest homologue of zebrafish Odf2b, with around 41% amino acid identity for the closest matching isoform of ODF2. As Odf2a is believed to be the zebrafish homologue of ODF2, with 48% amino acid identity, we sought to consider whether there may be another human protein that is equivalent to Odf2b. This lead us to discover another ODF2 related protein in the human database, termed ODF2-like (ODF2L) or BCAP. Although ODF2L shares only 21% amino acid identity with ODF2, we were interested to pursue the possible function of ODF2L. ODF2L may not be the human homologue of either Odf2a or Odf2b, since the four protein isoforms of ODF2L exhibit only 19-21% identity to either Odf2a or Odf2b (Table 4-1). Nevertheless, we sought to explore the function of ODF2L in relation to ciliogenesis, in human cells.

Outer dense fibre of sperm tails 2-like (ODF2L, also known as KIAA1229) was initially named as basal body centrosome-associated protein (BCAP) by Ponsard *et al*., (2007) and later classified as part of the ODF2 (also known as cenexin) family of proteins due to sequence similarity. ODF2L was reported to have 20% amino acid similarity to *H. sapiens* ODF2 (Ponsard *et al*.,2007). ODF2 was initially identified as a major component of the sperm tail (Brohmann *et al.*, 1997; Hoyer-Fender *et al.*, 1998; Petersen *et al.*, 1999) in which it localised to the medulla and cortex and the connecting piece (Schalles *et al.*, 1998). However, later studies identified ODF2 as a structural protein specifically localised to distal/subdistal appendages of the mother centriole (Nakagawa *et al.*, 2001). Furthermore, ODF2 has also been recognised to play an important role in anchoring the centriole/basal body when building the cilium. Silencing ODF2 resulted in a centrosome without appendages (Ishikawa *et al.*, 2005) and lacking the primary cilium. Furthermore, mice homozygous for a gene trap insertion in exon 9 of the *Odf2* gene, which results in a truncated

Odf2 protein, display pre-implantation lethality (Salmon *et al.*, 2006). This implies the absolute requirement of ODF2 for embryonic development and importance of the integrity of cellular components as centrioles, basal bodies, and/or primary cilia (Salmon *et al.*, 2006).

Ponsard *et al*., (2007) also reported that human ODF2L shares 45% similarity with *S. cerevisiae* SPC110, a component of spindle pole body that is required for correct execution of spindle pole body duplication. *ODF2L* mRNA is strongly expressed in trachea and testis where motile cilia and flagella are found and weakly expressed in brain, prostate, spinal cord and thyroids (Ponsard *et al,* 2007). Additionally, Ponsard *et al.* (2007) recognised two isoforms of *ODF2L* (L-BCAP: 2.8kb, S-BCAP: 2.3kb) and have demonstrated that expression of the different isoforms depends on the presence or absence of cilia; the longer isoform is always expressed, whereas the shorter isoform is only present when cilia are present. The change of expression in the isoforms before, during and after ciliation alluded to functional divergence of these isoforms in ciliogenesis. Furthermore, indirect immunofluorescence microscopy studies of ODF2L in human nasal epithelial (HNE) cells have shown it to localise to the centrosome and basal body. Although ODF2L was demonstrated to associate with centrosome and basal body in multi-ciliating cells, the functional role of ODF2L on ciliogenesis in primary cilia remains to be explored.

5.2 Structure and organisation of ODF2L

The human ODF2L is encoded by *ODF2L* gene (Gene ID: 57489, Ensembl: ENSG00000122417). The NCBI predicts 4 transcripts for human *ODF2L* to encode proteins based on prediction algorithms and EST data. Those transcripts are responsible for 4 isoforms: isoform a (Strausberg *et al.*, 2002) with 620 amino acids (aa), isoform b (Jakobsen *et al.*, 2011) with 636 aa which differs in the 5' UTR and coding region compared to isoform a, isoform c (Strausberg *et al.*, 2002) with 620 aa which contains multiple differences in the coding region compared to isoform a that result in a translational frameshift causing very distinct C-terminus but is the same length as

isoform a and, isoform d (Strausberg *et al.*, 2002) with 591 aa which contains multiple differences in the coding region compared to isoform a resulting from a frameshift which is responsible for a distinct C-terminus.

SMART domain structure analysis of all the isoforms shows a common N-terminus low complexity region followed by 3 to 4 coiled-coil domains to the C-terminus depending on the isoform (Figure 5.1). Isoforms b and c show a similar domain organisation and a common low complexity region in the middle of the sequence. However, those isoforms do not share the same sequences in the C-terminus (Figure 5.2 highlighted in blue). Furthermore, isoforms a and d also share a similar domain organisation but, again, differ at the C-terminus sequence. Multiple sequence alignment of the four isoforms shows that there is substantial identity between the isoforms but also regions of diversity that make each isoform unique (Figure 5.2).

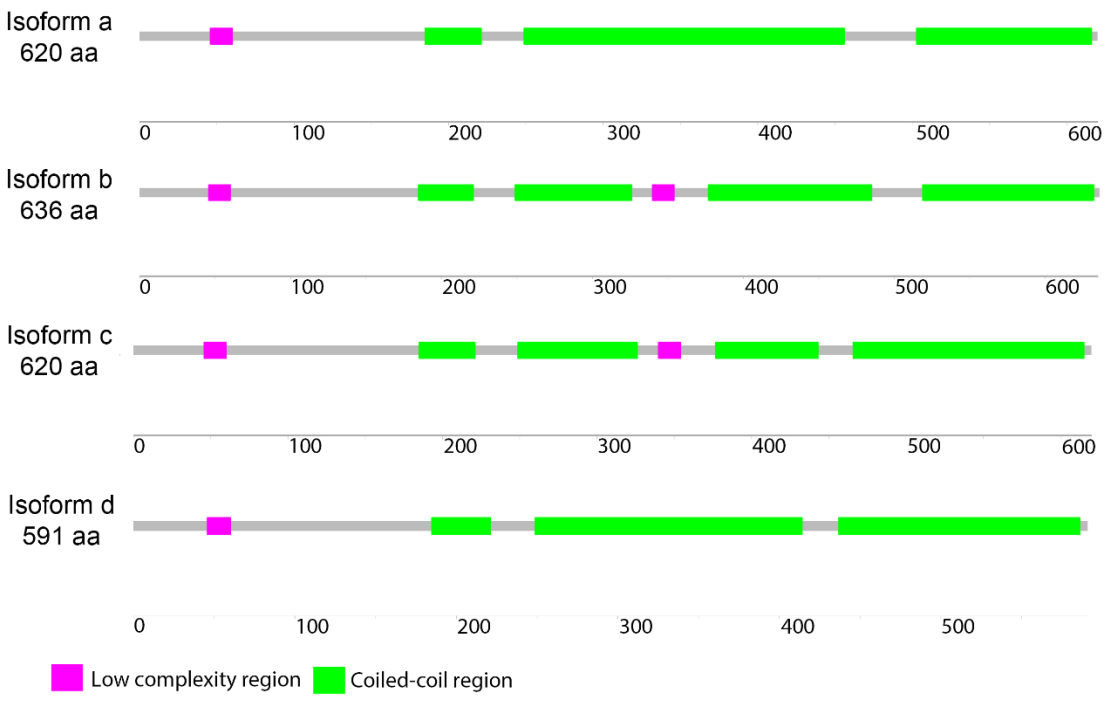

Figure 5-1 Predicted domain organisation of HsODF2L isoforms using SMART.

The SMART protein domain search recognised a common N-terminus in all four isoforms with a low complexity region and varying middle and C-terminus regions. Isoform A and D share a common domain architecture whereas isoform B and C share a common domain organisation.

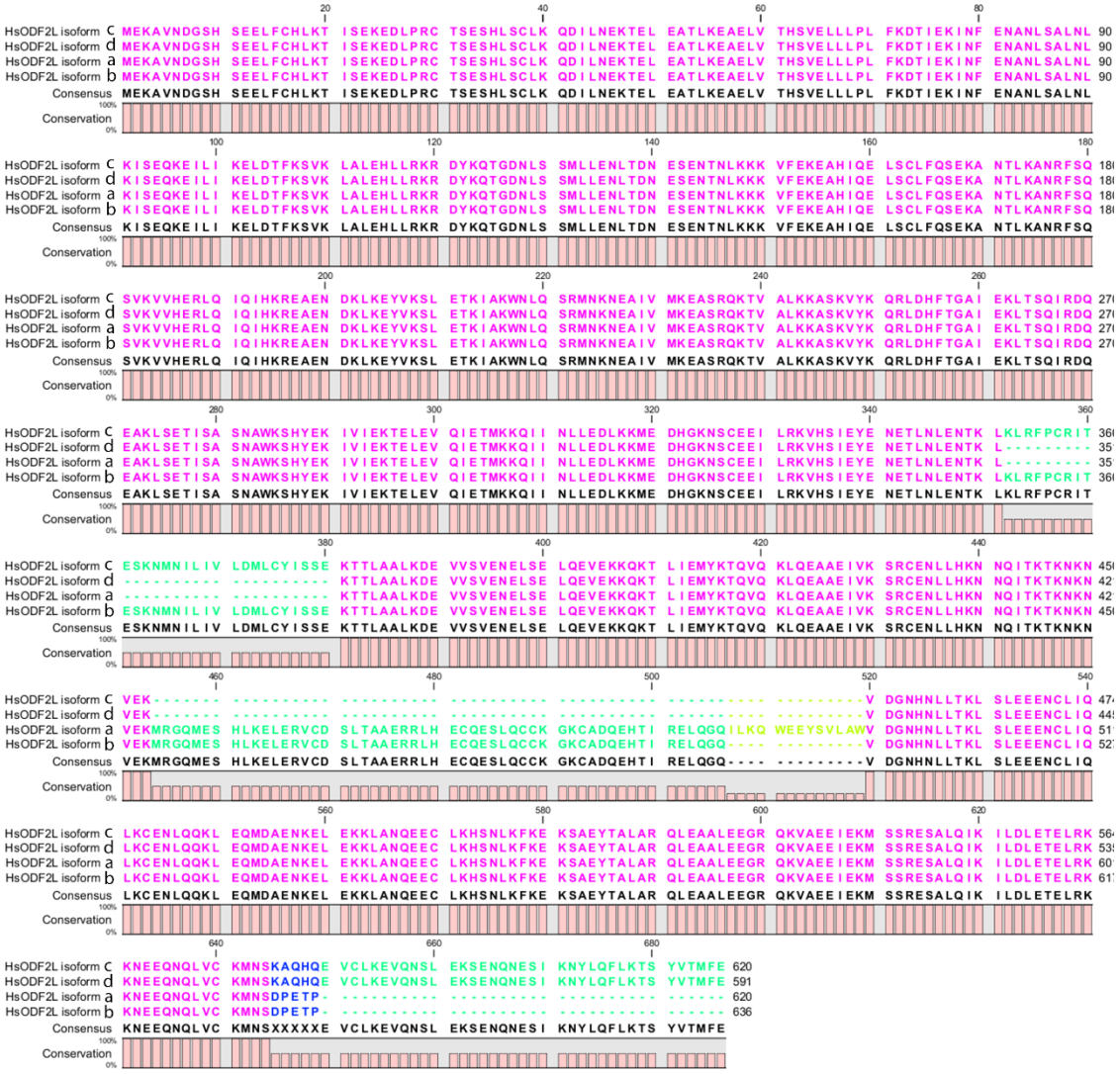

Figure 5-2 MUSCLE alignment of HsODF2L isoforms to show the protein sequence differences.

The conserved sequences are coloured in pink. Note that isoform a and b share a common C-terminus sequence, as do isoforms c and d, although this is 37 amino acids longer than in a/b.

5.3 ODF2L is a satellite protein

In order to investigate the localisation of ODF2L in mammalian cells, indirect immunofluorescence microscopy was conducted using a commercially available antibody purchased from Biorbyt™ (Cat# orb31049). This rabbit polyclonal antibody was raised to the C-terminus of human ODF2L isoform b (NCBI ID: NP_001007023.21; NM_001007022.21); however, the specific epitope was not given. Given the extent of similarity to other isoforms at the C-terminus, this antibody is likely to bind to at least one other isoform, and perhaps all four isoforms, depending on exactly where the epitope(s) lie.

Immunocytochemistry on NIH 3T3 cells showed the antibody immunostained a structure in the perinuclear region surrounding the centrosome in proliferating cells (Figure 5.3A). The cells were also co-stained with γ-tubulin as the marker for the centrosome (red) and ODF2L staining (green) was shown to concentrate around the centrioles (Figure 5.3). This staining pattern was similar to the centrosome satellite staining observed when using a known centriolar satellite marker such as PCM-1 (Figure 5.3 B).

Although the antibody has shown a staining pattern that resembles other centriolar satellite proteins in NIH 3T3 cells, we must always be cautious about whether an antibody is really specific to the protein target. Furthermore, ODF2L staining in NIH 3T3 cells often showed high background and non-specific binding even after fine-tuning the staining protocol with extended washing and blocking times. This may be due to the fact that the antibody was never tested in mice by the commercial provider and only optimised to react with human ODF2L antigen. Therefore, the antibody staining might be producing high background and non-specific staining with mouse cell lines such as NIH 3T3 cells. To resolve the high background, human hepatocellular carcinoma cells (HuH-7) were used to stain with the same antibody combinations; this showed substantial improvement with the background and reduced non-specific staining (Figure 5.4). The immunocytochemistry staining of ODF2L on HuH-7 cells showed a very

distinctive staining in the perinuclear compartment around the centriole, which was identified by γ-tubulin staining (Figure 5.4A). The γ-tubulin staining highlighted two intense spots in the cells, consistent with centriolar staining in HuH-7 cells, and these spots also showed co-localisation of ODF2L staining (Figure 5.4A). The staining was performed a number of times and the ODF2L localisation was observed to be consistent (Figure 5.4A).

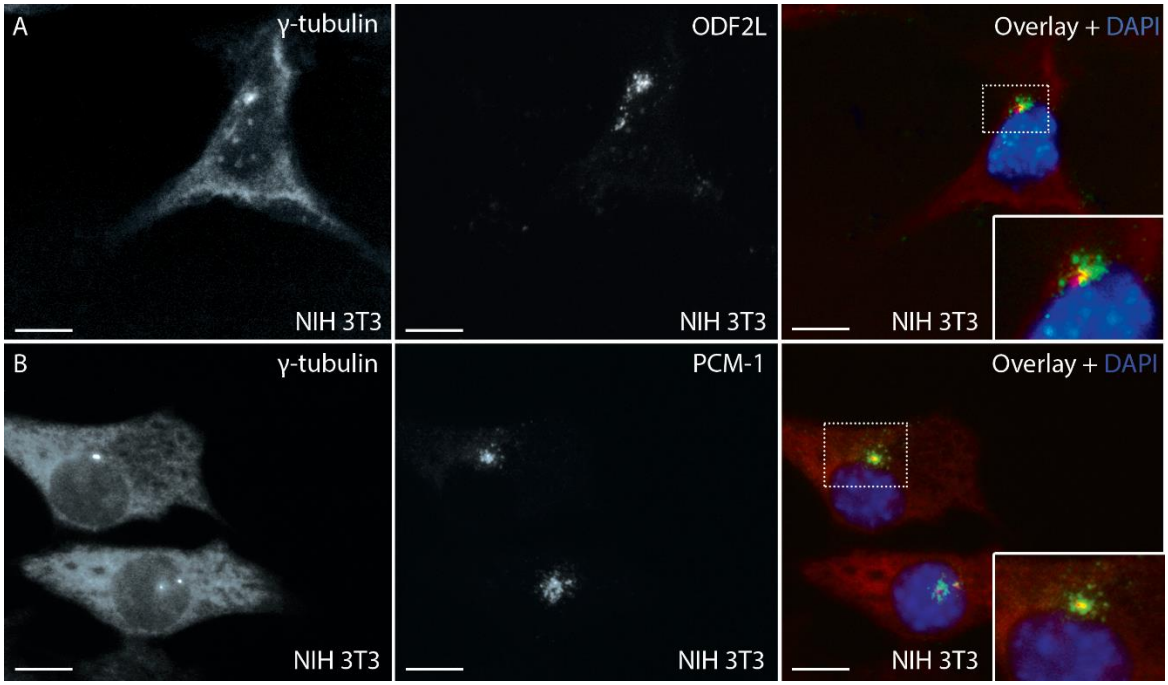

Figure 5-3 ODF2L and PCM-1 staining in proliferating NIH 3T3 cells.

(A) ODF2L staining (green) was shown to be localised around the centrioles which are co-stained with γ-tubulin (red). γ-tubulin intensely stains the centrioles and less intensely stains the cytoskeleton. **(B)** PCM-1 staining (green) shows a similar localization pattern to ODF2L, and is adjacent to the γ-tubulin stained centrioles (red). PCM-1 is a well-established satellite protein known to regulate ciliogenesis. DNA was stained with DAPI (blue). Inserts show higher magnification view of boxed area. Scale bar 10 µm.

PCM-1 staining in HuH-7 cells produced a fine, punctate localisation around the centrosome representing the centrosome satellites (Figure 5.4B). Although the localisation observed with anti-ODF2L antibody demonstrated a staining pattern comparable to centriolar satellites around the centrosome, the staining appeared to be more granular compared to PCM-1 staining (Figure 5.4A,B).

From the initial experiments, it appeared that ODF2L localised around the centrosome resembling centriolar satellites in cycling cells.

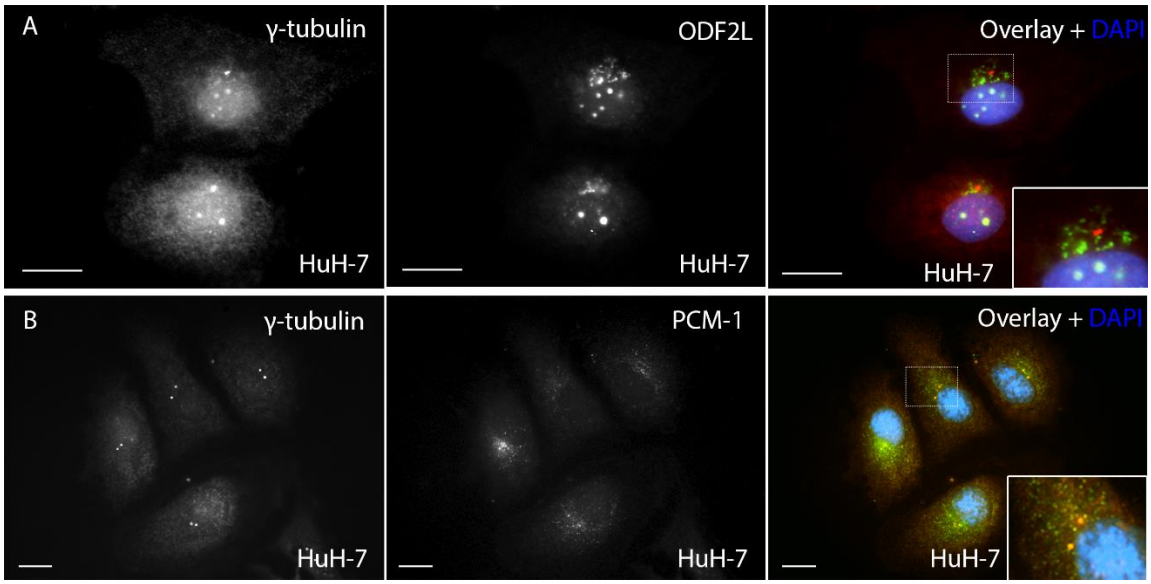

Figure 5-4 ODF2L and PCM-1 staining in proliferating HuH-7 cells.

(A) ODF2L staining in cycling HuH-7 cells (green) is localised on or around the centrioles which are intensely stained with γ-tubulin (red) **(B).** PCM-1 staining (green) in HuH-7 cells showed a fine scattered localisation around the centrioles, stained with γ-tubulin (red). Note the granular staining of ODF2L when compared to PCM-1. DNA stained with DAPI. Inserts show higher magnification view of boxed area. Scale bar: 10 µm.

5.4 Ciliation causes ODF2L to disappear from centriolar satellites

When HuH-7 cells were serum-deprived to attempt to induce ciliogenesis, ODF2L localisation disappeared from the periphery or satellites in many cells (Figure 5.5A). HuH-7 cells do not appear to form cilia. Therefore, hTERT-RPE1 cells were also examined for ODF2L localisation. In control serum-containing medium, ODF2L was localised in a diffuse pattern around the centrioles, consistent with centriolar satellite localisation (Figure 5.5B). Under serum free conditions, hTERT-RPE1 cells initiate ciliogenesis (Figure 5.5C). Under these conditions, ODF2L staining appeared to either disappear, or to localise to the centrioles/basal body (Figure 5.5C

white arrow), although this latter pattern was only observed when cells were fixed with formaldehyde, and not when cold methanol fixed.

The disappearance of ODF2L from the centrosome periphery at the onset of ciliogenesis might be due to the degradation of the protein or to the relocation of ODF2L to the centrosome. However, not all cells showed ODF2L localisation to the centrosome, nor was there a sufficient increase in the ODF2L fluorescence intensity at the centrosome to account for all the ODF2L relocalising there, in those cells where ODF2L was relocalised to the centrosome. Hence, to understand the true fate of the ODF2L in cycling and in quiescent cells, protein extracts were subjected to Western blot analysis.

The Western blot analysis recognised a single band of around 69-72 kDa band from the lysates of both HeLa and hTERT-RPE1 cells when cultured in control serum-containing medium (Figure 5.5D). This band corresponds to the theoretical molecular weights of ODF2L isoforms (predicted molecular weights for ODF2L isoform a: 72.5 kDa, b: 73.7 kDa, c: 72.6 kDa, and d: 68.6 kDa). The antibody was raised against the C-terminus of isoform b which shares the common C-terminus sequence with isoform a so is anticipated to recognise both a and b isoforms. Indeed, the antibody may bind to all four isoforms, depending on exactly where the epitope(s) reside. Theoretically the antibody should have recognised at least two isoforms in the Western blot analysis and therefore, should have resulted in two or more separate bands. The identification of only a single band on the Western blot may be due to the insufficient separation of isoforms with very similar molecular weights. The gel resolution is insufficient to separate isoform a, b and c bands where there is less than 1.2 kDa difference.

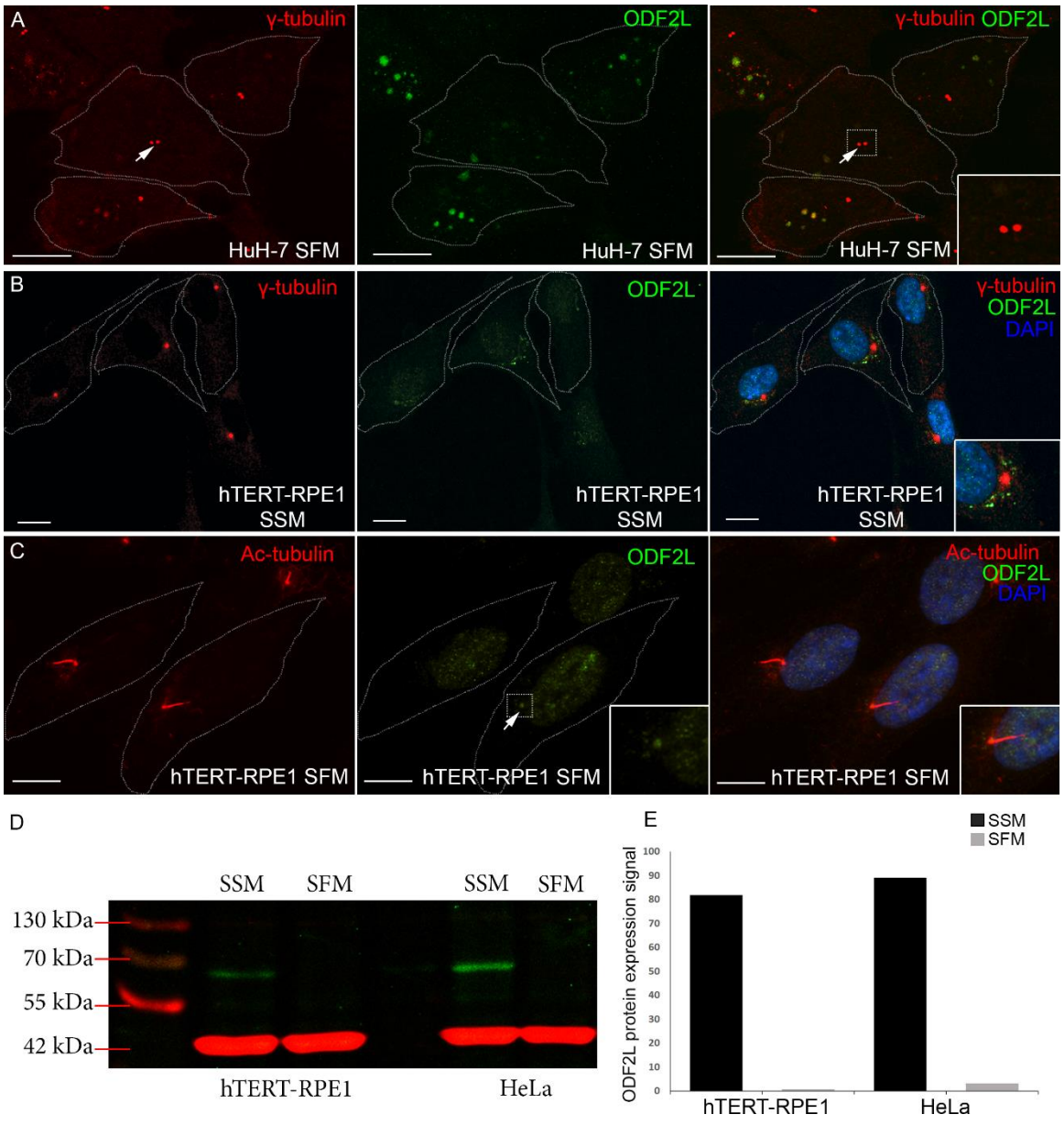

Figure 5-5 ODF2L localisation and level of protein expression in cycling and quiescent cells.

(A) ODF2L localisation (green) in HuH-7 cells following 24 hours culture in serum free medium (SFM). Note the absence of ODF2L staining from the centriolar satellites under these conditions (white arrow). Centrioles are stained for γ-tubulin (red); HuH-7 cells do not ciliate. **(B)** ODF2L localisation (green) in cycling hTERT-RPE-1 cells. ODF2L is localised to the centriolar satellites. Centrioles are stained with γ-tubulin (red). DNA stained with DAPI. **(C)** Localisation of ODF2L (green) in hTERT-RPE-1 cells when serum-deprived for 24 hours. It appeared that ODF2L has moved to the centrosome (white arrow; insert represents higher magnification view of boxed area). Cilia and centrioles are stained for acetylated tubulin and γ-tubulin (red). Green nuclear staining appears to be an artefact of formaldehyde fixation. DNA stained with DAPI. **(D)** Protein expression from two differenct cell lysates analysed by Western blotting for ODF2L (green) and β-actin (red). Cell lysates from hTERT-RPE-1 and HeLa cultures in serum supplemented medium (SSM) showed ODF2L presence (70 kDa band in green), whereas ODF2L was undetectable following 24 hours culture in serum free medium (SFM). The red band represents β-actin as a loading control and shows similar protein levels in each well. **(E)** Protein expression quantification, confirming the almost complete disappearance of ODF2L from both serum-starved cell lysates. Scale bar in A-C: 10 μm.

In contrast, the Western blot showed almost complete disappearance of the ODF2L band from cells cultured in serum free medium (Figure 5.5D,E). This is consistent with the degradation of ODF2L when cells were serum deprived. This result therefore confirmed the previous observations from immunocytochemistry of disappearance of ODF2L localisation from the centriolar satellites was due to the degradation of the protein when serum starved rather than due to the dispersal of the protein to the cell periphery.

5.5 GFP tagged ODF2L localises to centriolar satellites

In order to validate the antibody staining was specific to ODF2L, full length mouse *Odf2l* (cDNA clone MGC:28123 IMAGE:3979963 Gene Bank accession: BC020075.1) was GFP tagged (N-terminus) and cloned into an expression plasmid. Mouse Odf2l was used in this part of the study as a mouse cDNA clone could be purchased from the IMAGE library resource, whereas a human cDNA clone was not available. Mouse Odf2l and human ODF2L share about 71% amino acid sequence identity, although mouse has only two isoforms, compared to the four in humans.

The GFP-mOdf2l construct was transfected into HuH-7, HeLa and hTERT-RPE-1 cells and studied using immunofluorescence microscopy to investigate the localisation patterns. The GFP-tagged full length mOdf2l protein localised to the centrosome periphery in all 3 cell types (Figure 5.6 B-D). This is similar to the satellite localisation observed with the antibody staining for the endogenous mouse and human protein (Figure 5.3A, 5.4A, 5.5B). Moreover, GFP-mOdf2l transfected cells were also co-stained with anti-ODF2L antibodies, showing overlapping staining (Figure 5.6D). To validate the specificity of the ODF2L antibody, confocal images of the localisation were obtained and the Z-stacks were analysed with Coloc function in BITPLAN™ Imaris 7.6 software (Oxford Instruments, UK) to identify the colocalisation overlap. The Coloc function recognised 97% overlap with a Pearson correlation coefficient (PCC) of 0.6 (Figure 5.6D) therefore, strongly suggesting that the antibody recognised the mouse Odf2l protein.

Additionally, GFP-mOdf2l localisation with respect to endogenous PCM-1 was also studied using anti-PCM-1 antibody (Figure 5.6E). The analysis demonstrated a co-localisation of GFP-mOdf2l with PCM-1 with 80% overlap and PCC of 0.5. Hence, this supports the hypothesis that mOdf2l is a centriolar satellite protein which colocalises with PCM-1. However, the true nature of this localisation is yet to be studied.

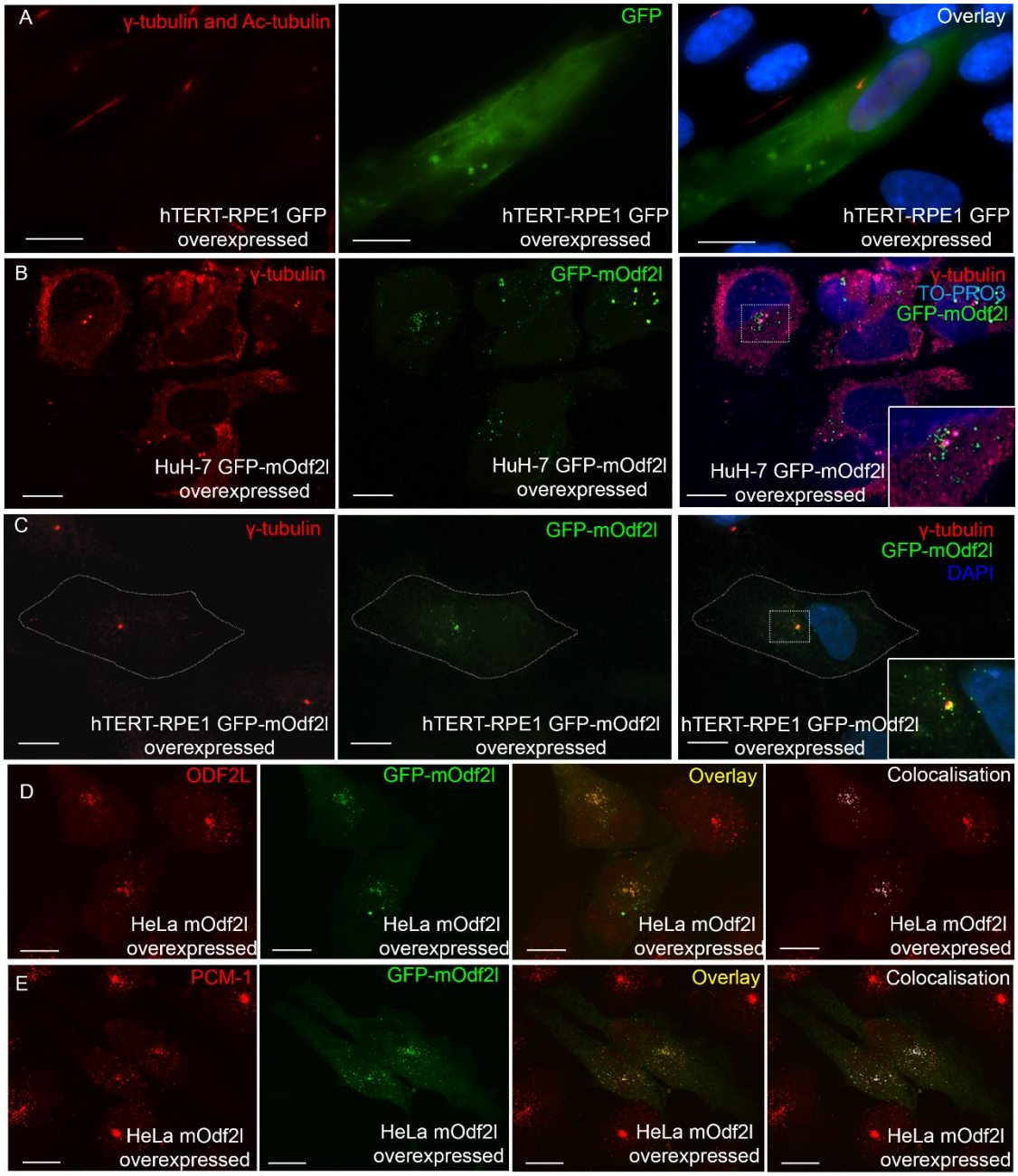

Figure 5-6 Transfection of GFP tagged mOdf2l construct to cells to study the localisation pattern.

(A) The GFP parental plasmid was transfected into HeLa cells. The localisation pattern of GFP is throughout the cell, and distinct from that observed when GFP is tagged to mOdf2l. **(B,C)** GFP-mOdf2l localisation (green) in HuH-7 cells **(B)** and hTERT-RPE-1 cells **(C),** showing GFP-mOdf2l is localised around the centrosome, consistent with satellite-like organisation (white arrow). γ-tubulin is stained in red. **(D)** The anti-ODF2L antibody (red) was tested for whether it can recognise the GFP-mOdf2l protein (green) and co-localisation was analysed with Pearson correlation coefficient (PCC); the co-localisation is coloured in white. The analysis show 97% overlap. (**E**) The GFP-mOdf2l localisation was also analysed with PCM-1 localisation (red), the PCC analysis showed 80% overlap. DNA is stained with DAPI. Scale bar: 10 µm.

5.6 Overexpression of ODF2L disrupt the ciliation in RPE-1 cells

From the above experiments, it appears that ODF2L was removed from satellites when the ciliation was induced by serum starvation. Therefore, I asked how the localisation might change if cells overexpressed ODF2L and were serum starved. In order to assess this, I wished to use antibodies to both γ-tubulin and acetylated tubulin to identify centrosomes and the cilia at the same time. This necessitated co-staining with both antibodies detected with the same secondary antibody, and thus analysed in the same fluorescence channel. To validate this co-staining, I compared the staining pattern obtained with the individual antibodies with that obtained when both antibodies were used together (Figure 5.7). This showed that the antibodies do not appear to interfere with each other, and can successfully be used for co-staining experiments in this way.

To examine whether ODF2L localisation changes under serum starvation, hTERT-RPE1 cells were transfected with GFP-mOdf2l expression construct and induced to ciliate by serum deprivation for 24 h after the transfection. Similarly, to above, the GFP-expressing parental plasmid was also transfected into hTERT-RPE-1 cells and subjected to serum deprivation (Figure 5.8A). After 24 h of serum deprivation, cells were fixed in 4% FA and studied using immunofluorescence microscopy.

About 30-40% of the hTERT-RPE-1 cells were shown to be transfected, when using either the GFP-expressing parental plasmid or the GFP-mOdf2l construct. The GFP-expressing parental plasmid resulted in GFP localisation throughout the cell (Figure 5.8A). In contrast, cells transfected with the GFP-mOdf2l construct showed localisation of GFP-mOdf2l around the centriole, consistent with satellite distribution (Figure 5.8B). However, when the transfected cells were examined in more detail, it appeared that none of the GFP-mOdf2l expressing cells formed a cilium (Figure 5.8B). Therefore, I serendipitously found that overexpressing Odf2l made cells unable to ciliate even after inducing ciliogenesis by serum starvation. However, all of

the non-transfected cells, and the control GFP-transfected cells, were able to ciliate following serum starvation (Figure 5.8A,B). The experiment was repeated three times and none of the observed GFP-mOdf2l transfected cells formed a cilium, in over 100 cells examined. Therefore, from these observations, I concluded that overexpression of Odf2l prevents ciliation in cells.

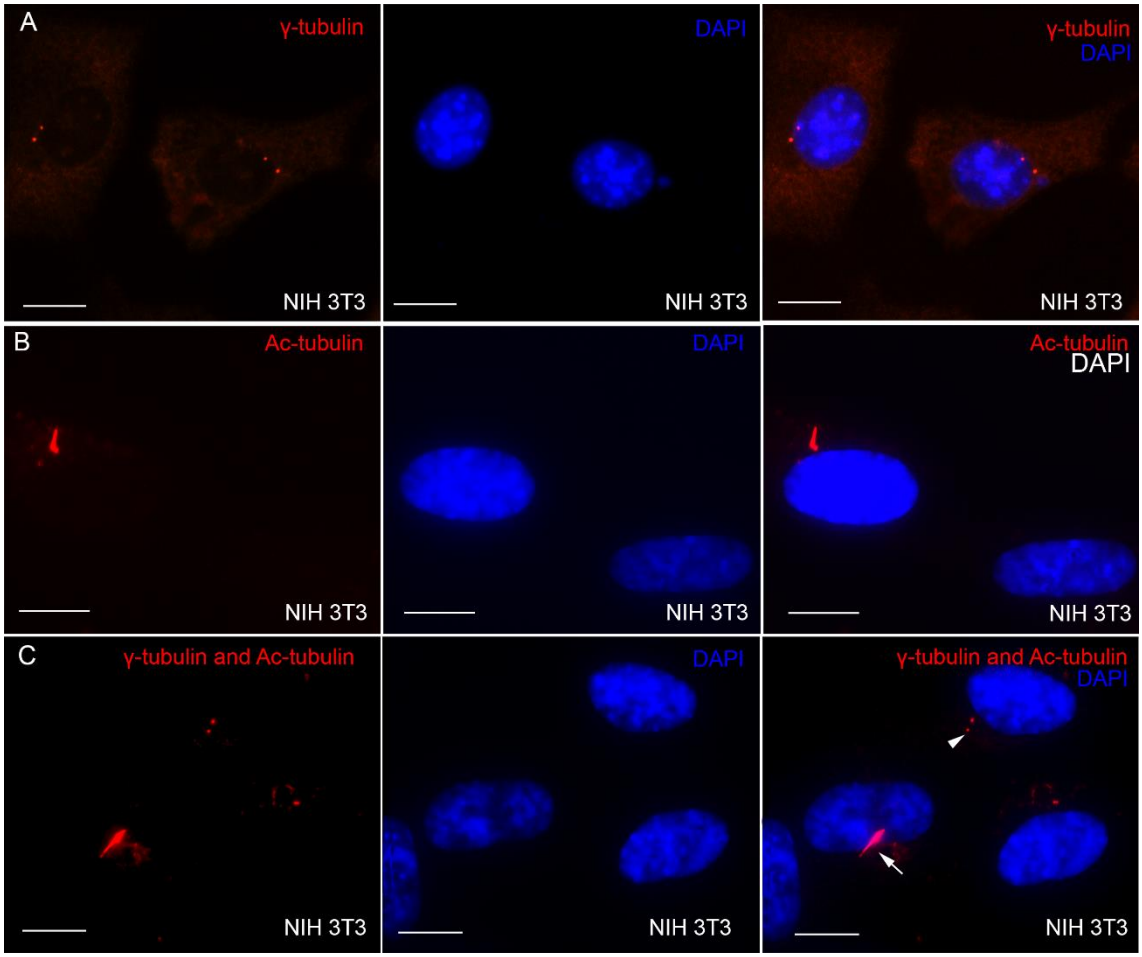

Figure 5-7 Comparison and validation of staining with antibodies for γ-tubulin and acetylated tubulin, in the same fluorescence channel.

NIH 3T3 cells stained with antibodies for γ-tubulin (**A**; red), acetylated tubulin (**B**; red) or both together (**C**; red). DNA is stained with DAPI (blue). Co-staining with both antibodies together works well, and gives the same results as seen with either antibody separately.

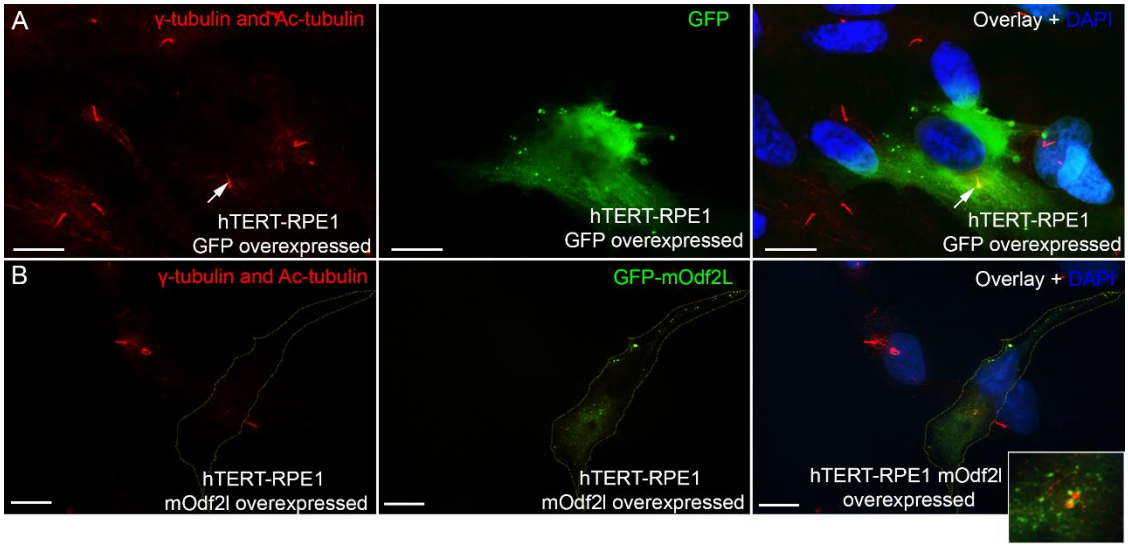

Figure 5-8 ODF2L overexpression can stop ciliogenesis.

(A) The GFP expressing parental plasmid was transfected into hTERT-RPE-1 cells and cells subjected to serum starvation for 24 hours. These cells were able to ciliate (white arrow) as shown with anti-acetylated tubulin and γ-tubulin staining (red) even when expressing GFP (green). **(B)** When GFP-mOdf2l was transfected, the overexpressing cells were unable to ciliate. The overexpression was repeated three times and all cells expressing GFP-mOdf2l had no cilium, whereas non-transfected cells showed cilia. DNA staining DAPI. Scale bar 10 µm.

Thus, I have shown that ODF2L appears to be removed from centriolar satellites when ciliation was induced following serum starvation (Section 5.3), and that when Odf2l was overexpressed, cells were unable to ciliate following serum starvation. Therefore, it appears that removal of ODF2L is essential for the initiation or progression of ciliogenesis; hence ODF2L appears to be negatively regulating ciliogenesis. This type of regulation is not unprecedented; a recent study has shown that satellite protein OFD1 negatively regulates ciliogenesis through an autophagy pathway and removal of OFD1 from satellites was crucial to the onset of ciliogenesis (Orhon *et al.*, 2015).

5.7 ODF2L knockdown encourage cycling RPE-1 cells to express cilia

Following on from the previous experiments, it was logical to investigate the effect on ciliogenesis when ODF2L was knocked-down in cells. To deplete the expression, siRNA oligo primers were designed to target all isoform transcripts of ODF2L. The siRNAs were transfected into hTERT-RPE-1 cells using RNAiMAX and depletion efficiency was analysed using immunocytochemistry and RT-PCR.

After knockdown of ODF2L with the siRNA oligos, ODF2L staining in the cells cultured in serum supplemented medium almost completely disappeared (Figure 5.9B), in contrast to robust expression around the centrosome in hTERT-RPE-1 cells transfected with non-target siRNA (Figure 5.9A). This was confirmed by using RT-PCR with a primer pair (isoform b region between 363-975 bp) designed to amplify a common area for all the isoforms from cDNA. In the RT-PCR, the primers amplified a product of 613 bp from controls (Figure 5.9C). However, this amplicon was absent from cells following transfection with either siRNA (Figure 5.9C).

From the previous behavioural observations of ODF2L, I postulated that knockdown of ODF2L should encourage ciliogenesis in hTERT-RPE-1 cells without serum deprivation. To test this notion, cells were cultured in serum supplemented culture media for 24 h after the siRNA knockdown and then fixed in PFA. Then cells were stained with anti-acetylated α-tubulin and anti γ-tubulin to stain cilia and centrosome respectively (Figure 5.9A,B) and the number of cells expressing a cilium was counted using immunofluorescence microscopy (Figure 5.9E,F). Furthermore, the cilium length was also measured using the measuring tool box in Nikon NIS-Element Basic Research software and analysed using ANOVA to analyse the statistical significance of the cilium length changes (Figure 5.9E).

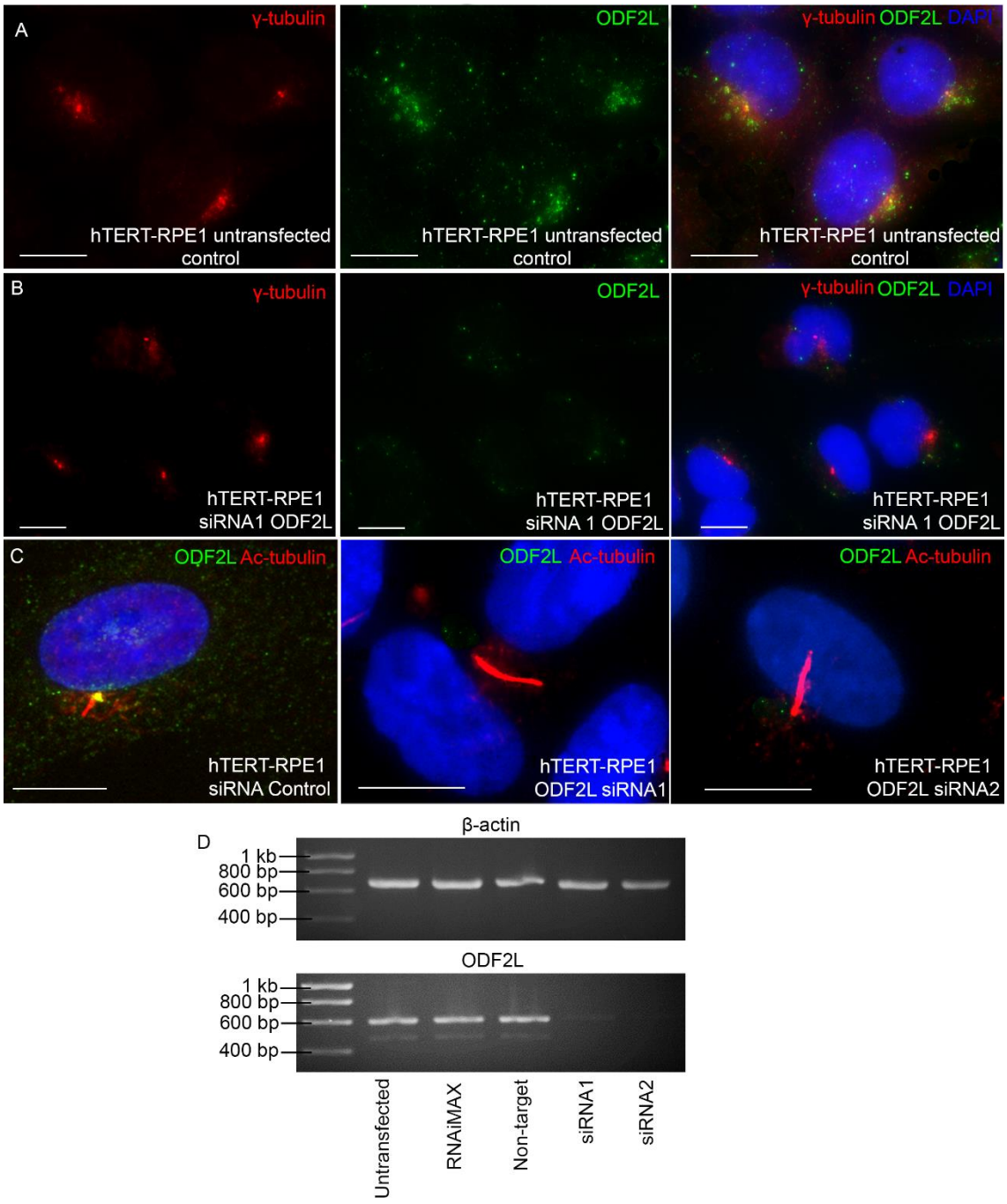
A
γ-tubulin
hTERT-RPE1 untransfected control
ODF2L
hTERT-RPE1 untransfected control
γ-tubulin ODF2L DAPI
hTERT-RPE1 untransfected control
B
γ-tubulin
hTERT-RPE1 siRNA1 ODF2L
ODF2L
hTERT-RPE1 siRNA 1 ODF2L
γ-tubulin ODF2L DAPI
hTERT-RPE1 siRNA 1 ODF2L
C
ODF2L Ac-tubulin
hTERT-RPE1 siRNA Control
ODF2L Ac-tubulin
hTERT-RPE1 ODF2L siRNA1
ODF2L Ac-tubulin
hTERT-RPE1 ODF2L siRNA2

D
β-actin
1 kb
800 bp
600 bp
400 bp
ODF2L
1 kb
800 bp
600 bp
400 bp
Untransfected
RNAiMAX
Non-target
siRNA1
siRNA2

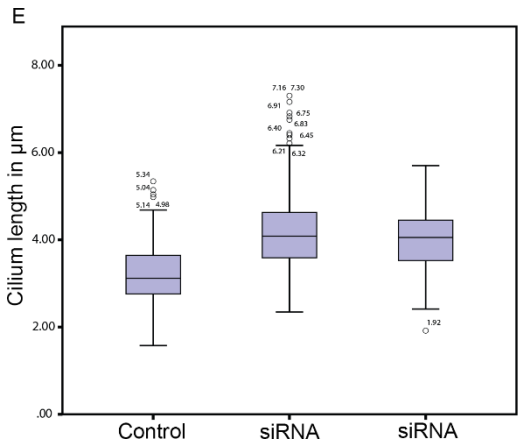
E
Cilium length in µm
8.00
6.00
4.00
2.00
.00
Control
siRNA
siRNA

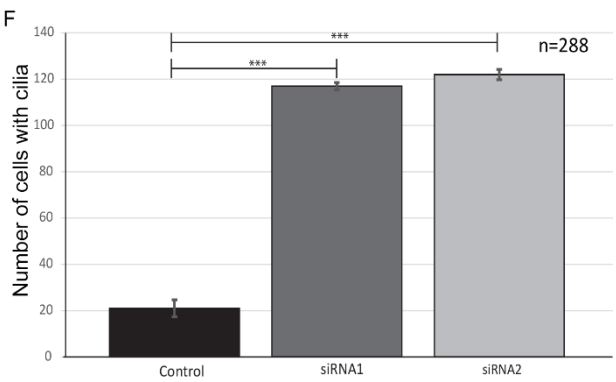
F
Number of cells with cilia
140
120
100
80
60
40
20
0
***
***
n=288
Control
siRNA1
siRNA2

Figure 5-9 siRNA knockdown analysis of ODF2L in hTERT-RPE-1 cells.

(A-C) ODF2L localisation (green) detected with anti-ODF2L antibody from Proteintech, in hTERT-RPE-1 cells that are untransfected **(A)** or transfected with either ODF2L-siRNA or control non-target siRNA, as indicated in each panel **(B,C).** ODF2L shows satellite-like staining in untransfected and control siRNA-transfected cells, but this staining disappears following ODF2L-siRNA transfection. γ-tubulin and acetylated tubulin were stained to show centrosomes and cilia (red). Higher power views **(C)** show increased cilium length following ODF2L-siRNA transfection compared to control siRNA-transfected cells. DNA is stained with DAPI (blue). Scale bars: 10 μm. **(D)** RT-PCR shows the presence of 613bp ODF2L band from untreated, RNAiMax and non-target siRNA transfected cells, but absence of ODF2L mRNA from ODF2L-targetted siRNA1/2 transfected cells. β-actin was amplified as a cDNA control. **(E)** Box and whisker plots showing that knockdown of ODF2L in hTERT-RPE-1 cells resulted in longer cilia (statistically significant, $P<0.0001$). **(F)** Bar chart showing number of cells with cilia in non-target siRNA (control) and ODF2L-targetted siRNA1/2 transfected cells, out of 288 cells counted for each condition. There was a six-fold increase in the number of cells with cilia, following ODF2L knockdown. Experiments were repeated three times. Error bars show SEM, $P<0.001$ with ANOVA.

In the ODF2L-siRNA knockdown cells, there was a six fold increase in the proportion of cells with a cilium, compared to the non-target siRNA transfected control cells (Figure 5.9E,F).The hTERT-RPE-1 cell line is commonly used for cilia-related studies due to the flat orientation of their cilia (Marshall, 2013) and known to extensively ciliate upon serum deprivation (Molla-Herman *et al.*, 2008; Molla-Herman *et al.*, 2010). However, these cells also tend to ciliate in a few cells (up to 20%) when grown in serum supplemented medium (Sloboda, 2009). The observed increase here in the proportion of cells with a cilium following siRNA knockdown of ODF2L is substantially higher (around 40%) so can only be explained as an effect due to the reduction of ODF2L. Therefore, the removal of ODF2L encourages cells to ciliate, hence it usually negatively regulates ciliation.

In addition to the increased cilia numbers, the cilium length of the ODF2L knockdown cells also appeared to be longer than the cilia of the non-target control cells (Figure 5.9C). The average cilium length from the control was 3.1 μm and the average length for the siRNA and siRNA2 were 4.08 μm and 4.10 μm respectively (Figure 5.9E). The analysis of variation (One-way ANOVA) of the cilium length revealed that the length increase in siRNA knockdown cells was statistical significant ($p<0.0001$). Thus, ODF2L appears to be involved not only in negatively regulating ciliogenesis, but also in controlling cilium length.

5.8 Commercial antibodies show differences in localisation of ODF2L

When this study started, only a single commercial antibody was available (Biorbyt™). However, during the study a few more commercial antibodies came onto the market (Novus Bio™, Proteintech™). Therefore, I verified those new antibodies with immunocytochemistry and Western blot analysis.

The Biorbyt™ antibody targets the C-terminus of isoforms a and b (the C-terminus differs from isoforms c and d, please see Figure 5.2) (Figure 5.10). Novus NBP-82922 antibody targets a region in the N-terminus common to all the isoforms, while Novus NBP-82920 only targets isoform b and Novus NBP-56559 targets the C-terminus of isoforms c and d (Figure 5.10). Finally, an anti-ODF2L antibody was purchased from Proteintech™ which recognises all four isoforms (Figure 5.10). All the antibodies were subjected to immunofluorescence microscopy and Western blot analysis to validate their specificity and sensitivity.

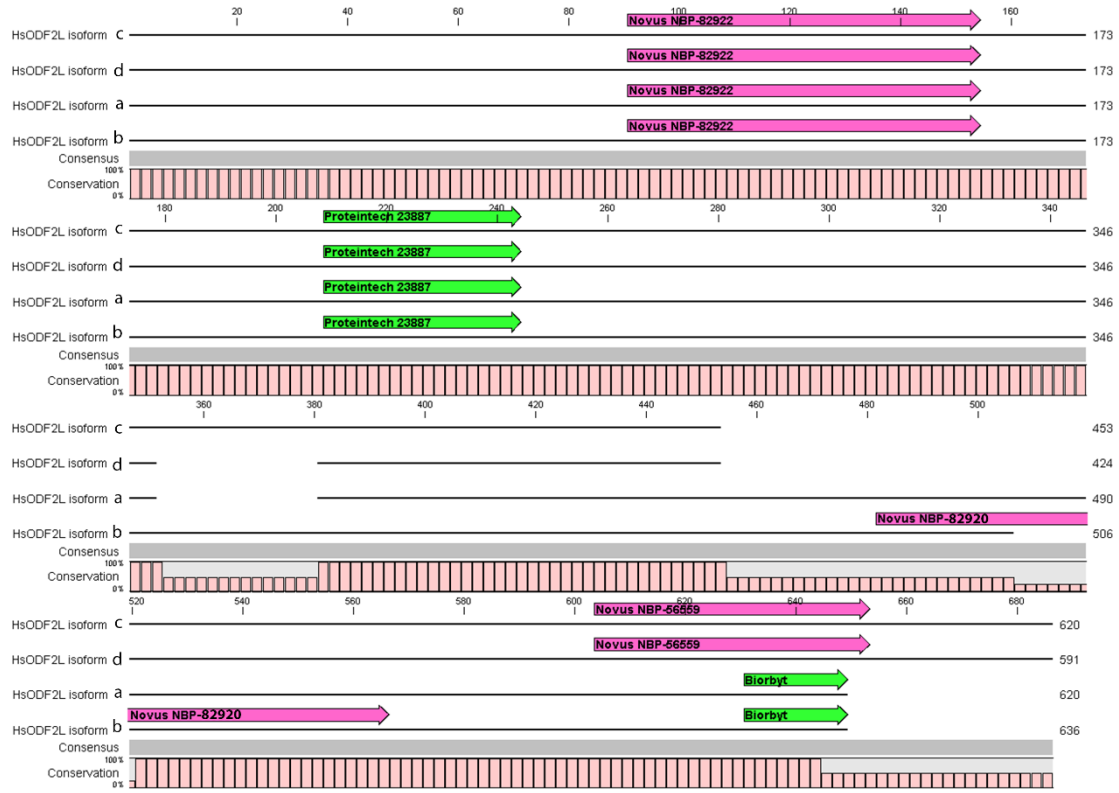

Figure 5-10 Binding regions of commercially available ODF2L antibodies.

The antibodies which show the correct staining by immunofluorescence microscopy and correct molecular weight by western blotting are shown in green. The antibodies that failed to detect ODF2L in either assay are shown in pink.

Three commercially available anti-ODF2L antibodies were purchased from Novus Bio™ and tested in both immunofluorescence and Western blotting. None of the antibodies demonstrated any centriolar satellite staining (Figure 5.11 A-C). In fact, only the NBP-56559 antibody showed any staining, and this appeared to be a rather diffuse nuclear staining (Figure 5.11C). In the Western blot analysis, none of the three antibodies detected a band at the expected molecular weight of ODF2L (69-72 kDa); rather, multiple bands were detected at other molecular weights, particularly either below 55 kDa or above 100 kDa, which may represent proteins other than ODF2L (Figure 5.11 D-F). Thus neither of these three antibodies seemed to work specifically to detect ODF2L, and were not used further.

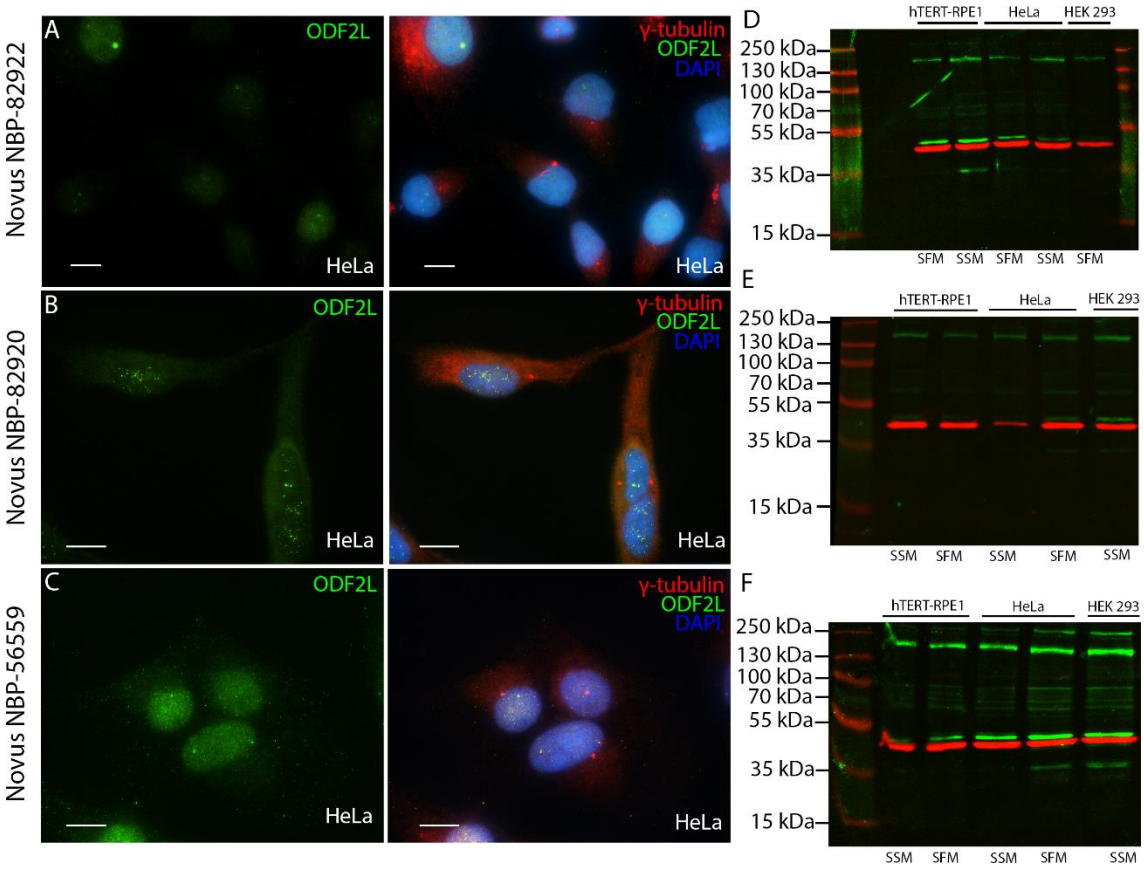

Figure 5-11 Immunofluorescence and Western blotting with three anti-ODF2L antibodies from Novus.

(A-C) Three commercially available antibodies for ODF2L (green) were tested by immunofluorescence on HeLa cells. Cells were co-stained with anti-γ-tubulin to detect centrosomes (red) and DAPI to stain DNA (blue). Neither of the three ODF2L antibodies showed any specific staining. **(D-F)** Western blots containing protein extracts from hTERT-RPE1, HeLa and HEK293 cells cultured with serum supplemented medium (SSM) or serum free medium (SFM). Immunodetection with each of the Novus anti-ODF2L antibodies showed multiple bands (green), though none at the expected size for ODF2L (69-72 kDa). B-actin was used as a loading control (red).

For the Proteintech™ anti-ODF2L antibody (which recognises all 4 isoforms), immunocytochemistry showed strong staining resembling centriolar satellites in cycling cells (Figure 5.12A). However, the staining did not disappear when cells were serum deprived; instead, the antibody stained a vesicular tubular structure which resembles the Golgi apparatus (Figure 5.12B). Also, in serum deprived cells, staining was occasionally observed away from the centrioles (Figure 5.12B, white arrows). In Western blotting, the antibody recognised a band of 70 kDa (Figure 5.12C). This band was also present when cell lysates from serum-deprived cells

were used in the Western blot (Figure 5.12C). Although a single band of 70 kDa was observed with hTERT-RPE-1 cells, there were multiple bands detected when HeLa cell lysates were used (Figure 5.12C). However, these bands were not as prominent nor as bright as the 70 kDa band. Comparison of ODF2L abundance in serum supplemented and serum free medium suggests that there is a slight reduction following culture in serum free conditions (about 25-30%), however ODF2L detection with this Proteintech™ antibody does not disappear completely (Figure 5.12C,D), in contrast to that observed with the Biorbyt™ antibody (Section 5.5).

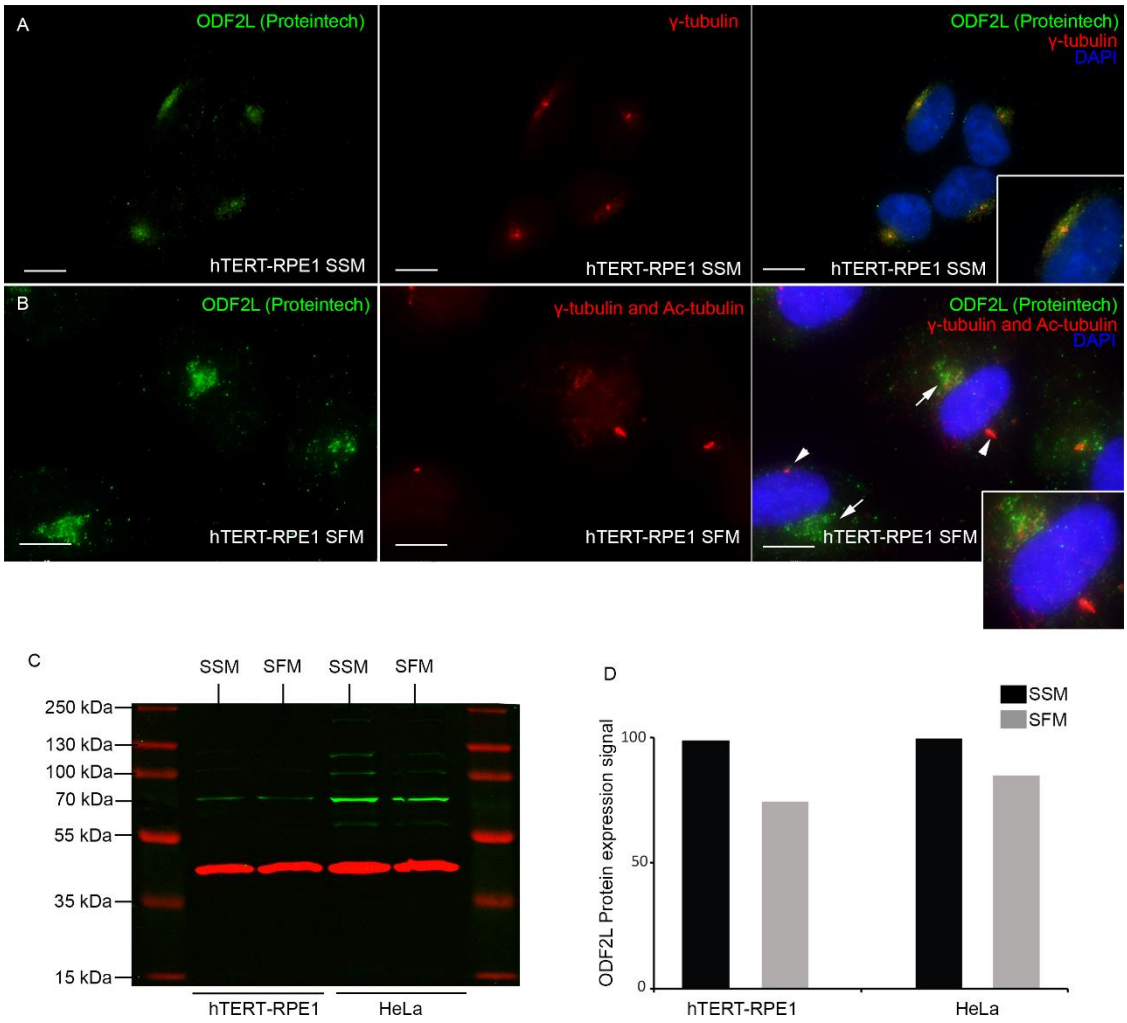

Figure 5-12 Testing of the Proteintech™ anti-ODF2L antibody.

(A, B) Proteintech™ anti-ODF2L antibody staining (green) on hTERT RPE-1 cells either with **(A)** or without **(B)** serum. Cells are co-stained for γ-tubulin and acetylated tubulin (red) and with DAPI (blue). The anti-ODF2L antibody showed a satellite-like staining pattern in continuously dividing cells **(A)** which became more granular and localised away (white arrows) from the centrosome or cilium (yellow arrows) in serum-starved cells **(B).** Scale bars: 10 µm. **(C)** Western bot analysis of lysates from hTERT-RPE1 and HeLa cells cultured either in serum-supplemented medium (SSM) or serum free medium (SFM), detected with Proteintech anti-ODF2L antibody staining (green) and β-actin (red). The anti-ODF2L antibody recognised a 70 kDa band in all lysates; serum starvation did not cause the band to disappear as previously observed with the Biorbyt antibody (Figure 5.5). The HeLa cell lysates showed additional faint bands that may repesent non-specific binding of the polyclonal antibody. **(D)** Quantitation of the ODF2L 70 kDa relative band intensity on the Western blot from SSM to SFM conditions, normalised to β-actin levels. This shows that in serum free medium there appears to be a slight reduction in ODF2L expression, but it does not disappear.

5.9 ODF2L may associate with the Golgi apparatus

The Golgi apparatus (GA) plays a central role in the secretory pathway where newly synthesized proteins are transported from the endoplasmic reticulum (ER) to the GA for the posttranslational modifications. Once the protein is in the GA, it is sorted into transport vesicles and delivered to intended targets such as the plasma membrane or endosomal-lysosomal system by using the microtubule (MT) network. The Golgi apparatus consists of stacks of flattened cisternae which connect laterally to create the membrane system called the Golgi ribbon. The Golgi ribbon is localised closer to the nucleus and surrounds the centrosome and actively maintains this position during interphase by rearranging microtubules and the actin cytoskeleton (Brownhill *et al.*, 2009).

In some hTERT-RPE1 cells cultured in either control (serum supplemented) or serum deprived media, immunofluorescence microscopy showed ODF2L localisation with a vesicular tubular localization, resembling the Golgi apparatus (Figure 5.13A). To establish whether ODF2L was indeed co-localised with the Golgi apparatus, the Golgi was stained with anti-Golgin-97 antibody and ODF2L was stained with the Proteintech™ anti-ODF2L antibody (Figure 5.13B). The co-localisation was analysed using the CoLoc function as described previously (Figure 5.13C). The Pearson's Correlation Coefficient was 0.85 which supports co-localisation, and localisation site analysis indicated an 80% overlap. Furthermore, the intensity profile showed a common intensity pattern between Golgin-97 and ODF2L (Figure 5.13D). Therefore, this suggested that ODF2L may localise to the Golgi apparatus when hTERT-RPE1 cells were serum starved. However, the isoform and the function of ODF2L in the Golgi apparatus is yet to be studied.

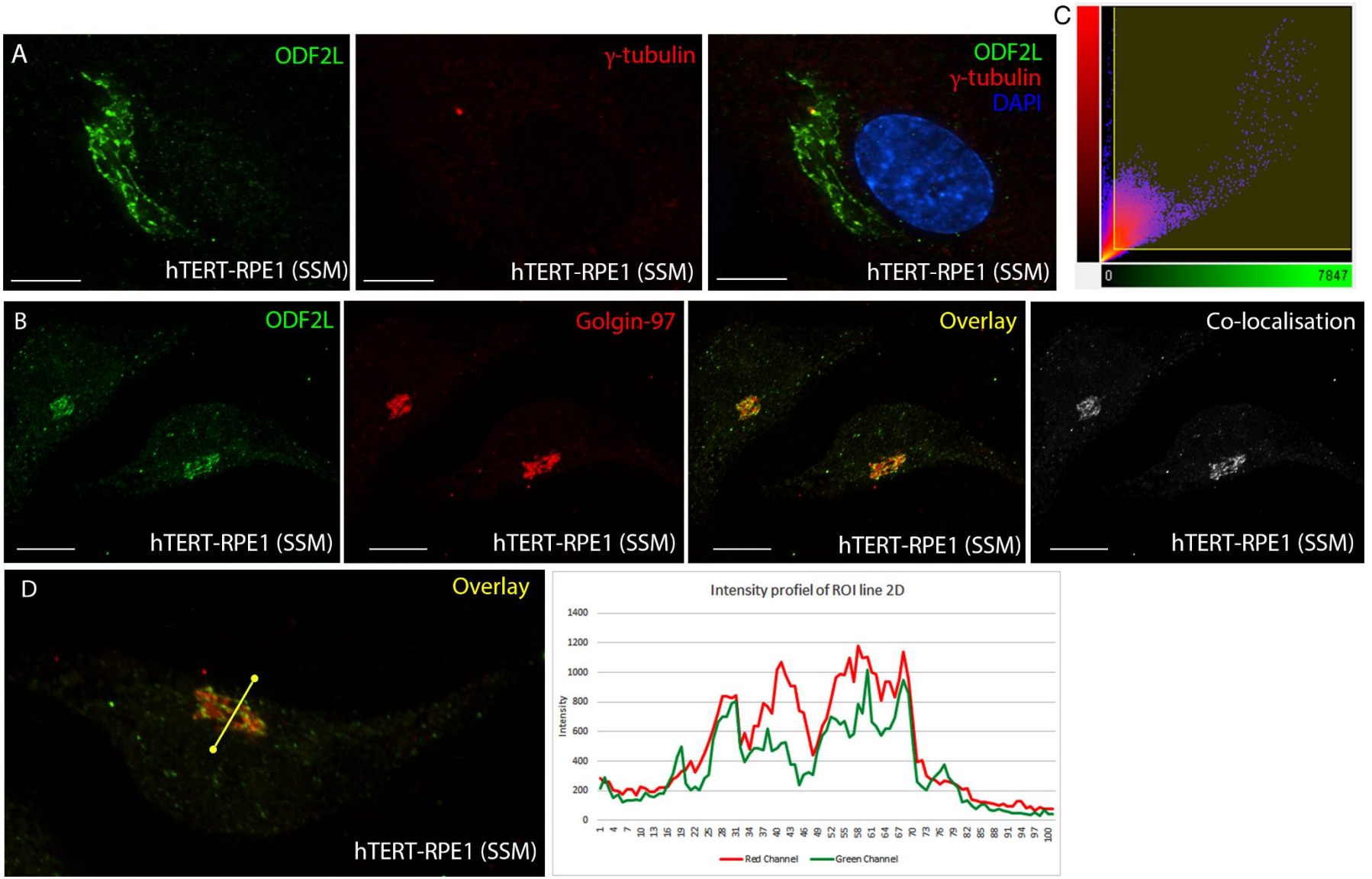
A
ODF2L
hTERT-RPE1 (SSM)
γ-tubulin
hTERT-RPE1 (SSM)
ODF2L
γ-tubulin
DAPI
hTERT-RPE1 (SSM)
C
0
7847
B
ODF2L
hTERT-RPE1 (SSM)
Golgin-97
hTERT-RPE1 (SSM)
Overlay
hTERT-RPE1 (SSM)
Co-localisation
hTERT-RPE1 (SSM)
D
Overlay
hTERT-RPE1 (SSM)
Intensity profiel of ROI line 2D
Intensity
Red Channel
Green Channel

Figure 5-13 ODF2L localisation to the Golgi apparatus.

(A,B) hTERT-RPE1 cells cultured in serum supplemented (control) medium (SSM) and immunostained with Proteintech™ anti-ODF2L antibody (green) and either anti-γ-tubulin (red, **A**) or anti-Golgin-97 antibody (red, **B**) and DAPI (blue). In some cells, ODF2L staining revealed a more tubular structure which resembles the Golgi apparatus (green, **A**). **(C)** Co-localisation histogram showing red and green channel pixel overlap and signal intensity, corresponding to co-localisation of protein expression in a region of interest. This co-localisation analysis was conducted on Z-stacks from confocal microscopy and showed an 80% overlap (white) between ODF2L and Golgin-97 staining. **(D)** Over the line shown in the left panel, the change in intensity in the green signal closesly matches the change in intensity in the red signal, supporting co-localisation of ODF2L and Golgin-97. Scale bar **(A)**: 5 µm, (B): 10 µm.

In recent discoveries, a number of centrosome proteins have been identified to associate with the Golgi apparatus. It has also been demonstrated that the Golgi apparatus retains the ability to nucleate its own microtubules (Miller *et al.*, 2009), suggesting overlapping functions between the centrosome and the Golgi apparatus. Furthermore, the Golgi apparatus and centrosome are known to play a major role in cell polarity and migration (Li *et al.*, 2005). Since ODF2L was observed to localise with the Golgi apparatus and centriolar satellites, I hypothesised that ODF2L may play a role in cell polarity and migration.

5.10 ODF2L is not involved with cell polarity, cell migration or microtubule reorganization

The scratch-wound assay is a simple assay commonly used to measure cell migration and polarity (Nobes and Hall, 1999). In this assay, cells are grown to confluence and then a thin wound is introduced with a pipette tip. The cells at the wound edge re-orientate and migrate into the wound space to close the wound (Cory, 2011). During wound closure, both the centrosome and Golgi are reorientated within the cell, to face the site of the wound. Therefore, close coordination between the centrosome and the Golgi apparatus is needed for the cells to locomote during wound closure. If ODF2L interacts with the Golgi to initiate ciliogenesis, it would be thought-provoking to consider whether there is a connection with cell polarity. To investigate the effect on cell polarity, ODF2L was knocked-down using siRNA and a scratch-wound assay was performed on the hTERT-RPE-1 cells. Cell locomotion and Golgi orientation were observed subsequent to the wound being created.

The wound closure and the migration pattern was checked after 7 h and 24 h. At 7h the wound was partially closed in both control (non-target siRNA) and ODF2L-siRNA transfected cells (Figure 5.14 B,E). By 24 h, the wound was completely closed in both control and ODF2L-siRNA transfected cells (Figure 5.14C,F). Therefore, no migration defects were observed in ODF2L

knockdown cells. Furthermore, the cell polarity was not affected in ODF2L knockdown cells as the Golgi apparatus was orientated towards the leading edge similar to that observed in the non-target siRNA control cells (Figure 5.15). Therefore, ODF2L appears to be not required for cell polarity and reorientation and locomotion during wound healing.

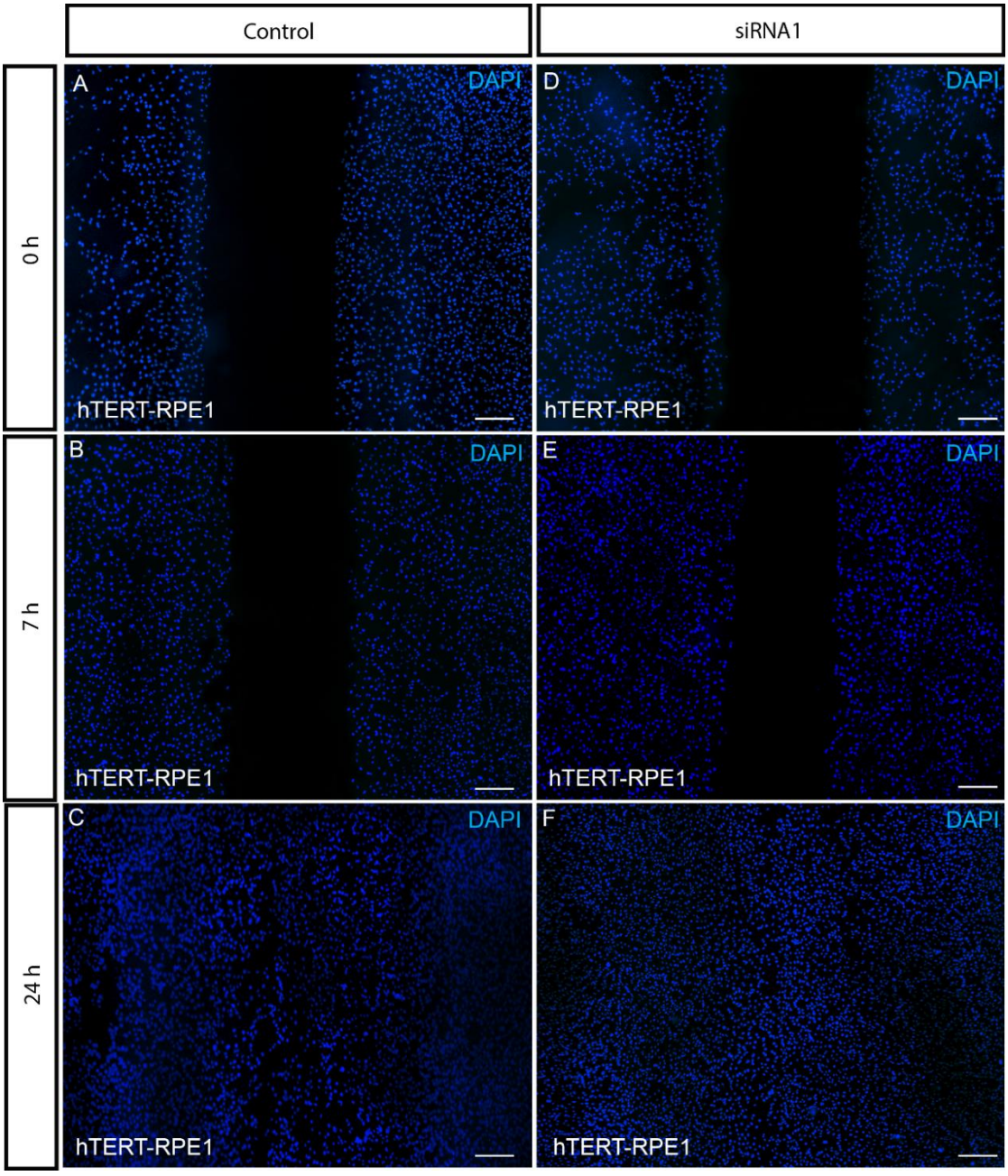

Figure 5-14 Scratch wound assay shows no migration defect in ODF2L-knockdown cells.

Confluent layers of hTERT-RPE1 cells were wounded using the scratch method. The wounds were fixed, stained with DAPI and photographed either immediately after making the wound, or after 7h or 24 h of culture. No difference was seen in the rate of closure for the ODF2L-siRNA transfected cells **(D-F)** compared to the non-target siRNA control cells **(A-C).**

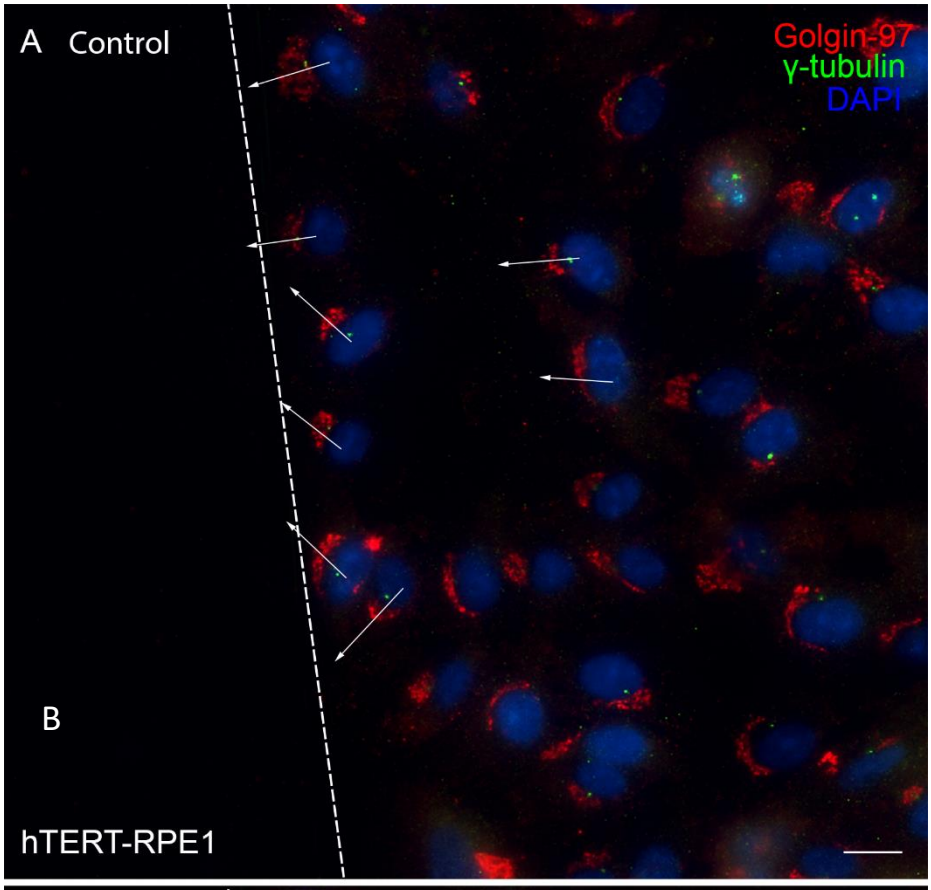
A Control
Golgin-97
γ-tubulin
DAPI
B
hTERT-RPE1

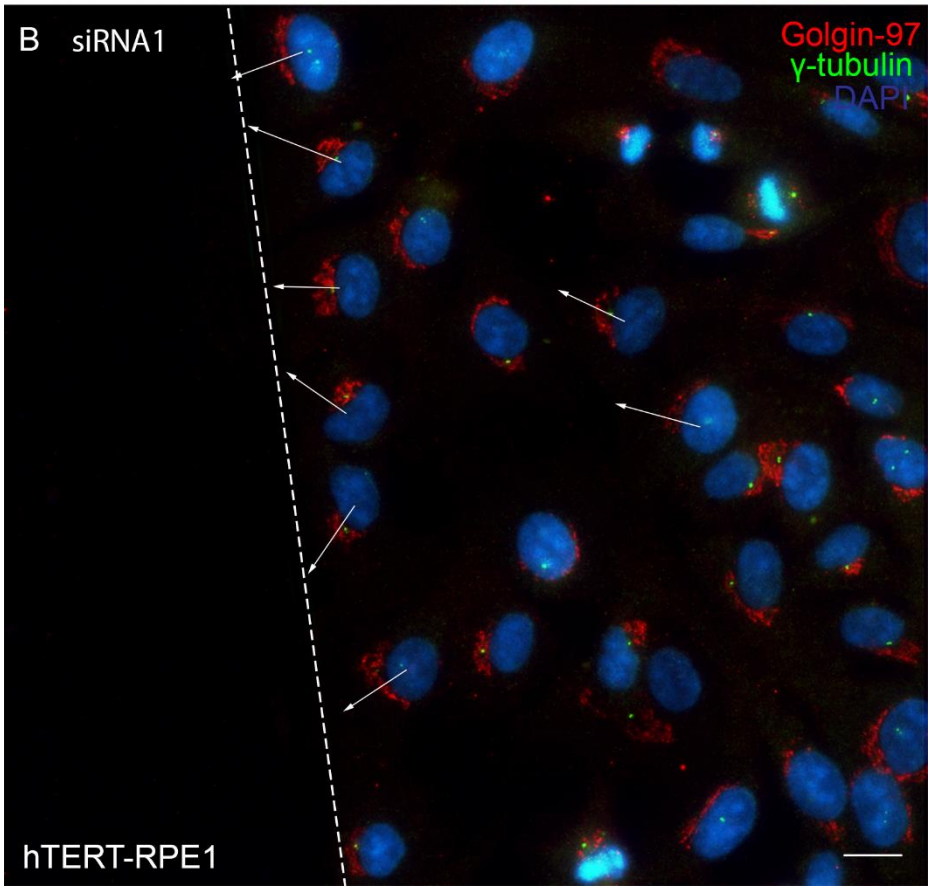
B siRNA1
Golgin-97
γ-tubulin
DAPI
hTERT-RPE1

Figure 5-15 Wound healing assay shows no defect in cell orientation following ODF2L knockdown.

(A-B) hTERT-RPE1 cells following transfection with siRNA to knockdown ODF2L **(A)** or non-target siRNA (**B),** 7 h after wounding, and immunostained for Golgin-97 to detect the Golgi apparatus (red), γ-tubulin to detect the centrosome (green) and DAPI (blue). Cells immediately adjacent to the wound were considered as correctly orientated if the Golgi and centrosome were orientated towards the edge of the scratch in the monolayer. ODF2L knockdown does not alter the ability of cells to orientate towards the wound edge. Scale bar: 10 µm.

A microtubule regrowth assay was performed, to test whether knocking down ODF2L might affect microtubule rearrangement and regrowth. Cultures of hTERT-RPE1 cells were cold treated to depolymerise the microtubules, and then rewarmed to allow the microtubules to repolymerise. Cells were fixed at several time points, to allow the microtubule organisation to be examined. Cells transfected with control non-target siRNA showed microtubule aster formation by 1.5 minutes, and no differences were observed in cells transfected with siRNA to knockdown ODF2L (Figure 5.16). Thus ODF2L knockdown appears not to interfere with microtubule organisation.

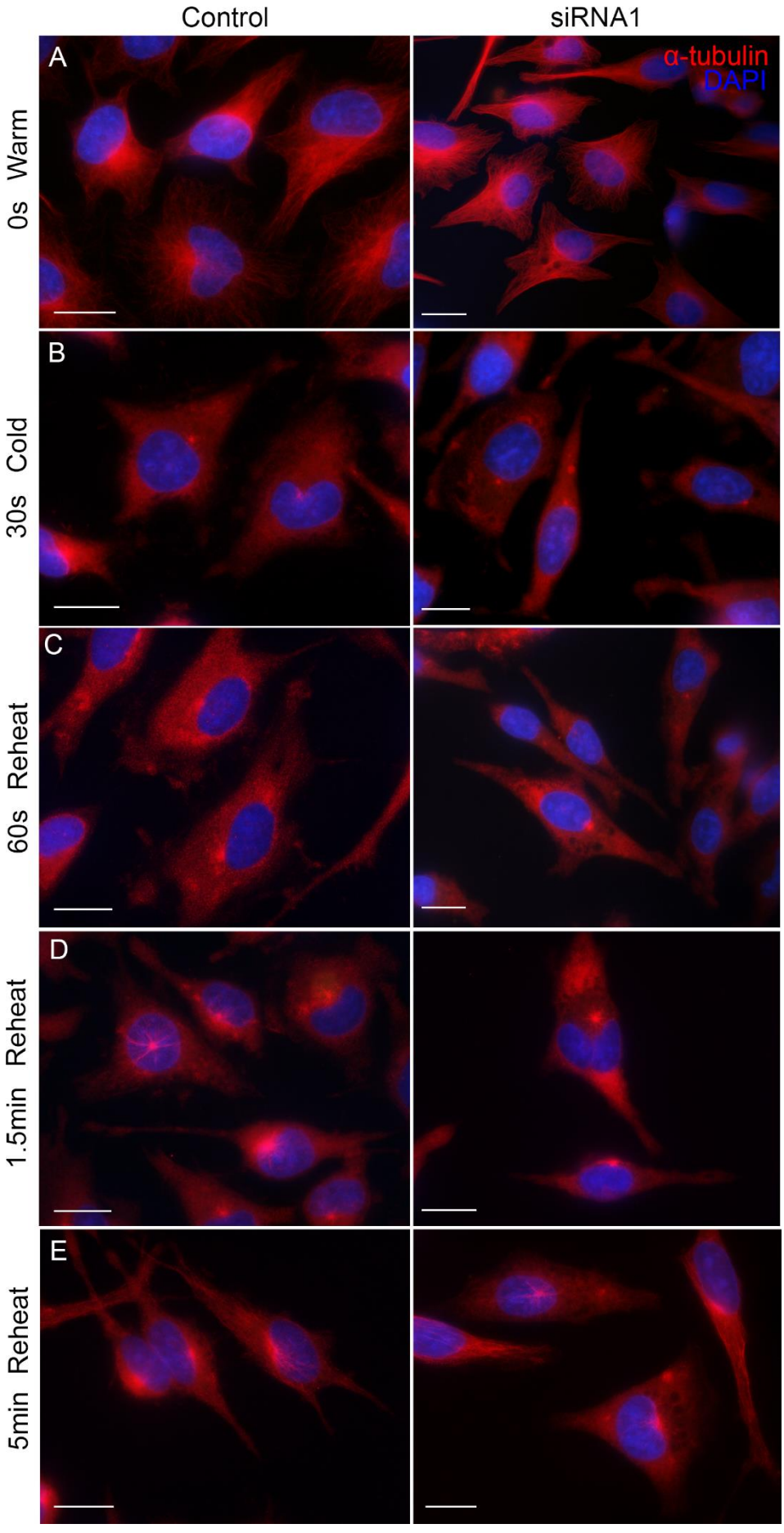
Control
siRNA1
α-tubulin
DAPI
A
0s Warm
B
30s Cold
C
60s Reheat
D
1.5min Reheat
E
5min Reheat

Figure 5-16 Microtubule regrowth assay shows no change following ODF2L knockdown.

Cultures of hTERT-RPE1 cells were taken from warm conditions **(A)** and treated with cold medium (4°C) for 30 seconds to cause microtubules to depolymerise **(B).** The medium was then replaced with warm (37°C) medium, and after a further 30 s **(C)**, 1 min **(D)** or 4.5 min **(E),** cells were fixed and stained. Microtubules were detected with anti-α-tubulin staining (red); nuclei were detected with DAPI (blue). Cells transfected with siRNA to knockdown ODF2L (right hand panels) show similar microtubule regrowth characteristics to the control cells transfected with non-target siRNA (left hand panels).

5.11 Localisation profile of ODF2L in interphase and during ciliation

In this chapter, I have shown that ODF2L appears to negatively regulate ciliogenesis in serum deprived cell cultures and may be associated with the Golgi. These observations paint a complex picture of the behaviour of the ODF2L during different cellular events. It is therefore important to determine how the localisation of ODF2L changes during ciliogenesis. To study the localisation profile, hTERT-RPE1 cells were plated on coverslips and grown to confluency. When cells reached 70-80% confluency, cells were treated with nocodazole as described in the Materials and Methods section, to synchronise the cells so they leave the cell cycle at the same time. After nocodazole treatment for 24 h, cells were carefully washed and released from the mitotic block by changing to fresh cell culture medium without serum. Then the cells were fixed at different time points with formaldehyde and immunostained for ODF2L, γ-tubulin and acetylated α-tubulin, to follow the localisation change of ODF2L during the process of ciliogenesis.

At the point of release from the mitotic block, ODF2L appeared to be scattered around the cytoplasm in several punctae (0 min time point, Figure 5.17). After this point, ODF2L staining disappeared, to reappear at 6 h, at which point ciliogenesis was well underway as seen by the dash-like staining of the anti-tubulin antibodies (6 h time point, Figure 5.17). ODF2L appears to be clustered around the base of the cilium (6 h time point onwards). The above observations are consistent with ODF2L negatively regulating the initiation of ciliogenesis.

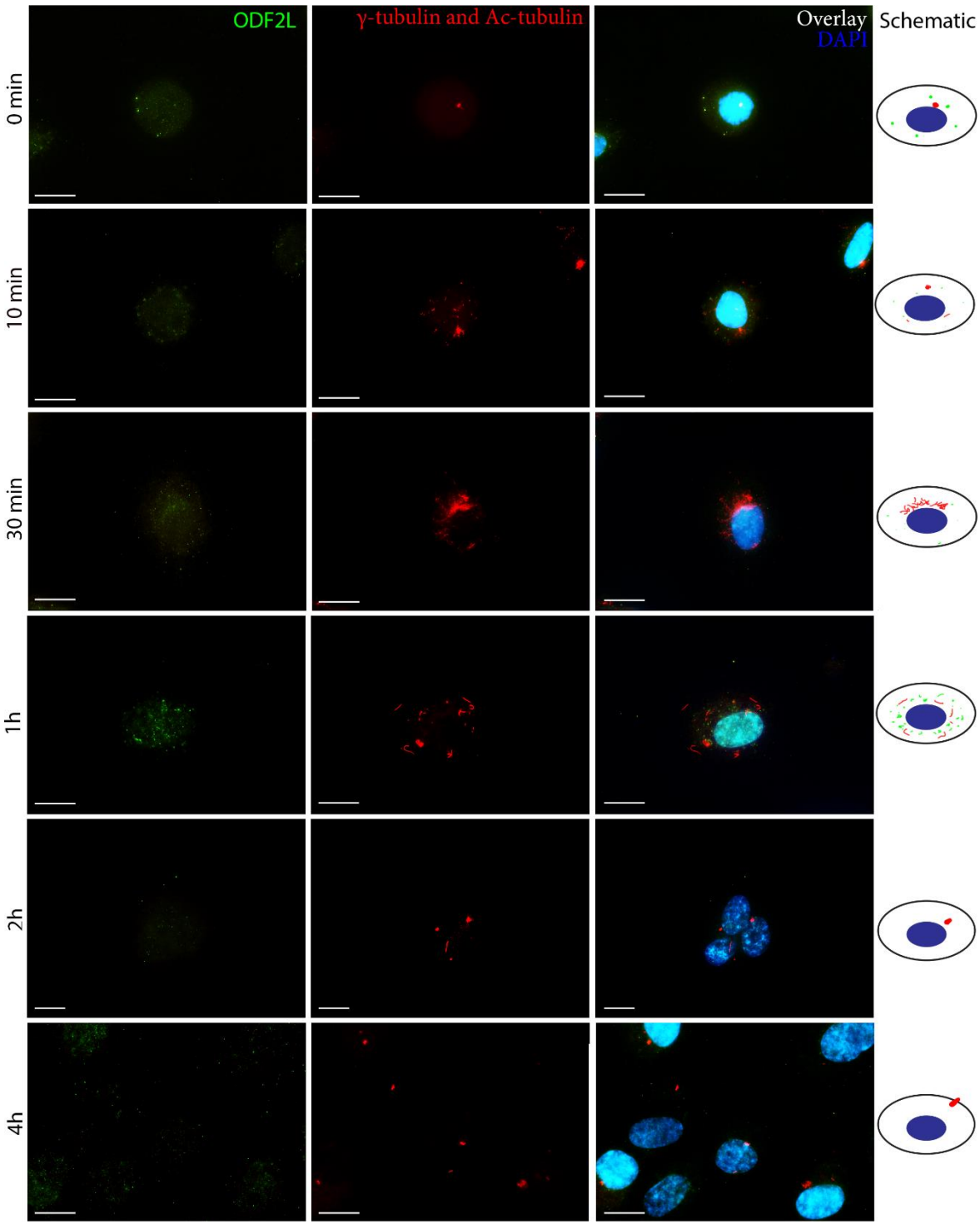
ODF2L
γ-tubulin and Ac-tubulin
Overlay
DAPI
Schematic
0 min
10 min
30 min
1h
2h
4h

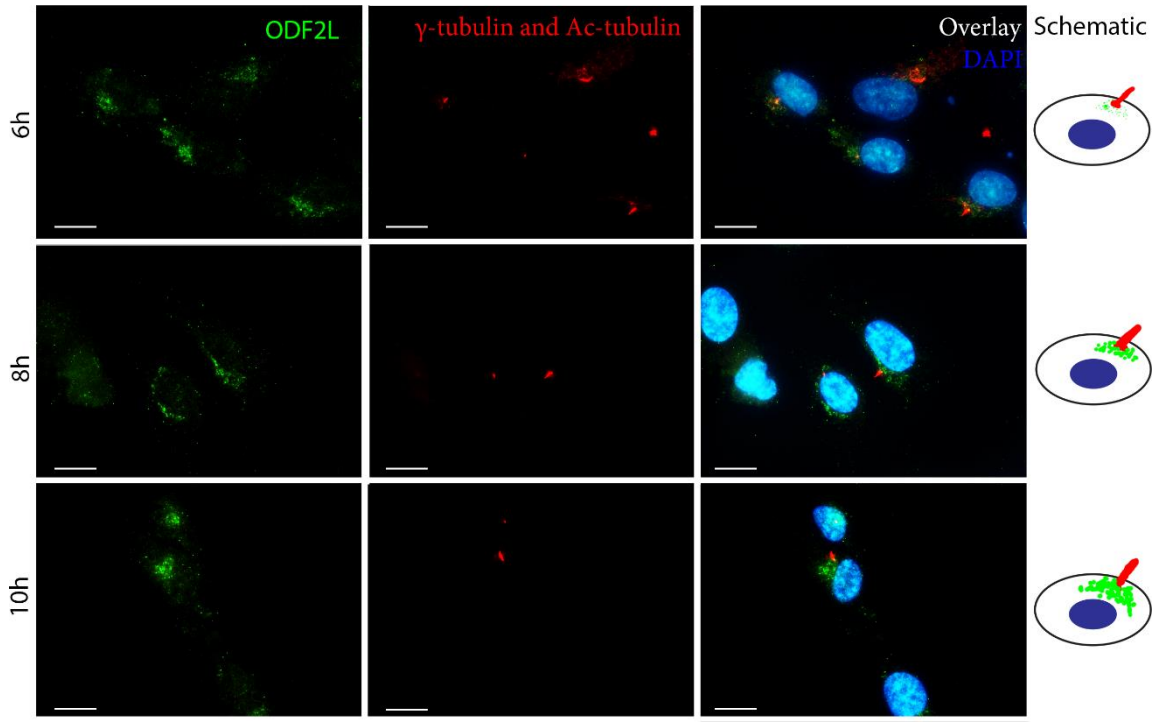

Figure 5-17 Cell synchronisation and release study examining ODF2L localisation during ciliogenesis.

hTERT-RPE1 cells were sychronised using nocodazole and released into serum-free medium. Cells were fixed at the time points indicated after release, and immunostained with Proteintech anti-ODF2L antibody (green), antibodies for γ-tubulin and acetylated α-tubulin (red) and with DAPI (blue). ODF2L staining shows a scattered localisation immediately after release from the mitotic block (0 min). The ODF2L signal then disappears, reappearing at 6 h, when ciliogenesis is well underway and a satellite-like localisation is observed. From 6 h the cilium is clearly evident, and ODF2L staining becomes progressively stronger at the base of the cilium from this time onwards. Diagrams to the right give a schematic representation of the progress of events. Scale bar: 10 μm.

.

5.12 Effect of ODF2L on cell cycle

To test if ODF2L is required for cells to progress through the cell cycle, cells were transfected with siRNA to knock down ODF2L and kept in serum starvation for 24 hours. The medium was then supplemented with 10% serum to allow the cells to re-enter the cell cycle, and cells were cultured for a further 24 hours before being analysed with FACS to determine the proportion in each phase of the cell cycle.

ODF2L knockdown by siRNA transfection showed only slight differences in G1 clustering (80% vs 75%) and G2 frequency (14% vs 19%), compared to the untransfected controls (Figure 5.18).

However, overall cell populations following ODF2L siRNA transfection were comparable to the control cells, therefore knockdown of ODF2L did not have a significant effect on the cell cycle.

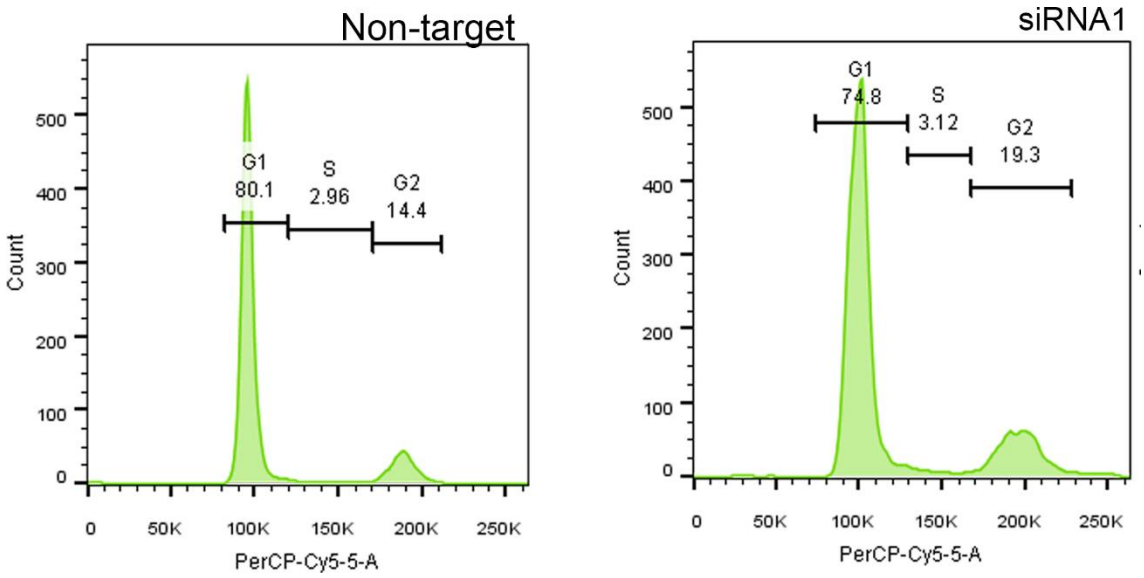

Figure 5-18 ODF2L knockdown has no effect on cell cycle.

FACS analysis of hTERT-RPE1 cells transfected with non-target siRNA (left) or with ODF2L siRNA (right) following 24 hours culture in serum supplemented medium after reentering the cell cycle following 24 hour culture in serum starvation. Proportion of cell population in each phase of the cell cycle is shown. Cell cycle analysis found no significant difference in the cell population between control and siRNA transfected cells (n=3).

5.13 Summary

In this Chapter, I have shown that *Homo sapiens* ODF2L is a 69-72 kDa protein that appears to localise to centriolar satellites in proliferating cells and also appears to associate with the Golgi in some cells. Its disappearance during ciliogenesis and the fact that depleting ODF2L results in cells forming cilia under conditions in which they usually do not, suggests that ODF2L is a negative regulator of ciliogenesis. Conversely, overexpression of ODF2L diminished the ability to ciliate even after the induction of ciliation via serum deprivation. The evidence from the two different antibodies we have used suggests that the different isoforms of ODF2L have subtly

different roles in this process. The a and b isoforms, recognised by the Biorbyt™ antibody, do not reappear once cilia have been formed. However, additional isoforms, recognised by the Proteintech™ antibody, probably have another role once cilia are established, but still need to be absent for ciliogenesis to occur.

The siRNAs used here are predicted to cause the depletion of all isoforms. When all isoforms are depleted, not only are cilia formed when they usually would not, but the cilia are also longer than those formed under the conditions of serum starvation. Our immunofluorescence data suggests that isoforms c and d would normally return after the initiation of ciliogenesis. However, when we deplete ODF2L via siRNA, isoforms c and d will also be depleted and *not* return after the initiation of ciliogenesis. This suggests that isoforms c and d of ODF2L may be involved in regulating the length of cilia. There is a wide variation of cilium lengths and morphologies that exist depending on the cilium function in specific tissues (Silverman and Leroux, 2009). Although a few proteins have been identified to control the cilium length, the mechanism involved in controlling the cilium length is not yet identified. In recent years, the balance point model has been proposed as to how the cell controls its cilium length by a balance between cilium assembly and disassembly rate (Engel *et al.*, 2009; Hilton *et al.*, 2013). Therefore, the length differences observed with siRNA knockdown cells might mean that ODF2L is involved in this mechanism. Nevertheless, further studies are needed to ascertain the complete mechanism by which ODF2L regulates cilium length.

Proteins involved in the control of ciliogenesis often have other roles in centrosome and cilium biochemistry (Spektor *et al.*, 2007; Tsang *et al.*, 2008; Tang *et al.*, 2013). We tested if depletion of all isoforms of ODF2L affected the ability of the cell to enter and progress through the cell cycle and if it affected the ability of the cell to locomote, which also reflects the ability of the cell to polarize in response to environmental cues. In both cases, we found depletion of ODF2L to have no effect on these processes. This is consistent with the role of ODF2L being restricted to

controlling the initiation of ciliogenesis and maybe modulating cilium length when this process is complete. However, further experiments testing other aspects of ciliogenesis will be required to confirm that this is the case.

5.14 Possible future work

In this study, the different ODF2L isoforms may be involved in both regulating the onset of ciliogenesis and in regulating the length of cilia formed. However, the results obtained do not differentiate the precise isoforms involved. Therefore, in future work it would be interesting to explore the expression of these isoforms using RT-PCR to analyse whether the ODF2L isoforms' expression is changed before and during ciliation. Once the presence of the multiple isoforms is established, it would be interesting to study individual isoform's localisation within the cell by cloning each isoform and tagging with GFP or RFP to observe the localisation. It would also be interesting to identify the binding partner(s) of each isoform, such as by using yeast two-hybrid screens or mass spectrometric analysis of proteins that co-immunoprecipitate or pull down with ODF2L. Results from initial pull-down experiments will be discussed in the next chapter.

The method used for induction of ciliation in this study was serum starvation, which is a commonly employed protocol in studies on cilia. It is commonly accepted that serum starvation stops cells proliferating, allowing them to ciliate. However, serum starvation has been suggested to not be the ideal mechanism for studying ciliogenesis, as this condition will likely stress cells in other ways (Pirkmajer and Chibalin, 2011). It would be interesting to examine whether ODF2L gives similar results if ciliogenesis is induced by other means, such as when artificially induced with chemical agents such as sphingolipid ceramide (Wang *et al.*, 2009a; He *et al.*, 2014).

Furthermore, the dynamic change of ODF2L was much harder to study by time lapse fixation methods therefore, another approach would be to stably express GFP-tagged ODF2L in cells and

use video microscopy to study the dynamic interaction of this protein with the satellites and the Golgi apparatus.

Chapter 6:

Exploring the Structural and Functional Relationship of ODF2L

6.1 Structural predictions

In the previous chapter, ODF2L was shown to exhibit centriolar satellite-like localisation, and knockdown of ODF2L is consistent with it acting to negatively regulate ciliogenesis in mammalian cells. However, the exact mechanism of action is unknown. Also, the localisation of ODF2L resembled the Golgi apparatus in some cells, suggesting that it may also be associated with trafficking vesicles from the Golgi.

ODF2L is likely to function through interactions with other proteins. In the previous chapter, protein structural motif analysis using the SMART database identified 3 or 4 coiled-coil domains (CCD) as well as low complexity regions (LCR) near the N-terminus in all ODF2L isoforms and another LCR domain in the middle region in two of the isoforms (Figure 5.1). Both CCD and LCR domains are known to be important for mediating protein interactions. Coiled-coil domains are autonomous folding units consisting of two to five α-helices wrapped around each other with a left-handed twist to form supercoiled regions with typically a rod-like structure. Genes encoding coiled-coil proteins comprise roughly 2-3% of the coding sequence of the eukaryotic genome implying an involvement in numerous cellular processes (Wolf *et al.*, 1997). These coiled-coil structures can also be modulated by phosphorylation (Szilak *et al.*, 1997) or by interaction with ions (Farah and Reinach, 1999) therefore making them versatile folding motifs (Burkhard *et al.*, 2001). These motifs are known to be involved in a broad range of different functions depending on the organisation of the coiled-coil domains, and are found in cytoskeletal, motor, Golgi, endosome and centrosome proteins, where a high degree of vesicle transport necessitates a large number of tethering factors (Gillingham and Munro, 2003). In fact, it has been proposed that the rod-like structure of coiled-coil proteins may enable them to assemble into arrays along a membrane, therefore increasing their local concentration and making a meshwork of tethers that could act to ensure that vesicles are selectively captured or repelled from a particular membrane (Gillingham and Munro, 2003). The proteins involved in secretory pathways often contain a discrete coiled-coil domain at their N or C terminus, which may mediate organelle-

specific targeting or interaction with other proteins, followed by a few other coiled-coil domains separated by small stretches of non-coiled-coil sequences. These non-coiled-coil spacer regions could act as hinges, enabling vesicles docking at one end of the tether to be physically moved closer to the membrane via mechanical bending. Low-complexity regions (LCRs) in a protein are areas with little diversity in the amino acid composition. LCRs are found abundantly in proteins and are believed to play important roles across a wide range of biological functions. A study conducted by Ekman *et al.* (2006) on yeast protein-protein interactions (PPI) noted that the highly connected 'hub' proteins contain an increased proportion of LCRs compared to non-hub proteins. Furthermore, LCRs positioned at the terminus of the sequences have more binding partners than LCRs positioned more internally within the protein due to the difference in accessibility (Coletta *et al.*, 2010). This increased accessibility of the terminal LCR domains has suggested that they may be involved in forming large protein complexes, such as with cargo proteins and chaperones. The accessibility of the centrally located LCRs may be regulated by protein conformation changes, such as in response to protein binding or phosphorylation cascades in signalling pathways (Ekman *et al.*, 2006). Therefore, given the coiled-coil and LCR domain organisation of ODF2L, it is reasonable to suggest that it may interact with a number of partners, which may also change depending on cell pathway activation.

6.2 ODF2L structural predictions

The earlier SMART analysis identified LCRs and coiled-coil domains in ODF2L, however a more comprehensive database was needed to search for additional protein motifs. Therefore, the ODF2L isoform sequences were analysed with NCBI-conserved domain search (NCBI-CDD) using Pfam v27.0 as the database. This search recognised an APG6 domain within the coiled-coil region near the C-terminus in all four isoforms of ODF2L (Figure 6.1B). The APG6 domain is found in many proteins, including yeast vascular sorting-associated protein 30 (Vsp30) and autophagy-

related protein 6 (Apg6), as well as in the mammalian homologue of Apg6, Beclin-1, and therefore may suggest a link to autophagy and membrane trafficking. (Kang *et al.*, 2011; Wirawan *et al.*, 2012).

In addition, a HOOK domain was recognised adjacent to the APG6 domain in isoform b, while an ADIP domain was identified in isoforms a and d (Figure 6.1A). The HOOK domain is found in HOOK family proteins and is involved in binding with Golgi membrane or with microtubules (Walenta *et al.*, 2001; Sano *et al.*, 2007). The Afadin and alpha-actin binding (ADIP) domain is an actin-binding region that can also facilitate the anchoring of the minus end of spindle microtubules to the centrosome or the spindle-pole-body (Toya *et al.*, 2007).

The four isoforms of ODF2L therefore have both similarities and differences in their protein domain organisation. Furthermore, the specific combination of domains in particular isoforms may affect the overall function. Further studies are necessary to validate the roles of the domains.

6.3 ODF2L post-translational modification prediction

The ODF2L sequences were analysed *in silico* for post-translational modifications (PMT) using ModPred (Pejaver *et al.*, 2014) software for sequence based and group based prediction analysis. The analysis predicted an identical phosphorylation pattern at the N-terminus of all four isoforms (Figure 6.1A), but with differences between isoforms in the middle and C-terminus (Figure 6.1B). The most strongly predicted phosphorylation sites were for T619 and T635 in isoform a and b respectively (Figure 6.1A; Score: 0.87). The sequences were also analysed for the kinases involved in phosphorylation, by using the Group-based Prediction System (GPS) tool (Xue *et al.*, 2005; Xue *et al.*, 2008). The GPS analysis identified T619 and T635 sites as putatively phosphorylated by many kinases, including MAPK/JNK (score 35.6), MAPK/ERK (score 30.6), CDK1 (score: 22.5), PEK (score: 21.6), GRK (Score 21.9), and FRAP (score: 20.16). Therefore, GPS

predicts that the common C-terminus region (LVCKMNSDPETP) of isoforms a and b may be phosphorylated by the CMGC group (including cyclin-dependent kinases (CDKs), mitogen-activated protein kinases (MAP kinases), glycogen synthase kinases (GSK) and CDK-like kinases) of kinases.

The small ubiquitin-like modifiers (SUMO) are capable of covalently modifying specific lysine residues (Hay, 2005) and enabling protein-protein interactions through cognate SUMO-interacting motifs (SIMs) (Hannich *et al.*, 2005); it has been identified as one of the most important types of post-translational modification. The enzymes involved in SUMOylation are present in the cytoplasm (Melchior *et al.*, 2003) and known to play roles in the endoplasmic reticulum (Dadke *et al.*, 2007), regulating intermediate filaments (Kaminsky *et al.*, 2009) and membrane receptors (Martin *et al.*, 2007). In recent years, SUMOylation has also been implicated for localisation of proteins to the cilium (Li *et al.*, 2012; McIntyre *et al.*, 2015) and SUMOylation motifs have been found in some centrosome proteins, such as ninein and centrin-2 (Cheng *et al.*, 2006; Klein and Nigg, 2009). Therefore, we analysed whether ODF2L may be a substrate for SUMOylation.

The ODF2L isoform sequences were analysed for putative SUMOylation by using Group-based Prediction System, GPS-SUMO version 1, set with a high threshold. Two possible SUMO-interacting motifs (SIMs; Figure 6.1A, red bars) and two putative sumoylation sites (Figure 6.1B, amino acids in red) were identified in isoforms B and C, while isoforms A and D contained a single predicted SIM site and two putative sumoylation sites (Figure 6.1B in red).

6.4 ODF2L 3D structure prediction

The 3D structures of the ODF2L isoforms were predicted using Raptor X (Kallberg *et al.*, 2012). Distinct structures were predicted for the four ODF2L isoforms (Figure 6.1C). Isoforms a and d are predicted to have an elongated filament-like organisation. However, isoform b is predicted

to have a “U”-shaped structure whereas isoform c shows a “Y”–shaped structure. These different predicted structures reinforce the possible functional differences between the isoforms.

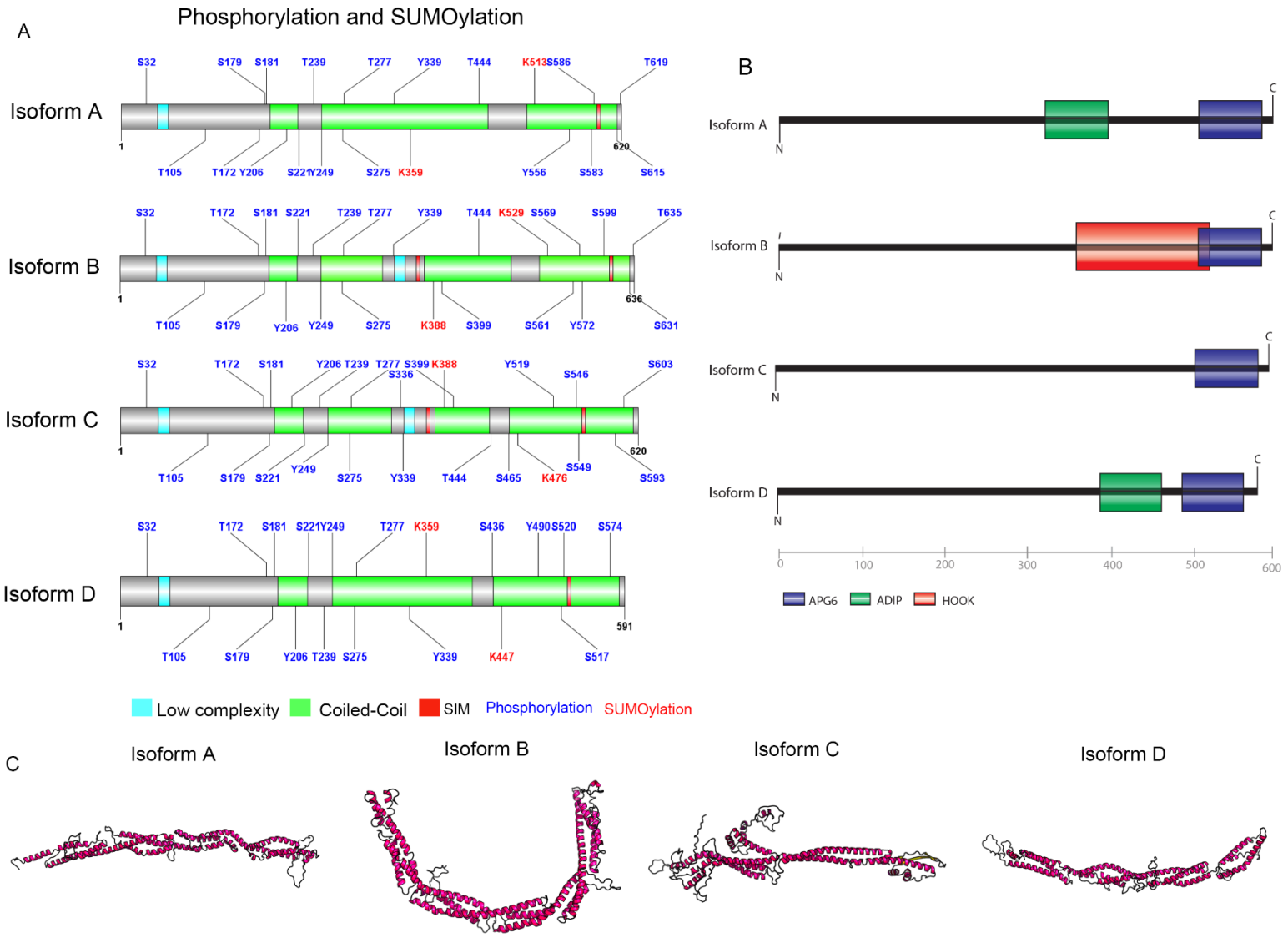
A
Phosphorylation and SUMOylation
Isoform A
S32 S179 S181 T239 T277 Y339 T444 K513 S586 T619
T105 T172 Y206 S221 Y249 S275 K359 Y556 S583 S615
Isoform B
S32 T172 S181 S221 T239 T277 Y339 T444 K529 S569 S599 T635
T105 S179 Y206 Y249 S275 K388 S399 S561 Y572 S631
Isoform C
S32 T172 S181 Y206 T239 T277 S399 K388 S336 Y519 S546 S603
T105 S179 S221 Y249 S275 Y339 T444 S465 K476 S549 S593
Isoform D
S32 T172 S181 S221 Y249 T277 K359 S436 Y490 S520 S574
T105 S179 Y206 T239 S275 Y339 K447 S517
Low complexity
Coiled-Coil
SIM
Phosphorylation
SUMOylation
B
Isoform A
Isoform B
Isoform C
Isoform D
N
C
0 100 200 300 400 500 600
APG6
ADIP
HOOK
C
Isoform A
Isoform B
Isoform C
Isoform D

Figure 6-1 Functional domain organisation, and predicted phosphorylation and SUMOylation of ODF2L isoforms.

(A) Predicted phosphorylation sites (blue), SUMOylation sites (red) and SIM motifs (red bars) in ODF2L isoforms. All the isoforms share a common phosphorylation pattern in the N-terminus but different pattern towards the C-terminus. T619 and T635 in isoforms a and b were identified as the putative phosphorylation sites with the highest confidence. **(B)** Pfam-based functional domain organisation of ODF2L isoforms. All the isoforms shared an APG6 domain (blue) in the C-terminus. A HOOK domain (red) was identified in isoform b. An ADIP domain (green) was identified in isoforms a and d. **(C)** Raptor X based tertiary structure prediction for the ODF2L isoforms. Isoform a and d show a similarly predicted tertiary organisation, while isoform b is predicted to form a U-shape and isoform c a Y-shape.

6.5 Overexpression of ODF2L and pull-down of the binding partners

The computer-based domain analysis above predicts the presence of a number of motifs and domains that may be involved in allowing the interaction of ODF2L with other proteins. Therefore, I set out to identify the binding partners of ODF2L by overexpressing mouse Odf2l in mammalian cells, isolating the interacting partners and then identifying these proteins using mass spectrometry.

In an ideal experimental setting, it would be important to use the endogenous ODF2L to assess the interacting partners and pull-down the interacting complexes using an anti-ODF2L primary antibody. However, all the commercially available ODF2L antibodies were polyclonal. The specificity of the tested ODF2L antibodies were not optimised for pull-down study and, indeed, multiple bands were observed in the Western blot analysis (Figure 5.12). Another problem was the difficulty of acquiring the pre immune serum for a commercial antibody. Therefore, the strategy used here was to increase the expression of ODF2L in cells by overexpressing the GFP tagged ODF2L and using an anti-GFP antibody to pull-down the ODF2L together with any interacting proteins.

6.5.1 Overexpression of ODF2L in mammalian cells

In the previous chapter, a GFP-tagged mOdf2l expression plasmid was constructed (Section 5.4) and validated to show centriolar satellite-like localisation of the GFP-mOdf2l fusion protein in immunocytochemistry studies (Figure 5.6). Therefore, the same expression construct was used to overexpress mOdf2l for the pull-down assay. To maximize the transfection and protein yield HEK293T cells were used, and transfected as described in the Materials and Methods (Section 2.2.3). Transfection efficiency was tested in our HEK293 cells by transfecting a GFP-expressing parental plasmid (pCS2P-eGFP) with subsequent analysis by FACS. The transfection efficiency for HEK293 was found to be about 60% (Figure 6.2).

HEK293 cells were transfected with pCS2P-eGFPN-mOdf2l (abbreviated to GFP-mOdf2l), grown to 90-95% confluency and then total cell lysates were prepared. The lysates were incubated with either Chromotek GFP-TRAP®-MA magnetic beads or GFP-TRAP®-A agarose beads, in which an anti-GFP antibody is conjugated to the beads. Incubation with the beads should enable the GFP-tagged Odf2l protein to be enriched, together with any interacting proteins. As a control, HEK293 cells transfected with the pCS2P-eGFP parental plasmid were processed in parallel with the GFP-TRAP®-MA magnetic beads. Before the enrichment with GFP-TRAP®-MA, the cell lysate was pre-cleared using unconjugated magnetic beads for 30 min to minimise the nonspecific binding.

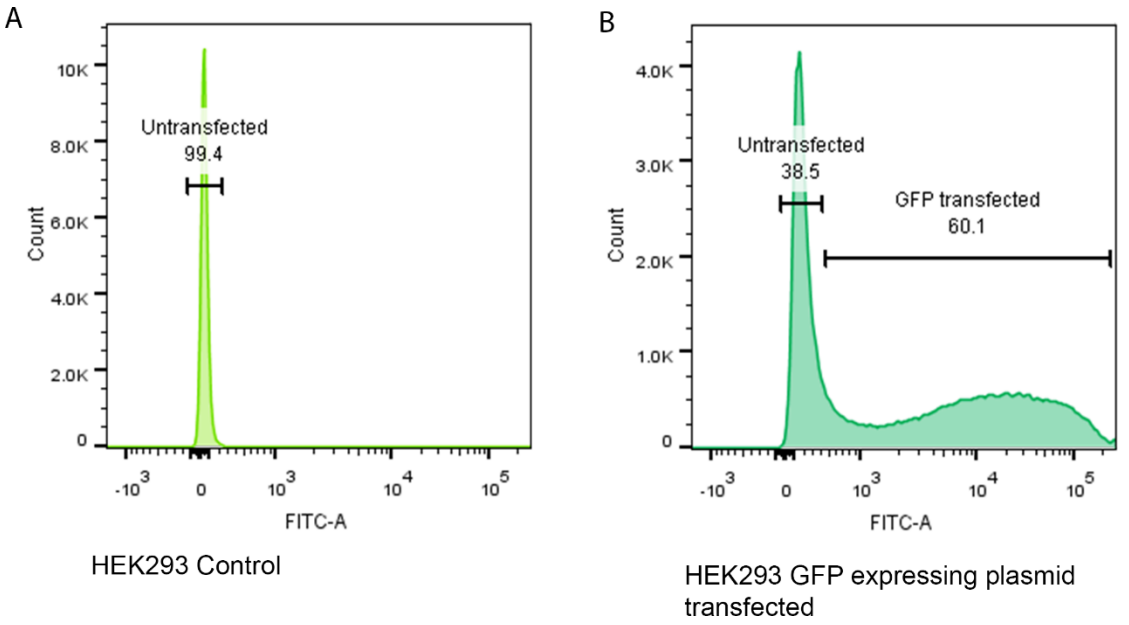

Figure 6-2 Analysis of transfection efficiency of HEK293T cells.

FACS analysis of the proportion of GFP-expressing and non-expressing cells in non-transfected HEK293 cells **(A)** or following transfection with the GFP expressing construct pCS2P-eGFPN **(B).** Transfected cells show about 60% transfection efficiency with the plasmid.

The pull-down of eGFPN-mOdf2l was verified by SDS-PAGE and Western blot analysis using monoclonal anti-GFP antibody and also an anti-ODF2L antibody (Proteintech™). The Western blots included samples of the clarified cell lysate before enrichment (lysate, lys), the unbound

material after incubation with the beads (unbound, unb) and the eluates from the antibody-conjugated beads following incubation and washing (eluate, elu). Pulled-downs were processed in parallel for both GFP and GFP-mOdf2l samples. For both GFP and GFP-mOdf2l, using either the magnetic or agarose beads, results were similar. The GFP or GFP-mOdf2l protein was clearly detected in the lysate, was partially reduced in the non-bound sample, and was present or enriched in the eluate (Figure 6.3 A,B). These results show that the GFP-pull down procedure has been successful, in that the GFP tagged protein was able to bind to the beads and then be released from the beads. The detection of β-actin was included as a control and showed robust detection in the lysates and non-bound fraction in each case, and was undetectable in the eluates, indicating that this has been successfully washed off the beads (Figure 6.3 A,B,C).

Eluted proteins were also analysed by SDS PAGE followed by either Coomassie or silver staining to detect the pulled-down proteins. Both Coomassie and silver staining identified a number of bands, including a prominent band of 100 kDa from the eGFP-mOdf2l pull-down and about 30 kDa from the eGFP pull down (Figure 6.3 D,E). The 100 kDa band corresponds to the expected molecular weight of the eGFP-mOdf2l (32.7kDa+68.01kDa), consistent with successful pull-down.

After silver staining, a number of bands with different molecular weights were witnessed from the eGFP-mOdf2l pull-down (Figure 6.3D), and the observed band pattern was distinct from that seen with the GFP pull-down samples. The presence of multiple bands in the eGFP-mOdf2l pull-down suggested that proteins that interact with Odf2l have been co-precipitated. To identify the co-precipitated proteins, LC MS-MS mass spectrometry was used.

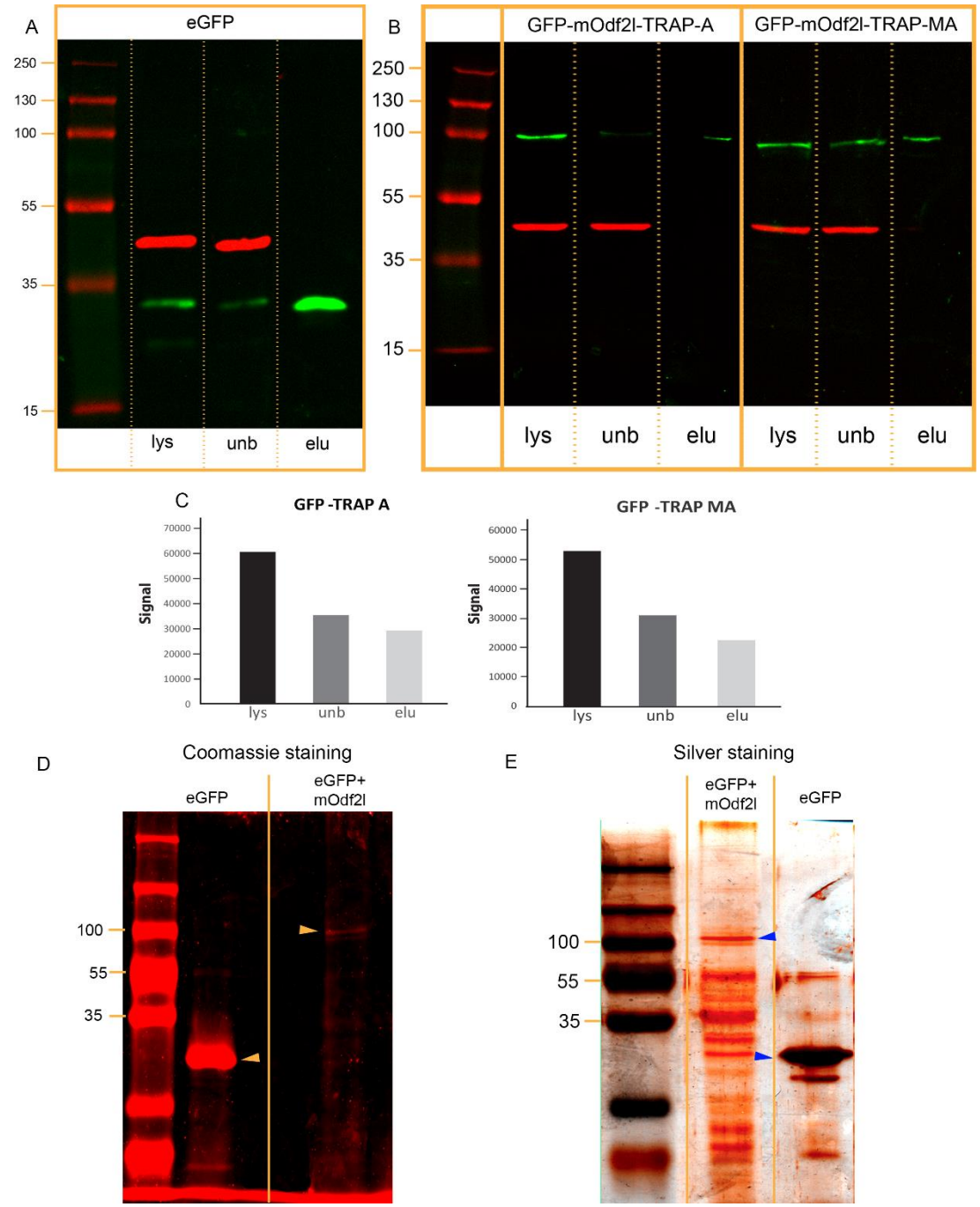

Figure 6-3 Analysis of GFP and eGFP-mOdf2l pull-down using Western blotting and SDS-PAGE.

(A,B) Western blot with immuno-detection of GFP (green) and β-actin (red) in samples from precleared cell lysate (lys), unbound material following incubation with the beads (unb) and eluate from the beads after incubation (elu). Lysates were prepared for pull-down experiments from HEK-293T cells transfected with either **(A)** pCS2P-eGFP or **(B)** pCS2P-eGFPN-mOdf2l constructs. Pull-downs were performed with either anti-GFP antibody-conjugated agarose beads (TRAP-A) or anti-GFP antibody-conjugated magnetic beads (TRAP-MA). Sizes of marker bands are indicated to the left. The GFP or GFP-Odf2l protein is present in the lysate, unbound fraction and eluate, in each case, while β-actin was strongly detected in the lysates and unbound samples, but not detectable in the eluate, confirming the specificity of the pull-down. **(C)** Pull-down signal quantification from GFP-TRAP A and GFP-TRAP MA. **(D)** Coomassie stained SDS-PAGE gel of eluates following anti-GFP TRAP-MA pull down of GFP and GFP-

mOdf2l; bands were seen most prominently at about 30 and 100 kDa (arrowheads). **(E)** Silver stained SDS-PAGE gel of eluates following anti-GFP TRAP-MA pull down of GFP and GFP-mOdf2l detected bands at 30 and 100 kDa, respectively (arrowheads) along with a number of other bands.

6.6 Mass Spectrometric Analysis

A typical proteomic protocol includes the isolation of the complexes and elution of the bait and interacting partners. The eluted samples are then separated by either one or two-dimensional SDS-PAGE, stained and the individual spots or bands are excised. Then the proteins are digested in-gel and analysed using LC-MS-MS (Domon and Aebersold, 2006). This pre-fractioning method was previously the established protocol as the sensitivity of the earlier mass spectrometers were limited by technical restraints and the resolution of the HPLC system. In recent years, these technical boundaries were resolved and the speed and sensitivity of both HPLC and MS vastly improved, therefore, decreasing the need for fractionation. As a result of these improvements, numerous in-solution strategies have been developed to bypass the laborious pre-processing, saving time.

In this study, I adapted the previously published (von Thun *et al.*, 2013; Turriziani *et al.*, 2014) on-bead digestion system to study the interacting partners of Odf2l. After the pull-down, beads were trypsinized for 24 h at 37°C to digest the bait protein and interacting proteins. The samples were then analysed using Ultimate ™ 3000 RSLCnano HPLC system (Thermo Scientific, Dionex) coupled with the Amazon Electron Transfer Dissociation (ETD) captive spray-ion trap mass spectrometer (Bruker).

Preliminary data from HEK293 lysate pull-downs and mass spectrometry, performed by others in the lab, have shown that the protocol was sensitive and reliable, at least for the antibodies previously used. For my experiments, HEK293 cells overexpressing GFP-mOdf2l were used to pull-down Odf2l, with the anti-GFP antibody, and lysates analysed by mass spectrometry using

the same protocols; the aim was to identify possible interacting partners of Odf2l. As a control, HEK293 cells overexpressing GFP were processed in parallel, and were used to subtract GFP-interacting proteins from the results. Three independent protein preparations were analysed for each pull-down, two using a mass spectrometer in Bruker, and the third using the same type of mass spectrometer but at Royal Holloway.

Following anti-GFP pull-down from GFP-mOdf2l expressing HEK293 cell lysate, mass spectrometric analysis recognised 387 proteins collectively from all three runs and 252 proteins from GFP-expressing cell lysates. Out of all samples, 165 proteins were recognised common to both GFP and GFP-mOdf2l samples, therefore, 222 proteins were identified only from the GFP-mOdf2l lysate. Out of these 222 proteins, many were recognised as DNA or RNA binding proteins which are commonly found as false positives from mass spectrometry and therefore can probably be discounted. Odf2l was identified as one of the top scoring hits (Table 6.1), which was expected, based on the nature of the experiment. Comparing the results from all the experiments identified three proteins present in all three replicates: RAB7B, MYH9 and MYO18A (Table 6.1). RAB7B has been linked to the lysosome sorting pathway (Yang *et al.*, 2004) and it also localises to the Golgi apparatus (Progida *et al.*, 2010). MYH9, non-muscle myosin IIA (NMIIA/MYH9) has been shown to mediate normal recycling of Golgi glycosyltransferases and Golgi fragments to the ER for proteasome degradation (Petrosyan *et al.*, 2012; Petrosyan and Cheng, 2014). MYO18A, another myosin, has a diverse set of roles and has been identified as a component of a complex that regulates Golgi trafficking (Cao *et al.*, 2016). Thus it is striking that the three proteins that were identified repeatedly are all associated with trafficking and the Golgi. This implies that ODF2L may also be involved with this process. A further 5 proteins were identified from two of the three replicate experiments, RANBP1, SRP72, CCT6A, HSP90AB1 and TUBA1A (Table 6.1). There is no obvious common function between these proteins.

Another 214 proteins were identified from a single GFP-mOdf2l pull-down and are therefore perhaps less likely to be genuine interactors with Odf2l. Those with the highest Mascot scores are listed in Table 6.1; the full list is provided in Appendix 2. Of the proteins identified in a single replicate, a number are likely to be false positives. These may include some highly abundant proteins, such as common DNA- or RNA-binding proteins, actin- or tubulin-binding proteins, ribosomal proteins, as well as proteins that bind to unfolded polypeptides, such as heat shock proteins (Wang *et al.*, 2009b). In addition, the pull-down experiment uses cell lysates, and therefore allows mixing of proteins from different compartments of the cell, so interactions may have been identified which do not actually exist in intact cells. In addition, ODF2L contains coiled-coil domains that enable protein interactions, and the fact that it is being over-expressed in cells may also allow artefactual interactions to occur. Additional replicates are essential to verify the most likely genuine interactions.

Our previous data have suggested ODF2L may function as a centrosomal satellite protein, or may associate with the Golgi apparatus. Therefore, we interrogated the data further for relevant proteins consistent with this role for ODF2L. The complete list of all the MS-MS recognised proteins from the pull-down with GFP-mOdf2l lysate, after removing those identified from the parallel experiments with GFP lysates, can be found in Appendix 2. Amongst this list of 214 proteins are Calnexin, Transitional endoplasmic reticulum ATPase, COPB2, COPZ1, COPA and SRP72 which are all proteins known to associate with the Golgi or ER, and found in vesicle-mediated transport pathways. However, the true interaction of these proteins with ODF2L is uncertain, as these proteins were identified only in a single experiment, and had a low Mascot score as the abundance of peptides, and number of different peptides from each protein (that is, the sequence coverage) were both low. It is interesting that the MS-MS also identified CDK1 as a possible ODF2L interactor, given the prediction that CDK1 may phosphorylate the end terminus of ODF2L isoforms a and b (Section 6.1); however, whether this interaction is genuine is also uncertain as the mascot score and sequence coverage is low.

The proteins discovered from this pull-down experiment were further analysed using STRING multiple protein interaction identifier to ascertain the probable clustering and functional interactions among them (Figure 6.4). This is particularly important since pull-downs can bring a whole interacting complex of proteins if proteins are tightly associated within the complex. The STRING analysis identified only 32 proteins of the 222 putative interactors as having a link with ODF2L. Of these, 15 proteins were found to be protein transporters (GO biological processors pathway ID: GO:0015031). These identified proteins are coloured in light blue in the interaction map (Figure 6.4).

I also analysed predicted ODF2L interactors from protein-protein interaction databases such as BioGRID (Stark *et al.*, 2006), IntAct (Orchard *et al.*, 2014), Human protein reference database (HPRD) (Prasad *et al.*, 2009) and Struc2Net (Singh *et al.*, 2006) (Table 6.2). BioGRID, IntAct and HPRD listed experimentally reported interactors with ODF2L, whereas Struc2Net uses structure-based computational algorithms to predict protein-protein interactions. BioGRID and IntAct both reported that PCM-1, ODF2 and CEP128 appear to interact with ODF2L, when using proximity label mass spectrometric proteomic profiling methods. Although my pull-down and mass-spectrometric data did not identify any of these proteins, I have shown that PCM-1 might be a potential interactor since it co-localises with ODF2L.

Struc2Net predicted a large number of potential interactors with ODF2L, based on a structural prediction algorithm. Out of these predictions, only two proteins were identified from the pull-down experiment, Vimentin (VIM) and Laminin β 1 (LAMB1). However, both these were hits from only a single replicate, and remain unverified interactions. Vimentin and Laminin β 1 are both intermediate filament proteins, making their interaction with ODF2L unlikely.

Proteins found by LC-MS/MS in all 3 replicates of the GFP-mOdf2l pull-down				
Protein name	Gene Name	Uniprot functional description	Mascot Score	Peptides
ODF2L			1001	23
Myosin-9	*MYH9*	Cellular myosin that appears to play a role in cytokinesis, cell shape, and specialized functions such as secretion and capping. During cell spreading, plays an important role in cytoskeleton reorganization, focal contacts formation (in the margins but not the central part of spreading cells), and lamellipodial retraction; this function is mechanically antagonized by MYH10	351.4	6
Unconventional myosin-XVIIIa	*MYO18A*	May link Golgi membranes to the cytoskeleton and participate in the tensile force required for vesicle budding from the Golgi. Thereby, may play a role in Golgi membrane trafficking and could indirectly give its flattened shape to the Golgi apparatus.	231.1	4
Ras-related protein Rab-7b	*RAB7B*	Controls vesicular trafficking from endosomes to the trans-Golgi network (TGN). Acts as a negative regulator of TLR9 signaling and can suppress TLR9-triggered TNFA, IL6, and IFNB production in macrophages by promoting TLR9 lysosomal degradation. Also negatively regulates TLR4 signaling in macrophages by promoting lysosomal degradation of TLR4.	141.9	3
Proteins found by LC-MS/MS in 2 replicates of the GFP-mOdf2l pull-down				
Heat shock protein HSP 90-beta	*HSP90AB1*	Molecular chaperone that promotes the maturation, structural maintenance and proper regulation of specific target proteins involved for instance in cell cycle control and signal transduction. Undergoes a functional cycle that is linked to its ATPase activity. This cycle probably induces conformational changes in the client proteins, thereby causing their activation. Interacts dynamically with various co-chaperones that modulate its substrate recognition, ATPase cycle and chaperone function. Engages with a range of client protein classes via its interaction with various co-chaperone proteins or complexes that act as adapters, simultaneously able to interact with the specific client and the central chaperone itself.	1710.8	32

Tubulin alpha-1A chain	*TUBA1A*	Tubulin is the major constituent of microtubules. It binds two moles of GTP, one at an exchangeable site on the beta chain and one at a non-exchangeable site on the alpha chain.	1010	21
T-complex protein 1 subunit zeta	*CCT6A*	Molecular chaperone; assists the folding of proteins upon ATP hydrolysis. Known to play a role, in vitro, in the folding of actin and tubulin.	365.63	18
Signal recognition particle 72 kDa protein	*SRP72*	Signal-recognition-particle assembly has a crucial role in targeting secretory proteins to the rough endoplasmic reticulum membrane. Binds the 7S RNA only in presence of SRP68. This ribonucleoprotein complex might interact directly with the docking protein in the ER membrane and possibly participate in the elongation arrest function.	132.9	2
Ran-specific GTPase-activating protein	*RANBP1*	Plays a role in RAN-dependent nucleocytoplasmic transport. Alleviates the TNPO1-dependent inhibition of RAN GTPase activity and mediates the dissociation of RAN from proteins involved in transport into the nucleus (By similarity). Induces a conformation change in the complex formed by XPO1 and RAN that triggers the release of the nuclear export signal of cargo proteins.	122.2	5
Proteins found by LC-MS/MS in only 1 replicate of the GFP-mOdf2l pull-down				
Elongation factor 2	EEF2	Catalyzes the GTP-dependent ribosomal translocation step during translation elongation. During this step, the ribosome changes from the pre-translocational (PRE) to the post-translocational (POST) state as the newly formed A-site-bound peptidyl-tRNA and P-site-bound deacylated tRNA move to the P and E sites, respectively. Catalyzes the coordinated movement of the two tRNA molecules, the mRNA and conformational changes in the ribosome.	1384.9	31
Stress-70 protein, mitochondrial	HSPA9	Chaperone protein which plays an important role in mitochondrial iron-sulfur cluster (ISC) biogenesis. Interacts with and stabilizes ISC cluster assembly proteins FXN, NFU1, NFS1 and ISCU.	713.6	16
DNA-dependent protein kinase catalytic subunit	PRKDC	Serine/threonine-protein kinase that acts as a molecular sensor for DNA damage. Involved in DNA non-homologous end joining (NHEJ) required for double-strand break (DSB) repair and V(D)J recombination. Must be bound to DNA to express its catalytic properties.	701.9	16

Tubulin beta-6 chain	TUBB6	Tubulin is the major constituent of microtubules. It binds two moles of GTP, one at an exchangeable site on the beta chain and one at a non-exchangeable site on the alpha chain .	637	11
ATP synthase subunit beta, mitochondrial	ATP5F1B	Mitochondrial membrane ATP synthase (F1F0 ATP synthase or Complex V) produces ATP from ADP in the presence of a proton gradient across the membrane which is generated by electron transport complexes of the respiratory chain.	615.7	13
Phosphoglycerate kinase 1	PGK1	In addition to its role as a glycolytic enzyme, it seems that PGK-1 acts as a polymerase alpha cofactor protein.	469.7	12
Nucleophosmin	NPM1	nvolved in diverse cellular processes such as ribosome biogenesis, centrosome duplication, protein chaperoning, histone assembly, cell proliferation, and regulation of tumor suppressors p53/TP53 and ARF. Binds ribosome presumably to drive ribosome nuclear export. Associated with nucleolar ribonucleoprotein structures and bind single-stranded nucleic acids.	449.3	10
Complement component 1 Q subcomponent-binding protein, mitochondrial	C1QBP	Is believed to be a multifunctional and multicompartmental protein involved in inflammation and infection processes, ribosome biogenesis, regulation of apoptosis, transcriptional regulation and pre-mRNA splicing.	413.4	7
14-3-3 protein beta/alpha	YWHAB	Adapter protein implicated in the regulation of a large spectrum of both general and specialized signaling pathways. Binds to a large number of partners, usually by recognition of a phosphoserine or phosphothreonine motif. Binding generally results in the modulation of the activity of the binding partner.	396.6	10
Alpha-1-antiproteinase	SERPINA1	Inhibitor of serine proteases. Its primary target is elastase, but it also has a moderate affinity for plasmin and thrombin. Irreversibly inhibits trypsin, chymotrypsin and plasminogen activator.	315.6	7
Multifunctional protein ADE2	PAICS	Catalytic activity.	314.4	10
Phosphoglycerate mutase 1	PGAM1	Interconversion of 3- and 2-phosphoglycerate with 2,3-bisphosphoglycerate as the primer of the reaction. Can also catalyze the reaction of EC 5.4.2.4 (synthase), but with a reduced activity.	306.8	8

Table 6-1 List of protein identified by LC-MS/MS from GFP-mOdf2l pull-down samples.
The columns show the Mascot score, number of peptides identified and Uniprot-defined function. Proteins that were pulled down also in the GFP control experiments have been excluded.

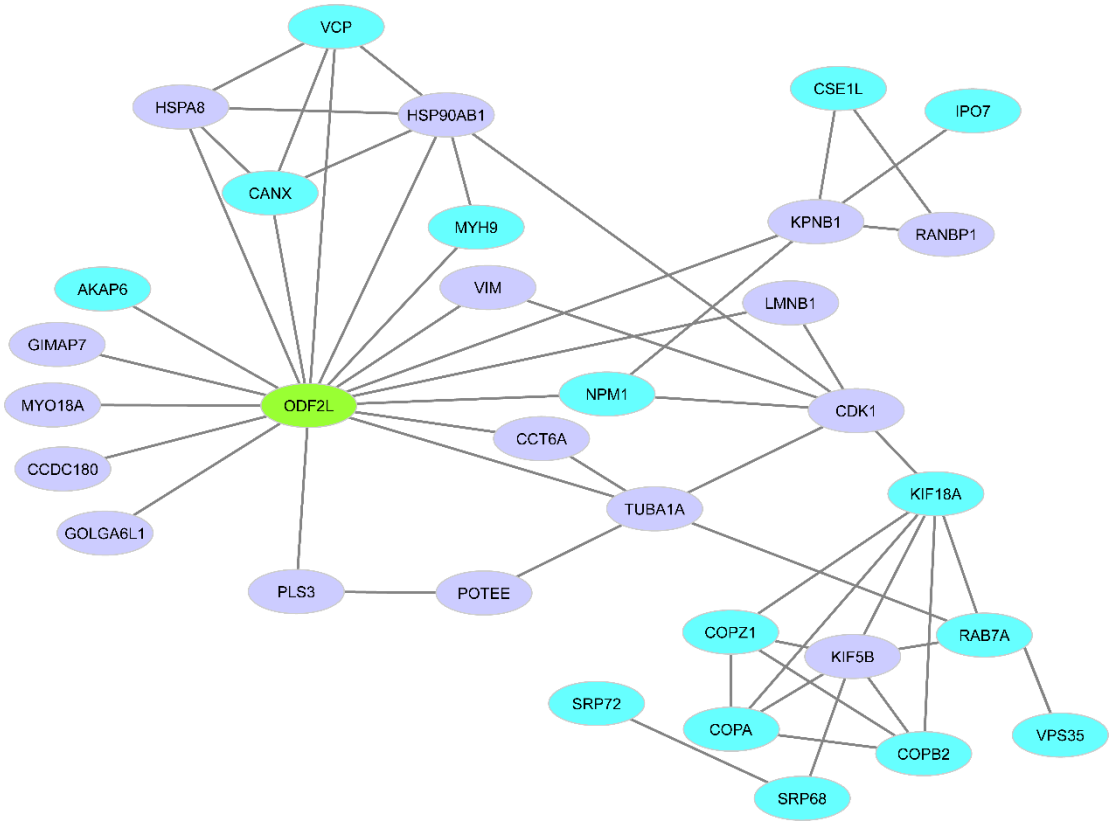

Figure 6-4 Probable ODF2L protein interaction map predicted by STRING.

The proteins identified from the pull-down were further analysed to identify potential clustering of the protein complexes. According to the predictions from the STRING analysis, ODF2L mainly associates with protein transport within the cell (those proteins are marked in light blue). The protein network was first analysed in STRING (total of 32 proteins) and then nodes and edges were imported to Cytoscape version 3.6 for further annotation.

BioGRID	IntAct	HRPD	Struc2net			
GAPDHS	HHT	CEP126	**VIM**	EMILIN1	CCDC123	SESTD1
ZMAT2	ppdk	ERBB3	PRPH	POF1B	FAM184B	KIAA1524
EMILIN1	cotE	PIPOX	LAMB3	TRIM68	IFT57	PPFIA1
HACL1	PIPOX	PRSS23	SMC2	SLC4A5	IFT74	CCDC21
NPM2	cueO		SMC4	ERC1	FILIP1	SCLT1
C17ORF59	mukB		**LMNB2**	CCDC102B	TRIM35	MIA3
NDC80	glsA2		LMNB1	TRIM29	DNAH10	LZTS1
CEP126 (KIAA1377)	CEP126		C14orf49	SCARA3	TRIM75	CEP63
PRSS23	PRSS23		LAMB3	RNF40	CCDC62	FKBP15
ERBB3	yapB		KRT78	ODF2	TRIM11	TRAK2
APP	NDC80		SMC1A	TRAK1	IQCE	TRIM16L
MED4	ERBB3		KRT7	C18orf34	NUF2	ERC2
ODF2	ureC		SMC1B	CALCOCO1	PIBF1	GRINL1A
CEP128	aspA		CEP135	TRIM47	NDE1	TRIM5
PCM1	PCM1		CCDC39	C20orf117	TEKT2	CCDC155
	ODF2		CCDC18	CCDC67	FGA	FILIP1L
	CEP128		LAMC2	CARD14	TEKT5	TEKT3
			KRT80	CCDC150	LUZP1	CCDC157
			CCDC88A	MMRN2	MCC	CCDC136
			CCDC110	GOLGA5	TRIML1	GRIPAP1
			SMC5	TAX1BP1	SH3BP5L	CKAP4
			CCDC146	TRIM41	TRIM8	ATP6V0A4
			USO1	NDC80	JAKMIP2	DYNC2H1
			PPFIA2	SYCP1	TRIM64B	TXLNA
			EMILIN3	RPGRIP1	EPS15L1	TRIM14
			CARD10	TEKT1	MMRN1	TRIM22
			SASS6	SPAG5	MORC3	CLIP2
			PMFBP1	GOLGA2	TRIM17	GCOM1
			CCDC40	C6orf97	BICD2	GOLGA1
			CARD11	RUFY3	HOOK1	HOOK2
			CGN	NUPL1	FIBCD1	ATP6V0A1
			IFFO1	FCHO2	TMF1	CCDC147
			CYTSB	PPFIA3	LZTS2	
			CTAGE5	TSKS	TRIM4	
			BICD1	TEKT4	C9orf117	

Table 6-2 List of ODF2L interactors predicted by protein interaction databases.
BioGRID, IntAct and HRPD use experimental evidence from yeast two hybrid screens (marked in blue), tandem affinity purification (in green), proximity-dependent biotin identification (in yellow), and affinity capture RNA (in grey) methods. Struc2Net uses structure base computational algorithm to predict the protein interactions. Proteins shown in **bold red** were identified also in the pull-down experiment.

6.7 FRET

ODF2L may interact with a number of binding partners (Section 6.6). Verification of genuine interactions requires considerable experimental analysis. One approach for testing interactions is using FRET (fluorescence resonance energy transfer). FRET has the advantage of enabling interactions to be tested both *in vitro* and *in vivo*. In recent years, FRET has become a key method of analysing protein-protein interactions and visualising cellular dynamics in living cells (Zhang *et al.*, 2002; Gaits and Hahn, 2003; Chhabra and dos Remedios, 2005; Jares-Erijman and Jovin, 2006). However, FRET had never before been used in our laboratory. Therefore, I wanted to establish the technique of FRET in our laboratory, with the long term aim of using this approach to further investigate ODF2L interactions.

Furthermore, I wanted to explore whether FRET is possible by using fragments of a protein, rather than whole proteins, since many coiled-coil domain interacting proteins are large and expressing the full length protein has proven to be problematic. Therefore, the aim of this experiment was to establish a positive control by using coiled-coil domain fragments of large PCM proteins to investigate whether FRET is possible between these fragments.

There are various methods used for FRET measurements to visualise protein-protein interactions (Wouters *et al.*, 2001) and the most widely used FRET-based reporters are cyan and yellow fluorescent proteins (CFP and YFP). However, this probe pair was known to have some limitations for FRET-based studies. Both CFP and YFP can undergo rapid multi-rate and reversible photo-bleaching (Shaner *et al.*, 2008), and YFP can sometimes photo-convert into cyan fluorescent species (Raarup *et al.*, 2009), so can then photo-activate at CFP-exciting wavelengths (Malkani and Schmid, 2011). Furthermore, the violet CFP excitation in live cells can be photo-toxic (Dixit and Cyr, 2003). Also, many CFP-YFP based FRET reporters produce only a small change in FRET. Therefore, detecting the FRET can be challenging, especially when the interactions are transient, and the signal may be little higher than background noise; however,

increasing the illumination to increase the signal can result in fluorophore bleaching. In recent years, alternative FRET pairs have become available, such as GFP and red fluorescent protein (RFP). Although the use of GFP and RFP proteins improves the dynamic detection range, standard RFP acceptors do not improve the energy transfer compared to CFP-YFP pairs (Piston and Kremers, 2007). However, the recent development of enhanced fluorescent proteins have shown the eGFP-mCherry pair can yield reproducible quantitative determination of energy transfer both *in vivo* and *in vitro* (Albertazzi *et al.*, 2009). The mCherry reporter is one of the most promising monomeric proteins derived from DsRed protein and reported as a good FRET acceptor (Tramier *et al.*, 2006). Therefore, in this experiment the combination of eGFP and mCherry fluorescent proteins was used to conduct FRET.

The CDK5RAP2 is a γ-tubulin complex binding protein that functions in γ-tubulin attachment to the centrosome as well as the Golgi complex (Wang *et al.*, 2010). It contains a γ-tubulin complex-binding domain called Centrosome Family Domain (CFD) as well as multiple coiled coil domains (Figure 6.4A). Pericentrin (Kendrin or PCNT) is another protein localised to the centrosome and contains a series of coiled-coil domains (Figure 6.5A) and a highly conserved PCM targeting motif, the PACT domain (Figure 6.5C) (Li *et al.*, 2001). The PACT domain consists of 90 amino acids located near the C-terminus and is responsible for recruiting proteins to the centrosome and attaching those to the centriolar wall in interphase (Kim and Rhee, 2014) (Figure 6.5B). In recent studies, CDK5RAP2 is shown to complex with PCNT in the presence of CEP192, therefore, playing a pivotal role in centrosome assembly (Gomez-Ferreria *et al.*, 2007; Zhu *et al.*, 2008). This protein complex organises to create highly ordered structures (Lawo *et al.*, 2012) (Figure 6.5B), therefore, making an ideal candidate for establishing FRET-based study in our lab. As only small parts in the proteins interact, I wanted to explore the possibility of whether these domains can be used to analyse interactions with FRET. If the FRET transfer can be confirmed, the method can be extended to study the interacting partners of ODF2L.

For this study, the 3' region of CDK5RAP2 was cloned into the mammalian expression vector pCS2P-eGFP, to generate a 140 amino acid C-terminal fragment containing the CNN2 domain and tagged at the N-terminus with eGFP. A domain in the centre of pericentrin was cloned into the mammalian expression vector pCS2P-mCherry, to generate a 300 amino acid fragment (1801-2100 aa) tagged at the N-terminus with mCherry. (All the cloning procedures were performed in collaboration with Dr Rivka Isaacson and Ewelina Krysztofinska at King's College, London).

Both constructs were transfected into HeLa cells. Cells were viewed using the Olympus FV1000 confocal microscope and localisation of eGFP-tagged CDK5RAP2 fragments was observed by exciting with Argon 488 laser and viewed through a 515/30 nm band pass filter (Figure 6.6A). The localisation of mCherry-tagged pericentrin central domain was observed by exciting with a Helium-Neon 543 laser and viewed through the 570LP band pass filter (Figure 6.6B). For both channels, 0.5 µm z-stack optical sections were collected. Then both channels were simultaneously collected for FRET by exciting only the donor channel while measuring the sensitised emission of the acceptor channel (Figure 6.6C-F). The sensitised emission was collected from 10 cells and the FRET energy transfer efficiency and FRET distance was measured using the FRET software toolkit for the microscope. The average FRET distance between CDK5RAP2 and PCNT fragments was found to be about 4.3 nm and at this distance, about 72% FRET energy was transferred between the two fluorophores, demonstrating protein-protein interaction (Figure 6.5 G,H). Thus, this confirms that we have established the technique of FRET in our laboratory, and that it is possible to detect FRET when using single domains of the proteins.

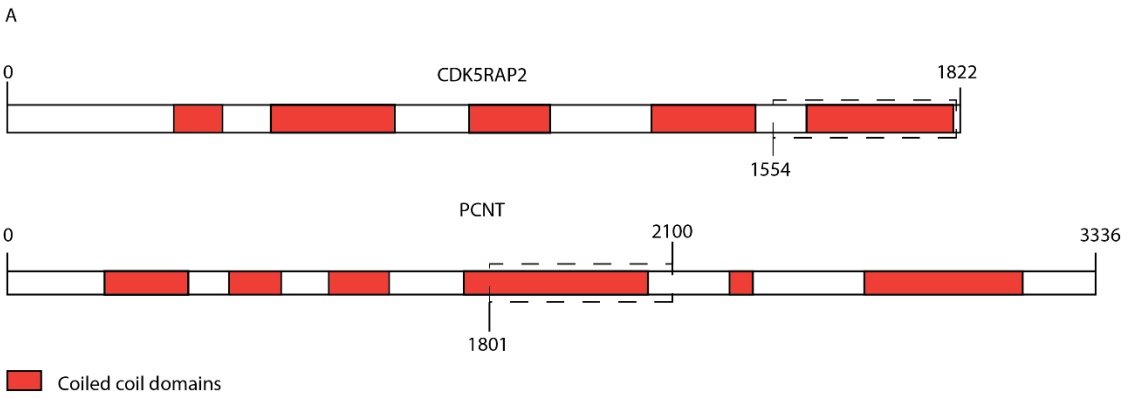
A
0
CDK5RAP2
1822
1554
PCNT
0
2100
3336
1801
Coiled coil domains

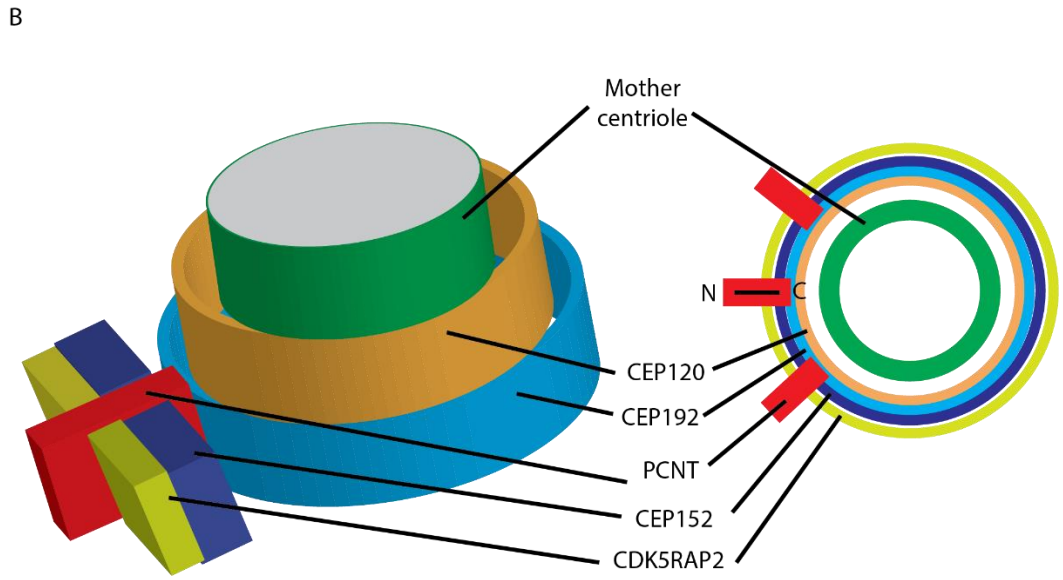
B
Mother centriole
N
C
CEP120
CEP192
PCNT
CEP152
CDK5RAP2

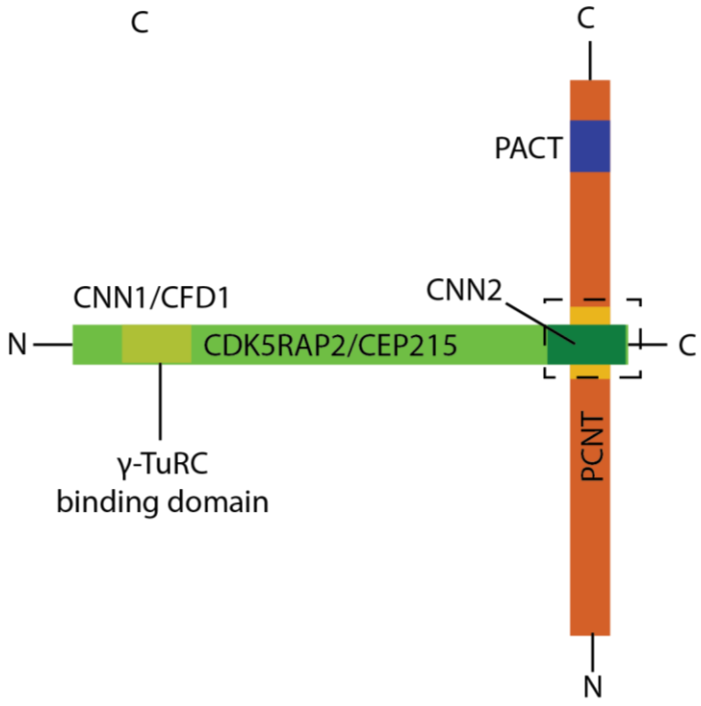
C
C
PACT
CNN1/CFD1
CNN2
N
CDK5RAP2/CEP215
C
γ-TuRC
binding domain
PCNT
N

Figure 6-5 Schematic diagram of domain structural organisation of CDK5RAP2 and PCNT.

(**A)** Coiled coil domain organisation and interacting sites on CDK5RAP2 and PCNT. The sites known to interact with each other are indicated with the dashed lines and are the sub-cloned fragments used for FRET.
(B) Schematic representation of the putative organisation of CDK5RAP2 and PCNT around the centrosome, together with other centrosome proteins.
(**C)** Representation of CDK5RAP2 and PCNT interaction together with other known protein interaction sites shown. The CNN2 domain of CDK5RAP2 interacts with PCNT. The CNN1 domain of CDK5RAP2 interacts with γ-TuRC. The PACT domain of PCNT interacts with AKAP450. Images were modified from Lawo *et al.* (2012).

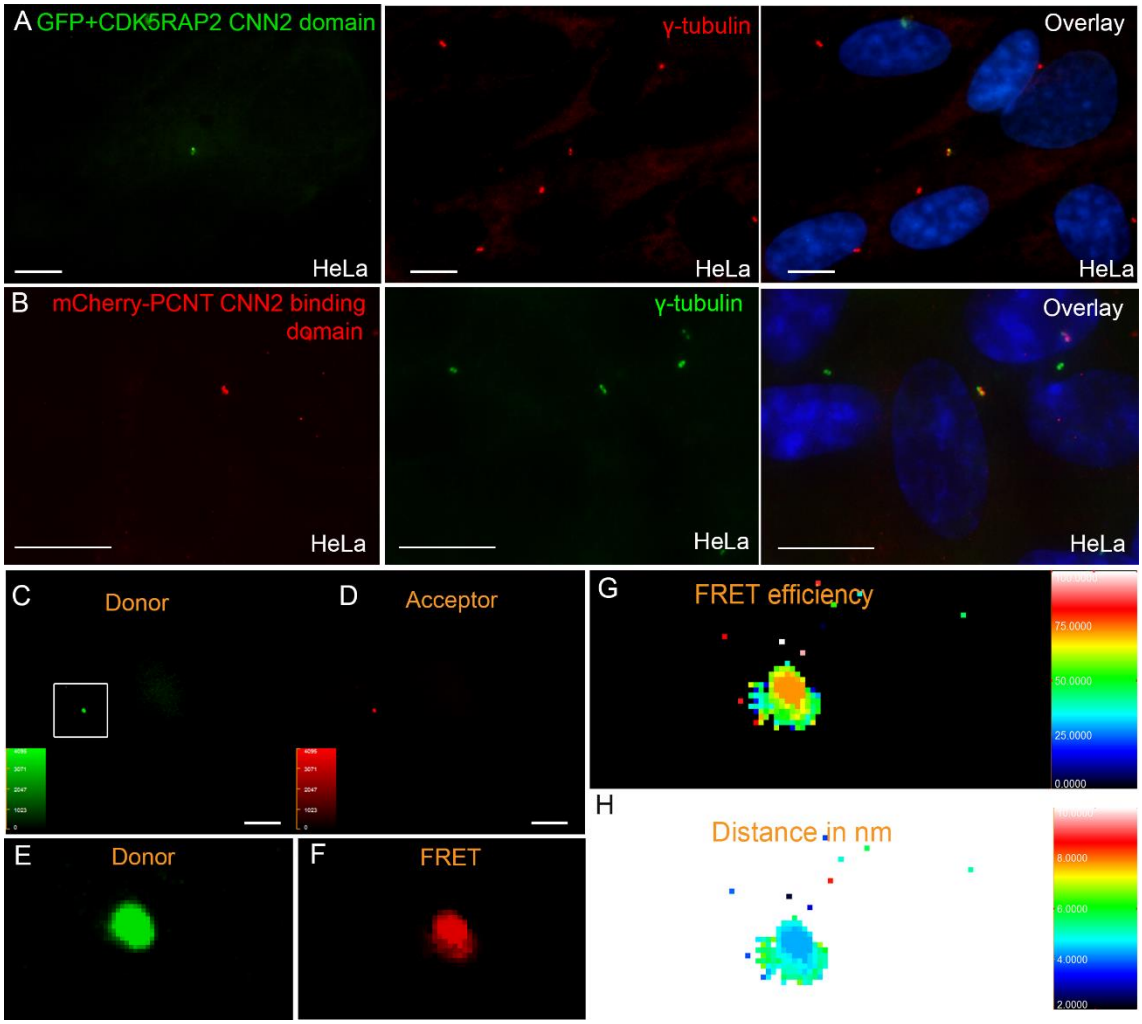

Figure 6-6 FRET based analysis of protein-protein interaction between fragments of CDK5RAP2 and PCNT.

(A) HeLa cells transfected with eGFP-CDK5RAP2 CNN2 fragment (green) and immunostained for γ-tubulin (red) and DAPI (blue). The GFP-tagged CDK5RAP2 localised to the centrosome. (**B)** HeLa cells transfected with mCherry-PCNT fragment (red) and immunostained for γ-tubulin (green) and DAPI (blue). **(C,D**) HeLa cells transfected with both eGFP-CDK5RAP2 fragment (green, **C**) and mCherry-PCNT fragment (red, **D**); donor excitation (green) causes acceptor excitation (red) due to the FRET energy transfer. **(E)** Enlarged view of donor channel (white box in C) showing the donor excitation. **(F)** Enlarged view of acceptor channel showing excitation of the acceptor due to FRET from the donor. (**G)** Representation of the FRET efficiency, showing how much energy was transferred from donor to acceptor channel. The centre of this region corresponds to approximately 72% energy transfer. **(H**) Calculated FRET distance (in nm) between the two proteins; the centre of this region represents a separation of 4.3 nm. Scale bar: 10 µm.

6.8 Summary

In this chapter, the functional domain organisation, phosphorylation and SUMOylation pattern of ODF2L were explored. The structural organisation of ODF2L isoforms consists of a number of motifs that can interact with many proteins, including coiled-coil and low complexity domains, as well as some additional domains.

The prediction of an APG6 domain in all the isoforms hints that ODF2L might be involved with autophagy. However, the actual function of this domain in ODF2L and whether it interacts with other components of the autophagy pathway is not known. The predicted ADIP and HOOK domains in some ODF2L isoforms implies that ODF2L may be involved with vesicle trafficking.

The unique phosphorylation sites found in the C-terminus of isoforms a and b may also play a role in regulating the function of ODF2L, and these sites may be phosphorylated by one of the CMGC group of kinases. This is particularly interesting since both of these isoforms seem to disappear from centriolar satellites at the onset of ciliogenesis. Perhaps these phosphorylation sites are involved in specifying the signal for these isoforms to be removed from satellites. Prediction of SIM and SUMOylation sites in isoforms also implicates association of some of the ciliary proteins with ODF2L.

In addition, in this chapter I set out to understand the ODF2L interacting partners by overexpressing GFP-tagged mouse Odf2l, pulling down the interacting proteins and identifying them by mass spectrometry. Three proteins – RAB7B, MYH9, MYO18A – were identified in all three replicate experiments. As all these proteins are part of the vesicle trafficking system from the Golgi, it is tempting to speculate that ODF2L may partner with these proteins to regulate the vesicle trafficking from the Golgi that is required for ciliogenesis. Further experiments would be required to confirm the interaction with ODF2L and to examine whether all four act together in the same pathway from Golgi to cilium.

Anticipating the need to show a close relationship between ODF2L and these proteins, I established the technique of FRET in our laboratory. I have also demonstrated that FRET is successful even when expressing only individual domains of the centrosome proteins. This is particularly important as proteins such as ODF2L contain multiple putative domains, so functional domains can be individually expressed and used to understand the nature of the interactions with those specific regions. Furthermore, this is a powerful technique to explore dynamic protein-protein interactions *in vitro* and *in vivo* and, once ODF2L interactors are better confirmed, will be a useful tool to help understand the function of ODF2L.

6.9 Possible future work

Overexpressing a protein in cells for a pull-down based study can always yield off-target effects. These off-target effects can produce false positive results by pulling-down non-specific or artefactual interactions, hence compromising the specificity of the assay. Furthermore, overexpression of a protein may perturb the normal cellular functions and affect the overall understanding of the protein's function within the cell. Therefore, it is also important to pull down the endogenous protein without overexpressing, to avoid these problems.

Pulling-down an endogenous protein requires a robust and specific antibody for immunoprecipitation. Unfortunately, the commercially available antibodies for ODF2L, used in co-localisation studies and for Western blot analysis, appeared to not be entirely specific for ODF2L; for instance, multiple bands were evident on the Westerns. In addition, pre-immune sera for these commercial antibodies was not available, thus an important control would have been missed. In the future, it would be ideal to raise an in-house antibody for ODF2L and use it for Co-IP studies, as the pre-immune serum would be available.

The pull-down proteins obtained here were analysed using mass-spectrometry. An alternative approach is to use Western blot analysis to test for the presence in the pull-down eluate of

specific predicted interacting proteins. In a previous study, CEP126 (KIAA1377) was reported to interact with ODF2L from a yeast two-hybrid screen (Stelzl *et al.*, 2005) and would therefore be an obvious candidate for analysis in this way. However, no antibody is available to detect CEP126, precluding this approach. Moreover, additional analysis of structure-based computational prediction of protein-protein interactions using BioGRID, IntAct, HRPD and Struc2net (Singh *et al.*, 2006; Singh *et al.*, 2010) recognised many potential interacting partners (Appendix 2). While all of these putative interactors would be interesting targets to validate using the above mentioned methods, it is not feasible to analyse them without further data to prioritise particular targets. Moreover, these are only predicted interactors (Struc2Net), based on some calculated algorithm, and may not actually occur. It is perhaps most noteworthy that only 3 of these predictions was replicated in the mass spec analysis performed here.

Another interesting avenue to consider in the future is to understand the phosphorylation patterns of the different ODF2L isoforms. The isoforms a and b were predicted to have CMGC kinase phosphorylation sites. CDK1 belongs to the CMGC kinase family and was also identified by MS-MS from the pull-down products. Furthermore, isoforms a and b disappear from the centriolar satellite region at the onset of ciliogenesis. Therefore, it can be hypothesised that phosphorylation of these isoforms may have a functional effect in initiating the removal of these proteins from the satellites prior to ciliogenesis. Protein PTMs can be studied using mass-spectrometer based analysis with ETD (Electron-transfer dissociation) or ECD (Electron-capture dissociation) modules, and this would be a further interesting approach for future experiments.

Chapter 7:

Discussion

7.1 Discussion

Centriolar satellites are conserved components of the vertebrate centrosome, but their function in ciliogenesis and centrosome function is poorly understood. In the last decade a number of new satellite proteins have been identified that regulate ciliogenesis. Although a large number of satellite proteins are positive regulators of ciliogenesis, there are only a few satellite proteins such as OFD1 that negatively regulate ciliogenesis in mammals. Furthermore, there are a number of ciliopathy-associated proteins that localise to centriolar satellites (Lopes *et al.*, 2011; Chamling *et al.*, 2014), but the functional relationship of those proteins in satellites have not been established. In the present study, I sought to characterise ODF2L and previously characterised CEP72 in mammalian cells and in zebrafish. I employed a variety of cell and molecular biology approaches to determine the localisation and characterise the function of these proteins in ciliogenesis.

7.2 Zebrafish Cep72 morphants display a ciliary phenotype

CEP72 was described as a satellite protein that associates with CEP290 and PCM-1 (Stowe *et al.*, 2012). Since CEP290 is mutated in Nephronophthisis (Helou *et al.*, 2007), in which cilium function is compromised, and CEP72 interacts with CEP290, I wondered whether there is a functional role played by CEP72 in ciliogenesis. In Chapter 3, I studied the function of zebrafish Cep72 in ciliogenesis by knocking down Cep72 using morpholinos.

The Cep72 knockdown morphants showed a classic “ciliary phenotype” with a curved back and ectopic otolith. These phenotypes are seen in several other mutants in which cilium structure is compromised (Kramer-Zucker *et al.*, 2005; Wilkinson *et al.*, 2009; Stowe *et al.*, 2012; Choksi *et al.*, 2014). However, the phenotype observed following Cep72 knockdown was not severe when compared to other satellite protein morphant phenotypes. Furthermore, in higher doses it seemed to severely affect the tail development and led to highly deformed embryos.

When the cilium structure in Cep72 morphants was analysed using confocal microscopy, the cilium length in the pronephric duct was not altered, compared to control embryos. Therefore the knockdown of Cep72 in zebrafish did not overtly affect ciliogenesis. This is in contrast to the effects observed from knockdown of other satellite proteins. However, we cannot rule out the possibility that there is a subtle defect in cilium structure, or that cilium function is disrupted following Cep72 knockdown. More detailed structural analysis or functional tests are needed, beyond the scope of this thesis, to pursue this further.

CEP72 may not play a *direct* role in ciliogenesis; rather, it may affect ciliogenesis indirectly, by regulating centrosome function. CEP72 recruits other centrosome-associated proteins and satellite proteins to the centrosome and the PCM. CEP72 is implicated in centrosomal microtubule nucleating activity from the γ-TuRCs and plays a critical role in forming a focused bipolar spindle (Oshimori *et al.*, 2009). The focused bipolar spindle is essential for proper tension generation between sister chromatids. CEP72 is required for recruiting KIZ, AKAP9 and γ-TuRCs to microtubules and the centrosome (Oshimori *et al.*, 2009). Recently, it has been demonstrated that CEP72 plays an important role in recruiting CDK5RAP22, CEP152, WDE62 and CEP63 to the centrosome and promotes the centrosomal localisation of CDK2 (Kodani *et al.*, 2015). Therefore, the morphant phenotype observed following the knockdown of Cep72 may be a result of compromised centrosome function, affecting cilium function through the interplay between centrosome and cilia.

7.3 Zebrafish Odf2a and Odf2b exhibit functional divergence

A previous study conducted in this lab looked at the phenotype following knockdown of zebrafish Odf2a. The Odf2a morphants have shown a severe ciliary phenotype, with complete absence of cilia in the perinephric duct (Anila Iqbal, unpublished data). The absence of cilia can be explained in morphants since vertebrate Odf2 localises to the distal appendages of centrioles

and is essential for centriole docking to the plasma membrane at the onset of ciliogenesis (Ishikawa *et al.*, 2005). Therefore, knockdown of Odf2a, the homologue of ODF2, should result in complete absence of cilia, as observed in the morphants.

Zebrafish contains another Odf2 family member, Odf2b. In order to test the function of Odf2b, I knocked this down in zebrafish. The initial Odf2b knockdown study using morpholino oligos revealed a distinct phenotype to that observed following Odf2a knockdown. Odf2b morphants retained cilia, but the cilia were shorter. In addition, Odf2b morphants showed ectopic otoliths and curved backs, phenotypes that are deemed characteristic of ciliogenesis disruption. Remarkably, the overall Odf2b morphant phenotype was very similar to that described for morphants of either Pcm-1 or Cep131 (Wilkinson *et al.*, 2009; Stowe *et al.*, 2012). The *pcm-1* morphant showed a ciliary phenotype with shortened cilia in the pronephric duct and unchanged basal body numbers (Stowe *et al.*, 2012). The shortening of the cilium length has also been observed with knockdown of other satellite proteins such as SSX2IP (Klinger *et al.*, 2014), CEP131 (Wilkinson *et al.*, 2009), and FOR20 (Sedjai *et al.*, 2010). The shortening of the cilium may be caused by inefficiencies in the recruiting of core ciliary axoneme proteins to the ciliary base and cilium.

The morphant phenotype led me to consider that Odf2b may be a satellite protein, particularly given the shortened (rather than absent) cilia phenotype observed with other satellite protein deficient morphants. Therefore, it invites the question whether Odf2b is a satellite protein, or is associated with regulating satellite proteins. Therefore, these results show that Odf2a and Odf2b, although related family members, exhibit functional divergence. Indeed, zebrafish Odf2a and Odf2b share only 48% amino acid identity, consistent with this divergence. It is interesting to note that in mammals, different isoforms of ODF2 appear to have distinct functions; only cenexin 1 (ODF2 isoform 9) is localised to the distal appendages (Chang *et al.*, 2013a), and the isoforms may have different roles in ciliogenesis.

ODF2L is another related family member, albeit with only about 21% identity to ODF2. Nevertheless, given that there is some similarity, and ODF2L had not previously been studied in relation to ciliogenesis, I decided to investigate the function of ODF2L in human cells.

7.4 ODF2L is a satellite protein that negatively regulates ciliation

ODF2L was previously described as basal body centrosome-associated protein (BCAP). However, the researchers only looked at the localisation in multiciliating primary human nasal epithelial (HNE) cells (Ponsard *et al.*, 2007). Ponsard et al., (2007) also identified two isoforms, the shorter BCAP (S-BCAP) and a longer BCAP (L-BCAP) and looked at the mRNA and protein expression during and after induced mucociliary differentiation (MCD). They observed a gradual reduction of S-BCAP protein expression level during the epidermoid differentiation (without RA) and an increase during the MCD (with RA). As for the L-BCAP, the expression level was only increased after when cells were fully differentiated. Furthermore, S-BCAP expressed in very low levels in proliferating cells and only increased during and after ciliation. Also, S-BCAP expression level appear to reduce even further when the ciliation initiated. All of these observations suggest that ODF2L isoform protein levels were altered during and after ciliation, therefore, may have a different regulatory role in ciliogenesis.

In this study, localisation and expression of ODF2L was studied during primary ciliogenesis in mammalian cells. I identified ODF2L as a satellite protein that co-localised with PCM-1. The NCBI database predicts that human ODF2L consists of four transcript sequences which can encode proteins. I have used two different polyclonal antibodies to study the localisation and protein expression in mammalian cells. The Biorbyt™ antibody only recognised isoforms a and b due to the C-terminus differences from isoform c and d while the Proteintech™ antibody recognised all four isoforms. The Biorbyt™ antibody shows the disappearance of isoform a and b during the ciliogenesis in mammalian cells in immunocytochemistry and in Western blot analysis. However

the Proteintech™ antibody did not show a disappearance of the proteins in Western blot analysis or in immunocytochemistry. One of the striking discoveries with the Proteintech™ antibody was that, after the ciliation, the ODF2L localisation was seen prominently in the Golgi apparatus. These results suggest that isoforms a and b may have a functionally similar role in ciliogenesis and most likely to negatively regulate ciliogenesis. Isoforms c and d may have a functionally different role to isoforms a and b and most likely to associate with the Golgi apparatus after the ciliation. Hence, it can be said that two different subsets of isoforms function differently to each other, and only one set is negatively regulating ciliogenesis. Perhaps each isoform in the pairs may have functional redundancy. This is further supported when considering the domain organisation of each isoform; the domain organisation of a and d are similar to each other whereas b and c show very similar domain organisation. Alternatively, this may be a mistake in the database, made during the EST-based sequence assembly, and that only two isoforms actually exist as described by Ponsard et al., (2007). Isoform function divergence has been observed for other centrosome proteins, such as ODF2, and therefore it is possible that the different isoforms of ODF2L have functional divergence.

The negative regulation of ciliogenesis was also confirmed using siRNA knockdown. Depletion of all ODF2L isoforms encouraged ciliation in proliferating cells. Conversely, overexpression of mouse Odf2L (isoform c) in mammalian cells inhibited ciliation in quiescent cells. Furthermore, knockdown of ODF2L also resulted in longer cilia. Thus it may be the case that ODF2L is involved with the balance point model of regulating cilium length by affecting the cilium assembly and disassembly rate.

There are a number of negative regulators of ciliogenesis recently described. OFD1 is a satellite protein now known to negatively regulate ciliogenesis through an autophagy pathway (Tang *et al.*, 2013). Branched F-actin and CP110 are also recognised as negative regulators of ciliogenesis. CP110 is a MT capping protein that localises to the distal end of the centrioles; it needs removing

at the onset of ciliogenesis for the axoneme to grow by MT polymerisation (Schmidt *et al.*, 2009). Branched F-actin is most likely to inhibit the migration of the centrosome to the apical surface and impact on membrane trafficking at the onset of ciliogenesis. F-actin has also been identified to regulate the length of the cilium (Bershteyn *et al.*, 2010; Kim *et al.*, 2010). More recently, members of CCT/TRiC molecular chaperone complex interacting protein, Nubp1 (nucleotide-binding protein) and Nubp2 have also been recognised to negatively regulate ciliogenesis (Kypri *et al.*, 2014).

My data suggest that ODF2L is also localised to the Golgi apparatus especially after ciliation. This type of behaviour has been observed with several centrosome-cilium associated proteins such as IFT20 (Follit *et al.*, 2008), AKAP450 (Rivero *et al.*, 2009), Rab8 (Nachury *et al.*, 2007; Yoshimura *et al.*, 2007) and GM130 (GOLGA2) (Kodani and Sutterlin, 2008). These proteins are involved in regulating the cargo trafficking fom Golgi apparatus to centrosome or cilium (Sutterlin and Colanzi, 2010; Rios, 2014). Hence, the Golgi-centrosome association is essential for building and maintaining the cilium.

7.5 ODF2L might be involved with vesicle trafficking or autophagy

In order for ciliogenesis to occur, a number of simultaneous events must occur in the cell. First, the ciliary vesicle should be able to dock to the distal appendages of the mother centriole. The ciliary vesicle is produced by the Golgi apparatus and transportation and docking are known to be regulated by IFT20 and CCDC41 (Joo *et al.*, 2013). Second, the centrosome should be able to move to the apical surface of the cell for the mother centriole to dock to the membrane. This process seems to be regulated by re-arranging the actin cytoskeleton and MTs (Kim *et al.*, 2010; Cao *et al.*, 2012; Zhang *et al.*, 2016). Third, the centriole should be able to dock to the membrane through distal appendages and form a “ciliary gate” by forming special structures like transitional fibres and the ciliary necklace (Tanos *et al.*, 2013). Finally, the extension of the

axoneme and establishment of the IFT based ciliary transport system occurs. This stage is also influenced by IFT20 and actin cytoskeleton dynamics (Follit *et al.*, 2006; Kim *et al.*, 2010). Given the co-IP data and the domain organisation, ODF2L may be involved in the first, second and final stages of the ciliogenesis.

My pull-down and mass spectrometry data suggest that several proteins involved in vesicle trafficking and the Golgi may associate with ODF2L. RAB7B controls vesiclular trafficking from endosomes to the trans-Golgi network, (Progida *et al.*, 2010). MYH9 has been shown to mediate normal recycling of Golgi glycosyltransferases and Golgi fragments to the ER for proteasome degradation and maintaining the Golgi morphology (Petrosyan *et al.*, 2014; Petrosyan *et al.*, 2016). MYO18A interacts with Golgin45 and plays a role in forming Golgi apparatus and organising F-acting bundles (Cao *et al.*, 2016). MYO18A has also been linked to Golgi membrane trafficking, vesicle budding (Dippold *et al.*, 2009) and maintaining the Golgi morphology (Ng *et al.*, 2013). None of these proteins RAB7B, MYH9, and MYO18A – are reported to associate directly with each other but all localise to the same organelle. ODF2L may therefore regulate cilium-targetted vesicle traffic from the Golgi via its interatction with these proteins and maybe others. Further experiments would be required to show these intereactions conclusively and to show that ODF2L and the other proteins are operating in the same pathway.

At the onset of ciliogenesis, Golgi-derived ciliary vesicles bind with the distal appendages of the centrioles and are required for a steady supply of protein from the Golgi apparatus to the centriole. This ciliary vesicle binding phase and the cilium directed cargo delivery are mediated by a number of proteins including IFT20. In a cycling cell, this cargo delivery is inhibited by autophagy or by interaction with satellite proteins that can inhibit the transport of certain Golgi-derived proteins to the centrosome (Pampliega *et al.*, 2013). During ciliogenesis, autophagy might remove these interacting satellite proteins and enable these cargo proteins to move to the centrioles and basal body (Orhon *et al.*, 2015; Pampliega and Cuervo, 2016).

Isoform ‘b’ could function as a recruiter of Golgi-derived ciliogenesis promoters such as IFT20 and CDC41C and block the migration to the mother centriole of the Golgi-derived primary cilium vesicle when ciliogenesis is not required. At the onset of ciliogenesis, ODF2L temporarily disappears from centriolar satellites. This window of disappearance from centriolar satellites may enable ciliogenesis promoters such as IFT20 and CCDC41 to localise to mother centrioles.

This model seems to fit well with OFD1 and IFT20 regulating ciliogenesis and extension of the cilium respectively. Under basal autophagy (Wang *et al.*, 2015; Pampliega and Cuervo, 2016), ciliogenesis is prevented by degradation of ciliogenesis-promoting proteins such as IFT20, which is known to deliver the ciliary vesicle to the mother centriole. During early-starvation autophagy, endogenous ciliary inhibitors like OFD1 and proteins associated with blocking and delivery of IFT20 to centrioles must be removed for ciliogenesis to progress (Pampliega *et al.*, 2013; Tang *et al.*, 2013).

Therefore it is also possible, given the prediction of an autophagy domain in ODF2L, that the removal of ODF2L from satellites at the onset of ciliogenesis may be linked to the autophagic processes required during ciliogenesis. However, this hypothasis lacks experimental evidence and is only based on structrul and domain predictions of ODF2L therefore, is less compelling. Hence, further experiments showing that ODF2L is subject to autophagy during ciliogenesis and-or controls it before ciliogenesis initiates, would be required to give this idea some strength.

Isoforms containing ADIP domains might also be inhibiting the function of the actin-based vesicle trafficking and actin remodeling in cycling cells to inhibit the migration of the centrosome to the apical surface. ODF2L isoform ‘a’ and ‘d’ both contain an ADIP domain before the APG-6 domain. Therefore, those isoforms might be inhibiting the actin-based vesicle tafficking and actin re-modeling required for the centriole migration to the apical surface, and so are removed temporarily at the onset of ciliogenesis. The ADIP domain which, alongside roles in the actin cytoskeleton, is also capable of directly binding with COPB subunits in the coatomer complex

and is recognised to be involved with vesicle trafficking from Golgi (Asada *et al.*, 2004). COPB2, COPZ1 and COPA were also identified in the pull-down although with lower confident scores.

Once ciliogenesis is initiated, ODF2L localises to the Golgi more prominently. This may be particularly important in regulating the cilium length since ODF2L localisation to the Golgi might be selectively blocking some of the Golgi-derived, cilia-targetted cargo from reaching the basal body. ODF2L isoform b is predicted to contain a HOOK domain. The HOOK domain was originally discovered in the proteins HOOK1, 2, 3 that associate with the Golgi, microtubules and centrosome (Walenta *et al.*, 2001; Szebenyi *et al.*, 2007; Xu *et al.*, 2008; Pallesi-Pocachard *et al.*, 2016). Recently, HOOK2 and HOOK3 have been demonstrated to localise to centriolar satellites via a PCM-1 dependent pathway (Ge *et al.*, 2010; Baron Gaillard *et al.*, 2011). HOOK3 normally localises to the Golgi membrane (Walenta *et al.*, 2001) and can associate with PCM-1 via its C-terminus. This association between Golgi and centriolar satellites implicates HOOK3 in mediating the trafficking of cargo proteins from Golgi apparatus to the satellites and to the centrosome (Ge *et al.*, 2010). HOOK2 is an adaptor protein that also interacts with PCM-1 and is implicated in trafficking cargo from the Golgi apparatus to the centrosome (Baron Gaillard *et al.*, 2011). HOOK1 was recently implicated in uni-directional endosomal transport (Maldonado-Baez *et al.*, 2013) using dynein-dynactin based cargo attachments (Maldonado-Baez *et al.*, 2013; Bielska *et al.*, 2014; Olenick *et al.*, 2016). Hence, the predicted HOOK binding site suggests that ODF2L might be involved with HOOK-based cargo delivery from the Golgi. Furthermore, experimental confirmation of Golgi localising/interacting proteins RAB7B, MYH9 and MYO18A as ODF2L interactors also strengthen the probability of the above hypothesis. However, further experiments are required to conclude the actual link between the ODF2L domain and the interactors.

An alternative way of regulating ciliogenesis is via interacting with other satellite proteins and ODF2L might be inhibiting ciliogenesis through preventing satellites from acting to promote

ciliogenesis. A yeast two-hybrid screen has suggested that CEP126 interacts with ODF2L (Stelzl *et al.*, 2005). CEP126 is another centrosome satellite protein that is required for ciliogenesis (Bonavita *et al.*, 2014), so inhibiting this protein would result in inhibition of ciliogenesis.

Given the domain organisation of ODF2L isoforms and the experimental evidence, we are encouraged to consider that ODF2L regulates ciliogenesis through one of the known pathways: autophagy, actin dynamics, satellite proteins or either through Golgi associated vesicle trafficking. Our evidence currently favours the latter. ODF2L might have a multi-functional role, depending on the isoform and stage of ciliogenesis.

7.6 Summary

In this study, I have ventured into the characterisation of two satellite proteins using various cell and molecular biology techniques. My work concludes that Cep72 is not directly involved with ciliogenesis in zebrafish while ODF2L acts as a satellite protein and negatively regulates ciliogenesis in mammals. My work emphasises the significance of studying centriolar satellites as they play significant roles in ciliogenesis.

7.7 Further developments in the study of ODF2L

The studies described in this thesis were subsequently extended by another PhD student in the laboratory of Dr Wilkinson. Combined with the results described here, they were published in Journal of Cell Science, the protein referred to as BCAP rather than ODF2L (de Saram *et al.*, 2017).

In this paper, ODF2L/BCAP was confirmed as a centriolar satellite protein, with depletion of PCM-1, a core satellite component, causing dispersal of ODF2L/BCAP away from the satellites.

The cellular phenotype induced by RNAi-mediated depletion of both isoforms could be rescued by overexpression of mouse Odf2l/Bcap, confirming the role of this protein as a ciliogenesis inhibitor.

In this thesis, it was proposed that there were probably two isoforms of ODF2L with slightly different roles in control of ciliogenesis, based on sequence analysis, structural predictions and cell biology studies. It was also proposed that both isoforms are degraded upon initiation of ciliation but one returns to the centriole / satellites once ciliogenesis is underway.

Additional experiments described in the paper revealed that, in hTERT-RPE1 cells at least, only two isoforms of ODF2L are present, ODF2Lα/BCAPα and ODF2Lδ/BCAPδ, corresponding to ODF2L isoforms a and d respectively. The two isoforms were overexpressed and depleted individually, further defining the roles of each splice variant. Both isoforms inhibit ciliogenesis and are partially redundant: the effect of depleting both isoforms simultaneously (siRNA1 or 2) is stronger than depletion of each individual isoform; ODF2Lα/BCAPα is able to suppress ciliogenesis in ODF2Lδ/BCAPδ-depleted cells and vice-versa. In addition, ODF2Lδ/BCAPδ controls cilium length, with ODF2Lδ/BCAPδ -depleted cells only displaying abnormally long cilia. Both isoforms localise to centriolar satellites but ODF2Lδ/BCAPδ is also localised to centrioles. This explains why ODF2L/BCAP signal returns to the (centriole) satellites, as one isoform is required to control cilium length once cilia have been formed. However, the exact mechanism of how ODF2Lδ controls the cilium length or the exact mechanism of how ODF2L controls ciliogenesis is yet to be discovered.

Appendix

Appendix -1

1.1 Zebrafish Cep72 sequence information

Name	Transcript ID	bp	Protein	Biotype	UniProt	RefSeq	Flags
cep72-201	ENSDART00000163151.2	1820	532aa	Protein coding	A0A0R4IXQ3	NM_001319132 NP_001306061	APPRIS P1

1.1.1 cDNA sequence (*cep72*)

```
   1 attcttcaaa acaatggcgg tagacggttt gcccataaca gaacagtgga tcagagagaa
  61 actcaacctt cagcatcgat gtttagcgga tgtccgatca ttgactctac caggaacata
 121 cgaagggaaa atctgtcatt taggaacatc actgaagaac tttgtccgtc tgaaatcgct
 181 ggatctctca tataacgcac tggtcacagt tcaggggatt gagcatctgg agctgctgga
 241 gagactgaat ctgtactata acagactggc gtctctgcag gacatctttt ccctgcacaa
 301 actacagaat ttaaagcaac tggacctgcg actgaatcct gtggttaaga agcatccaca
 361 ctaccgcctt tacctggtcc acgcaatccc caaactccgc agactcgatg actgtcccgt
 421 gcgagaccga gaaagaaagg cagctctaat gcatttctca tctgaggaaa atctagactc
 481 cgatcataag aagcaagtgt ttatacagga cacaactgcc agaagcagtg atctcagaat
 541 aaaagcgatg cagaagatgg tgaagatgct ctcgcttctg gagggaaatg aggaagttgc
 601 actaaatgat agttcaagaa aaagcgggaa gaggaggaat cttcaaactc tctccgtccg
 661 ctgcgagaat gaatgcagtc ctcttctggc acacgaaaat ccatctgaat ctgatattgt
 721 atatttattc aatgattccg attgcagacg ctcatcaaaa cataagcagg agtctgctcc
 781 ctccaagagc tcggattata agaatgatgc tcgggccggt cctcatcgag tgaggtttgt
 841 aagtcctgtc atactgaggc attcatcagt tcgaggagag agtgttttta cagcacatcc
 901 agattcacac aaacagcctc attcacatga aaacgattcc tcgtctccta aatggcaaaa
 961 ccaacttcta gatcgagcta atctcgtcct gcatcctccc agactgactt acagcactgc
1021 agaaaccaaa gacagaagca caaaaacact gaagggcaca tacagaaagc caatggagct
1081 cctgctgagc atgatggagg atctctggtc cgagaagaag gagaatcagc aaaacaggac
1141 atttctcatg aagatggttc agatcctcag catgatggag caggaggttt caggaggaga
1201 acaggagatc cagactctga aagccgctct gaaagcctcc atcgctcaag ctgatgtgca
1261 ggagaaacag catcagtctg agattgaaga gctgacgctg caacaacagc aggcgcacga
1321 gtccatcaag cgtcttaatg agcagacgaa gagtctgttg gaggagaacg tgtctttaca
1381 gaaacagctg atcagagcag aacacaagct gctggcgtcc cgactcaaga acatcccaca
1441 cacacaggac agaggagtgc agtctgttcc tgaagagttc aacacaaaga gagacataat
1501 cgctgatgat gaggacggcg gagtcggtga gcagcagcag agctacaggt ctttgattgc
1561 cagaaatgag cgtttgctgc agcagctgga ggaggcttta atgagcaaat gaagaaggtg
1621 cttctgatag acaaacacat tcatagaggg gtttttcaat ctaatctgtg ctttgaaaga
1681 ttataaaaat ggtcaaacat atttaaaaaa aagccctgtt ttaaatacac tatgagcagc
1741 tttattcaca tgtccagctg aatcaaacgt gtttgttttt ggtgttgaca aaaacaaata
1801 aacaacgatt ttcttagtgt
```

1.1.2 Protein sequence (Cep72)

MAVDGLPITEQWIREKLNLQHRCLADVRSLTLPGTYEGKICHLGTSLKNFVRLKSLDLSY
NALVTVQGIEHLELLERLNLYYNRLASLQDIFSLHKLQNLKQLDLRLNPVVKKHPHYRLY
LVHAIPKLRRLDDCPVRDRERKAALMHFSSEENLDSDHKKQVFIQDTTARSSDLRIKAMQ
KMVKMLSLLEGNEEVALNDSSRKSGKRRNLQTLSVRCENECSPLLAHENPSESDIVYLFN
DSDCRRSSKHKQESAPSKSSDYKNDARAGPHRVRFVSPVILRHSSVRGESVFTAHPDSHK
QPHSHENDSSSPKWQNQLLDRANLVLHPPRLTYSTAETKDRSTKTLKGTYRKPMELLLSM
MEDLWSEKKENQQNRTFLMKMVQILSMMEQEVSGGEQEIQTLKAALKASIAQADVQEKQH
QSEIEELTLQQQQAHESIKRLNEQTKSLLEENVSLQKQLIRAEHKLLASRLKNIPHTQDR
GVQSVPEEFNTKRDIIADDEDGGVGEQQQSYRSLIARNERLLQQLEEALMSK

1.2 Zebrafish Odf2a sequence information

Name	Transcript ID	bp	Protein	Biotype	UniProt	Flags
odf2a-202	ENSDART00000179221.2	4852	831aa	Protein coding	E7F186	APPRIS P1
odf2a-201	ENSDART00000081426.5	2992	831aa	Protein coding	E7F186	APPRIS P1

1.2.1 cDNA sequence *(odf2a)*

```
1 GGGTTTCAAGACTGTGGGATGACACAAGTAGTTCGCAACTATTTTTATGCACGTTTTGCT
  ............................................................
 61 CATATCGGCGTTTGAATGTTTGTAATTTCGCATGAAGAAATCAGTGAGAACAAGGTCCTC
  ...............................ATGAAGAAATCAGTGAGAACAAGGTCCTC
121 CTCCCCACCCCTGCATGTGCACGTGAACGAGAGCACACCTGTGCATGTTCATGTGAAGAA
 30 CTCCCCACCCCTGCATGTGCACGTGAACGAGAGCACACCTGTGCATGTTCATGTGAAGAA
181 GAGCACGAAATGCAGCCCTACCAAGACAGCCCAGGTTAAGTCAAAAACTGGCTTGCATCC
 90 GAGCACGAAATGCAGCCCTACCAAGACAGCCCAGGTTAAGTCAAAAACTGGCTTGCATCC
241 TACTGCTAAGGTGAAGACAAGAGTTCCATGGATTCCCCCTGGCAAGGTCTCAGCCCGAGA
150 TACTGCTAAGGTGAAGACAAGAGTTCCATGGATTCCCCCTGGCAAGGTCTCAGCCCGAGA
301 GACCTCATATAAGTGGGATGGACCATCCCATCGTCTGGAAATAACGGCTCCACAGGAGCC
210 GACCTCATATAAGTGGGATGGACCATCCCATCGTCTGGAAATAACGGCTCCACAGGAGCC
      R                                                R
361 TGAGCGTTCCCAGTCTCCTATGCGAATAGAAGATCTGTCCACCAATGAAGAAGAGGCACT
270 TGAGCGTTCCCAGTCTCCTATGCGAATAGAAGATCTGTCCACCAATGAAGAAGAGGCACT
421 GCATGGACGCATAAATCAGTACGAGAGGAAGATCGACAGTCTGATGACAGAGGTCAGCTC
330 GCATGGACGCATAAATCAGTACGAGAGGAAGATCGACAGTCTGATGACAGAGGTCAGCTC
              S
481 TCTGAAAAAGGAGGTAGAGCTTCGTAAGAAGGAGCAGCTGCTTGAGCGTCAGTCGGAGAG
390 TCTGAAAAAGGAGGTAGAGCTTCGTAAGAAGGAGCAGCTGCTTGAGCGTCAGTCGGAGAG
                                    M
541 GTTGAGCGCATCCCAGCGTGTCATCGCTGAACAGGAAGAGGAGCTTGCAGAAGTCGCCCG
450 GTTGAGCGCATCCCAGCGTGTCATCGCTGAACAGGAAGAGGAGCTTGCAGAAGTCGCCCG
          R
601 AGAGCTCGAGGCCACAGAGCAGGAGAACTCACGTCTACGAGAGTCCATGGAGAAGATGCT
510 AGAGCTGGAGGCCACAGAGCAGGAGAACTCACGTCTACGAGAGTCCATGGAGAAGATGCT
                                        R           Y
661 GGCAGAGAATGATTTCGGGAGAGTAGAGAGGGACGGCATGCAGCTTGACAAAGATGTTCT
570 GGCAGAGAATGATTTCGGGAGAGTAGAGAGGGACGGCATGCAGCTTGACAAAGATGTTCT
721 ACTCAGGAAGCTGCTGGAAGCAGAGATGGACAGCAGTGCGGCTGCAAAACAGGTTTCGGC
630 ACTCAGGAAGCTGCTGGAAGCAGAGATGGACAGCAGTGCGGCTGCAAAACAGGTTTCGGC
781 CCTTCGCGAAACGGTCAGCCAAATGTCTAGGAGTACAAGTGAGAAAAAGATGTCAGGATC
690 CCTTCGCGAAACGGTCAGCCAAATGTCTAGGAGTACAAGTGAGAAAAAGATGTCAGGATC
841 AGACTCGACACTTTTGGTTCGACAAAAGGAGATGTTACTGCAGAAGCTGGAGACTTTTGA
750 AGACTCGACACTTTTGGTTCGACAAAAGGAGATGTTACTGCAGAAGCTGGAGACTTTTGA
901 GAGCACCAACAGAACTCTTAGGCATCTTCTTAGAGAACAGCATAGCAGAGAGATGGACTC
810 GAGCACCAACAGAACTCTTAGGCATCTTCTTAGAGAACAGCATAGCAGAGAGATGGACTC
961 ACTTAGACTCTTGGAACAGAAAGATGCACTGCTGAAAAGGCTTTCTGATGTAGAAGAAGA
870 ACTTAGACTCTTGGAACAGAAAGATGCACTGCTGAAAAGGCTTTCTGATGTAGAAGAAGA


1021 GAATTCGCGTATTCTTGTAAAGCTTCAAGACAAAGAAAGAGAGGTCAACCAGCTCACTTC
 930 GAATTCGCGTATTCTTGTAAAGCTTCAAGACAAAGAAAGAGAGGTCAACCAGCTCACTTC
1081 CATATTAGAGAGTGAAAAGGAAAGCTCAAAAACCACCAGCGAACTGTCCAAAGTCTTAGA
 990 CATATTAGAGAGTGAAAAGGAAAGCTCAAAAACCACCAGCGAACTGTCCAAAGTCTTAGA
1141 GTCCACCCGTGCACATCTACAGGGTCAACTGCGAAATAAAGAAGCAGAGAATAACCGCCT
1050 GTCCACCCGTGCACATCTACAGGGTCAACTGCGAAATAAAGAAGCAGAGAATAACCGCCT
1201 TAACGTTCAGATCAGGAATCTGGAGCGATCCCTCAGCCAGCAGCAGGGGGAGATGGACCA
1110 TAACGTTCAGATCAGGAATCTGGAGCGATCCCTCAGCCAGCAGCAGGGGGAGATGGACCA
1261 CCTGCAGAACCAGCTGCGAGACCTCAGGCAGCAGGCGGAGGCTGATAAGGAGGCCCTAAA
1170 CCTGCAGAACCAGCTGCGAGACCTCAGGCAGCAGGCGGAGGCTGATAAGGAGGCCCTAAA
                                    W
1321 GAAAGCCACGCGGGCACAGAAACTGCGGGCACAGCGCAGTGAAGACACTGTCGGACAGCT
1230 GAAAGCCACGCGGGCACAGAAACTGCGGGCACAGCGCAGTGAAGACACTGTCGGACAGCT
                R
1381 CAGTGGCCAGCTCTTAGAGATAGAAAAACAATTGGCAGAGGCTGTGACAGCTGCAGAAAA
1290 CAGTGGCCAGCTCTTAGAGATAGAAAAACAATTGGCAGAGGCTGTGACAGCTGCAGAAAA
1441 CTGGAGCAGTCGCCACGCAAAAGAGATGAAGGACAAAGGACAGCTTGAGGTGGAGATCGC
1350 CTGGAGCAGTCGCCACGCAAAAGAGATGAAGGACAAAGGACAGCTTGAGGTGGAGATCGC
```

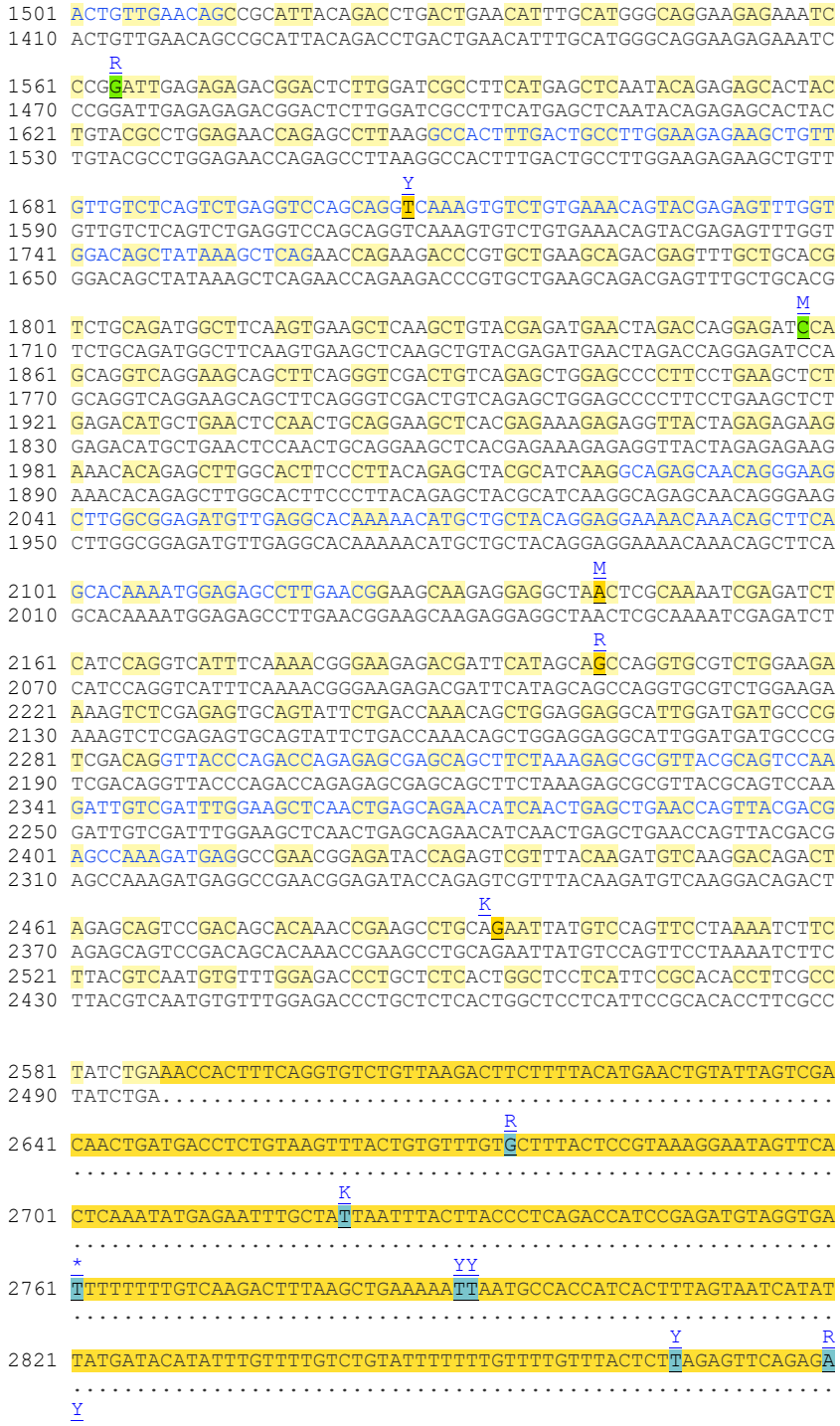

```
1501 ACTGTTGAACAGCCGCATTACAGACCTGACTGAACATTTGCATGGGCAGGAAGAGAAATC
1410 ACTGTTGAACAGCCGCATTACAGACCTGACTGAACATTTGCATGGGCAGGAAGAGAAATC
         R
1561 CCGGATTGAGAGAGACGGACTCTTGGATCGCCTTCATGAGCTCAATACAGAGAGCACTAC
1470 CCGGATTGAGAGAGACGGACTCTTGGATCGCCTTCATGAGCTCAATACAGAGAGCACTAC
1621 TGTACGCCTGGAGAACCAGAGCCTTAAGGCCACTTTGACTGCCTTGGAAGAGAAGCTGTT
1530 TGTACGCCTGGAGAACCAGAGCCTTAAGGCCACTTTGACTGCCTTGGAAGAGAAGCTGTT
                          Y
1681 GTTGTCTCAGTCTGAGGTCCAGCAGGTCAAAGTGTCTGTGAAACAGTACGAGAGTTTGGT
1590 GTTGTCTCAGTCTGAGGTCCAGCAGGTCAAAGTGTCTGTGAAACAGTACGAGAGTTTGGT
1741 GGACAGCTATAAAGCTCAGAACCAGAAGACCCGTGCTGAAGCAGACGAGTTTGCTGCACG
1650 GGACAGCTATAAAGCTCAGAACCAGAAGACCCGTGCTGAAGCAGACGAGTTTGCTGCACG
                                                           M
1801 TCTGCAGATGGCTTCAAGTGAAGCTCAAGCTGTACGAGATGAACTAGACCAGGAGATCCA
1710 TCTGCAGATGGCTTCAAGTGAAGCTCAAGCTGTACGAGATGAACTAGACCAGGAGATCCA
1861 GCAGGTCAGGAAGCAGCTTCAGGGTCGACTGTCAGAGCTGGAGCCCCTTCCTGAAGCTCT
1770 GCAGGTCAGGAAGCAGCTTCAGGGTCGACTGTCAGAGCTGGAGCCCCTTCCTGAAGCTCT
1921 GAGACATGCTGAACTCCAACTGCAGGAAGCTCACGAGAAAGAGAGGTTACTAGAGAGAAG
1830 GAGACATGCTGAACTCCAACTGCAGGAAGCTCACGAGAAAGAGAGGTTACTAGAGAGAAG
1981 AAACACAGAGCTTGGCACTTCCCTTACAGAGCTACGCATCAAGGCAGAGCAACAGGGAAG
1890 AAACACAGAGCTTGGCACTTCCCTTACAGAGCTACGCATCAAGGCAGAGCAACAGGGAAG
2041 CTTGGCGGAGATGTTGAGGCACAAAAACATGCTGCTACAGGAGGAAAACAAACAGCTTCA
1950 CTTGGCGGAGATGTTGAGGCACAAAAACATGCTGCTACAGGAGGAAAACAAACAGCTTCA
                                                 M
2101 GCACAAAATGGAGAGCCTTGAACGGAAGCAAGAGGAGGCTAACTCGCAAAATCGAGATCT
2010 GCACAAAATGGAGAGCCTTGAACGGAAGCAAGAGGAGGCTAACTCGCAAAATCGAGATCT
                                                 R
2161 CATCCAGGTCATTTCAAAACGGGAAGAGACGATTCATAGCAGCCAGGTGCGTCTGGAAGA
2070 CATCCAGGTCATTTCAAAACGGGAAGAGACGATTCATAGCAGCCAGGTGCGTCTGGAAGA
2221 AAAGTCTCGAGAGTGCAGTATTCTGACCAAACAGCTGGAGGAGGCATTGGATGATGCCCG
2130 AAAGTCTCGAGAGTGCAGTATTCTGACCAAACAGCTGGAGGAGGCATTGGATGATGCCCG
2281 TCGACAGGTTACCCAGACCAGAGAGCGAGCAGCTTCTAAAGAGCGCGTTACGCAGTCCAA
2190 TCGACAGGTTACCCAGACCAGAGAGCGAGCAGCTTCTAAAGAGCGCGTTACGCAGTCCAA
2341 GATTGTCGATTTGGAAGCTCAACTGAGCAGAACATCAACTGAGCTGAACCAGTTACGACG
2250 GATTGTCGATTTGGAAGCTCAACTGAGCAGAACATCAACTGAGCTGAACCAGTTACGACG
2401 AGCCAAAGATGAGGCCGAACGGAGATACCAGAGTCGTTTACAAGATGTCAAGGACAGACT
2310 AGCCAAAGATGAGGCCGAACGGAGATACCAGAGTCGTTTACAAGATGTCAAGGACAGACT
                                     K
2461 AGAGCAGTCCGACAGCACAAACCGAAGCCTGCAGAATTATGTCCAGTTCCTAAAATCTTC
2370 AGAGCAGTCCGACAGCACAAACCGAAGCCTGCAGAATTATGTCCAGTTCCTAAAATCTTC
2521 TTACGTCAATGTGTTTGGAGACCCTGCTCTCACTGGCTCCTCATTCCGCACACCTTCGCC
2430 TTACGTCAATGTGTTTGGAGACCCTGCTCTCACTGGCTCCTCATTCCGCACACCTTCGCC


2581 TATCTGAAACCACTTTCAGGTGTCTGTTAAGACTTCTTTTACATGAACTGTATTAGTCGA
2490 TATCTGA.....................................................
                                            R
2641 CAACTGATGACCTCTGTAAGTTTACTGTGTTTGTGCTTTACTCCGTAAAGGAATAGTTCA
     ............................................................
                         K
2701 CTCAAATATGAGAATTTGCTATTAATTTACTTACCCTCAGACCATCCGAGATGTAGGTGA
     ............................................................
     *                             YY
2761 TTTTTTTTGTCAAGACTTTAAGCTGAAAAATTAATGCCACCATCACTTTAGTAATCATAT
     ............................................................
                                                 Y          R
2821 TATGATACATATTTGTTTTGTCTGTATTTTTTTGTTTTGTTTACTCTTAGAGTTCAGAGA
     ............................................................
     Y
```

1.2.2 Protein sequence (Odf2a)

```
MKKSVRTRSSSPPLHVHVNESTPVHVHVKKSTKCSPTKTAQVKSKTGLHPTAKVKTRVPW
IPPGKVSARETSYKWDGPSHRLEITAPQEPERSQSPMRIEDLSTNEEEALHGRINQYERK
IDSLMTEVSSLKKEVELRKKEQLLERQSERLSASQRVIAEQEEELAEVARELEATEQENS
RLRESMEKMLAENDFGRVERDGMQLDKDVLLRKLLEAEMDSSAAAKQVSALRETVSQMSR
STSEKKMSGSDSTLLVRQKEMLLQKLETFESTNRTLRHLLREQHSREMDSLRLLEQKDAL
LKRLSDVEEENSRILVKLQDKEREVNQLTSILESEKESSKTTSELSKVLESTRAHLQGQL
RNKEAENNRLNVQIRNLERSLSQQQGEMDHLQNQLRDLRQQAEADKEALKKATRAQKLRA
QRSEDTVGQLSGQLLEIEKQLAEAVTAAENWSSRHAKEMKDKGQLEVEIALLNSRITDLT
EHLHGQEEKSRIERDGLLDRLHELNTESTTVRLENQSLKATLTALEEKLLLSQSEVQQVK
VSVKQYESLVDSYKAQNQKTRAEADEFAARLQMASSEAQAVRDELDQEIQQVRKQLQGRL
SELEPLPEALRHAELQLQEAHEKERLLERRNTELGTSLTELRIKAEQQGSLAEMLRHKNM
LLQEENKQLQHKMESLERKQEEANSQNRDLIQVISKREETIHSSQVRLEEKSRECSILTK
QLEEALDDARRQVTQTRERAASKERVTQSKIVDLEAQLSRTSTELNQLRRAKDEAERRYQ
SRLQDVKDRLEQSDSTNRSLQNYVQFLKSSYVNVFGDPALTGSSFRTPSPI
```

1.2.3 A list of best BLASTsearch matches to Odf2a

Description	Total score	Query cover	E value	Ident	Accession
PREDICTED: outer dense fiber protein 2-like [Lepisosteus oculatus]	724	99%	0.0	52%	XP_006640818.1
PREDICTED: outer dense fiber protein 2 [Danio rerio]	701	99%	0.0	49%	XP_001332564.5
outer dense fiber protein 2 isoform d [Mus musculus]	563	99%	0.0	42%	NP_001171130.1
outer dense fiber protein 2 isoform 11 [Homo sapiens]	553	99%	0.0	41%	NP_001229281.1
outer dense fiber protein 2 isoform 9 [Homo sapiens]	518	99%	6e-170	41%	NP_002531.3
outer dense fiber protein 2 isoform 2 [Homo sapiens]	518	97%	9e-170	41%	NP_702911.1
outer dense fiber protein 2 isoform 1 [Homo sapiens]	517	99%	3e-168	41%	NP_702913.1

1.3 Zebrafish Odf2b sequence information

Name	Transcript ID	bp	Protein	Biotype	UniProt	RefSeq
odf2b-202	ENSDART00000143604.3	3233	810aa	Protein coding	B0S753	NM_001123232 NP_001116704
odf2b-201	ENSDART00000130870.4	648	173aa	Protein coding	B0S752	-
odf2b-203	ENSDART00000145851.2	808	No protein	Retained intron	-	-

Protein sequence for odf2b-202 was considered for all the works in this thesis.

1.3.1 cDNA sequence (*odf2b)*

```
   1 GGGTAGTGCAAACAACATTACCCGGGGGATGCAACGTTGTATACTTGACTTGAGGTTGTA
     ............................................................
  61 ATATTTTTTTAATTCATATTTACCATTTAATGTACACGAATTGCTTTTTCAAACGTATTT
     ............................................................
 121 CCGATCATGCCGATTTAACTGGTTGCAGTGCGTAAACTAAAATAACGACTCAGAACTACA
     ............................................................
 181 AACATCGTTGAATGTGGACAAAGTGGACGCTTGTTTCGTAACACTTCTTTTTTATTTTTC
     ............................................................
 241 TTACAAGTTTCTGACACACATCTGGGACACTTTTTCATACCTGTAACTGTTTTAAGACCG
     ............................................................
 301 TCTTACTAAAGTGAAGGGATGAAAACACGGTCGTCTTCTCCGCCCGTTCATGTTCATATC
     ..................ATGAAAACACGGTCGTCTTCTCCGCCCGTTCATGTTCATATC
 361 CCAGACTCCACATCTGTGCATGTTCACCTGAAGAAGAGCCCACAGAGGAGCCAGCAGGCA
  43 CCAGACTCCACATCTGTGCATGTTCACCTGAAGAAGAGCCCACAGAGGAGCCAGCAGGCA
 421 AAAGTGAGCAGTTTGCGATCCACTGCCAGTGTGAAGGTCCGAGCTCCATGGGTTCCTCCT
 103 AAAGTGAGCAGTTTGCGATCCACTGCCAGTGTGAAGGTCCGAGCTCCATGGGTTCCTCCT
 481 GGAAAGAGCTCAACACGAAGACAGTACAAATGGGAGGGGGCTACTCGCTGCTTGGAGATC
 163 GGAAAGAGCTCAACACGAAGACAGTACAAATGGGAGGGGGCTACTCGCTGCTTGGAGATC
 541 ACTCCTGGACTCTCCTCTTCCTCACCTCCACTCCGGCTCACTGACCTGTCCAGTGAAGAA
 223 ACTCCTGGACTCTCCTCTTCCTCACCTCCACTCCGGCTCACTGACCTGTCCAGTGAAGAA
 601 GAGGATCCAGGAGGAGCCATCAACAAATATGAGAGAAAACTCGAAAGCCTAATGTCGGAG
 283 GAGGATCCAGGAGGAGCCATCAACAAATATGAGAGAAAACTCGAAAGCCTAATGTCGGAG
 661 GTTGACTGTTTAAAAAATGAGGTGAAATTACGGCAAGCAGAGGAGCACCTGAAGCACCAG
 343 GTTGACTGTTTAAAAAATGAGGTGAAATTACGGCAAGCAGAGGAGCACCTGAAGCACCAG
 721 TCACAGCAGCTGAGTGCCTGTCAGCATTTGATTGACCAGCATGAGGAAAGACTTGAGGAA
 403 TCACAGCAGCTGAGTGCCTGTCAGCATTTGATTGACCAGCATGAGGAAAGACTTGAGGAA
 781 GCTAGTAAAAGCTTGAGGAGGTCAAAACGTGAAAACACAGATCTGCGTAGCTCTGCAGAC
 463 GCTAGTAAAAGCTTGAGGAGGTCAAAACGTGAAAACACAGATCTGCGTAGCTCTGCAGAC
 841 GGGACACAGGGTGAACCTGGAGAAATCAGATCAGATGCAGGACCACTGCACCAGGAGCTA
 523 GGGACACAGGGTGAACCTGGAGAAATCAGATCAGATGCAGGACCACTGCACCAGGAGCTA
 901 GAAACTCTGCTGAGGAAACTGGTGGAAGCTGAAATTGATGGTCAGGCCGCAGCCAAACAA
 583 GAAACTCTGCTGAGGAAACTGGTGGAAGCTGAAATTGATGGTCAGGCCGCAGCCAAACAA
 961 GTGGTGCTTCTGAAGGAATCTGTGGGCAAACTCAAAAAGGAGAAAAAACAGTCAAAGGTA
 643 GTGGTGCTTCTGAAGGAATCTGTGGGCAAACTCAAAAAGGAGAAAAAACAGTCAAAGGTA
1021 AACTCGGATCAGCTGGGCCGTCAACATGAGCTACTTGAACAGAAGTTGGACAAATTTGTG
 703 AACTCGGATCAGCTGGGCCGTCAACATGAGCTACTTGAACAGAAGTTGGACAAATTTGTG
1081 GAGACAAACCGAACTCTCAGACGCCTTTTGAGGGAGCAGCATGGGCGTGAGACAGATGCT
 763 GAGACAAACCGAACTCTCAGACGCCTTTTGAGGGAGCAGCATGGGCGTGAGACAGATGCT
1141 TTGAAGATGACTGATGAGAGAGAGATTCTAATGAGGAAGCTAGCAGATTCTGAAGCTGAG
 823 TTGAAGATGACTGATGAGAGAGAGATTCTAATGAGGAAGCTAGCAGATTCTGAAGCTGAG
1201 AGAAGGAAACTTGAGACTAAACTTAGCAGGAGAGAAAGAGAGGCCAATCAGATGGCTGAG
 883 AGAAGGAAACTTGAGACTAAACTTAGCAGGAGAGAAAGAGAGGCCAATCAGATGGCTGAG
1261 AATTTGGAAACTGAAAAGGAGCATATGAAAGCCACAGGAGAGCTGTCCAAGGTTCTTGAA
 943 AATTTGGAAACTGAAAAGGAGCATATGAAAGCCACAGGAGAGCTGTCCAAGGTTCTTGAA
1321 TCAACCCGCAGTCGCTTGCAGAACAATCTGCTTAAGAAGGAAGCTGAAAATAAACGTCAG
1003 TCAACCCGCAGTCGCTTGCAGAACAATCTGCTTAAGAAGGAAGCTGAAAATAAACGTCAG
1381 GAGGCTCAGATCCAAAGACTGGAAGAGACACTGCAGCATCAGCAGGATGAGGTTCAAGGC
```

```
1063 GAGGCTCAGATCCAAAGACTGGAAGAGACACTGCAGCATCAGCAGGATGAGGTTCAAGGC
1441 CTGCTGGAGCAGATGAGAGAGTTGAAGCAGCACTGTGAAGGAGACGTCCACAAACAGGTC
1123 CTGCTGGAGCAGATGAGAGAGTTGAAGCAGCACTGTGAAGGAGACGTCCACAAACAGGTC
1501 TTGGAGGAACACAGAAAACAGGCAGAGAAAAGTGTGAATACTGCTGCACAGCTTTCTGCA
1183 TTGGAGGAACACAGAAAACAGGCAGAGAAAAGTGTGAATACTGCTGCACAGCTTTCTGCA
1561 CAGCTCCTGGAAAAGGAGGCTCAGTTAACAGAGGCTCTCTCCAGTGCTGAGGAGCTTCAG
1243 CAGCTCCTGGAAAAGGAGGCTCAGTTAACAGAGGCTCTCTCCAGTGCTGAGGAGCTTCAG
1621 CAGCGTTTCTCCAAACAGAGCCGAGAGAAAAGCCAGCTGGAGCTGCAGATCACCACCTTA
1303 CAGCGTTTCTCCAAACAGAGCCGAGAGAAAAGCCAGCTGGAGCTGCAGATCACCACCTTA
1681 AATAATCGTCTCAGTGAGTTGAGTGATCAGTTGTGCAGTTGTGAGCAGAAGTCCTGTGCC
1363 AATAATCGTCTCAGTGAGTTGAGTGATCAGTTGTGCAGTTGTGAGCAGAAGTCCTGTGCC
1741 GAGAGAGAGGGTCTTCTCAACCGTCTGCACTTCCTCACCTCAGAAAACACTTCCACCAAA
1423 GAGAGAGAGGGTCTTCTCAACCGTCTGCACTTCCTCACCTCAGAAAACACTTCCACCAAA
1801 CTGGAGAACCAGAGACTCAAGAGCACTCTGTCAGCTGCAGAGGACAGGCTGTGTTTGTCT
1483 CTGGAGAACCAGAGACTCAAGAGCACTCTGTCAGCTGCAGAGGACAGGCTGTGTTTGTCT
1861 CAGGCTGAGGTGCAGCAGCTGAAGGTCTCACTCAAAGACTTCGAGAGTCTGGTGGAAGGC
1543 CAGGCTGAGGTGCAGCAGCTGAAGGTCTCACTCAAAGACTTCGAGAGTCTGGTGGAAGGC
1921 TACAAAAGTCAGTTGCAGAAGACGCATCTGGAGTCTGAGCAATGGAGGCTGAGACTGGAG
1603 TACAAAAGTCAGTTGCAGAAGACGCATCTGGAGTCTGAGCAATGGAGGCTGAGACTGGAG
1981 ATGATGGAGGAGGCGGCAGAAAGCGAGCGTGTGGAGGTGGACAGAGAGATGGAGCATGGC
1663 ATGATGGAGGAGGCGGCAGAAAGCGAGCGTGTGGAGGTGGACAGAGAGATGGAGCATGGC
2041 CGCAAGCAGCTCCAGGCCCGGATGAAAGAGATGGAGAAGCTGCGCGAAGCTCTAAAGCTC
1723 CGCAAGCAGCTCCAGGCCCGGATGAAAGAGATGGAGAAGCTGCGCGAAGCTCTAAAGCTC
2101 CTGGAGGATGAGCTCAGAGAGACCAAAGAGAACCGGATCATCCAGGACAGGAGAAACACT
1783 CTGGAGGATGAGCTCAGAGAGACCAAAGAGAACCGGATCATCCAGGACAGGAGAAACACT
2161 GAACACAGCTGCGCTCTGGCTGAACTCAGGACAAAAGTGGAGCAGCAGAGTAGTAAAATA
1843 GAACACAGCTGCGCTCTGGCTGAACTCAGGACAAAAGTGGAGCAGCAGAGTAGTAAAATA
2221 GAGTCACTCCAGGAGAAGAACTTATTTCTGCTTGAAGAAAATATGCAGCTGAAACGCTCA
1903 GAGTCACTCCAGGAGAAGAACTTATTTCTGCTTGAAGAAAATATGCAGCTGAAACGCTCA
2281 ACGGAAAGCATTGAAAGGAAGATGGAGGACACGAGTGCTCAGAACAAGGATCTTCTTCAG
1963 ACGGAAAGCATTGAAAGGAAGATGGAGGACACGAGTGCTCAGAACAAGGATCTTCTTCAG
2341 CTGGTCTCCAAGCGTGAAGAGACCATCAAGAGCTGCCAGCAGCATCTGGAGGAGAAGAGC
2023 CTGGTCTCCAAGCGTGAAGAGACCATCAAGAGCTGCCAGCAGCATCTGGAGGAGAAGAGC
2401 CGCGAGTGTGAGTGTCTGTTCAGACAGCTGGAGCAGAGCAGAGTGGAGGCACAGAGACAG
2083 CGCGAGTGTGAGTGTCTGTTCAGACAGCTGGAGCAGAGCAGAGTGGAGGCACAGAGACAG
2461 GGGGAGCAGAGTCTGGAGCGGCTGATTTCTAAAGAGCGATCCACTCAGTCCAGAATGCTG
2143 GGGGAGCAGAGTCTGGAGCGGCTGATTTCTAAAGAGCGATCCACTCAGTCCAGAATGCTG
2521 GATCTGGAGAGCCAACTGAGCCTGGCCAAAAATGAGCTGAGTCAAACACGCCGCAGCAAA
2203 GATCTGGAGAGCCAACTGAGCCTGGCCAAAAATGAGCTGAGTCAAACACGCCGCAGCAAA
2581 GATGATATGGAGAAGAGATTTCAGTGTAAACTACAAGACATGAAGAATCAGCTGGAGCAG
2263 GATGATATGGAGAAGAGATTTCAGTGTAAACTACAAGACATGAAGAATCAGCTGGAGCAG
2641 GTGAACAGCTCAAACCGCAGCCTGCAGAACTACGTCAACTACCTTAAAGCTTCATACGCT
2323 GTGAACAGCTCAAACCGCAGCCTGCAGAACTACGTCAACTACCTTAAAGCTTCATACGCT
2701 GATGTGTTTGGAGACTCCTCGCTGACCAGCGCACTCAATCCACACATCTGATTTATCAAA
2383 GATGTGTTTGGAGACTCCTCGCTGACCAGCGCACTCAATCCACACATCTGA.........
2761 TGTTAAAACTGTCATTTACTAATCCTCATGTCATGCCGAAATGCCGATGATTTTTTTTGT
     ............................................................
2821 CTCTGGGGAAAAATCCTGTGGATTCACTACGCATGTGTTTCAGTAAAATTGTAATATTTG
     ............................................................
2881 TTTCATTTTATAAAGGTCTTTATTTATTTGTTGTGACTGAAAAATCAAGGTTATTCCAAG
     ............................................................
2941 TTAAAACATGGGTATTGTGGAAAATAATAATACTGTGATTTTAAATTTGGATTTGGAAAG
     ............................................................
3001 AAATGCCATCACATTTTTTACGATAACTTTACTAAACAAAAAATGACTAATGCAGAGAGA
     ............................................................
3061 CAAAATGTAAAAGCGCTCTCATTTTATATCTGTCCACTGGAAATAAGGTTAGAAAAGTTA
     ............................................................
3121 TGGAATAACATGAGGATAAATAAAAGTCAATCTTTTTTCATGATGCAGTTCTTTTTACCC
     ............................................................
3181 ATAATGTACTTGAATTTGTTTTGTTAACTTTTTAATAAAACATCATTGCGACA
     ...................................................
```

1.3.2 Protein sequence (Odf2b)

```
MKTRSSSPPVHVHIPDSTSVHVHLKKSPQRSQQAKVSSLRSTASVKVRAPWVPPGKSSTR
RQYKWEGATRCLEITPGLSSSSPPLRLTDLSSEEEDPGGAINKYERKLESLMSEVDCLKN
EVKLRQAEEHLKHQSQQLSACQHLIDQHEERLEEASKSLRRSKRENTDLRSSADGTQGEP
GEIRSDAGPLHQELETLLRKLVEAEIDGQAAAKQVVLLKESVGKLKKEKKQSKVNSDQLG
RQHELLEQKLDKFVETNRTLRRLLREQHGRETDALKMTDEREILMRKLADSEAERRKLET
KLSRREREANQMAENLETEKEHMKATGELSKVLESTRSRLQNNLLKKEAENKRQEAQIQR
LEETLQHQQDEVQGLLEQMRELKQHCEGDVHKQVLEEHRKQAEKSVNTAAQLSAQLLEKE
AQLTEALSSAEELQQRFSKQSREKSQLELQITTLNNRLSELSDQLCSCEQKSCAEREGLL
NRLHFLTSENTSTKLENQRLKSTLSAAEDRLCLSQAEVQQLKVSLKDFESLVEGYKSQLQ
KTHLESEQWRLRLEMMEEAAESERVEVDREMEHGRKQLQARMKEMEKLREALKLLEDELR
ETKENRIIQDRRNTEHSCALAELRTKVEQQSSKIESLQEKNLFLLEENMQLKRSTESIER
KMEDTSAQNKDLLQLVSKREETIKSCQQHLEEKSRECECLFRQLEQSRVEAQRQGEQSLE
RLISKERSTQSRMLDLESQLSLAKNELSQTRRSKDDMEKRFQCKLQDMKNQLEQVNSSNR
SLQNYVNYLKASYADVFGDSSLTSALNPHI
```

1.3.3 List of best BLAST search matches to Odf2b

Description	Total score	Query cover	E value	Ident	Accession
PREDICTED: outer dense fiber protein 2-like [Lepisosteus oculatus]	724	99%	0.0	52%	XP_006640818.1
PREDICTED: outer dense fiber protein 2 [Danio rerio]	701	99%	0.0	49%	XP_001332564.5
outer dense fiber protein 2 isoform d [Mus musculus]	563	99%	0.0	42%	NP_001171130.1
outer dense fiber protein 2 isoform 11 [Homo sapiens]	553	99%	0.0	41%	NP_001229281.1
outer dense fiber protein 2 isoform 9 [Homo sapiens]	518	99%	6e-170	41%	NP_002531.3
outer dense fiber protein 2 isoform 2 [Homo sapiens]	518	97%	9e-170	41%	NP_702911.1
outer dense fiber protein 2 isoform 1 [Homo sapiens]	517	99%	3e-168	41%	NP_702913.1

Appendix -2

2.1 List of protein identified from mass spectrometric analysis

A list of proteins identified from mass spectrometric analysis from all experiments sorted according the mascot scores.

Gene name	Name	Meta Score	Peptides
HSP90AB1	Heat shock protein HSP 90-beta	1710.8	32
EEF2	Elongation factor 2	1384.9	31
TUBA1A	TUBA1A	1010	21
HSPA9	Stress-70 protein, mitochondrial	713.6	16
PRKDC	DNA-dependent protein kinase catalytic subunit	701.9	16
TUBB6	Tubulin beta-6 chain	637	11
ATP5B	ATP synthase subunit beta, mitochondrial	615.7	13
PGK1	Phosphoglycerate kinase 1	469.7	12
NPM1	Nucleophosmin	449.3	10
C1QBP	Complement component 1 Q subcomponent-binding protein, mitochondrial	413.4	7
YWHAB	14-3-3 protein beta/alpha	396.6	10
MYH9	Myosin-9	351.4	6
CCT6A	T-complex protein 1 subunit zeta	365.63	18
SERPINA1	Alpha-1-antiproteinase	315.6	7
PAICS	Multifunctional protein ADE2	314.4	10
PGAM1	Phosphoglycerate mutase 1	306.8	8
HNRNPA2B1	Heterogeneous nuclear ribonucleoproteins A2/B1	294.2	6
YWHAG	14-3-3 protein gamma	291.2	6
ACLY	ATP-citrate synthase	274.8	9
AHCY	Adenosylhomocysteinase	265.2	7
VIM	Vimentin	253	10
NONO	Non-POU domain-containing octamer-binding protein	251	6
LARS	Leucine--tRNA ligase, cytoplasmic	240.5	5
HNRNPU	Heterogeneous nuclear ribonucleoprotein U	240	5
PLS3	Plastin-3	237.7	7
VCP	Transitional endoplasmic reticulum ATPase	233.3	5
KPNB1	Importin subunit beta-1	232	7
ATIC	Bifunctional purine biosynthesis protein PURH	223.9	8
MYO18A	Unconventional myosin-XVIIIa	231.1	4
PARP1	Poly [ADP-ribose] polymerase 1	219.6	6
MTHFD1	C-1-tetrahydrofolate synthase, cytoplasmic	219.6	6
YWHAH	14-3-3 protein eta	216.9	5
NACA	Nascent polypeptide-associated complex subunit alpha, muscle-specific form	204.7	2
ALDH18A1	Delta-1-pyrroline-5-carboxylate synthase	199.9	4
CANX	Calnexin	198.3	5
SFPQ	Splicing factor, proline- and glutamine-rich	197	7
DDX3X	ATP-dependent RNA helicase DDX3X	195	5
SSB	Lupus La protein	194.6	6
TXN	Thioredoxin	193.8	5

DDX17	Probable ATP-dependent RNA helicase DDX17	189.8	7
STOML2	Stomatin-like protein 2	180.7	5
RPL3	60S ribosomal protein L3	178.2	4
NME1	Nucleoside diphosphate kinase A	177.8	5
TF	Serotransferrin	177.3	5
EEF1B2	Elongation factor 1-beta	175.6	3
RPS5	40S ribosomal protein S5	175.3	4
ST13	Hsc70-interacting protein	173.6	5
IARS	Isoleucine--tRNA ligase, cytoplasmic	169.3	5
STIP1	Stress-induced-phosphoprotein 1	166.5	5
GCN1L	Translational activator GCN1	166.1	4
HNRNPH1	Heterogeneous nuclear ribonucleoprotein H	163.4	4
PDIA6	Protein disulfide-isomerase A6	159.6	4
EIF4B	Eukaryotic translation initiation factor 4B	158.4	4
ANXA5	Annexin A5	157.5	3
RPL13	60S ribosomal protein L13	155.2	4
PRPS1	Ribose-phosphate pyrophosphokinase 1	153.6	3
KPNA2	Importin subunit alpha-2	152	4
RL10A	60S ribosomal protein L10a	147.7	4
SHMT2	Serine hydroxymethyltransferase, mitochondrial	147.5	4
PARK7	Protein DJ-1 O	146.5	5
PEBP1	Phosphatidylethanolamine-binding protein 1	146.2	3
EIF5A	Eukaryotic translation initiation factor 5A	142.7	5
SF3B3	Splicing factor 3B subunit 3	142.6	4
RAB7B	Ras-Related Protein Rab-7b	141.9	3
UQCRC1	Cytochrome b-c1 complex subunit 1, mitochondrial	141.6	3
A2M	Alpha-2-macroglobulin	139.9	2
PHB	Prohibitin	137.9	4
AIFM1	Apoptosis-inducing factor 1, mitochondrial	136	3
DNJA1	DnaJ homolog subfamily A member 1	134.3	2
ASNS	Asparagine synthetase [glutamine-hydrolyzing]	133.3	3
SRP72	Signal recognition particle 72 kDa protein	132.9	2
RPLP1	60S acidic ribosomal protein P1	131.3	3
PPA1	Inorganic pyrophosphatase	130.4	3
STRAP	Serine-threonine kinase receptor-associated protein	129.7	3
PTBP1	Polypyrimidine tract-binding protein 1	129.6	5
RPS26	40S ribosomal protein S26	129.1	3
CYB5R3	NADH-cytochrome b5 reductase 3	126.7	2
KIF5B	Kinesin-1 heavy chain	125.1	2
COPB2	Coatomer subunit beta'	124.7	3
HPRT1	Hypoxanthine-guanine phosphoribosyltransferase	124.3	2
EIF2S1	Eukaryotic translation initiation factor 2 subunit 1	123.4	1
RANBP1	Ran-Specific GTPase-Activating Protein	122.2	5
PPP1CA	Serine/threonine-protein phosphatase PP1-alpha catalytic subunit	120.2	2
PSME3	Proteasome activator complex subunit 3	112.9	3
S100A11	Protein S100-A11	112.1	2
FHL1	Four and a half LIM domains protein 1	110.3	3
CDK1	Cyclin-dependent kinase 1	109.4	3
RPS24	40S ribosomal protein S24	108.5	2
DHX9	ATP-dependent RNA helicase A	108.4	3
DYNC1I2	Cytoplasmic dynein 1 intermediate chain 2	108.2	1
RPS16	40S ribosomal protein S16	106.1	2

HADHA	Trifunctional enzyme subunit alpha, mitochondrial	103.6	3
HNRNPC	Heterogeneous nuclear ribonucleoproteins C1/C2	102.5	1
BASP1	Brain acid soluble protein 1	102.3	3
DX39B	Spliceosome RNA helicase DDX39B	102.2	3
ANP32A	Acidic leucine-rich nuclear phosphoprotein 32 family member A	102.2	3
RPS15A	40S ribosomal protein S15a	102.2	3
RPS6	40S ribosomal protein S6	102	2
P4HB	Protein disulfide-isomerase	100.4	2
COPZ1	Coatomer subunit zeta-1	100.1	2
RPL11	60S ribosomal protein L11	100	3
SSBP1	Single-stranded DNA-binding protein, mitochondrial	98.8	4
PSMB5	Proteasome subunit beta type-5	96.2	2
DBNL	Drebrin-like protein	95.5	2
MAT2A	S-adenosylmethionine synthase isoform type-2	94.3	3
NAA15	N-alpha-acetyltransferase 15, NatA auxiliary subunit	93.6	3
TTLL12	Tubulin--tyrosine ligase-like protein 12	93.5	2
PGM1	Phosphoglucomutase-1	92.3	2
HNRNPAB	Heterogeneous nuclear ribonucleoprotein A/B	91.5	2
EIF3A	Eukaryotic translation initiation factor 3 subunit A	90.8	3
PSMA7	Proteasome subunit alpha type-7	89.8	3
SRP68	Signal recognition particle 68 kDa protein	89	3
ANP32B	Acidic leucine-rich nuclear phosphoprotein 32 family member B	88.9	3
BCAP31	B-cell receptor-associated protein 31	86.8	1
ATP5D	ATP synthase subunit delta, mitochondrial	86.5	1
ALYREF	THO complex subunit 4	86	2
FUS	RNA-binding protein FUS	86	3
PPP2R1A	Serine/threonine-protein phosphatase 2A 65 kDa regulatory subunit A alpha isoform	85.7	3
ALDH9A1	4-trimethylaminobutyraldehyde dehydrogenase	85.4	3
RPL35A	60S ribosomal protein L35a	85	3
RPS27A	Ubiquitin-40S ribosomal protein S27a	83.9	2
ILF2	Interleukin enhancer-binding factor 2	82.8	3
RPL15	60S ribosomal protein L15 (Fragment)	82.2	2
CPSF7	Cleavage and polyadenylation specificity factor subunit 7	82	2
CAPRIN1	Caprin-1	81.8	3
SUMO4	Small ubiquitin-related modifier 4	81.7	1
PRMT	Protein arginine N-methyltransferase 1	80.7	2
VPS35	Vacuolar protein sorting-associated protein 35	80	2
RPS27	40S ribosomal protein S27	79.5	2
ACTR1A	Alpha-centractin	79.2	2
OAT	Ornithine aminotransferase, mitochondrial	78.6	1
PDIA3	Protein disulfide-isomerase A3 (Fragments)	78.1	1
APOA1	Apolipoprotein A-I	77.5	2
COPA	Coatomer subunit alpha	76.6	3
ADRM1	Proteasomal ubiquitin receptor ADRM1	76.6	1
LMNB1_RAT	Lamin-B1	75.8	2
CROCC	Rootletin	74.7	1
CLASP1	CLIP-associating protein 1	74.2	1
PABPC1	Polyadenylate-binding protein 1	74	2
SFXN1	Sideroflexin-1	74	2
PPIB	Peptidyl-prolyl cis-trans isomerase B	71.7	2
ATP5H	ATP synthase subunit d, mitochondrial	71.5	2

HUWE1	E3 ubiquitin-protein ligase HUWE1	70.6	2
TARDBP	TAR DNA-binding protein 43	70.1	2
DVL3	Segment polarity protein dishevelled homolog DVL-3	69.7	1
CAD	CAD protein	68.8	2
PSMD14	26S proteasome non-ATPase regulatory subunit 14	68.7	1
MPDH2	Inosine-5'-monophosphate dehydrogenase 2	68.4	3
PFN2	Profilin-2	67.5	1
GLUD1	Glutamate dehydrogenase 1, mitochondrial	67.4	2
GOT2	Aspartate aminotransferase, mitochondrial	67	2
PTMS	Parathymosin	66.8	1
FAM120A	Constitutive coactivator of PPAR-gamma-like protein 1	66.8	2
LUC7L2	Putative RNA-binding protein Luc7-like 2	66.5	2
RPL27A	60S ribosomal protein L27a	66.4	2
FAM186A	Protein FAM186A	65.8	2
TSN	Translin	65.6	2
MY12B	Myosin regulatory light chain 12B	65.6	2
TBCA	Tubulin-specific chaperone A	65.2	2
EIF4A3	Eukaryotic initiation factor 4A-III	65.2	2
DUT	Deoxyuridine 5'-triphosphate nucleotidohydrolase, mitochondrial	64.7	2
SF3B2	Splicing factor 3B subunit 2	64.3	1
SDHA	Succinate dehydrogenase [ubiquinone] flavoprotein subunit, mitochondrial	63.6	1
MYBB1A	Myb-binding protein 1A	63.6	1
FARSA	Phenylalanine--tRNA ligase alpha subunit	63.6	2
RBM26	RNA-binding protein 26	63.2	1
ROS1	Proto-oncogene tyrosine-protein kinase ROS	62.6	1
SHCGP1L	SHC SH2 domain-binding protein 1-like protein	62.1	1
GSTM3	Glutathione S-transferase Mu 3	61.8	1
PSMD12	26S proteasome non-ATPase regulatory subunit 12	61.5	2
RPL13A	60S ribosomal protein	61.5	2
DENR	Density-regulated protein	61.3	2
SSR4	Translocon-associated protein subunit delta	60.9	1
EIF2S3X	Eukaryotic translation initiation factor 2 subunit 3, X-linked	60.9	2
ATXN10	Ataxin-10	60.7	1
RRM1	Ribonucleoside-diphosphate reductase large subunit	60.2	2
SNRPB2	U2 small nuclear ribonucleoprotein	60	1
IPO7	Importin-7	59.9	1
RHOA	Transforming protein RhoA	59	1
ECHS1	Enoyl-CoA hydratase, mitochondrial	58.8	1
SRP14	Signal recognition particle 14 kDa protein	58.7	2
CAP1	Adenylyl cyclase-associated protein 1	56.5	1
RPL24	60S ribosomal protein L24	56.3	1
AKR1B1	Aldose reductase	56.3	2
GEMIN5	Gem-associated protein 5	55.8	2
USMG5_HUMAN	Up-regulated during skeletal muscle growth protein 5	55.3	1
TOMM22	Mitochondrial import receptor subunit TOM22 homolog	55	2
WDR61	WD repeat-containing protein 61	54.7	1
ATP5L	ATP synthase subunit g, mitochondrial	54.2	1
SBNO2	Protein strawberry notch homolog 2	53.9	1
CHTOP	Chromatin target of PRMT1 protein	53.6	1
WDR77	Methylosome protein 50	53.1	1
NAMPT	Nicotinamide phosphoribosyltransferase	51.4	1

RPL37A	60S ribosomal protein L37a	50.2	1
RPL18A	60S ribosomal protein L18a	50	1
MTPN	Myotrophin	48.8	1
NAA11	N-alpha-acetyltransferase 11	48.4	1
CLNS1A	Methylosome subunit pICln	47.8	1
HADH	Hydroxyacyl-coenzyme A dehydrogenase, mitochondrial	47.7	1
BRI3B	BRI3-binding protein	46.6	1
MRPL12	39S ribosomal protein L12, mitochondrial	45.5	1
CDK9	Cyclin-dependent kinase 9	44.4	1
DPYSL3	Dihydropyrimidinase-related protein 3	43.8	1
DNJA2	DnaJ homolog subfamily A member 2	43.3	1
RCC2	Protein RCC2	43	1
NASP	Nuclear autoantigenic sperm protein	41.8	1
TPD52L2	Tumor protein D54	41.7	1
HMGB1	High mobility group protein B1 (Fragment)	41.7	1
PPIF	Peptidyl-prolyl cis-trans isomerase F,	41.7	1
GEMIN4	Gem-associated protein 4	41.4	1
ADH5	Alcohol dehydrogenase class-3	41.4	1
HNRNPH3	Heterogeneous nuclear ribonucleoprotein H3	41.3	1
ARHGDIA	Rho GDP-dissociation inhibitor 1	40.3	1
GIMAP7	GTPase IMAP family member 7	30.1	1
KIF18A	Kinesin-like protein KIF18A	18	1
CCDC180	Coiled-coil domain-containing protein 180	28	1
AKAP6	A-kinase anchor protein 6	14	1
GOLGA6L1	Golgin subfamily A member 6-like protein 1	14	1

References

Adams, M., Smith, U. M., Logan, C. V. & Johnson, C. A. (2008). Recent advances in the molecular pathology, cell biology and genetics of ciliopathies. *J Med Genet,* **45**, 257-67.

Adams, N. A., Awadein, A. & Toma, H. S. (2007). The retinal ciliopathies. *Ophthalmic Genet,* **28**, 113-25.

Akimov, V., Rigbolt, K. T., Nielsen, M. M. & Blagoev, B. (2011). Characterization of ubiquitination dependent dynamics in growth factor receptor signaling by quantitative proteomics. *Mol Biosyst,* **7**, 3223-33.

Albertazzi, L., Arosio, D., Marchetti, L., Ricci, F. & Beltram, F. (2009). Quantitative FRET analysis with the EGFP-mCherry fluorescent protein pair. *Photochem Photobiol,* **85**, 287-97.

Alieva, I. B. & Vorobjev, I. A. (2004). Vertebrate primary cilia: a sensory part of centrosomal complex in tissue cells, but a "sleeping beauty" in cultured cells? *Cell Biol Int,* **28**, 139-50.

Andersen, J. S., Wilkinson, C. J., Mayor, T., Mortensen, P., Nigg, E. A. & Mann, M. (2003). Proteomic characterization of the human centrosome by protein correlation profiling. *Nature,* **426**, 570-4.

Anderson, R. G. (1972). The three-dimensional structure of the basal body from the rhesus monkey oviduct. *J Cell Biol,* **54**, 246-65.

Asada, M., Irie, K., Yamada, A. & Takai, Y. (2004). Afadin- and alpha-actinin-binding protein ADIP directly binds beta'-COP, a subunit of the coatomer complex. *Biochem Biophys Res Commun,* **321**, 350-4.

Azimzadeh, J., Hergert, P., Delouvee, A., Euteneuer, U., Formstecher, E., Khodjakov, A. & Bornens, M. (2009). hPOC5 is a centrin-binding protein required for assembly of full-length centrioles. *J Cell Biol,* **185**, 101-14.

Azimzadeh, J. & Marshall, W. F. (2010). Building the centriole. *Curr Biol,* **20**, R816-25.

Balczon, R., Bao, L. & Zimmer, W. E. (1994). PCM-1, A 228-kD centrosome autoantigen with a distinct cell cycle distribution. *J Cell Biol,* **124**, 783-93.

Balczon, R., Varden, C. E. & Schroer, T. A. (1999). Role for microtubules in centrosome doubling in Chinese hamster ovary cells. *Cell Motil Cytoskeleton,* **42**, 60-72.

Balczon, R. & West, K. (1991). The identification of mammalian centrosomal antigens using human autoimmune anticentrosome antisera. *Cell Motil Cytoskeleton,* **20**, 121-35.

Barenz, F., Inoue, D., Yokoyama, H., Tegha-Dunghu, J., Freiss, S., Draeger, S., Mayilo, D., Cado, I., Merker, S., Klinger, M., Hoeckendorf, B., Pilz, S., Hupfeld, K., Steinbeisser, H., Lorenz, H., Ruppert, T., Wittbrodt, J. & Gruss, O. J. (2013). The centriolar satellite protein SSX2IP promotes centrosome maturation. *J Cell Biol,* **202**, 81-95.

Barenz, F., Mayilo, D. & Gruss, O. J. (2011). Centriolar satellites: busy orbits around the centrosome. *Eur J Cell Biol,* **90**, 983-9.

Baron Gaillard, C. L., Pallesi-Pocachard, E., Massey-Harroche, D., Richard, F., Arsanto, J. P., Chauvin, J. P., Lecine, P., Kramer, H., Borg, J. P. & Le Bivic, A. (2011). Hook2 is involved in the morphogenesis of the primary cilium. *Mol Biol Cell,* **22**, 4549-62.

Barr, F. A., Sillje, H. H. & Nigg, E. A. (2004). Polo-like kinases and the orchestration of cell division. *Nat Rev Mol Cell Biol,* **5**, 429-40.

Baye, L. M., Patrinostro, X., Swaminathan, S., Beck, J. S., Zhang, Y., Stone, E. M., Sheffield, V. C. & Slusarski, D. C. (2011). The N-terminal region of centrosomal protein 290 (CEP290) restores vision in a zebrafish model of human blindness. *Hum Mol Genet,* **20**, 1467-77.

Bedell, V. M., Wang, Y., Campbell, J. M., Poshusta, T. L., Starker, C. G., Krug, R. G., 2nd, Tan, W., Penheiter, S. G., Ma, A. C., Leung, A. Y., Fahrenkrug, S. C., Carlson, D. F., Voytas, D. F.,

Clark, K. J., Essner, J. J. & Ekker, S. C. (2012). In vivo genome editing using a high-efficiency TALEN system. *Nature,* **491**, 114-8.

Beisson, J. & Wright, M. (2003). Basal body/centriole assembly and continuity. *Curr Opin Cell Biol,* **15**, 96-104.

Bernhard, W. & de Harven, E. (1960). L'ultrastructure du centriole et d'autres éléments de l'appareil achromatique. *In:* Bargmann, W., Peters, D. & Wolpers, C. (eds.) *Verhandlungen Band II / Biologisch-Medizinischer Teil.* Springer Berlin Heidelberg.

Berns, M. W., Rattner, J. B., Brenner, S. & Meredith, S. (1977). The role of the centriolar region in animal cell mitosis. A laser microbeam study. *J Cell Biol,* **72**, 351-67.

Bershteyn, M., Atwood, S. X., Woo, W. M., Li, M. & Oro, A. E. (2010). MIM and cortactin antagonism regulates ciliogenesis and hedgehog signaling. *Dev Cell,* **19**, 270-83.

Bessis, M. & Breton-Gorius, J. (1958). [On an pericentral inframicroscopic structure; electron microscopy of mammalian leukocytes]. *C R Hebd Seances Acad Sci,* **246**, 1289-91.

Bettencourt-Dias, M., Rodrigues-Martins, A., Carpenter, L., Riparbelli, M., Lehmann, L., Gatt, M. K., Carmo, N., Balloux, F., Callaini, G. & Glover, D. M. (2005). SAK/PLK4 is required for centriole duplication and flagella development. *Curr Biol,* **15**, 2199-207.

Bielska, E., Schuster, M., Roger, Y., Berepiki, A., Soanes, D. M., Talbot, N. J. & Steinberg, G. (2014). Hook is an adapter that coordinates kinesin-3 and dynein cargo attachment on early endosomes. *J Cell Biol,* **204**, 989-1007.

Bjourson, A. J. & Cooper, J. E. (1992). Band-stab PCR: a simple technique for the purification of individual PCR products. *Nucleic Acids Res,* **20**, 4675.

Blagden, S. P. & Glover, D. M. (2003). Polar expeditions--provisioning the centrosome for mitosis. *Nat Cell Biol,* **5**, 505-11.

Bobinnec, Y., Khodjakov, A., Mir, L. M., Rieder, C. L., Edde, B. & Bornens, M. (1998). Centriole disassembly in vivo and its effect on centrosome structure and function in vertebrate cells. *J Cell Biol,* **143**, 1575-89.

Bonavita, R., Walas, D., Brown, A. K., Luini, A., Stephens, D. J. & Colanzi, A. (2014). Cep126 is required for pericentriolar satellite localisation to the centrosome and for primary cilium formation. *Biol Cell,* **106**, 254-67.

Bornens, M. (2002). Centrosome composition and microtubule anchoring mechanisms. *Curr Opin Cell Biol,* **14**, 25-34.

Bornens, M. & Gonczy, P. (2014). Centrosomes back in the limelight. *Philos Trans R Soc Lond B Biol Sci,* **369**.

Boveri, T. (1887). *Ueber den Antheil des Spermatozoon an der Teilung des Eies.*: Sitzungsber. Ges. Morph. Physiol. München.

Boveri, T. (1900). *Zellen-Studien: Über die Natur der Centrosomen.* G. Fischer.

Brazelton, W. J., Amundsen, C. D., Silflow, C. D. & Lefebvre, P. A. (2001). The bld1 mutation identifies the Chlamydomonas osm-6 homolog as a gene required for flagellar assembly. *Curr Biol,* **11**, 1591-4.

Brohmann, H., Pinnecke, S. & Hoyer-Fender, S. (1997). Identification and characterization of new cDNAs encoding outer dense fiber proteins of rat sperm. *J Biol Chem,* **272**, 10327-32.

Brown, N. J., Marjanovic, M., Luders, J., Stracker, T. H. & Costanzo, V. (2013). Cep63 and cep152 cooperate to ensure centriole duplication. *PLoS One,* **8**, e69986.

Brownhill, K., Wood, L. & Allan, V. (2009). Molecular motors and the Golgi complex: staying put and moving through. *Semin Cell Dev Biol,* **20**, 784-92.

Bruno, I. G., Jin, W. & Cote, G. J. (2004). Correction of aberrant FGFR1 alternative RNA splicing through targeting of intronic regulatory elements. *Hum Mol Genet,* **13**, 2409-20.

Bujakowska, K. M., Liu, Q. & Pierce, E. A. (2017). Photoreceptor Cilia and Retinal Ciliopathies. *Cold Spring Harb Perspect Biol,* **9**.

Burkhard, P., Stetefeld, J. & Strelkov, S. V. (2001). Coiled coils: a highly versatile protein folding motif. *Trends Cell Biol,* **11**, 82-8.

Candiano, G., Bruschi, M., Musante, L., Santucci, L., Ghiggeri, G. M., Carnemolla, B., Orecchia, P., Zardi, L. & Righetti, P. G. (2004). Blue silver: a very sensitive colloidal Coomassie G-250 staining for proteome analysis. *Electrophoresis,* **25**, 1327-33.

Cao, J., Shen, Y., Zhu, L., Xu, Y., Zhou, Y., Wu, Z., Li, Y., Yan, X. & Zhu, X. (2012). miR-129-3p controls cilia assembly by regulating CP110 and actin dynamics. *Nat Cell Biol,* **14**, 697-706.

Cao, J. M., Cheng, X. N., Li, S. Q., Heller, S., Xu, Z. G. & Shi, D. L. (2016). Identification of novel MYO18A interaction partners required for myoblast adhesion and muscle integrity. *Sci Rep,* **6**, 36768.

Cartegni, L., Wang, J., Zhu, Z., Zhang, M. Q. & Krainer, A. R. (2003). ESEfinder: A web resource to identify exonic splicing enhancers. *Nucleic Acids Res,* **31**, 3568-71.

Chabin-Brion, K., Marceiller, J., Perez, F., Settegrana, C., Drechou, A., Durand, G. & Pous, C. (2001). The Golgi complex is a microtubule-organizing organelle. *Mol Biol Cell,* **12**, 2047-60.

Chamling, X., Seo, S., Searby, C. C., Kim, G., Slusarski, D. C. & Sheffield, V. C. (2014). The centriolar satellite protein AZI1 interacts with BBS4 and regulates ciliary trafficking of the BBSome. *PLoS Genet,* **10**, e1004083.

Chang, B., Khanna, H., Hawes, N., Jimeno, D., He, S., Lillo, C., Parapuram, S. K., Cheng, H., Scott, A., Hurd, R. E., Sayer, J. A., Otto, E. A., Attanasio, M., O'Toole, J. F., Jin, G., Shou, C., Hildebrandt, F., Williams, D. S., Heckenlively, J. R. & Swaroop, A. (2006). In-frame deletion in a novel centrosomal/ciliary protein CEP290/NPHP6 perturbs its interaction with RPGR and results in early-onset retinal degeneration in the rd16 mouse. *Hum Mol Genet,* **15**, 1847-57.

Chang, J., Seo, S. G., Lee, K. H., Nagashima, K., Bang, J. K., Kim, B. Y., Erikson, R. L., Lee, K. W., Lee, H. J., Park, J. E. & Lee, K. S. (2013a). Essential role of Cenexin1, but not Odf2, in ciliogenesis. *Cell Cycle,* **12**, 655-62.

Chang, N., Sun, C., Gao, L., Zhu, D., Xu, X., Zhu, X., Xiong, J. W. & Xi, J. J. (2013b). Genome editing with RNA-guided Cas9 nuclease in zebrafish embryos. *Cell Res,* **23**, 465-72.

Chen, J. V. & Megraw, T. L. (2013). Cenexin1 and Odf2: splice variants with diverged cilium functions. *Cell Cycle,* **12**, 869.

Chen, Y., Wu, B., Xu, L., Li, H., Xia, J., Yin, W., Li, Z., Shi, D., Li, S., Lin, S., Shu, X. & Pei, D. (2012). A SNX10/V-ATPase pathway regulates ciliogenesis in vitro and in vivo. *Cell Res,* **22**, 333-45.

Chen, Z., Indjeian, V. B., McManus, M., Wang, L. & Dynlacht, B. D. (2002). CP110, a cell cycle-dependent CDK substrate, regulates centrosome duplication in human cells. *Dev Cell,* **3**, 339-50.

Cheng, T. S., Chang, L. K., Howng, S. L., Lu, P. J., Lee, C. I. & Hong, Y. R. (2006). SUMO-1 modification of centrosomal protein hNinein promotes hNinein nuclear localization. *Life Sci,* **78**, 1114-20.

Chhabra, D. & dos Remedios, C. G. (2005). Cofilin, actin and their complex observed in vivo using fluorescence resonance energy transfer. *Biophys J,* **89**, 1902-8.

Chhabra, E. S. & Higgs, H. N. (2007). The many faces of actin: matching assembly factors with cellular structures. *Nat Cell Biol,* **9**, 1110-21.

Chih, B., Liu, P., Chinn, Y., Chalouni, C., Komuves, L. G., Hass, P. E., Sandoval, W. & Peterson, A. S. (2012). A ciliopathy complex at the transition zone protects the cilia as a privileged membrane domain. *Nat Cell Biol,* **14**, 61-72.

Choksi, S. P., Babu, D., Lau, D., Yu, X. & Roy, S. (2014). Systematic discovery of novel ciliary genes through functional genomics in the zebrafish. *Development,* **141**, 3410-9.

Chomczynski, P. & Sacchi, N. (1987). Single-step method of RNA isolation by acid guanidinium thiocyanate-phenol-chloroform extraction. *Anal Biochem,* **162**, 156-9.

Chomczynski, P. & Sacchi, N. (2006). The single-step method of RNA isolation by acid guanidinium thiocyanate-phenol-chloroform extraction: twenty-something years on. *Nat Protoc,* **1**, 581-5.

Cole, N. B., Sciaky, N., Marotta, A., Song, J. & Lippincott-Schwartz, J. (1996). Golgi dispersal during microtubule disruption: regeneration of Golgi stacks at peripheral endoplasmic reticulum exit sites. *Mol Biol Cell,* **7**, 631-50.

Coletta, A., Pinney, J. W., Solis, D. Y., Marsh, J., Pettifer, S. R. & Attwood, T. K. (2010). Low-complexity regions within protein sequences have position-dependent roles. *BMC Syst Biol,* **4**, 43.

Cory, G. (2011). Scratch-wound assay. *Methods Mol Biol,* **769**, 25-30.

Craige, B., Tsao, C. C., Diener, D. R., Hou, Y., Lechtreck, K. F., Rosenbaum, J. L. & Witman, G. B. (2010). CEP290 tethers flagellar transition zone microtubules to the membrane and regulates flagellar protein content. *J Cell Biol,* **190**, 927-40.

Czarnecki, P. G. & Shah, J. V. (2012). The ciliary transition zone: from morphology and molecules to medicine. *Trends Cell Biol,* **22**, 201-10.

Dadke, S., Cotteret, S., Yip, S. C., Jaffer, Z. M., Haj, F., Ivanov, A., Rauscher, F., 3rd, Shuai, K., Ng, T., Neel, B. G. & Chernoff, J. (2007). Regulation of protein tyrosine phosphatase 1B by sumoylation. *Nat Cell Biol,* **9**, 80-5.

Dammermann, A., Maddox, P. S., Desai, A. & Oegema, K. (2008). SAS-4 is recruited to a dynamic structure in newly forming centrioles that is stabilized by the gamma-tubulin-mediated addition of centriolar microtubules. *J Cell Biol,* **180**, 771-85.

Dammermann, A. & Merdes, A. (2002). Assembly of centrosomal proteins and microtubule organization depends on PCM-1. *J Cell Biol,* **159**, 255-66.

Das, A. & Guo, W. (2011). Rabs and the exocyst in ciliogenesis, tubulogenesis and beyond. *Trends Cell Biol,* **21**, 383-6.

Dawe, H. R., Adams, M., Wheway, G., Szymanska, K., Logan, C. V., Noegel, A. A., Gull, K. & Johnson, C. A. (2009). Nesprin-2 interacts with meckelin and mediates ciliogenesis via remodelling of the actin cytoskeleton. *J Cell Sci,* **122**, 2716-26.

Dawe, H. R., Farr, H. & Gull, K. (2007a). Centriole/basal body morphogenesis and migration during ciliogenesis in animal cells. *J Cell Sci,* **120**, 7-15.

Dawe, H. R., Smith, U. M., Cullinane, A. R., Gerrelli, D., Cox, P., Badano, J. L., Blair-Reid, S., Sriram, N., Katsanis, N., Attie-Bitach, T., Afford, S. C., Copp, A. J., Kelly, D. A., Gull, K. & Johnson, C. A. (2007b). The Meckel-Gruber Syndrome proteins MKS1 and meckelin interact and are required for primary cilium formation. *Hum Mol Genet,* **16**, 173-86.

de Saram, P., Iqbal, A., Murdoch, J. N. & Wilkinson, C. J. (2017). BCAP is a centriolar satellite protein and inhibitor of ciliogenesis. *J Cell Sci,* **130**, 3360-3373.

Deane, J. A., Cole, D. G., Seeley, E. S., Diener, D. R. & Rosenbaum, J. L. (2001). Localization of intraflagellar transport protein IFT52 identifies basal body transitional fibers as the docking site for IFT particles. *Curr Biol,* **11**, 1586-90.

Delattre, M., Leidel, S., Wani, K., Baumer, K., Bamat, J., Schnabel, H., Feichtinger, R., Schnabel, R. & Gonczy, P. (2004). Centriolar SAS-5 is required for centrosome duplication in C. elegans. *Nat Cell Biol,* **6**, 656-64.

Dippell, R. V. (1968). The development of basal bodies in paramecium. *Proc Natl Acad Sci U S A,* **61**, 461-8.

Dippold, H. C., Ng, M. M., Farber-Katz, S. E., Lee, S. K., Kerr, M. L., Peterman, M. C., Sim, R., Wiharto, P. A., Galbraith, K. A., Madhavarapu, S., Fuchs, G. J., Meerloo, T., Farquhar, M. G., Zhou, H. & Field, S. J. (2009). GOLPH3 bridges phosphatidylinositol-4- phosphate and actomyosin to stretch and shape the Golgi to promote budding. *Cell,* **139**, 337-51.

Dishinger, J. F., Kee, H. L., Jenkins, P. M., Fan, S., Hurd, T. W., Hammond, J. W., Truong, Y. N., Margolis, B., Martens, J. R. & Verhey, K. J. (2010). Ciliary entry of the kinesin-2 motor KIF17 is regulated by importin-beta2 and RanGTP. *Nat Cell Biol,* **12**, 703-10.

Dixit, R. & Cyr, R. (2003). Cell damage and reactive oxygen species production induced by fluorescence microscopy: effect on mitosis and guidelines for non-invasive fluorescence microscopy. *Plant J,* **36**, 280-90.

Dixon-Salazar, T., Silhavy, J. L., Marsh, S. E., Louie, C. M., Scott, L. C., Gururaj, A., Al-Gazali, L., Al-Tawari, A. A., Kayserili, H., Sztriha, L. & Gleeson, J. G. (2004). Mutations in the AHI1 gene, encoding jouberin, cause Joubert syndrome with cortical polymicrogyria. *Am J Hum Genet,* **75**, 979-87.

Domon, B. & Aebersold, R. (2006). Mass spectrometry and protein analysis. *Science,* **312**, 212-7.

Dong, G. (2015). Building a ninefold symmetrical barrel: structural dissections of centriole assembly. *Open Biol,* **5**.

Doolin, P. F. & Birge, W. J. (1966). Ultrastructural organization of cilia and basal bodies of the epithelium of the choroid plexus in the chick embryo. *J Cell Biol,* **29**, 333-45.

Doxsey, S. J., Stein, P., Evans, L., Calarco, P. D. & Kirschner, M. (1994). Pericentrin, a highly conserved centrosome protein involved in microtubule organization. *Cell,* **76**, 639-50.

Draper, B. W., Morcos, P. A. & Kimmel, C. B. (2001). Inhibition of zebrafish fgf8 pre-mRNA splicing with morpholino oligos: a quantifiable method for gene knockdown. *Genesis,* **30**, 154-6.

Duan, D. (2011). *Muscle gene therapy : methods and protocols.* New York, NY: Humana.

Duldulao, N. A., Li, J. & Sun, Z. (2010). Cilia in cell signaling and human disorders. *Protein Cell,* **1**, 726-36.

Dutcher, S. K. (1995). Flagellar assembly in two hundred and fifty easy-to-follow steps. *Trends Genet,* **11**, 398-404.

Eisen, J. S. & Smith, J. C. (2008). Controlling morpholino experiments: don't stop making antisense. *Development,* **135**, 1735-43.

Ekker, S. C. (2000). Morphants: a new systematic vertebrate functional genomics approach. *Yeast,* **17**, 302-306.

Ekman, D., Light, S., Bjorklund, A. K. & Elofsson, A. (2006). What properties characterize the hub proteins of the protein-protein interaction network of Saccharomyces cerevisiae? *Genome Biol,* **7**, R45.

Elbashir, S. M., Harborth, J., Lendeckel, W., Yalcin, A., Weber, K. & Tuschl, T. (2001). Duplexes of 21-nucleotide RNAs mediate RNA interference in cultured mammalian cells. *Nature,* **411**, 494-8.

Engel, B. D., Ludington, W. B. & Marshall, W. F. (2009). Intraflagellar transport particle size scales inversely with flagellar length: revisiting the balance-point length control model. *J Cell Biol,* **187**, 81-9.

Engelender, S., Sharp, A. H., Colomer, V., Tokito, M. K., Lanahan, A., Worley, P., Holzbaur, E. L. & Ross, C. A. (1997). Huntingtin-associated protein 1 (HAP1) interacts with the p150Glued subunit of dynactin. *Hum Mol Genet,* **6**, 2205-12.

Failler, M., Gee, H. Y., Krug, P., Joo, K., Halbritter, J., Belkacem, L., Filhol, E., Porath, J. D., Braun, D. A., Schueler, M., Frigo, A., Alibeu, O., Masson, C., Brochard, K., Hurault de Ligny, B., Novo, R., Pietrement, C., Kayserili, H., Salomon, R., Gubler, M. C., Otto, E. A., Antignac, C., Kim, J., Benmerah, A., Hildebrandt, F. & Saunier, S. (2014). Mutations of CEP83 cause infantile nephronophthisis and intellectual disability. *Am J Hum Genet,* **94**, 905-14.

Farah, C. S. & Reinach, F. C. (1999). Regulatory properties of recombinant tropomyosins containing 5-hydroxytryptophan: Ca2+-binding to troponin results in a conformational change in a region of tropomyosin outside the troponin binding site. *Biochemistry,* **38**, 10543-51.

Ferrante, M. I., Zullo, A., Barra, A., Bimonte, S., Messaddeq, N., Studer, M., Dolle, P. & Franco, B. (2006). Oral-facial-digital type I protein is required for primary cilia formation and left-right axis specification. *Nat Genet,* **38**, 112-7.

Firat-Karalar, E. N., Rauniyar, N., Yates, J. R., 3rd & Stearns, T. (2014). Proximity interactions among centrosome components identify regulators of centriole duplication. *Curr Biol,* **24**, 664-70.

Fisch, C. & Dupuis-Williams, P. (2011). Ultrastructure of cilia and flagella - back to the future! *Biol Cell,* **103**, 249-70.

Flemming, W. (1875). *Studien in der Entwicklungsgeschichte der Najaden.* Wien : K. K. Staatsdruckerei: 71: 81–147.

Flemming, W. (1891). Verhandlungen der anatomischen Gesellschaft, Jahrg. 6, München (found as item 60 vol II in Collected Papers of Walther Flemming in M.B.L. Library, reprint collection). *Anatomische Gesellschaft.* .

Follit, J. A., San Agustin, J. T., Xu, F., Jonassen, J. A., Samtani, R., Lo, C. W. & Pazour, G. J. (2008). The Golgin GMAP210/TRIP11 anchors IFT20 to the Golgi complex. *PLoS Genet,* **4**, e1000315.

Follit, J. A., Tuft, R. A., Fogarty, K. E. & Pazour, G. J. (2006). The intraflagellar transport protein IFT20 is associated with the Golgi complex and is required for cilia assembly. *Mol Biol Cell,* **17**, 3781-92.

Forsythe, E. & Beales, P. L. (2013). Bardet-Biedl syndrome. *Eur J Hum Genet,* **21**, 8-13.

Gadde, S. & Heald, R. (2004). Mechanisms and molecules of the mitotic spindle. *Curr Biol,* **14**, R797-805.

Gaits, F. & Hahn, K. (2003). Shedding light on cell signaling: interpretation of FRET biosensors. *Sci STKE,* **2003**, PE3.

Garcia-Gonzalo, F. R., Corbit, K. C., Sirerol-Piquer, M. S., Ramaswami, G., Otto, E. A., Noriega, T. R., Seol, A. D., Robinson, J. F., Bennett, C. L., Josifova, D. J., Garcia-Verdugo, J. M., Katsanis, N., Hildebrandt, F. & Reiter, J. F. (2011). A transition zone complex regulates mammalian ciliogenesis and ciliary membrane composition. *Nat Genet,* **43**, 776-84.

Garcia-Gonzalo, F. R. & Reiter, J. F. (2012). Scoring a backstage pass: mechanisms of ciliogenesis and ciliary access. *J Cell Biol,* **197**, 697-709.

Gard, D. L. & Kirschner, M. W. (1987). A microtubule-associated protein from Xenopus eggs that specifically promotes assembly at the plus-end. *J Cell Biol,* **105**, 2203-15.

Ge, X., Frank, C. L., Calderon de Anda, F. & Tsai, L. H. (2010). Hook3 interacts with PCM1 to regulate pericentriolar material assembly and the timing of neurogenesis. *Neuron,* **65**, 191-203.

Geimer, S. & Melkonian, M. (2004). The ultrastructure of the Chlamydomonas reinhardtii basal apparatus: identification of an early marker of radial asymmetry inherent in the basal body. *J Cell Sci,* **117**, 2663-74.

Geimer, S. & Melkonian, M. (2005). Centrin scaffold in Chlamydomonas reinhardtii revealed by immunoelectron microscopy. *Eukaryot Cell,* **4**, 1253-63.

Gherman, A., Davis, E. E. & Katsanis, N. (2006). The ciliary proteome database: an integrated community resource for the genetic and functional dissection of cilia. *Nat Genet,* **38**, 961-2.

Gillingham, A. K. & Munro, S. (2003). Long coiled-coil proteins and membrane traffic. *Biochim Biophys Acta,* **1641**, 71-85.

Gilula, N. B. & Satir, P. (1972). The ciliary necklace. A ciliary membrane specialization. *J Cell Biol,* **53**, 494-509.

Glover, D. M., Leibowitz, M. H., McLean, D. A. & Parry, H. (1995). Mutations in aurora prevent centrosome separation leading to the formation of monopolar spindles. *Cell,* **81**, 95-105.

Goetz, S. C. & Anderson, K. V. (2010). The primary cilium: a signalling centre during vertebrate development. *Nat Rev Genet,* **11**, 331-44.

Goetz, S. C., Liem, K. F., Jr. & Anderson, K. V. (2012). The spinocerebellar ataxia-associated gene Tau tubulin kinase 2 controls the initiation of ciliogenesis. *Cell,* **151**, 847-58.

Goley, E. D. & Welch, M. D. (2006). The ARP2/3 complex: an actin nucleator comes of age. *Nat Rev Mol Cell Biol,* **7**, 713-26.

Gomez-Ferreria, M. A., Rath, U., Buster, D. W., Chanda, S. K., Caldwell, J. S., Rines, D. R. & Sharp, D. J. (2007). Human Cep192 is required for mitotic centrosome and spindle assembly. *Curr Biol,* **17**, 1960-6.

Gould, R. R. & Borisy, G. G. (1977). The pericentriolar material in Chinese hamster ovary cells nucleates microtubule formation. *J Cell Biol,* **73**, 601-15.

Graser, S., Stierhof, Y. D., Lavoie, S. B., Gassner, O. S., Lamla, S., Le Clech, M. & Nigg, E. A. (2007). Cep164, a novel centriole appendage protein required for primary cilium formation. *J Cell Biol,* **179**, 321-30.

Grisendi, S., Bernardi, R., Rossi, M., Cheng, K., Khandker, L., Manova, K. & Pandolfi, P. P. (2005). Role of nucleophosmin in embryonic development and tumorigenesis. *Nature,* **437**, 147-53.

Guichard, P., Chretien, D., Marco, S. & Tassin, A. M. (2010). Procentriole assembly revealed by cryo-electron tomography. *EMBO J,* **29**, 1565-72.

Gunawardane, R. N., Lizarraga, S. B., Wiese, C., Wilde, A. & Zheng, Y. (2000). gamma-Tubulin complexes and their role in microtubule nucleation. *Curr Top Dev Biol,* **49**, 55-73.

Gupta, G. D., Coyaud, E., Goncalves, J., Mojarad, B. A., Liu, Y., Wu, Q., Gheiratmand, L., Comartin, D., Tkach, J. M., Cheung, S. W., Bashkurov, M., Hasegan, M., Knight, J. D., Lin, Z. Y., Schueler, M., Hildebrandt, F., Moffat, J., Gingras, A. C., Raught, B. & Pelletier, L. (2015). A Dynamic Protein Interaction Landscape of the Human Centrosome-Cilium Interface. *Cell,* **163**, 1484-99.

Habedanck, R., Stierhof, Y. D., Wilkinson, C. J. & Nigg, E. A. (2005). The Polo kinase Plk4 functions in centriole duplication. *Nat Cell Biol,* **7**, 1140-6.

Hames, R. S., Crookes, R. E., Straatman, K. R., Merdes, A., Hayes, M. J., Faragher, A. J. & Fry, A. M. (2005). Dynamic recruitment of Nek2 kinase to the centrosome involves microtubules, PCM-1, and localized proteasomal degradation. *Mol Biol Cell,* **16**, 1711-24.

Hannich, J. T., Lewis, A., Kroetz, M. B., Li, S. J., Heide, H., Emili, A. & Hochstrasser, M. (2005). Defining the SUMO-modified proteome by multiple approaches in Saccharomyces cerevisiae. *J Biol Chem,* **280**, 4102-10.

Hay, R. T. (2005). SUMO: a history of modification. *Mol Cell,* **18**, 1-12.

He, Q., Wang, G., Wakade, S., Dasgupta, S., Dinkins, M., Kong, J. N., Spassieva, S. D. & Bieberich, E. (2014). Primary cilia in stem cells and neural progenitors are regulated by neutral sphingomyelinase 2 and ceramide. *Mol Biol Cell,* **25**, 1715-29.

Heasman, J. (2002). Morpholino oligos: making sense of antisense? *Dev Biol,* **243**, 209-14.

Helou, J., Otto, E. A., Attanasio, M., Allen, S. J., Parisi, M. A., Glass, I., Utsch, B., Hashmi, S., Fazzi, E., Omran, H., O'Toole, J. F., Sayer, J. A. & Hildebrandt, F. (2007). Mutation analysis of NPHP6/CEP290 in patients with Joubert syndrome and Senior-Loken syndrome. *J Med Genet,* **44**, 657-63.

Hilton, L. K., Gunawardane, K., Kim, J. W., Schwarz, M. C. & Quarmby, L. M. (2013). The kinases LF4 and CNK2 control ciliary length by feedback regulation of assembly and disassembly rates. *Curr Biol,* **23**, 2208-14.

Hodges, M. E., Scheumann, N., Wickstead, B., Langdale, J. A. & Gull, K. (2010). Reconstructing the evolutionary history of the centriole from protein components. *J Cell Sci,* **123**, 1407-13.

Hori, A., Ikebe, C., Tada, M. & Toda, T. (2014). Msd1/SSX2IP-dependent microtubule anchorage ensures spindle orientation and primary cilia formation. *EMBO Rep,* **15**, 175-84.

Hou, Y., Qin, H., Follit, J. A., Pazour, G. J., Rosenbaum, J. L. & Witman, G. B. (2007). Functional analysis of an individual IFT protein: IFT46 is required for transport of outer dynein arms into flagella. *J Cell Biol,* **176**, 653-65.

Howard, M. T., Gesteland, R. F. & Atkins, J. F. (2004). Efficient stimulation of site-specific ribosome frameshifting by antisense oligonucleotides. *RNA,* **10**, 1653-61.

Howe, K., Clark, M. D., Torroja, C. F., Torrance, J., Berthelot, C., Muffato, M., Collins, J. E., Humphray, S., McLaren, K., Matthews, L., McLaren, S., Sealy, I., Caccamo, M., Churcher, C., Scott, C., Barrett, J. C., Koch, R., Rauch, G. J., White, S., Chow, W., Kilian, B., Quintais, L. T., Guerra-Assuncao, J. A., Zhou, Y., Gu, Y., Yen, J., Vogel, J. H., Eyre, T., Redmond, S., Banerjee, R., Chi, J., Fu, B., Langley, E., Maguire, S. F., Laird, G. K., Lloyd, D., Kenyon, E., Donaldson, S., Sehra, H., Almeida-King, J., Loveland, J., Trevanion, S., Jones, M., Quail, M., Willey, D., Hunt, A., Burton, J., Sims, S., McLay, K., Plumb, B., Davis, J., Clee, C., Oliver, K., Clark, R., Riddle, C., Elliot, D., Threadgold, G., Harden, G., Ware, D., Begum, S., Mortimore, B., Kerry, G., Heath, P., Phillimore, B., Tracey, A., Corby, N., Dunn, M., Johnson, C., Wood, J., Clark, S., Pelan, S., Griffiths, G., Smith, M., Glithero, R., Howden, P., Barker, N., Lloyd, C., Stevens, C., Harley, J., Holt, K., Panagiotidis, G., Lovell, J., Beasley, H., Henderson, C., Gordon, D., Auger, K., Wright, D., Collins, J., Raisen, C., Dyer, L., Leung, K., Robertson, L., Ambridge, K., Leongamornlert, D., McGuire, S., Gilderthorp, R., Griffiths, C., Manthravadi, D., Nichol, S., Barker, G., et al. (2013). The zebrafish reference genome sequence and its relationship to the human genome. *Nature,* **496**, 498-503.

Hoyer-Fender, S., Petersen, C., Brohmann, H., Rhee, K. & Wolgemuth, D. J. (1998). Mouse Odf2 cDNAs consist of evolutionary conserved as well as highly variable sequences and encode outer dense fiber proteins of the sperm tail. *Mol Reprod Dev,* **51**, 167-75.

Hu, Q., Milenkovic, L., Jin, H., Scott, M. P., Nachury, M. V., Spiliotis, E. T. & Nelson, W. J. (2010). A septin diffusion barrier at the base of the primary cilium maintains ciliary membrane protein distribution. *Science,* **329**, 436-9.

Huang, L., Szymanska, K., Jensen, V. L., Janecke, A. R., Innes, A. M., Davis, E. E., Frosk, P., Li, C., Willer, J. R., Chodirker, B. N., Greenberg, C. R., McLeod, D. R., Bernier, F. P., Chudley, A. E., Muller, T., Shboul, M., Logan, C. V., Loucks, C. M., Beaulieu, C. L., Bowie, R. V., Bell, S. M., Adkins, J., Zuniga, F. I., Ross, K. D., Wang, J., Ban, M. R., Becker, C., Nurnberg, P., Douglas, S., Craft, C. M., Akimenko, M. A., Hegele, R. A., Ober, C., Utermann, G., Bolz, H. J., Bulman, D. E., Katsanis, N., Blacque, O. E., Doherty, D., Parboosingh, J. S., Leroux, M. R., Johnson, C. A. & Boycott, K. M. (2011). TMEM237 is mutated in individuals with a Joubert syndrome related disorder and expands the role of the TMEM family at the ciliary transition zone. *Am J Hum Genet,* **89**, 713-30.

Huang, L., Xiao, A., Wecker, A., McBride, D. A., Choi, S. Y., Zhou, W. & Lipschutz, J. H. (2014). A possible zebrafish model of polycystic kidney disease: knockdown of wnt5a causes cysts in zebrafish kidneys. *J Vis Exp*.

Huber, D. & Hoyer-Fender, S. (2007). Alternative splicing of exon 3b gives rise to ODF2 and Cenexin. *Cytogenet Genome Res,* **119**, 68-73.

Hurd, T. W., Fan, S. & Margolis, B. L. (2011). Localization of retinitis pigmentosa 2 to cilia is regulated by Importin beta2. *J Cell Sci,* **124**, 718-26.

Hutagalung, A. H. & Novick, P. J. (2011). Role of Rab GTPases in membrane traffic and cell physiology. *Physiol Rev,* **91**, 119-49.

Ibi, M., Zou, P., Inoko, A., Shiromizu, T., Matsuyama, M., Hayashi, Y., Enomoto, M., Mori, D., Hirotsune, S., Kiyono, T., Tsukita, S., Goto, H. & Inagaki, M. (2011). Trichoplein controls microtubule anchoring at the centrosome by binding to Odf2 and ninein. *J Cell Sci,* **124**, 857-64.

Insolera, R., Shao, W., Airik, R., Hildebrandt, F. & Shi, S. H. (2014). SDCCAG8 regulates pericentriolar material recruitment and neuronal migration in the developing cortex. *Neuron,* **83**, 805-22.

Iomini, C., Li, L., Esparza, J. M. & Dutcher, S. K. (2009). Retrograde intraflagellar transport mutants identify complex A proteins with multiple genetic interactions in Chlamydomonas reinhardtii. *Genetics,* **183**, 885-96.

Ishikawa, H., Kubo, A., Tsukita, S. & Tsukita, S. (2005). Odf2-deficient mother centrioles lack distal/subdistal appendages and the ability to generate primary cilia. *Nat Cell Biol,* **7**, 517-24.

Jakobsen, L., Vanselow, K., Skogs, M., Toyoda, Y., Lundberg, E., Poser, I., Falkenby, L. G., Bennetzen, M., Westendorf, J., Nigg, E. A., Uhlen, M., Hyman, A. A. & Andersen, J. S. (2011). Novel asymmetrically localizing components of human centrosomes identified by complementary proteomics methods. *EMBO J,* **30**, 1520-35.

Jana, S. C., Marteil, G. & Bettencourt-Dias, M. (2014). Mapping molecules to structure: unveiling secrets of centriole and cilia assembly with near-atomic resolution. *Curr Opin Cell Biol,* **26**, 96-106.

Janke, C. & Bulinski, J. C. (2011). Post-translational regulation of the microtubule cytoskeleton: mechanisms and functions. *Nat Rev Mol Cell Biol,* **12**, 773-86.

Jares-Erijman, E. A. & Jovin, T. M. (2006). Imaging molecular interactions in living cells by FRET microscopy. *Curr Opin Chem Biol,* **10**, 409-16.

Jiang, K., Toedt, G., Montenegro Gouveia, S., Davey, N. E., Hua, S., van der Vaart, B., Grigoriev, I., Larsen, J., Pedersen, L. B., Bezstarosti, K., Lince-Faria, M., Demmers, J., Steinmetz, M. O., Gibson, T. J. & Akhmanova, A. (2012). A Proteome-wide screen for mammalian SxIP motif-containing microtubule plus-end tracking proteins. *Curr Biol,* **22**, 1800-7.

Jin, H. & Nachury, M. V. (2009). The BBSome. *Curr Biol,* **19**, R472-3.

Jin, H., White, S. R., Shida, T., Schulz, S., Aguiar, M., Gygi, S. P., Bazan, J. F. & Nachury, M. V. (2010). The conserved Bardet-Biedl syndrome proteins assemble a coat that traffics membrane proteins to cilia. *Cell,* **141**, 1208-19.

Joo, K., Kim, C. G., Lee, M. S., Moon, H. Y., Lee, S. H., Kim, M. J., Kweon, H. S., Park, W. Y., Kim, C. H., Gleeson, J. G. & Kim, J. (2013). CCDC41 is required for ciliary vesicle docking to the mother centriole. *Proc Natl Acad Sci U S A,* **110**, 5987-92.

Kallberg, M., Wang, H., Wang, S., Peng, J., Wang, Z., Lu, H. & Xu, J. (2012). Template-based protein structure modeling using the RaptorX web server. *Nat Protoc,* **7**, 1511-22.

Kaminsky, R., Denison, C., Bening-Abu-Shach, U., Chisholm, A. D., Gygi, S. P. & Broday, L. (2009). SUMO regulates the assembly and function of a cytoplasmic intermediate filament protein in C. elegans. *Dev Cell,* **17**, 724-35.

Kamiya, A., Tan, P. L., Kubo, K., Engelhard, C., Ishizuka, K., Kubo, A., Tsukita, S., Pulver, A. E., Nakajima, K., Cascella, N. G., Katsanis, N. & Sawa, A. (2008). Recruitment of PCM1 to the centrosome by the cooperative action of DISC1 and BBS4: a candidate for psychiatric illnesses. *Arch Gen Psychiatry,* **65**, 996-1006.

Kang, R., Zeh, H. J., Lotze, M. T. & Tang, D. (2011). The Beclin 1 network regulates autophagy and apoptosis. *Cell Death Differ,* **18**, 571-80.

Kee, H. L., Dishinger, J. F., Blasius, T. L., Liu, C. J., Margolis, B. & Verhey, K. J. (2012). A size-exclusion permeability barrier and nucleoporins characterize a ciliary pore complex that regulates transport into cilia. *Nat Cell Biol,* **14**, 431-7.

Kee, Y., Yoo, J. S., Hazuka, C. D., Peterson, K. E., Hsu, S. C. & Scheller, R. H. (1997). Subunit structure of the mammalian exocyst complex. *Proc Natl Acad Sci U S A,* **94**, 14438-43.

Keller, L. C., Geimer, S., Romijn, E., Yates, J., 3rd, Zamora, I. & Marshall, W. F. (2009). Molecular architecture of the centriole proteome: the conserved WD40 domain protein POC1 is required for centriole duplication and length control. *Mol Biol Cell,* **20**, 1150-66.

Keryer, G., Pineda, J. R., Liot, G., Kim, J., Dietrich, P., Benstaali, C., Smith, K., Cordelieres, F. P., Spassky, N., Ferrante, R. J., Dragatsis, I. & Saudou, F. (2011). Ciliogenesis is regulated by a huntingtin-HAP1-PCM1 pathway and is altered in Huntington disease. *J Clin Invest,* **121**, 4372-82.

Kim, J., Krishnaswami, S. R. & Gleeson, J. G. (2008). CEP290 interacts with the centriolar satellite component PCM-1 and is required for Rab8 localization to the primary cilium. *Hum Mol Genet,* **17**, 3796-805.

Kim, J., Lee, J. E., Heynen-Genel, S., Suyama, E., Ono, K., Lee, K., Ideker, T., Aza-Blanc, P. & Gleeson, J. G. (2010). Functional genomic screen for modulators of ciliogenesis and cilium length. *Nature,* **464**, 1048-51.

Kim, J. C., Badano, J. L., Sibold, S., Esmail, M. A., Hill, J., Hoskins, B. E., Leitch, C. C., Venner, K., Ansley, S. J., Ross, A. J., Leroux, M. R., Katsanis, N. & Beales, P. L. (2004). The Bardet-Biedl protein BBS4 targets cargo to the pericentriolar region and is required for microtubule anchoring and cell cycle progression. *Nat Genet,* **36**, 462-70.

Kim, K., Lee, K. & Rhee, K. (2012). CEP90 is required for the assembly and centrosomal accumulation of centriolar satellites, which is essential for primary cilia formation. *PLoS One,* **7**, e48196.

Kim, K. & Rhee, K. (2011). The pericentriolar satellite protein CEP90 is crucial for integrity of the mitotic spindle pole. *J Cell Sci,* **124**, 338-47.

Kim, S. & Rhee, K. (2014). Importance of the CEP215-pericentrin interaction for centrosome maturation during mitosis. *PLoS One,* **9**, e87016.

Kimmel, C. B., Ballard, W. W., Kimmel, S. R., Ullmann, B. & Schilling, T. F. (1995). Stages of embryonic development of the zebrafish. *Dev Dyn,* **203**, 253-310.

Kinzel, D., Boldt, K., Davis, E. E., Burtscher, I., Trumbach, D., Diplas, B., Attie-Bitach, T., Wurst, W., Katsanis, N., Ueffing, M. & Lickert, H. (2010). Pitchfork regulates primary cilia disassembly and left-right asymmetry. *Dev Cell,* **19**, 66-77.

Klein, U. R. & Nigg, E. A. (2009). SUMO-dependent regulation of centrin-2. *J Cell Sci,* **122**, 3312-21.

Klinger, M., Wang, W., Kuhns, S., Barenz, F., Drager-Meurer, S., Pereira, G. & Gruss, O. J. (2014). The novel centriolar satellite protein SSX2IP targets Cep290 to the ciliary transition zone. *Mol Biol Cell,* **25**, 495-507.

Knodler, A., Feng, S., Zhang, J., Zhang, X., Das, A., Peranen, J. & Guo, W. (2010). Coordination of Rab8 and Rab11 in primary ciliogenesis. *Proc Natl Acad Sci U S A,* **107**, 6346-51.

Kobayashi, T. & Dynlacht, B. D. (2011). Regulating the transition from centriole to basal body. *J Cell Biol,* **193**, 435-44.

Kobayashi, T., Tsang, W. Y., Li, J., Lane, W. & Dynlacht, B. D. (2011). Centriolar kinesin Kif24 interacts with CP110 to remodel microtubules and regulate ciliogenesis. *Cell,* **145**, 914-25.

Kodani, A., Kristensen, I., Huang, L. & Sutterlin, C. (2009). GM130-dependent control of Cdc42 activity at the Golgi regulates centrosome organization. *Mol Biol Cell,* **20**, 1192-200.

Kodani, A. & Sutterlin, C. (2008). The Golgi protein GM130 regulates centrosome morphology and function. *Mol Biol Cell,* **19**, 745-53.

Kodani, A., Tonthat, V., Wu, B. & Sutterlin, C. (2010). Par6 alpha interacts with the dynactin subunit p150 Glued and is a critical regulator of centrosomal protein recruitment. *Mol Biol Cell,* **21**, 3376-85.

Kodani, A., Yu, T. W., Johnson, J. R., Jayaraman, D., Johnson, T. L., Al-Gazali, L., Sztriha, L., Partlow, J. N., Kim, H., Krup, A. L., Dammermann, A., Krogan, N. J., Walsh, C. A. & Reiter, J. F. (2015). Centriolar satellites assemble centrosomal microcephaly proteins to recruit CDK2 and promote centriole duplication. *Elife,* **4**.

Kollman, J. M., Greenberg, C. H., Li, S., Moritz, M., Zelter, A., Fong, K. K., Fernandez, J. J., Sali, A., Kilmartin, J., Davis, T. N. & Agard, D. A. (2015). Ring closure activates yeast gammaTuRC for species-specific microtubule nucleation. *Nat Struct Mol Biol,* **22**, 132-7.

Kollman, J. M., Merdes, A., Mourey, L. & Agard, D. A. (2011). Microtubule nucleation by gamma-tubulin complexes. *Nat Rev Mol Cell Biol,* **12**, 709-21.

Kozminski, K. G., Johnson, K. A., Forscher, P. & Rosenbaum, J. L. (1993). A motility in the eukaryotic flagellum unrelated to flagellar beating. *Proc Natl Acad Sci U S A,* **90**, 5519-23.

Kramer-Zucker, A. G., Olale, F., Haycraft, C. J., Yoder, B. K., Schier, A. F. & Drummond, I. A. (2005). Cilia-driven fluid flow in the zebrafish pronephros, brain and Kupffer's vesicle is required for normal organogenesis. *Development,* **132**, 1907-21.

Kubo, A., Sasaki, H., Yuba-Kubo, A., Tsukita, S. & Shiina, N. (1999). Centriolar satellites: molecular characterization, ATP-dependent movement toward centrioles and possible involvement in ciliogenesis. *J Cell Biol,* **147**, 969-80.

Kubo, A. & Tsukita, S. (2003). Non-membranous granular organelle consisting of PCM-1: subcellular distribution and cell-cycle-dependent assembly/disassembly. *J Cell Sci,* **116**, 919-28.

Kurtulmus, B., Wang, W., Ruppert, T., Neuner, A., Cerikan, B., Viol, L., Duenas-Sanchez, R., Gruss, O. J. & Pereira, G. (2016). WDR8 is a centriolar satellite and centriole-associated protein that promotes ciliary vesicle docking during ciliogenesis. *J Cell Sci,* **129**, 621-36.

Kypri, E., Christodoulou, A., Maimaris, G., Lethan, M., Markaki, M., Lysandrou, C., Lederer, C. W., Tavernarakis, N., Geimer, S., Pedersen, L. B. & Santama, N. (2014). The nucleotide-binding proteins Nubp1 and Nubp2 are negative regulators of ciliogenesis. *Cell Mol Life Sci,* **71**, 517-38.

Lawo, S., Hasegan, M., Gupta, G. D. & Pelletier, L. (2012). Subdiffraction imaging of centrosomes reveals higher-order organizational features of pericentriolar material. *Nat Cell Biol,* **14**, 1148-58.

Lechtreck, K. F. (2015). IFT-Cargo Interactions and Protein Transport in Cilia. *Trends Biochem Sci,* **40**, 765-778.

Lee, J. Y. & Stearns, T. (2013). FOP is a centriolar satellite protein involved in ciliogenesis. *PLoS One,* **8**, e58589.

Leidel, S., Delattre, M., Cerutti, L., Baumer, K. & Gonczy, P. (2005). SAS-6 defines a protein family required for centrosome duplication in C. elegans and in human cells. *Nat Cell Biol,* **7**, 115-25.

Leigh, M. W., Pittman, J. E., Carson, J. L., Ferkol, T. W., Dell, S. D., Davis, S. D., Knowles, M. R. & Zariwala, M. A. (2009). Clinical and genetic aspects of primary ciliary dyskinesia/Kartagener syndrome. *Genet Med,* **11**, 473-87.

Lemullois, M., Boisvieux-Ulrich, E., Laine, M. C., Chailley, B. & Sandoz, D. (1988). Development and functions of the cytoskeleton during ciliogenesis in metazoa. *Biol Cell,* **63**, 195-208.

Letunic, I., Doerks, T. & Bork, P. (2015). SMART: recent updates, new developments and status in 2015. *Nucleic Acids Res,* **43**, D257-60.

Li, Q., Hansen, D., Killilea, A., Joshi, H. C., Palazzo, R. E. & Balczon, R. (2001). Kendrin/pericentrin-B, a centrosome protein with homology to pericentrin that complexes with PCM-1. *J Cell Sci,* **114**, 797-809.

Li, S., Guan, J. L. & Chien, S. (2005). Biochemistry and biomechanics of cell motility. *Annu Rev Biomed Eng,* **7**, 105-50.

Li, Y., Zhang, Q., Wei, Q., Zhang, Y., Ling, K. & Hu, J. (2012). SUMOylation of the small GTPase ARL-13 promotes ciliary targeting of sensory receptors. *J Cell Biol,* **199**, 589-98.

Lim, Y. S. & Tang, B. L. (2013). Getting into the cilia: nature of the barrier(s). *Mol Membr Biol,* **30**, 350-4.

Loncarek, J., Hergert, P., Magidson, V. & Khodjakov, A. (2008). Control of daughter centriole formation by the pericentriolar material. *Nat Cell Biol,* **10**, 322-8.

Lopes, C. A., Prosser, S. L., Romio, L., Hirst, R. A., O'Callaghan, C., Woolf, A. S. & Fry, A. M. (2011). Centriolar satellites are assembly points for proteins implicated in human ciliopathies, including oral-facial-digital syndrome 1. *J Cell Sci,* **124**, 600-12.

Lupas, A., Van Dyke, M. & Stock, J. (1991). Predicting coiled coils from protein sequences. *Science,* **252**, 1162-4.

Magiera, M. M. & Janke, C. (2014). Post-translational modifications of tubulin. *Curr Biol,* **24**, R351-4.

Maldonado-Baez, L., Cole, N. B., Kramer, H. & Donaldson, J. G. (2013). Microtubule-dependent endosomal sorting of clathrin-independent cargo by Hook1. *J Cell Biol,* **201**, 233-47.

Malkani, N. & Schmid, J. A. (2011). Some secrets of fluorescent proteins: distinct bleaching in various mounting fluids and photoactivation of cyan fluorescent proteins at YFP-excitation. *PLoS One,* **6**, e18586.

Marchler-Bauer, A., Anderson, J. B., Chitsaz, F., Derbyshire, M. K., DeWeese-Scott, C., Fong, J. H., Geer, L. Y., Geer, R. C., Gonzales, N. R., Gwadz, M., He, S., Hurwitz, D. I., Jackson, J. D., Ke, Z., Lanczycki, C. J., Liebert, C. A., Liu, C., Lu, F., Lu, S., Marchler, G. H., Mullokandov, M., Song, J. S., Tasneem, A., Thanki, N., Yamashita, R. A., Zhang, D., Zhang, N. & Bryant, S. H. (2009). CDD: specific functional annotation with the Conserved Domain Database. *Nucleic Acids Res,* **37**, D205-10.

Marchler-Bauer, A., Derbyshire, M. K., Gonzales, N. R., Lu, S., Chitsaz, F., Geer, L. Y., Geer, R. C., He, J., Gwadz, M., Hurwitz, D. I., Lanczycki, C. J., Lu, F., Marchler, G. H., Song, J. S., Thanki, N., Wang, Z., Yamashita, R. A., Zhang, D., Zheng, C. & Bryant, S. H. (2015). CDD: NCBI's conserved domain database. *Nucleic Acids Res,* **43**, D222-6.

Marshall, W. F. (2001). Centrioles take center stage. *Curr Biol,* **11**, R487-96.

Marshall, W. F. (2008). Basal bodies platforms for building cilia. *Curr Top Dev Biol,* **85**, 1-22.

Marshall, W. F. (2009). Centriole evolution. *Curr Opin Cell Biol,* **21**, 14-9.

Marshall, W. F. (2013). *Cilia, Part A.* First edition. ed.: Academic Press.

Marshall, W. F., Qin, H., Rodrigo Brenni, M. & Rosenbaum, J. L. (2005). Flagellar length control system: testing a simple model based on intraflagellar transport and turnover. *Mol Biol Cell,* **16**, 270-8.

Marshall, W. F. & Rosenbaum, J. L. (2001). Intraflagellar transport balances continuous turnover of outer doublet microtubules: implications for flagellar length control. *J Cell Biol,* **155**, 405-14.

Martin, S., Nishimune, A., Mellor, J. R. & Henley, J. M. (2007). SUMOylation regulates kainate-receptor-mediated synaptic transmission. *Nature,* **447**, 321-5.

Matsuura, K., Lefebvre, P. A., Kamiya, R. & Hirono, M. (2004). Bld10p, a novel protein essential for basal body assembly in Chlamydomonas: localization to the cartwheel, the first ninefold symmetrical structure appearing during assembly. *J Cell Biol,* **165**, 663-71.

Mazelova, J., Ransom, N., Astuto-Gribble, L., Wilson, M. C. & Deretic, D. (2009). Syntaxin 3 and SNAP-25 pairing, regulated by omega-3 docosahexaenoic acid, controls the delivery of rhodopsin for the biogenesis of cilia-derived sensory organelles, the rod outer segments. *J Cell Sci,* **122**, 2003-13.

McEwen, D. P., Koenekoop, R. K., Khanna, H., Jenkins, P. M., Lopez, I., Swaroop, A. & Martens, J. R. (2007). Hypomorphic CEP290/NPHP6 mutations result in anosmia caused by the selective loss of G proteins in cilia of olfactory sensory neurons. *Proc Natl Acad Sci U S A,* **104**, 15917-22.

McIntosh, J. R. & Euteneuer, U. (1984). Tubulin hooks as probes for microtubule polarity: an analysis of the method and an evaluation of data on microtubule polarity in the mitotic spindle. *J Cell Biol,* **98**, 525-33.

McIntyre, J. C., Joiner, A. M., Zhang, L., Iniguez-Lluhi, J. & Martens, J. R. (2015). SUMOylation regulates ciliary localization of olfactory signaling proteins. *J Cell Sci,* **128**, 1934-45.

Melchior, F., Schergaut, M. & Pichler, A. (2003). SUMO: ligases, isopeptidases and nuclear pores. *Trends Biochem Sci,* **28**, 612-8.

Michaud, E. J. & Yoder, B. K. (2006). The primary cilium in cell signaling and cancer. *Cancer Res,* **66**, 6463-7.

Miller, P. M., Folkmann, A. W., Maia, A. R., Efimova, N., Efimov, A. & Kaverina, I. (2009). Golgi-derived CLASP-dependent microtubules control Golgi organization and polarized trafficking in motile cells. *Nat Cell Biol,* **11**, 1069-80.

Molla-Herman, A., Boularan, C., Ghossoub, R., Scott, M. G., Burtey, A., Zarka, M., Saunier, S., Concordet, J. P., Marullo, S. & Benmerah, A. (2008). Targeting of beta-arrestin2 to the centrosome and primary cilium: role in cell proliferation control. *PLoS One,* **3**, e3728.

Molla-Herman, A., Ghossoub, R., Blisnick, T., Meunier, A., Serres, C., Silbermann, F., Emmerson, C., Romeo, K., Bourdoncle, P., Schmitt, A., Saunier, S., Spassky, N., Bastin, P. & Benmerah, A. (2010). The ciliary pocket: an endocytic membrane domain at the base of primary and motile cilia. *J Cell Sci,* **123**, 1785-95.

Morcos, P. A. (2001). Achieving efficient delivery of morpholino oligos in cultured cells. *Genesis,* **30**, 94-102.

Morcos, P. A. (2007). Achieving targeted and quantifiable alteration of mRNA splicing with Morpholino oligos. *Biochem Biophys Res Commun,* **358**, 521-7.

Moritz, M., Braunfeld, M. B., Guenebaut, V., Heuser, J. & Agard, D. A. (2000). Structure of the gamma-tubulin ring complex: a template for microtubule nucleation. *Nat Cell Biol,* **2**, 365-70.

Moser, J. J., Fritzler, M. J., Ou, Y. & Rattner, J. B. (2010). The PCM-basal body/primary cilium coalition. *Semin Cell Dev Biol,* **21**, 148-55.

Mukhopadhyay, S. & Jackson, P. K. (2013). Cilia, tubby mice, and obesity. *Cilia,* **2**, 1.

Nachury, M. V., Loktev, A. V., Zhang, Q., Westlake, C. J., Peranen, J., Merdes, A., Slusarski, D. C., Scheller, R. H., Bazan, J. F., Sheffield, V. C. & Jackson, P. K. (2007). A core complex of BBS proteins cooperates with the GTPase Rab8 to promote ciliary membrane biogenesis. *Cell,* **129**, 1201-13.

Nagase, T., Kikuno, R., Ishikawa, K., Hirosawa, M. & Ohara, O. (2000). Prediction of the coding sequences of unidentified human genes. XVII. The complete sequences of 100 new cDNA clones from brain which code for large proteins in vitro. *DNA Res,* **7**, 143-50.

Nakagawa, Y., Yamane, Y., Okanoue, T., Tsukita, S. & Tsukita, S. (2001). Outer dense fiber 2 is a widespread centrosome scaffold component preferentially associated with mother centrioles: its identification from isolated centrosomes. *Mol Biol Cell,* **12**, 1687-97.

Ng, M. M., Dippold, H. C., Buschman, M. D., Noakes, C. J. & Field, S. J. (2013). GOLPH3L antagonizes GOLPH3 to determine Golgi morphology. *Mol Biol Cell,* **24**, 796-808.

Nicklas, R. B., Kubai, D. F. & Hays, T. S. (1982). Spindle microtubules and their mechanical associations after micromanipulation in anaphase. *J Cell Biol,* **95**, 91-104.

Nigg, E. A. & Raff, J. W. (2009). Centrioles, centrosomes, and cilia in health and disease. *Cell,* **139**, 663-78.

Nobes, C. D. & Hall, A. (1999). Rho GTPases control polarity, protrusion, and adhesion during cell movement. *J Cell Biol,* **144**, 1235-44.

Novorol, C., Burkhardt, J., Wood, K. J., Iqbal, A., Roque, C., Coutts, N., Almeida, A. D., He, J., Wilkinson, C. J. & Harris, W. A. (2013). Microcephaly models in the developing zebrafish retinal neuroepithelium point to an underlying defect in metaphase progression. *Open Biol,* **3**, 130065.

O'Brien, L. L., Albee, A. J., Liu, L., Tao, W., Dobrzyn, P., Lizarraga, S. B. & Wiese, C. (2005). The Xenopus TACC homologue, maskin, functions in mitotic spindle assembly. *Mol Biol Cell,* **16**, 2836-47.

Oda, T., Chiba, S., Nagai, T. & Mizuno, K. (2014). Binding to Cep164, but not EB1, is essential for centriolar localization of TTBK2 and its function in ciliogenesis. *Genes Cells,* **19**, 927-40.

Oh, E. C. & Katsanis, N. (2012). Cilia in vertebrate development and disease. *Development,* **139**, 443-8.

Okabe, N., Xu, B. & Burdine, R. D. (2008). Fluid dynamics in zebrafish Kupffer's vesicle. *Dev Dyn,* **237**, 3602-12.

Okuda, M., Horn, H. F., Tarapore, P., Tokuyama, Y., Smulian, A. G., Chan, P. K., Knudsen, E. S., Hofmann, I. A., Snyder, J. D., Bove, K. E. & Fukasawa, K. (2000). Nucleophosmin/B23 is a target of CDK2/cyclin E in centrosome duplication. *Cell,* **103**, 127-40.

Olenick, M. A., Tokito, M., Boczkowska, M., Dominguez, R. & Holzbaur, E. L. (2016). Hook Adaptors Induce Unidirectional Processive Motility by Enhancing the Dynein-Dynactin Interaction. *J Biol Chem,* **291**, 18239-51.

Omori, Y., Zhao, C., Saras, A., Mukhopadhyay, S., Kim, W., Furukawa, T., Sengupta, P., Veraksa, A. & Malicki, J. (2008). Elipsa is an early determinant of ciliogenesis that links the IFT particle to membrane-associated small GTPase Rab8. *Nat Cell Biol,* **10**, 437-44.

Omran, H. (2010). NPHP proteins: gatekeepers of the ciliary compartment. *J Cell Biol,* **190**, 715-7.

Orchard, S., Ammari, M., Aranda, B., Breuza, L., Briganti, L., Broackes-Carter, F., Campbell, N. H., Chavali, G., Chen, C., del-Toro, N., Duesbury, M., Dumousseau, M., Galeota, E., Hinz, U., Iannuccelli, M., Jagannathan, S., Jimenez, R., Khadake, J., Lagreid, A., Licata, L., Lovering, R. C., Meldal, B., Melidoni, A. N., Milagros, M., Peluso, D., Perfetto, L., Porras, P., Raghunath, A., Ricard-Blum, S., Roechert, B., Stutz, A., Tognolli, M., van Roey, K., Cesareni, G. & Hermjakob, H. (2014). The MIntAct project--IntAct as a common curation platform for 11 molecular interaction databases. *Nucleic Acids Res,* **42**, D358-63.

Orhon, I., Dupont, N., Pampliega, O., Cuervo, A. M. & Codogno, P. (2015). Autophagy and regulation of cilia function and assembly. *Cell Death Differ,* **22**, 389-97.

Oshimori, N., Li, X., Ohsugi, M. & Yamamoto, T. (2009). Cep72 regulates the localization of key centrosomal proteins and proper bipolar spindle formation. *EMBO J,* **28**, 2066-76.

Oshimori, N., Ohsugi, M. & Yamamoto, T. (2006). The Plk1 target Kizuna stabilizes mitotic centrosomes to ensure spindle bipolarity. *Nat Cell Biol,* **8**, 1095-101.

Paintrand, M., Moudjou, M., Delacroix, H. & Bornens, M. (1992). Centrosome organization and centriole architecture: their sensitivity to divalent cations. *J Struct Biol,* **108**, 107-28.

Pallesi-Pocachard, E., Bazellieres, E., Viallat-Lieutaud, A., Delgrossi, M. H., Barthelemy-Requin, M., Le Bivic, A. & Massey-Harroche, D. (2016). Hook2, a microtubule-binding protein, interacts with Par6alpha and controls centrosome orientation during polarized cell migration. *Sci Rep,* **6**, 33259.

Palmer, K. J., MacCarthy-Morrogh, L., Smyllie, N. & Stephens, D. J. (2011). A role for Tctex-1 (DYNLT1) in controlling primary cilium length. *Eur J Cell Biol,* **90**, 865-71.

Pampliega, O. & Cuervo, A. M. (2016). Autophagy and primary cilia: dual interplay. *Curr Opin Cell Biol,* **39**, 1-7.

Pampliega, O., Orhon, I., Patel, B., Sridhar, S., Diaz-Carretero, A., Beau, I., Codogno, P., Satir, B. H., Satir, P. & Cuervo, A. M. (2013). Functional interaction between autophagy and ciliogenesis. *Nature,* **502**, 194-200.

Pan, J., Seeger-Nukpezah, T. & Golemis, E. A. (2013). The role of the cilium in normal and abnormal cell cycles: emphasis on renal cystic pathologies. *Cell Mol Life Sci,* **70**, 1849-74.

Pan, J. & Snell, W. (2007). The primary cilium: keeper of the key to cell division. *Cell,* **129**, 1255-7.

Paoletti, A., Moudjou, M., Paintrand, M., Salisbury, J. L. & Bornens, M. (1996). Most of centrin in animal cells is not centrosome-associated and centrosomal centrin is confined to the distal lumen of centrioles. *J Cell Sci,* **109 (Pt 13)**, 3089-102.

Pedersen, L. B. & Rosenbaum, J. L. (2008). Intraflagellar transport (IFT) role in ciliary assembly, resorption and signalling. *Curr Top Dev Biol,* **85**, 23-61.

Pejaver, V., Hsu, W. L., Xin, F., Dunker, A. K., Uversky, V. N. & Radivojac, P. (2014). The structural and functional signatures of proteins that undergo multiple events of post-translational modification. *Protein Sci,* **23**, 1077-93.

Pelletier, L., O'Toole, E., Schwager, A., Hyman, A. A. & Muller-Reichert, T. (2006). Centriole assembly in Caenorhabditis elegans. *Nature,* **444**, 619-23.

Perkins, L. A., Hedgecock, E. M., Thomson, J. N. & Culotti, J. G. (1986). Mutant sensory cilia in the nematode Caenorhabditis elegans. *Dev Biol,* **117**, 456-87.

Petersen, C., Fuzesi, L. & Hoyer-Fender, S. (1999). Outer dense fibre proteins from human sperm tail: molecular cloning and expression analyses of two cDNA transcripts encoding proteins of approximately 70 kDa. *Mol Hum Reprod,* **5**, 627-35.

Petrosyan, A., Ali, M. F., Verma, S. K., Cheng, H. & Cheng, P. W. (2012). Non-muscle myosin IIA transports a Golgi glycosyltransferase to the endoplasmic reticulum by binding to its cytoplasmic tail. *Int J Biochem Cell Biol,* **44**, 1153-65.

Petrosyan, A., Casey, C. A. & Cheng, P. W. (2016). The role of Rab6a and phosphorylation of non-muscle myosin IIA tailpiece in alcohol-induced Golgi disorganization. *Sci Rep,* **6**, 31962.

Petrosyan, A. & Cheng, P. W. (2014). Golgi fragmentation induced by heat shock or inhibition of heat shock proteins is mediated by non-muscle myosin IIA via its interaction with glycosyltransferases. *Cell Stress Chaperones,* **19**, 241-54.

Petrosyan, A., Holzapfel, M. S., Muirhead, D. E. & Cheng, P. W. (2014). Restoration of compact Golgi morphology in advanced prostate cancer enhances susceptibility to galectin-1-induced apoptosis by modifying mucin O-glycan synthesis. *Mol Cancer Res,* **12**, 1704-16.

Pigino, G., Geimer, S., Lanzavecchia, S., Paccagnini, E., Cantele, F., Diener, D. R., Rosenbaum, J. L. & Lupetti, P. (2009). Electron-tomographic analysis of intraflagellar transport particle trains in situ. *J Cell Biol,* **187**, 135-48.

Pirkmajer, S. & Chibalin, A. V. (2011). Serum starvation: caveat emptor. *Am J Physiol Cell Physiol,* **301**, C272-9.

Piston, D. W. & Kremers, G. J. (2007). Fluorescent protein FRET: the good, the bad and the ugly. *Trends Biochem Sci,* **32**, 407-14.

Ponsard, C., Seltzer, V., Perret, E., Tournier, F. & Middendorp, S. (2007). Identification of BCAP, a new protein associated with basal bodies and centrioles. *Front Biosci,* **12**, 3683-93.

Prasad, T. S., Kandasamy, K. & Pandey, A. (2009). Human Protein Reference Database and Human Proteinpedia as discovery tools for systems biology. *Methods Mol Biol,* **577**, 67-79.

Preble, A. M., Giddings, T. M., Jr. & Dutcher, S. K. (2000). Basal bodies and centrioles: their function and structure. *Curr Top Dev Biol,* **49**, 207-33.

Preisinger, C., Short, B., De Corte, V., Bruyneel, E., Haas, A., Kopajtich, R., Gettemans, J. & Barr, F. A. (2004). YSK1 is activated by the Golgi matrix protein GM130 and plays a role in cell migration through its substrate 14-3-3zeta. *J Cell Biol,* **164**, 1009-20.

Progida, C., Cogli, L., Piro, F., De Luca, A., Bakke, O. & Bucci, C. (2010). Rab7b controls trafficking from endosomes to the TGN. *J Cell Sci,* **123**, 1480-91.

Pugacheva, E. N., Jablonski, S. A., Hartman, T. R., Henske, E. P. & Golemis, E. A. (2007). HEF1-dependent Aurora A activation induces disassembly of the primary cilium. *Cell,* **129**, 1351-63.

Raarup, M. K., Fjorback, A. W., Jensen, S. M., Muller, H. K., Kjaergaard, M. M., Poulsen, H., Wiborg, O. & Nyengaard, J. R. (2009). Enhanced yellow fluorescent protein photoconversion to a cyan fluorescent protein-like species is sensitive to thermal and diffusion conditions. *J Biomed Opt,* **14**, 034039.

Rattner, J. B. (1992). 2 - Ultrastructure of Centrosome Domains and Identification of Their Protein Components. *In:* Kalnins, V. I. (ed.) *The Centrosome.* Academic Press.

Reiter, J. F., Blacque, O. E. & Leroux, M. R. (2012). The base of the cilium: roles for transition fibres and the transition zone in ciliary formation, maintenance and compartmentalization. *EMBO Rep,* **13**, 608-18.

Rios, R. M. (2014). The centrosome-Golgi apparatus nexus. *Philos Trans R Soc Lond B Biol Sci,* **369**.

Rivero, S., Cardenas, J., Bornens, M. & Rios, R. M. (2009). Microtubule nucleation at the cis-side of the Golgi apparatus requires AKAP450 and GM130. *EMBO J,* **28**, 1016-28.

Robbins, E., Jentzsch, G. & Micali, A. (1968). The centriole cycle in synchronized HeLa cells. *J Cell Biol,* **36**, 329-39.

Romio, L., Fry, A. M., Winyard, P. J., Malcolm, S., Woolf, A. S. & Feather, S. A. (2004). OFD1 is a centrosomal/basal body protein expressed during mesenchymal-epithelial transition in human nephrogenesis. *J Am Soc Nephrol,* **15**, 2556-68.

Romio, L., Wright, V., Price, K., Winyard, P. J., Donnai, D., Porteous, M. E., Franco, B., Giorgio, G., Malcolm, S., Woolf, A. S. & Feather, S. A. (2003). OFD1, the gene mutated in oral-facial-digital syndrome type 1, is expressed in the metanephros and in human embryonic renal mesenchymal cells. *J Am Soc Nephrol,* **14**, 680-9.

Rosen, J. N., Sweeney, M. F. & Mably, J. D. (2009). Microinjection of zebrafish embryos to analyze gene function. *J Vis Exp*.

Rual, J. F., Venkatesan, K., Hao, T., Hirozane-Kishikawa, T., Dricot, A., Li, N., Berriz, G. F., Gibbons, F. D., Dreze, M., Ayivi-Guedehoussou, N., Klitgord, N., Simon, C., Boxem, M., Milstein, S., Rosenberg, J., Goldberg, D. S., Zhang, L. V., Wong, S. L., Franklin, G., Li, S., Albala, J. S., Lim, J., Fraughton, C., Llamosas, E., Cevik, S., Bex, C., Lamesch, P., Sikorski, R. S., Vandenhaute, J., Zoghbi, H. Y., Smolyar, A., Bosak, S., Sequerra, R., Doucette-Stamm, L., Cusick, M. E., Hill, D. E., Roth, F. P. & Vidal, M. (2005). Towards a proteome-scale map of the human protein-protein interaction network. *Nature,* **437**, 1173-8.

Sahlender, D. A., Roberts, R. C., Arden, S. D., Spudich, G., Taylor, M. J., Luzio, J. P., Kendrick-Jones, J. & Buss, F. (2005). Optineurin links myosin VI to the Golgi complex and is involved in Golgi organization and exocytosis. *J Cell Biol,* **169**, 285-95.

Salisbury, J. L. (2003). Centrosomes: coiled-coils organize the cell center. *Curr Biol,* **13**, R88-90.

Salmon, N. A., Reijo Pera, R. A. & Xu, E. Y. (2006). A gene trap knockout of the abundant sperm tail protein, outer dense fiber 2, results in preimplantation lethality. *Genesis,* **44**, 515-22.

Sano, H., Ishino, M., Kramer, H., Shimizu, T., Mitsuzawa, H., Nishitani, C. & Kuroki, Y. (2007). The microtubule-binding protein Hook3 interacts with a cytoplasmic domain of scavenger receptor A. *J Biol Chem,* **282**, 7973-81.

Sathananthan, A. H., Kola, I., Osborne, J., Trounson, A., Ng, S. C., Bongso, A. & Ratnam, S. S. (1991). Centrioles in the beginning of human development. *Proc Natl Acad Sci U S A,* **88**, 4806-10.

Satir, P. & Christensen, S. T. (2007). Overview of structure and function of mammalian cilia. *Annu Rev Physiol,* **69**, 377-400.

Satish Tammana, T. V., Tammana, D., Diener, D. R. & Rosenbaum, J. (2013). Centrosomal protein CEP104 (Chlamydomonas FAP256) moves to the ciliary tip during ciliary assembly. *J Cell Sci,* **126**, 5018-29.

Schalles, U., Shao, X., van der Hoorn, F. A. & Oko, R. (1998). Developmental expression of the 84-kDa ODF sperm protein: localization to both the cortex and medulla of outer dense fibers and to the connecting piece. *Dev Biol,* **199**, 250-60.

Schatten, H. (2008). The mammalian centrosome and its functional significance. *Histochem Cell Biol,* **129**, 667-86.

Scheer, U. (2014). Historical roots of centrosome research: discovery of Boveri's microscope slides in Wurzburg. *Philos Trans R Soc Lond B Biol Sci,* **369**.

Schiebel, E. (2000). gamma-tubulin complexes: binding to the centrosome, regulation and microtubule nucleation. *Curr Opin Cell Biol,* **12**, 113-8.

Schmidt, K. N., Kuhns, S., Neuner, A., Hub, B., Zentgraf, H. & Pereira, G. (2012). Cep164 mediates vesicular docking to the mother centriole during early steps of ciliogenesis. *J Cell Biol,* **199**, 1083-101.

Schmidt, T. I., Kleylein-Sohn, J., Westendorf, J., Le Clech, M., Lavoie, S. B., Stierhof, Y. D. & Nigg, E. A. (2009). Control of centriole length by CPAP and CP110. *Curr Biol,* **19**, 1005-11.

Schultz, J., Milpetz, F., Bork, P. & Ponting, C. P. (1998). SMART, a simple modular architecture research tool: identification of signaling domains. *Proc Natl Acad Sci U S A,* **95**, 5857-64.

Sedjai, F., Acquaviva, C., Chevrier, V., Chauvin, J. P., Coppin, E., Aouane, A., Coulier, F., Tolun, A., Pierres, M., Birnbaum, D. & Rosnet, O. (2010). Control of ciliogenesis by FOR20, a novel centrosome and pericentriolar satellite protein. *J Cell Sci,* **123**, 2391-401.

Sedmak, T. & Wolfrum, U. (2010). Intraflagellar transport molecules in ciliary and nonciliary cells of the retina. *J Cell Biol,* **189**, 171-86.

Shaner, N. C., Lin, M. Z., McKeown, M. R., Steinbach, P. A., Hazelwood, K. L., Davidson, M. W. & Tsien, R. Y. (2008). Improving the photostability of bright monomeric orange and red fluorescent proteins. *Nat Methods,* **5**, 545-51.

Sharma, N., Kosan, Z. A., Stallworth, J. E., Berbari, N. F. & Yoder, B. K. (2011). Soluble levels of cytosolic tubulin regulate ciliary length control. *Mol Biol Cell,* **22**, 806-16.

Shi, Y., Su, Y., Lipschutz, J. H. & Lobo, G. P. (2017). Zebrafish as models to study ciliopathies of the eye and kidney. *Clin Nephrol Res,* **1**, 6-9.

Shu, X., Fry, A. M., Tulloch, B., Manson, F. D., Crabb, J. W., Khanna, H., Faragher, A. J., Lennon, A., He, S., Trojan, P., Giessl, A., Wolfrum, U., Vervoort, R., Swaroop, A. & Wright, A. F. (2005). RPGR ORF15 isoform co-localizes with RPGRIP1 at centrioles and basal bodies and interacts with nucleophosmin. *Hum Mol Genet,* **14**, 1183-97.

Silva, E., Betleja, E., John, E., Spear, P., Moresco, J. J., Zhang, S., Yates, J. R., 3rd, Mitchell, B. J. & Mahjoub, M. R. (2016). Ccdc11 is a novel centriolar satellite protein essential for ciliogenesis and establishment of left-right asymmetry. *Mol Biol Cell,* **27**, 48-63.

Silverman, M. A. & Leroux, M. R. (2009). Intraflagellar transport and the generation of dynamic, structurally and functionally diverse cilia. *Trends Cell Biol,* **19**, 306-16.

Singh, R., Park, D., Xu, J., Hosur, R. & Berger, B. (2010). Struct2Net: a web service to predict protein-protein interactions using a structure-based approach. *Nucleic Acids Res,* **38**, W508-15.

Singh, R., Xu, J. & Berger, B. (2006). Struct2net: integrating structure into protein-protein interaction prediction. *Pac Symp Biocomput*, 403-14.

Singla, V. & Reiter, J. F. (2006). The primary cilium as the cell's antenna: signaling at a sensory organelle. *Science,* **313**, 629-33.

Singla, V., Romaguera-Ros, M., Garcia-Verdugo, J. M. & Reiter, J. F. (2010). Ofd1, a human disease gene, regulates the length and distal structure of centrioles. *Dev Cell,* **18**, 410-24.

Sloboda, R. D. (2009). *Primary cilia.* Amsterdam ; London: Academic Press.

Soares, D. C., Carlyle, B. C., Bradshaw, N. J. & Porteous, D. J. (2011). DISC1: Structure, Function, and Therapeutic Potential for Major Mental Illness. *ACS Chem Neurosci,* **2**, 609-632.

Song, Y. & Brady, S. T. (2015). Post-translational modifications of tubulin: pathways to functional diversity of microtubules. *Trends Cell Biol,* **25**, 125-36.

Song, Z., Zhang, X., Jia, S., Yelick, P. C. & Zhao, C. (2016). Zebrafish as a Model for Human Ciliopathies. *J Genet Genomics,* **43**, 107-20.

Sorokin, S. (1962). Centrioles and the formation of rudimentary cilia by fibroblasts and smooth muscle cells. *J Cell Biol,* **15**, 363-77.

Spalluto, C., Wilson, D. I. & Hearn, T. (2013). Evidence for centriolar satellite localization of CDK1 and cyclin B2. *Cell Cycle,* **12**, 1802-3.

Spektor, A., Tsang, W. Y., Khoo, D. & Dynlacht, B. D. (2007). Cep97 and CP110 suppress a cilia assembly program. *Cell,* **130**, 678-90.

Srayko, M., Kaya, A., Stamford, J. & Hyman, A. A. (2005). Identification and characterization of factors required for microtubule growth and nucleation in the early C. elegans embryo. *Dev Cell,* **9**, 223-36.

Staples, C. J., Myers, K. N., Beveridge, R. D., Patil, A. A., Howard, A. E., Barone, G., Lee, A. J., Swanton, C., Howell, M., Maslen, S., Skehel, J. M., Boulton, S. J. & Collis, S. J. (2014). Ccdc13 is a novel human centriolar satellite protein required for ciliogenesis and genome stability. *J Cell Sci,* **127**, 2910-9.

Staples, C. J., Myers, K. N., Beveridge, R. D., Patil, A. A., Lee, A. J., Swanton, C., Howell, M., Boulton, S. J. & Collis, S. J. (2012). The centriolar satellite protein Cep131 is important for genome stability. *J Cell Sci,* **125**, 4770-9.

Stark, C., Breitkreutz, B. J., Reguly, T., Boucher, L., Breitkreutz, A. & Tyers, M. (2006). BioGRID: a general repository for interaction datasets. *Nucleic Acids Res,* **34**, D535-9.

Stelzl, U., Worm, U., Lalowski, M., Haenig, C., Brembeck, F. H., Goehler, H., Stroedicke, M., Zenkner, M., Schoenherr, A., Koeppen, S., Timm, J., Mintzlaff, S., Abraham, C., Bock, N., Kietzmann, S., Goedde, A., Toksoz, E., Droege, A., Krobitsch, S., Korn, B., Birchmeier, W., Lehrach, H. & Wanker, E. E. (2005). A human protein-protein interaction network: a resource for annotating the proteome. *Cell,* **122**, 957-68.

Stephan, A., Vaughan, S., Shaw, M. K., Gull, K. & McKean, P. G. (2007). An essential quality control mechanism at the eukaryotic basal body prior to intraflagellar transport. *Traffic,* **8**, 1323-30.

Stooke-Vaughan, G. A., Obholzer, N. D., Baxendale, S., Megason, S. G. & Whitfield, T. T. (2015). Otolith tethering in the zebrafish otic vesicle requires Otogelin and alpha-Tectorin. *Development,* **142**, 1137-45.

Stowe, T. R., Wilkinson, C. J., Iqbal, A. & Stearns, T. (2012). The centriolar satellite proteins Cep72 and Cep290 interact and are required for recruitment of BBS proteins to the cilium. *Mol Biol Cell,* **23**, 3322-35.

Strausberg, R. L., Feingold, E. A., Grouse, L. H., Derge, J. G., Klausner, R. D., Collins, F. S., Wagner, L., Shenmen, C. M., Schuler, G. D., Altschul, S. F., Zeeberg, B., Buetow, K. H., Schaefer, C. F., Bhat, N. K., Hopkins, R. F., Jordan, H., Moore, T., Max, S. I., Wang, J., Hsieh, F., Diatchenko, L., Marusina, K., Farmer, A. A., Rubin, G. M., Hong, L., Stapleton, M., Soares, M. B., Bonaldo, M. F., Casavant, T. L., Scheetz, T. E., Brownstein, M. J., Usdin, T. B., Toshiyuki, S., Carninci, P., Prange, C., Raha, S. S., Loquellano, N. A., Peters, G. J., Abramson, R. D., Mullahy, S. J., Bosak, S. A., McEwan, P. J., McKernan, K. J., Malek, J. A., Gunaratne, P. H., Richards, S., Worley, K. C., Hale, S., Garcia, A. M., Gay, L. J., Hulyk, S. W., Villalon, D. K., Muzny, D. M., Sodergren, E. J., Lu, X., Gibbs, R. A., Fahey, J., Helton, E., Ketteman, M., Madan, A., Rodrigues, S., Sanchez, A., Whiting, M., Madan, A., Young, A. C., Shevchenko, Y., Bouffard, G. G., Blakesley, R. W., Touchman, J. W., Green, E. D., Dickson, M. C., Rodriguez, A. C., Grimwood, J., Schmutz, J., Myers, R. M., Butterfield, Y. S., Krzywinski, M. I., Skalska, U., Smailus, D. E., Schnerch, A., Schein, J. E., Jones, S. J., Marra, M. A. & Mammalian Gene Collection Program, T. (2002). Generation and initial analysis of more than 15,000 full-length human and mouse cDNA sequences. *Proc Natl Acad Sci U S A,* **99**, 16899-903.

Strnad, P. & Gonczy, P. (2008). Mechanisms of procentriole formation. *Trends Cell Biol,* **18**, 389-96.

Strnad, P., Leidel, S., Vinogradova, T., Euteneuer, U., Khodjakov, A. & Gonczy, P. (2007). Regulated HsSAS-6 levels ensure formation of a single procentriole per centriole during the centrosome duplication cycle. *Dev Cell,* **13**, 203-13.

Sud, R., Geller, E. T. & Schellenberg, G. D. (2014). Antisense-mediated Exon Skipping Decreases Tau Protein Expression: A Potential Therapy For Tauopathies. *Mol Ther Nucleic Acids,* **3**, e180.

Sullivan-Brown, J., Schottenfeld, J., Okabe, N., Hostetter, C. L., Serluca, F. C., Thiberge, S. Y. & Burdine, R. D. (2008). Zebrafish mutations affecting cilia motility share similar cystic phenotypes and suggest a mechanism of cyst formation that differs from pkd2 morphants. *Dev Biol,* **314**, 261-75.

Summerton, J. (1999). Morpholino antisense oligomers: the case for an RNase H-independent structural type. *Biochim Biophys Acta,* **1489**, 141-58.

Summerton, J. & Weller, D. (1997). Morpholino antisense oligomers: design, preparation, and properties. *Antisense Nucleic Acid Drug Dev,* **7**, 187-95.

Summerton, J. E. (2007). Morpholino, siRNA, and S-DNA compared: impact of structure and mechanism of action on off-target effects and sequence specificity. *Curr Top Med Chem,* **7**, 651-60.

Sun, Z., Amsterdam, A., Pazour, G. J., Cole, D. G., Miller, M. S. & Hopkins, N. (2004). A genetic screen in zebrafish identifies cilia genes as a principal cause of cystic kidney. *Development,* **131**, 4085-93.

Sutterlin, C. & Colanzi, A. (2010). The Golgi and the centrosome: building a functional partnership. *J Cell Biol,* **188**, 621-8.

Szebenyi, G., Hall, B., Yu, R., Hashim, A. I. & Kramer, H. (2007). Hook2 localizes to the centrosome, binds directly to centriolin/CEP110 and contributes to centrosomal function. *Traffic,* **8**, 32-46.

Szilak, L., Moitra, J. & Vinson, C. (1997). Design of a leucine zipper coiled coil stabilized 1.4 kcal mol-1 by phosphorylation of a serine in the e position. *Protein Sci,* **6**, 1273-83.

Tachi, S., Tachi, C. & Lindner, H. R. (1974). Influence of ovarian hormones on formation of solitary cilia and behavior of the centrioles in uterine epithelial cells of the rat. *Biol Reprod,* **10**, 391-403.

Tang, C. J., Fu, R. H., Wu, K. S., Hsu, W. B. & Tang, T. K. (2009). CPAP is a cell-cycle regulated protein that controls centriole length. *Nat Cell Biol,* **11**, 825-31.

Tang, Z., Lin, M. G., Stowe, T. R., Chen, S., Zhu, M., Stearns, T., Franco, B. & Zhong, Q. (2013). Autophagy promotes primary ciliogenesis by removing OFD1 from centriolar satellites. *Nature,* **502**, 254-7.

Tanos, B. E., Yang, H. J., Soni, R., Wang, W. J., Macaluso, F. P., Asara, J. M. & Tsou, M. F. (2013). Centriole distal appendages promote membrane docking, leading to cilia initiation. *Genes Dev,* **27**, 163-8.

Taylor, J. S., Braasch, I., Frickey, T., Meyer, A. & Van de Peer, Y. (2003). Genome duplication, a trait shared by 22000 species of ray-finned fish. *Genome Res,* **13**, 382-90.

TerBush, D. R., Maurice, T., Roth, D. & Novick, P. (1996). The Exocyst is a multiprotein complex required for exocytosis in Saccharomyces cerevisiae. *EMBO J,* **15**, 6483-94.

Theg, D. E. (1964). Cytoplasmic Microtubules in Different Animal Cells. *J Cell Biol,* **23**, 265-75.

Tollenaere, M. A., Mailand, N. & Bekker-Jensen, S. (2015). Centriolar satellites: key mediators of centrosome functions. *Cell Mol Life Sci,* **72**, 11-23.

Toya, M., Sato, M., Haselmann, U., Asakawa, K., Brunner, D., Antony, C. & Toda, T. (2007). Gamma-tubulin complex-mediated anchoring of spindle microtubules to spindle-pole bodies requires Msd1 in fission yeast. *Nat Cell Biol,* **9**, 646-53.

Tramier, M., Zahid, M., Mevel, J. C., Masse, M. J. & Coppey-Moisan, M. (2006). Sensitivity of CFP/YFP and GFP/mCherry pairs to donor photobleaching on FRET determination by fluorescence lifetime imaging microscopy in living cells. *Microsc Res Tech,* **69**, 933-9.

Tsang, W. Y., Bossard, C., Khanna, H., Peranen, J., Swaroop, A., Malhotra, V. & Dynlacht, B. D. (2008). CP110 suppresses primary cilia formation through its interaction with CEP290, a protein deficient in human ciliary disease. *Dev Cell,* **15**, 187-97.

Tsujikawa, M. & Malicki, J. (2004). Intraflagellar transport genes are essential for differentiation and survival of vertebrate sensory neurons. *Neuron,* **42**, 703-16.

Turriziani, B., Garcia-Munoz, A., Pilkington, R., Raso, C., Kolch, W. & von Kriegsheim, A. (2014). On-beads digestion in conjunction with data-dependent mass spectrometry: a shortcut to quantitative and dynamic interaction proteomics. *Biology (Basel),* **3**, 320-32.

Uetake, Y. & Sluder, G. (2007). Cell-cycle progression without an intact microtuble cytoskeleton. *Curr Biol,* **17**, 2081-6.

Vaisse, C., Reiter, J. F. & Berbari, N. F. (2017). Cilia and Obesity. *Cold Spring Harb Perspect Biol,* **9**.

Valente, E. M., Silhavy, J. L., Brancati, F., Barrano, G., Krishnaswami, S. R., Castori, M., Lancaster, M. A., Boltshauser, E., Boccone, L., Al-Gazali, L., Fazzi, E., Signorini, S., Louie, C. M.,

Bellacchio, E., International Joubert Syndrome Related Disorders Study, G., Bertini, E., Dallapiccola, B. & Gleeson, J. G. (2006). Mutations in CEP290, which encodes a centrosomal protein, cause pleiotropic forms of Joubert syndrome. *Nat Genet,* **38**, 623-5.

van Beneden, É. (1876). *Contributions à l'histoire de la vésicule germinative et du premier noyau embryonnaire.* F. Hayez, Bull Acad R Belg 42:35–97.

van Breugel, M., Hirono, M., Andreeva, A., Yanagisawa, H. A., Yamaguchi, S., Nakazawa, Y., Morgner, N., Petrovich, M., Ebong, I. O., Robinson, C. V., Johnson, C. M., Veprintsev, D. & Zuber, B. (2011). Structures of SAS-6 suggest its organization in centrioles. *Science,* **331**, 1196-9.

Vicente-Manzanares, M., Zareno, J., Whitmore, L., Choi, C. K. & Horwitz, A. F. (2007). Regulation of protrusion, adhesion dynamics, and polarity by myosins IIA and IIB in migrating cells. *J Cell Biol,* **176**, 573-80.

Villumsen, B. H., Danielsen, J. R., Povlsen, L., Sylvestersen, K. B., Merdes, A., Beli, P., Yang, Y. G., Choudhary, C., Nielsen, M. L., Mailand, N. & Bekker-Jensen, S. (2013). A new cellular stress response that triggers centriolar satellite reorganization and ciliogenesis. *EMBO J,* **32**, 3029-40.

Vladar, E. K. & Stearns, T. (2007). Molecular characterization of centriole assembly in ciliated epithelial cells. *J Cell Biol,* **178**, 31-42.

von Thun, A., Preisinger, C., Rath, O., Schwarz, J. P., Ward, C., Monsefi, N., Rodriguez, J., Garcia-Munoz, A., Birtwistle, M., Bienvenut, W., Anderson, K. I., Kolch, W. & von Kriegsheim, A. (2013). Extracellular signal-regulated kinase regulates RhoA activation and tumor cell plasticity by inhibiting guanine exchange factor H1 activity. *Mol Cell Biol,* **33**, 4526-37.

Walenta, J. H., Didier, A. J., Liu, X. & Kramer, H. (2001). The Golgi-associated hook3 protein is a member of a novel family of microtubule-binding proteins. *J Cell Biol,* **152**, 923-34.

Wang, G., Chen, Q., Zhang, X., Zhang, B., Zhuo, X., Liu, J., Jiang, Q. & Zhang, C. (2013). PCM1 recruits Plk1 to the pericentriolar matrix to promote primary cilia disassembly before mitotic entry. *J Cell Sci,* **126**, 1355-65.

Wang, G., Krishnamurthy, K. & Bieberich, E. (2009a). Regulation of primary cilia formation by ceramide. *J Lipid Res,* **50**, 2103-10.

Wang, P., Bouwman, F. G. & Mariman, E. C. (2009b). Generally detected proteins in comparative proteomics--a matter of cellular stress response? *Proteomics,* **9**, 2955-66.

Wang, S., Livingston, M. J., Su, Y. & Dong, Z. (2015). Reciprocal regulation of cilia and autophagy via the MTOR and proteasome pathways. *Autophagy,* **11**, 607-16.

Wang, Z., Wu, T., Shi, L., Zhang, L., Zheng, W., Qu, J. Y., Niu, R. & Qi, R. Z. (2010). Conserved motif of CDK5RAP2 mediates its localization to centrosomes and the Golgi complex. *J Biol Chem,* **285**, 22658-65.

Waterman, R. E. & Bell, D. H. (1984). Epithelial fusion during early semicircular canal formation in the embryonic zebrafish, Brachydanio rerio. *Anat Rec,* **210**, 101-14.

Waters, A. M. & Beales, P. L. (2011). Ciliopathies: an expanding disease spectrum. *Pediatr Nephrol,* **26**, 1039-56.

Wells, C. M. & Parsons, M. (2011). *Cell migration : developmental methods and protocols.* 2nd ed. New York: Humana Press ; Springer.

Westerfield, M. (1993). *The zebrafish book : a guide for the laboratory use of zebrafish (Brachydanio rerio).* Eugene, OR: M. Westerfield.

Westlake, C. J., Baye, L. M., Nachury, M. V., Wright, K. J., Ervin, K. E., Phu, L., Chalouni, C., Beck, J. S., Kirkpatrick, D. S., Slusarski, D. C., Sheffield, V. C., Scheller, R. H. & Jackson, P. K. (2011). Primary cilia membrane assembly is initiated by Rab11 and transport protein particle II (TRAPPII) complex-dependent trafficking of Rabin8 to the centrosome. *Proc Natl Acad Sci U S A,* **108**, 2759-64.

Wiese, C. & Zheng, Y. (2006). Microtubule nucleation: gamma-tubulin and beyond. *J Cell Sci,* **119**, 4143-53.

Wilkinson, C. J., Carl, M. & Harris, W. A. (2009). Cep70 and Cep131 contribute to ciliogenesis in zebrafish embryos. *BMC Cell Biol,* **10**, 17.

Williams, C. L., Li, C., Kida, K., Inglis, P. N., Mohan, S., Semenec, L., Bialas, N. J., Stupay, R. M., Chen, N., Blacque, O. E., Yoder, B. K. & Leroux, M. R. (2011). MKS and NPHP modules cooperate to establish basal body/transition zone membrane associations and ciliary gate function during ciliogenesis. *J Cell Biol,* **192**, 1023-41.

Wirawan, E., Lippens, S., Vanden Berghe, T., Romagnoli, A., Fimia, G. M., Piacentini, M. & Vandenabeele, P. (2012). Beclin1: a role in membrane dynamics and beyond. *Autophagy,* **8**, 6-17.

Wittmann, T., Wilm, M., Karsenti, E. & Vernos, I. (2000). TPX2, A novel xenopus MAP involved in spindle pole organization. *J Cell Biol,* **149**, 1405-18.

Wolf, E., Kim, P. S. & Berger, B. (1997). MultiCoil: a program for predicting two- and three-stranded coiled coils. *Protein Sci,* **6**, 1179-89.

Woodruff, J. B., Wueseke, O. & Hyman, A. A. (2014). Pericentriolar material structure and dynamics. *Philos Trans R Soc Lond B Biol Sci,* **369**.

Wouters, F. S., Verveer, P. J. & Bastiaens, P. I. (2001). Imaging biochemistry inside cells. *Trends Cell Biol,* **11**, 203-11.

Xin, X., Rual, J. F., Hirozane-Kishikawa, T., Hill, D. E., Vidal, M., Boone, C. & Thierry-Mieg, N. (2009). Shifted Transversal Design smart-pooling for high coverage interactome mapping. *Genome Res,* **19**, 1262-9.

Xu, L., Sowa, M. E., Chen, J., Li, X., Gygi, S. P. & Harper, J. W. (2008). An FTS/Hook/p107(FHIP) complex interacts with and promotes endosomal clustering by the homotypic vacuolar protein sorting complex. *Mol Biol Cell,* **19**, 5059-71.

Xue, Y., Ren, J., Gao, X., Jin, C., Wen, L. & Yao, X. (2008). GPS 2.0, a tool to predict kinase-specific phosphorylation sites in hierarchy. *Mol Cell Proteomics,* **7**, 1598-608.

Xue, Y., Zhou, F., Zhu, M., Ahmed, K., Chen, G. & Yao, X. (2005). GPS: a comprehensive www server for phosphorylation sites prediction. *Nucleic Acids Res,* **33**, W184-7.

Yadav, S., Puri, S. & Linstedt, A. D. (2009). A primary role for Golgi positioning in directed secretion, cell polarity, and wound healing. *Mol Biol Cell,* **20**, 1728-36.

Yan, X. & Zhu, X. (2013). Branched F-actin as a negative regulator of cilia formation. *Exp Cell Res,* **319**, 147-51.

Yang, M., Chen, T., Han, C., Li, N., Wan, T. & Cao, X. (2004). Rab7b, a novel lysosome-associated small GTPase, is involved in monocytic differentiation of human acute promyelocytic leukemia cells. *Biochem Biophys Res Commun,* **318**, 792-9.

Ye, X., Zeng, H., Ning, G., Reiter, J. F. & Liu, A. (2014). C2cd3 is critical for centriolar distal appendage assembly and ciliary vesicle docking in mammals. *Proc Natl Acad Sci U S A,* **111**, 2164-9.

Yen, H. J., Tayeh, M. K., Mullins, R. F., Stone, E. M., Sheffield, V. C. & Slusarski, D. C. (2006). Bardet-Biedl syndrome genes are important in retrograde intracellular trafficking and Kupffer's vesicle cilia function. *Hum Mol Genet,* **15**, 667-77.

Yoshimura, S., Egerer, J., Fuchs, E., Haas, A. K. & Barr, F. A. (2007). Functional dissection of Rab GTPases involved in primary cilium formation. *J Cell Biol,* **178**, 363-9.

Zhang, C., Zhang, W., Lu, Y., Yan, X., Yan, X., Zhu, X., Liu, W., Yang, Y. & Zhou, T. (2016). NudC regulates actin dynamics and ciliogenesis by stabilizing cofilin 1. *Cell Res,* **26**, 239-53.

Zhang, D. & Aravind, L. (2010). Identification of novel families and classification of the C2 domain superfamily elucidate the origin and evolution of membrane targeting activities in eukaryotes. *Gene,* **469**, 18-30.

Zhang, J., Campbell, R. E., Ting, A. Y. & Tsien, R. Y. (2002). Creating new fluorescent probes for cell biology. *Nat Rev Mol Cell Biol,* **3**, 906-18.

Zhang, Q., Yu, D., Seo, S., Stone, E. M. & Sheffield, V. C. (2012). Intrinsic protein-protein interaction-mediated and chaperonin-assisted sequential assembly of stable bardet-biedl syndrome protein complex, the BBSome. *J Biol Chem,* **287**, 20625-35.

Zhu, F., Lawo, S., Bird, A., Pinchev, D., Ralph, A., Richter, C., Muller-Reichert, T., Kittler, R., Hyman, A. A. & Pelletier, L. (2008). The mammalian SPD-2 ortholog Cep192 regulates centrosome biogenesis. *Curr Biol,* **18**, 136-41.

Zimmerman, W. & Doxsey, S. J. (2000). Construction of centrosomes and spindle poles by molecular motor-driven assembly of protein particles. *Traffic,* **1**, 927-34.

Zuker, M. (2003). Mfold web server for nucleic acid folding and hybridization prediction. *Nucleic Acids Res,* **31**, 3406-15.

Zuo, X., Fogelgren, B. & Lipschutz, J. H. (2011). The small GTPase Cdc42 is necessary for primary ciliogenesis in renal tubular epithelial cells. *J Biol Chem,* **286**, 22469-77.